

**Microwave-assisted Desorption and Monitoring of Volatile Organic Compounds on Adsorbents**

by

Arman Peyravi

A thesis submitted in partial fulfillment of the requirements for the degree of

Doctor of Philosophy

in

Environmental Engineering

Department of Civil and Environmental Engineering

University of Alberta

© Arman Peyravi, 2021

## ABSTRACT

Adsorption is a widely used method for abatement of volatile organic compound (VOC) emissions due to its high efficiency and relatively low operating cost. Following adsorption, desorption is usually used to regenerate the adsorbent. Adsorbent regeneration, often known as the most limiting step in the adsorption process, is a time-consuming stage and is often completed through using hot purge gas or superheated steam. In the thermal regeneration process, regeneration time directly impacts energy consumption, and thus, the operating cost of the air treatment facility. In recent years, microwave (MW) regeneration has been proposed as a potential alternative to conventional thermal regeneration techniques. For an effective MW regeneration process, the adsorbent/adsorbate system should be able to absorb MW and convert it to heat. However, there are many adsorbent/adsorbate systems that are transparent to MW. In this research, different techniques were developed in chapters 3 to 6 to improve MW regeneration of porous MW-transparent adsorbents. Additionally, chapter 7 explores a novel technique to monitor VOC desorption process using a non-contact MW sensor and to determine the required time for adsorbent regeneration.

The effect of purge gas relative humidity (RH) on MW absorption of two MW-transparent adsorbents (a beta type zeolite and a hypercrosslinked polystyrene resin) was first investigated (Chapter 3). Dielectric properties and water adsorption capacity of each adsorbent were measured at different purge gas RH and applied MW power. Furthermore, polar and nonpolar adsorbates were used to investigate VOC adsorption and MW-assisted desorption under dry and humid conditions. Finally, complete desorption of selected adsorbates in both dry and humid conditions was compared in terms of regeneration time and energy consumption. Obtained results indicated

that continuous exposure of adsorbent bed to water saturated purge gas during MW heating enhances its MW absorption. Using water saturated purge gas reduced the MW energy needed for complete regeneration of the polymeric resin and zeolite by up to 30 % and 73 %, respectively. This study shows that the interaction of water molecules with the adsorbent in a MW field enhances the MW regeneration of adsorbents with poor dielectric properties.

Another approach to enhancing MW regeneration of MW-transparent adsorbents is to alter their dielectric loss factor and MW penetration depth (Chapter 4). In this regard, the influence of carbon nanotubes (CNT) addition to a commercially available styrene-divinylbenzene porous adsorbent resin beads, Optipore V503, was studied. CNTs were selected as a MW absorptive material (MAM) due to their large loss factor and electrical conductivity. CNTs were dispersed in sodium dodecyl sulfate solution and physically deposited on the surface of adsorbent at different weight percent (wt%). CNT-coated samples were characterized using helium ion microscopy (HIM), Raman spectroscopy, thermal gravimetry analysis, dielectric property analysis, and N<sub>2</sub> and n-heptane adsorption isotherms. In addition, 5 cycles of n-heptane adsorption and MW-assisted regeneration were completed for CNT-coated and as-received adsorbent samples. Obtained results revealed that coating the adsorbent with 0.1 to 0.3 wt% of CNTs resulted in a 3 to 28 % decrease in its total pore volume and increased its dielectric loss factor by 5 to 29 times. The deposition of a very small amount of CNTs (0.1 to 0.3 wt %) on the adsorbent increased the MW-assisted desorption efficiency by 103 % to 284 % compared to the as-received adsorbent.

In-situ polymerization of a porous composite with large surface area and MW absorption ability was also investigated (Chapter 5). In this regard, porous hypercrosslinked polymers (HCP) of (4, 4'-bis((chloromethyl)-1, 1'-biphenyl- benzyl chloride)) with different carbon black (CB) contents

were synthesized via the Friedel-Crafts reaction. CB was selected as the filler due to its low cost and high dielectric loss and was embedded inside the polymer structure during in-situ polymerization. Fourier-transform infrared spectroscopy (FTIR) and HIM confirmed the synthesis of the HCP and the presence of CB in the HCP structure, respectively. Thermo-gravimetric analysis, dielectric property measurement, Bruner–Emmett-Teller (BET) analysis and gravimetric sorption analysis were used to characterize the thermal stability, MW absorption ability, specific surface area, and adsorption performance, respectively, of the resulting composites. CB-containing composites showed enhanced thermal stability at elevated temperatures and more than a 90-times increase in the dielectric loss factor, which is favorable for MW regeneration. BET surface area analysis demonstrated that CB presence in the polymer structure nonlinearly decreases the surface area and total pore volume (by 38 % and 26 %, respectively at the highest CB load). Based on the characterization testing, 4 wt% of CB was found to be an optimum filler content, having the highest MW absorption and minimal effect on the adsorbent porosity. HCP with 4 wt% CB allowed a substantial increase in the desorption temperature and yielded more than a 450 % enhancement in the desorption efficiency compared to HCP without CB.

HCP/graphene oxide (GO) nanocomposites with large surface area and enhanced MW absorption ability were synthesized by solution mixing technique for use in VOC adsorption and MW regeneration (Chapter 6). Polymers of 4, 4'-bis ((chloromethyl)-1, 1' -biphenyl- benzyl chloride) were hypercrosslinked through the Friedel-Crafts reactions. GO nano-sheets were synthesized through the Hummer's method. Then, ethanol was selected as the solvent to prepare a series of nanocomposites with different GO contents (1-8 wt%) by solution mixing method. XRD and FTIR studies indicated the correct fabrication of GO, hypercrosslinked polymer (HCP), and GO-filled

nanocomposite. The morphology of synthesized samples and GO dispersion were characterized by scanning electron microscopy, HIM, and transmission electron microscopy analysis. Thermogravimetry analysis revealed a large enhancement in the thermal stability of GO-filled nanocomposites compared to pristine polymer. N<sub>2</sub> adsorption isotherm analysis showed 7 % and 10 % reduction in BET surface area and total pore volume of the nanocomposite with 8 wt% GO. Compared to the pristine polymer, the dielectric constant and dielectric loss factor increased from 5 to 17 and 0.05 to 1.6, respectively, for the nanocomposites with 8 wt% GO. Toluene adsorption isotherms of synthesized samples showed less than 10 % reduction in the adsorption capacity of nanocomposites at 8 wt% GO content. MW-assisted desorption of toluene from samples revealed more than 160 °C and 4 times improvement in the desorption temperature and desorption efficiency, respectively, by addition of 4 wt% GO to the polymer.

A non-contact MW sensor was developed for real-time monitoring of the desorption process (Chapter 7). The main sensing element of the proposed desorption monitoring platform was a chipless flexible MW split-ring resonator, ‘tag’, which was electromagnetically coupled to a read-out circuit, ‘reader’. A styrene-divinylbenzene adsorbent was loaded with heptane (nonpolar) and n-propyl alcohol (polar) at different concentrations to evaluate the use of the sensor for desorption monitoring. After verifying the sensor's temperature stability, the desorption was carried out at 175 °C. The sensor response was compared to effluent adsorbate concentration measured by a flame ionization detector (FID), and thereby, adsorbent dielectric properties were related to adsorbate load on the adsorbent. A linear correlation ( $R^2 > 0.95$ ) between the adsorbate load and the measured frequency shift was observed. The saturation time and regeneration time determined based on the non-contact sensor showed more than 95 % and 75 % consistency, respectively, with

corresponding values obtained from concentration measurements by FID. The proposed sensor has the potential to be integrated as a low-cost sensing device. The proposed chipless MW resonator sensor demonstrates the capability of real-time distant monitoring and detection, making it suitable for use in harsh environments and high-temperature sensing applications.

In summary, this study showed the critical impact of MAMs on the regeneration of MW-transparent adsorbents. While the presence of a MAM in the adsorbent structure is needed for efficient MW heating, it reduces the adsorption capacity to some extent. Future research could explore the effect of hybrid fillers (e.g., polymer-MAM nanofillers) which could potentially have better dispersion in the matrix and result in better VOC adsorption capacity and MW-assisted regeneration performance. Last but not the least, this study showed that the chipless MW resonator sensor can be used to monitor high temperature adsorbent regeneration process.

## PREFACE

This Ph.D. dissertation contains the result of a research conducted by me, Arman Peyravi, in the Department of Civil and Environmental Engineering at the University of Alberta. Chapters 3 to 6 have been submitted or ready for the submission to peer-reviewed journals. My co-authors from the Air Quality Characterization Laboratory in the Department of Civil & Environmental Engineering at the University of Alberta, Department of Electrical and Computer Engineering at the University of Alberta, Nanomaterials and Polymer Nanocomposites Laboratory in the School of Engineering at the University of British Columbia, and collaborators from our industrial sponsor, Ford Motor Company, were responsible for conducting part of laboratory tests and/or reviewing the manuscript drafts.

Chapter 3 is ready for the submission to a peer-reviewed journal.

Chapter 4 was published as Arman Peyravi, Zaher Hashisho, David Crompton, James E. Anderson. Enhanced microwave regeneration of a polymeric adsorbent through carbon nanotubes deposition. *Separation and Purification Technology* (2021): 119616.

Chapter 5 has been submitted (under review) as Arman Peyravi, Zaher Hashisho, David Crompton, James E. Anderson. Porous carbon black-polymer composites for VOC adsorption and efficient microwave-assisted desorption.

Chapter 6 has been submitted (under review) as Arman Peyravi, Farhad Ahmadijokani, Mohammad Arjmand, Zaher Hashisho. VOC Adsorption and Microwave Absorption study of Porous Polymer/Graphene Oxide Nanocomposites.

Chapter 7 has been submitted (under review) as Arman Peyravi, Zahra Abbasi, Zaher Hashisho, Mojgan Daneshmand. Real-time Noncontact VOC Desorption Monitoring Sensor.

*To my parents, Masoud and Farideh and to my siblings, Amir and Elham.*

*This humble work is a sign of my love to you!*

## ACKNOWLEDGMENTS

I would like to express my deep and sincere gratitude to my research supervisor, Prof. Zaher Hashisho, for giving me the opportunity to do research and providing invaluable guidance throughout these years. His vision, sincerity and motivation have been always inspiring. I would also like to thank him for his friendship and empathy that helped me to get through difficult times.

My sincere thanks also go to Dr. Pedram Mousavi and Dr. Mojgan Daneshmandi for providing technical support and instrumentation. I express my thanks to Mr. Peng Li, characterization group manager, and his colleagues at Nanofabrication and Characterization Facility, for their genuine supports in characterization experiments of this research.

I am extending my thanks to Ford Motor Company and the Natural Sciences and Engineering Research Council of Canada for their financial support during my research work.

I would like also to say thanks to my friends and colleagues, Sam Ranjbar, Farzad Ahmadi, Farhad Ahmadi, Daniel Unsworth, Mohammad Feizbakhshan, Keyvan Rahmani, and Amin Sadeghi for their support and friendship.

I also acknowledge my defense committee members, Dr. Rajender Gupta, Dr. Yaman Boluk, Dr. Bipro Dhar, Dr. Erin Bobicki and Dr. David Ramirez for their precious advice and time spent on this work.

Last but not the least, I am extremely grateful to my parents for their love, caring and sacrifices for educating and preparing me for my future.

# TABLE OF CONTENTS

<b>ABSTRACT.....</b>	<b>II</b>
<b>PREFACE.....</b>	<b>VII</b>
<b>ACKNOWLEDGMENTS .....</b>	<b>X</b>
<b>TABLE OF CONTENTS .....</b>	<b>XI</b>
<b>LIST OF TABLES .....</b>	<b>XIX</b>
<b>LIST OF FIGURES .....</b>	<b>XX</b>
<b>GLOSSARY OF ACRONYMS .....</b>	<b>XXVI</b>
<b>CHAPTER 1 : INTRODUCTION AND RESEARCH OBJECTIVES .....</b>	<b>1</b>
1.1 BACKGROUND AND MOTIVATIONS.....	1
1.1.1 VOC Adsorption and Desorption .....	1
1.1.2 Microwave-assisted Regeneration.....	2
1.1.3 Enhancing Microwave Absorption.....	3
1.1.4 Regeneration Time and MW Sensing.....	4
1.2 PROBLEM STATEMENT AND HYPOTHESIS .....	5
1.3 GOAL AND OBJECTIVES.....	6
1.4 RESEARCH SIGNIFICANCE .....	8
1.5 THESIS OUTLINE .....	8
1.6 REFERENCES .....	9
<b>CHAPTER 2 : LITRATURE REVIEW .....</b>	<b>16</b>

2.1 ADSORPTION .....	16
2.1.1 Adsorbent Materials .....	16
2.2 REGENERATION OF ADSORBENTS .....	18
2.3 MICROWAVE-ASSISTED REGENERATION .....	19
2.4 MICROWAVE HEATING PRINCIPLES.....	22
2.4.1 Microwave Heating Mechanisms.....	22
2.4.2 Materials Behavior in Microwave Field .....	23
2.4.3 Measurement of Dielectric Properties .....	26
2.5 NANOCOMPOSITE PREPARATION METHODS .....	27
2.5.1.1 In-situ polymerization.....	27
2.5.1.2 Solution mixing .....	28
2.5.1.3 Melt processing.....	28
2.6 PREVIOUS WORKS ON THE PREPARATION OF MICROWAVE ABSORPTIVE COMPOSITES .....	28
2.7 MICROWAVE SENSING .....	32
2.7.1 Microwave sensing applications in gas phase concentration monitoring .....	32
2.8 REFERENCES .....	34
<b>CHAPTER 3 : PURGE GAS HUMIDITY IMPROVES MICROWAVE ABSORPTION OF POLYMERIC AND ZEOLITE ADSORBENTS.....</b>	<b>50</b>
3.1 CHAPTER OVERVIEW .....	50
3.2 INTRODUCTION.....	51
3.3 EXPERIMENTAL SECTION .....	53
3.3.1 Adsorbents and Adsorbates .....	53

3.3.2 Methods.....	54
3.3.2.1 Microwave heating .....	54
3.3.2.2 Dielectric permittivity measurement.....	55
3.3.2.3 Water adsorption under microwave irradiation .....	56
3.3.2.4 VOC adsorption & desorption .....	56
3.4 RESULTS AND DISCUSSION.....	57
3.4.1 Effect of Microwave Applied Power .....	57
3.4.2 Relative Humidity Effect.....	60
3.4.3 VOC Adsorption and Desorption .....	61
3.4.4 Energy Consumption.....	65
3.5 CONCLUSIONS .....	66
3.6 REFERENCES .....	68
<b>CHAPTER 4 : ENHANCED MICROWAVE REGENERATION OF A POLYMERIC ADSORBENT THROUGH CARBON NANOTUBES DEPOSITION .....</b>	<b>73</b>
4.1 CHAPTER OVERVIEW .....	73
4.2 INTRODUCTION.....	74
4.3 EXPERIMENTAL SECTION .....	78
4.3.1 Material .....	78
4.3.2 Sample Preparation .....	79
4.3.3 Characterizations and Measurements.....	80
4.3.3.1 Raman spectroscopy.....	80
4.3.3.2 Scanning helium ion microscopy .....	80

4.3.3.3 Micropore surface analysis.....	80
4.3.3.4 Heptane adsorption isotherm .....	81
4.3.3.5 Derivative thermo-gravimetric analysis .....	81
4.3.3.6 Dielectric property measurement.....	82
4.3.3.7 Heating rate and microwave heating capacity.....	82
4.3.4 Cyclic Heptane Adsorption and Microwave-assisted Desorption .....	83
4.3.4.1 Adsorption setup.....	83
4.3.4.2 Microwave regeneration setup.....	83
4.4 RESULTS AND DISCUSSION.....	85
4.4.1 Raman Spectroscopy and HIM.....	85
4.4.2 Surface Property Measurement.....	88
4.4.3 Heptane Adsorption Isotherms.....	89
4.4.4 DTG Analysis.....	91
4.4.5 Dielectric Property Analysis.....	91
4.4.6 Heating Rate and Microwave Heating Capacity.....	93
4.4.7 Microwave-assisted Desorption .....	94
4.5 CONCLUSIONS .....	101
4.6 REFERENCES .....	103
<b>CHAPTER 5 : POROUS CARBON BLACK/POLYMER COMPOSITES FOR VOC ADSORPTION AND EFFICIENT MICROWAVE-ASSISTED DESORPTION.....</b>	<b>111</b>
5.1 CHAPTER OVERVIEW .....	111
5.2 INTRODUCTION.....	112

5.3 EXPERIMENTAL SECTION .....	116
5.3.1 Materials .....	116
5.3.2 Synthesis of Hypercrosslinked Polymer .....	116
5.3.2.1 Preparation of carbon black/polymer composites .....	117
5.3.3 Characterizations and Measurements.....	117
5.3.3.1 FTIR analysis.....	117
5.3.3.2 HIM analysis.....	118
5.3.3.3 TGA analysis.....	119
5.3.3.4 Micropore surface analysis.....	119
5.3.3.5 VOC adsorption isotherm.....	120
5.3.3.6 Dielectric properties .....	120
5.3.3.7 Microwave heating rate and capacity .....	120
5.3.3.8 Hexane adsorption and microwave-assisted desorption .....	121
5.4 RESULTS AND DISCUSSION.....	122
5.4.1 CB Dispersion Stability in 1, 2-dichloroethane .....	122
5.4.2 FTIR.....	123
5.4.3 HIM.....	124
5.4.4 TGA.....	126
5.4.5 Textural Analysis .....	127
5.4.6 Toluene Adsorption Isotherm .....	129
5.4.7 Dielectric Properties Measurement .....	132
5.4.8 Microwave Heating.....	133

5.4.9 Microwave-assisted Desorption .....	134
5.5 CONCLUSIONS .....	136
5.6 REFERENCES .....	138
<b>CHAPTER 6 : VOC ADSORPTION AND MICROWAVE ABSORPTION STUDY OF POROUS GRAPHENE OXIDE/POLYMER NANOCOMPOSITES .....</b>	<b>148</b>
6.1 CHAPTER OVERVIEW .....	148
6.2 INTRODUCTION.....	149
6.3 EXPERIMENTAL SECTION .....	151
6.3.1 Materials .....	151
6.3.2 Synthesis of Graphene Oxide.....	151
6.3.3 Synthesis of Hypercrosslinked Polymer .....	151
6.3.4 Preparation of Graphene Oxide/Polymer Nanocomposites .....	152
6.3.5 Characterizations and Measurements.....	153
6.3.5.1 XRD analysis.....	153
6.3.5.2 FTIR analysis.....	153
6.3.5.3 Microscopy study .....	153
6.3.5.4 TGA analysis .....	154
6.3.5.5 Micropore surface analysis.....	154
6.3.5.6 VOC adsorption isotherm.....	155
6.3.5.7 Dielectric properties and penetration depth.....	155
6.3.5.8 Microwave heating rate and capacity .....	156
6.3.5.9 Toluene adsorption and microwave-assisted desorption.....	157

6.4 RESULTS AND DISCUSSION.....	158
6.4.1 XRD.....	158
6.4.2 FTIR.....	158
6.4.3 Microscopic Studies.....	160
6.4.4 Thermal Properties of Adsorbents.....	163
6.4.5 Textural Analysis.....	165
6.4.6 Toluene Adsorption Isotherm.....	166
6.4.7 Dielectric Properties Measurement.....	167
6.4.8 Microwave Heating.....	168
6.4.9 Microwave-assisted Desorption.....	169
6.5 CONCLUSIONS.....	170
6.6 REFERENCES.....	172

## **CHAPTER 7 : REAL-TIME NONCONTACT VOC DESORPTION MONITORING**

<b>SENSOR.....</b>	<b>182</b>
7.1 CHAPTER OVERVIEW.....	182
7.2 INTRODUCTION.....	183
7.3 EXPERIMENTAL SET-UP AND METHODS.....	185
7.3.1 Material.....	185
7.3.2 VOC Adsorption and Desorption.....	186
7.3.3 Dielectric Property Measurement.....	188
7.3.4 VOC Adsorption Isotherm.....	193
7.4 RESULT AND DISCUSSION.....	194

7.4.1 Thermal stability.....	194
7.4.2 VOC adsorption/desorption monitoring.....	195
7.4.3 Saturation & Regeneration time prediction.....	200
7.5 CONCLUSIONS.....	202
7.6 REFERENCES.....	203
<b>CHAPTER 8 : CONCLUSIONS AND RECOMMENDATIONS.....</b>	<b>208</b>
8.1 DISSERTATION OVERVIEW.....	208
8.2 CONCLUSIONS.....	208
8.3 RECOMMENDATIONS.....	212
<b>BIBLIOGRAPHY.....</b>	<b>214</b>
<b>APPENDIX A: SUPPLEMENTARY INFORMATION.....</b>	<b>250</b>

## LIST OF TABLES

Table 2-1. Comparison of properties of various heat sources, adopted from Harikoshi et al. <sup>48</sup> ...	21
Table 2-2. Microwave properties some selected materials. ....	24
Table 3-1. Physical properties of selected adsorbents .....	53
Table 3-2. Physical properties of tested adsorbates .....	54
Table 3-3. The results of Cyhex and IPA adsorption on Optipore V503 and Zeolite HSZ980. Values are reported as mean $\pm$ standard deviation of three rounds of measurement.....	65
Table 5-1. Surface property and toluene adsorption capacities of various adsorbents as compared to that of synthesized HCP and CB/HCP composites.....	131
Table 7-1. Physical properties of tested adsorbates .....	186

## LIST OF FIGURES

Figure 1-1. Classification of approaches set to attain the final goal of this study. ....	7
Figure 2-1. MW heating mechanisms. ....	23
Figure 3-1. Schematic diagram of MW assisted regeneration setup. ....	55
Figure 3-2. MW heating effect on Optipore V503 and Zeolite HSZ980: a) temperature evolution, b) Water vapour adsorption c) dielectric constant, and d) dielectric loss factor. The error bars represent standard deviations calculated based on three rounds of experiments. ....	58
Figure 3-3. Temperature difference between humid and dry MW heating at constant applied power of 380 W and purge gas flow rate of 1 l/min. The error bars represent standard deviations calculated based on three rounds of experiments. ....	61
Figure 3-4. Desorption of Cyhex and IPA off Zeolite HSZ980. Effluent concentration and Zeolite HSZ980 temperature profiles during desorption of Cyhex (a) and IPA (b); Desorption efficiency of Cyhex (c) and IPA (d) at 0 and 100 % RH and constant applied power of 380 W. ....	63
Figure 3-5. Desorption of Cyhex and IPA off Optipore V503. Effluent concentration and Optipore V503 temperature profiles during desorption of Cyhex (a) and IPA (b); Desorption efficiency of Cyhex (c) and IPA (d) at 0 and 100 % RH and constant applied power of 380 W. ....	64
Figure 3-6. Energy consumption during the desorption of Cyhex and IPA on a) Optipore v503 and b) Zeolite HSZ980. The error bars represent standard deviations calculated based on three rounds of experiments. ....	66
Figure 4-1. Schematic diagram of MW-assisted regeneration setup. ....	85

## List of Figures

Figure 4-2. Raman spectra of CNT-coated and as-received Optipore V503 samples. ....	86
Figure 4-3. HIM images obtained for a) 0.0 wt%, b) 0.1 wt%, c) 0.2 wt%, and d) 0.3 wt% of CNT on Optipore V503. ....	87
Figure 4-4. Effect of SDS and CNT deposition on a) pore volume and b) BET surface area of Optipore V503. ....	89
Figure 4-5. Pore size distribution of the CNT and SDS coated Optipore V503. ....	89
Figure 4-6. Heptane adsorption isotherms of virgin Optipore V503, CNT-coated Optipore V503, and CNT. The error bars represent standard deviations of two runs. ....	90
Figure 4-7. Thermograms of virgin adsorbent and CNT-coated Optipore V503 ....	91
Figure 4-8. Effect of CNT and SDS loading on a) dielectric properties and b) penetration depth of virgin adsorbent and CNT-coated adsorbent. ....	93
Figure 4-9. a) Effect of MW power level on the heating rate; b) Effect of CNT loading on the MW heating capacity. The error bars represent standard deviations calculated based on three rounds of experiments. ....	94
Figure 4-10. Adsorption breakthrough curves of heptane on a) 0 wt% CNT, b) 0.1 wt% CNT, c) 0.2 wt% CNT, and d) 0.3 wt% CNT-coated adsorbent. ....	96
Figure 4-11. Heptane concentration and bed temperature during the regeneration of a) 0 wt% CNT, b) 0.1 wt% CNT, c) 0.2 wt% CNT, and d) 0.3 wt% CNT-coated adsorbent. ....	98
Figure 4-12. Heptane desorption efficiency of a) 0 wt% CNT, b) 0.1 wt% CNT, c) 0.2 wt% CNT, and d) 0.3 wt% CNT coated adsorbent. ....	100
Figure 4-13. 1st and 5th cycle adsorption capacity of CNT coated and as-received Optipore V503. Error bars represent standard deviation of two runs. ....	101

## List of Figures

Figure 5-1. CB/HCP composite synthesis steps. ....	118
Figure 5-2. a) CB UV-vis absorbance; b) Change in CB concentration in DCE with time. ....	124
Figure 5-3. FTIR spectra acquired for 0 wt% and 6 wt% CB/HCP.....	124
Figure 5-4. HIM micrographs of synthesized HCPs with 0 wt% CB (a & c) and 4 wt% CB (b & d). ....	125
Figure 5-5. a) Weight percent, b) weight loss rate versus temperature, and c) weight loss of composites with different CB content at 887 °C. The error bars represent the maximum based on three rounds of analysis. ....	127
Figure 5-6. a) BET surface area, b) Pore volume, and c) Pore size distribution of synthesized composites. ....	129
Figure 5-7. a) Toluene adsorption isotherms of CB/HCPs at 25 °C; b) Toluene adsorption capacity of CB/HCPs at 0.02 and 0.9 toluene relative vapor pressures. The error bars represent standard deviations calculated based on three rounds of analysis. ....	130
Figure 5-8. Effect of CB loading on a) dielectric properties and b) MW penetration depth. The error bars represent standard deviations calculated based on three rounds of measurements. ....	133
Figure 5-9. Effect of CB loading on a) heat up rate and b) MW heating capacity. The error bars represent standard deviations calculated based on three rounds of analysis. ....	134
Figure 5-10. Hexane adsorption/MW assisted regeneration of HCPs with 0 and 4 wt% CB; a) hexane adsorption breakthrough curves, b) desorption temperature, c) effluent hexane concentration during the desorption, and d) desorption efficiency versus desorption time. ....	136

## List of Figures

Figure 6-1. XRD spectrum of synthesized GO.....	158
Figure 6-2. FTIR spectra acquired for 0 wt% and 8 wt% GO/HCP. ....	159
Figure 6-3. SEM image of synthesized GO sheets. ....	161
Figure 6-4. HIM images of synthesized HCPs with 0 wt% GO (a & c) and 8 wt% GO (b & d). .....	162
Figure 6-5. TEM images of synthesized HCPs with 0 wt% GO (a) and 8 wt% GO (b). Red circles indicate areas abundant in GO. ....	162
Figure 6-6. a) Percent weight loss, and b) weight loss rate versus temperature of synthesized GO/HCPs. ....	164
Figure 6-7. a) BET surface area, total pore volume, and b) pore size distribution of synthesized GO/HCPs. Error bars represent the standard deviation of two measurments. ....	165
Figure 6-8. Toluene adsorption isotherms of GO/HCPs at 25 °C.....	166
Figure 6-9. Effect of GO on a) dielectric properties and b) MW penetration depth. Error bars represent the standard deviation of two measurments. ....	168
Figure 6-10. Effect of GO content on a) heating rate and b) MW heating capacity. Error bars represent the standard deviation of three measurments. ....	169
Figure 6-11. a) Effluenet concentration and adsorbent temperature profiles during desorption of toluene, and b) Toluene desorption efficiency. Error bars represent the standard deviation of two measurments. ....	170
Figure 7-1. (a) Schematic diagram of the adsorption and desorption process. (1) Mass flow controller; (2) Syringe pump; (3) Tee; (4) FID & Data acquisition; (5) Sensing tag and	

## List of Figures

reader; (6) Heating loop; (7) Adsorbent Bed. (b) Picture of MW reader-tag sensor used for distant desorption monitoring. ....	187
Figure 7-2. (a) The main structure of the chip-less MW sensor, (b) the transmission response of the system indicating a resonance in the spectrum of the whole structure. (c) the tag, reader, and the ground plane with their dimensions identified in mm: $W_{r1}=33.3$ , $L_{r1}=25.4$ , $W_{r2}=7$ , $L_{r2}=24.6$ , $L_{g1}=57.27$ , $L_{g2}=95.8$ , $L_{g3}=40$ , $W_g=14$ , $L_{t1}=45$ , $L_{t2}=21.4$ , $L_{t3}=20.5$ , $W_{t1}=9$ , $W_{t2}=1$ , and $g_1, g_2=1.4$ .....	189
Figure 7-3. Transmission response of the tag-reader sensor while the distance between the tag and reader changes from 10 mm to 60 mm. ....	191
Figure 7-4. Simulation results showing the resonant frequency variation for four different effective permittivities ( $\epsilon_r$ ) of the sample under the test (SUT).....	193
Figure 7-5. Change in temperature and frequency shift during the heating of the adsorbent bed. ....	194
Figure 7-6. Heptane and 1-propanol adsorption isotherms.....	195
Figure 7-7. a) Adsorption breakthrough curves, b) Dowex Optipore V503 adsorption capacities, c) effluent VOC concentration during the desorption, and d) frequency shift variation during the adsorption and consecutive desorption. Error bars represent the standard deviation of three rounds of analysis. Arrows indicate the transition from the adsorption to the desorption.....	197
Figure 7-8. Adsorbate load and frequency shift change during adsorption/desorption of a) 100 ppm 1-Propanol, b) 1000 ppm 1-propanol, c) 100 ppm Heptane, and d) 1000 ppm Heptane. Arrows indicate the transition from the adsorption to the desorption. ....	199

## List of Figures

Figure 7-9. Relative frequency shift versus relative adsorbate load in adsorption/desorption of a) Heptane and b) 1-Propanol. ....	200
Figure 7-10. Resonant frequency shift of adsorbent with 1 % adsorbate load. Error bars show the standard deviation of three rounds of experiments. ....	200
Figure 7-11. Measured adsorbent saturation time, $t_{\text{sat}}$ . (a) and regeneration time, $t_{\text{Reg}}$ . (b) based on concentration and frequency data. Error bars show the standard deviation of three rounds of experiments. ....	201
Figure A-1. Adsorption isotherms of water on Zeolite HSZ980 and Optipore V503 without MW heating. ....	250
Figure A-2. Desorption rate of a) Cyhex from Optipore V503, b) IPA from Optipore V503, c) Cyhex from Zeolite HSZ980, and d) IPA from Zeolite HSZ980 at 0 and 100 % RH and constant applied power of 380 W. ....	251
Figure A-3. Dispersed CNT concentration versus time. ....	251

## GLOSSARY OF ACRONYMS

AC	Activated Carbon
ACFC	Activated Carbon Fiber Cloth
BCH	Benzyl Chloride
BCMB	4, 4'-Bis(Chloromethyl)-1, 1'-Biphenyl
BET	Brunauer-Emmett-Teller
CB	Carbon Black
CMOS	Complementary Metal-Oxide Semiconductor
CNT	Carbon Nanotube
Cyhex	Cyclohexane
DA	Data Acquisition
DFT	Density Functional Theory
DI	Deionized
DMM	Dimethoxy Methane
DTG	Derivative Thermo-Gravimetric
EDC	1, 2-Dichloroethane
EM	Electromagnetic
EPA	Environmental Protection Agency
ETS-10	Engelhard Titanosilicate Molecular Sieve
FC	Iron (III) Chloride
FID	Flame Ionization Detector
FTIR	Fourier-transform Infrared
GO	Graphene Oxide
HCP	Hypercrosslinked Polymer
HIM	Helium Ion Microscopy
IPA	Isopropyl Alcohol
MAM	Microwave Absorbing Material
MFC	Mass Flow Controller
MOF	Metal Organic Framework

## Glossary of Acronyms

MW	Microwave
MWCNT	Multiwall Carbon Nanotubes
PD	Penetration Depth
phr	Parts Per Hundred Rubber
PSA	Pressure Swing Adsorption
PSD	Pore Size Distribution
QSDFT	Quenched Solid Density Functional Theory
RGO	Reduced Graphene Oxide
RH	Relative Humidity
SD	Standard Deviation
SDS	Sodium Dodecyl Sulfate
SEM	Scanning Electron Microscopy
SLPM	Standard Liter Per Minute
SRR	Split-Ring Resonator
SUT	Sample Under Test
TEM	Transmission Electron Microscopy
TGA	Thermo-Gravimetric Analysis
TSA	Temperature Swing Adsorption
UV-vis	Ultraviolet-Visible
VNA	Vector Network Analyzer
VOC	Volatile Organic Compound
wt%	Weight Percent
XRD	X-Ray Diffraction

# CHAPTER 1: INTRODUCTION AND RESEARCH OBJECTIVES

## 1.1 Background and Motivations

### 1.1.1 VOC Adsorption and Desorption

Volatile organic compounds (VOCs) are compounds of carbon, excluding carbon monoxide, carbon dioxide, carbonic acid, metallic carbides or carbonates, and ammonium carbonate, that contribute to atmospheric photochemical reactions.<sup>1</sup> VOCs are released from several sources of indoor environment, industrial plants and vehicles. VOC emissions may be transported over distances in atmosphere and cause adverse environmental and significant public health problems.<sup>2-4</sup> The increase in VOC emission into atmosphere and the strict environmental regulations makes VOC emission control more imperative. Up to now, numerous methods including absorption, adsorption, condensation, and oxidation have been used to treat VOC polluted streams.<sup>5-7</sup> Among them, adsorption has been a prime option that provides many advantages such as high efficiency and relatively low operating cost in the recovery of high-value adsorbates.<sup>8,9</sup> Furthermore, the principle of adsorption separation is already mature which makes it one of widely used methods for VOC capture in industry.<sup>8,9</sup>

Adsorbents used in VOC separation must be regenerated to be used in further adsorption cycles. Several techniques are available to regenerate adsorbents. These methods are typically categorized into pressure swing regeneration, temperature swing regeneration, and reactive regeneration.<sup>10,11</sup> Among aforementioned techniques, temperature swing regeneration is the most used method, and typically involves providing heat by hot purge gas or superheated steam. However, high volume of purge gas has to be used in these methods to reach suitable regeneration temperatures due to the

low heat capacity of purge gas. Using large volumes of purge gas dilutes the desorbed VOCs, thus further separation usually would be needed for VOC recovery purposes. Moreover, when steam is applied, the adsorbent bed requires a drying step after each desorption cycle. All these shortcomings increase the energy penalty of conventional thermal regeneration, necessitating the need for alternative methods of thermal regeneration.

In recent years, microwave (MW) regeneration has emerged as a potential alternative to conventional thermal regeneration.<sup>12-14</sup> MW regeneration has several advantages over conventional thermal regeneration including faster heating, higher adsorbate recovery due to lower purge gas consumption, and ability to heat the bed to higher temperatures as there is no temperature limitation associated with a purge gas. Furthermore, the energy loss in MW heating is substantially less than in conventional heating which heats unnecessary parts of the facility in hot gas/steam generation unit.<sup>15-17</sup> However, to meet the basic purpose of MW regeneration which is maintaining the adsorption capacity of adsorbents for reuse, the adsorbent and/or adsorbate system should have a reasonable MW absorption to provide an effective heating.

### **1.1.2 Microwave-assisted Regeneration**

MW heating has been extensively used in industrial drying due to the advantages associated to its selective volumetric heating of water. Several researchers have extended the application of MW to the regeneration of adsorbents since 1980. Burkholder et al. found that the desorption of ethanol from molecular sieve can be improved by MW heating since it selectively heats the ethanol without directly heating the adsorbent.<sup>18</sup> Researchers recognized the potential for using MW regeneration to enhance solvent recovery. Gibson et al. reported that the ethylene oxide desorption time from

polyvinyl chloride (PVC) can be reduced by 400% using MW heating instead of conventional heating for the same regeneration temperature.<sup>19</sup> More recently, Hashisho et al. investigated the effect of activated carbon fiber cloth (ACFC) functional groups on its MW absorption performance.<sup>20</sup> Different densities of functional groups were produced on ACFCs surface during acid and hydrogen treatments and their effect on MW absorption was studied. It was reported that hydrogen -treated samples showed a 50 % increase in MW attenuation constant, while it dropped by 89 % for the acid-treated samples. Shariaty et al. studied the effect of ETS-10 ion exchange on its dielectric properties.<sup>21</sup> They demonstrated that using monovalent and divalent cations by ion exchange, in ETS-10 increases its water adsorption capacity and decreases its dielectric properties which can be useful during the regeneration of polar compounds from the adsorbent. Meng et al found that changing the hydrophobicity of styrene-divinylbenzene porous resin during the sulfonation process can improve its MW regeneration efficiency.<sup>22</sup> Based on their experimental results, better MW absorption was mainly attributed to water adsorption enhancement after sulfonation. All these studies showed that MW heating would be an effective method for adsorbent regeneration when adsorbent/adsorbate systems can convert MW to heat. However, there are many circumstances where both adsorbent and adsorbate are MW transparent which limits the effectiveness of MW heating.

### **1.1.3 Enhancing Microwave Absorption**

Different forms of MW absorptive materials (MAMs) such as graphene oxides (GO), carbon nanotubes (CNTs), sodium dodecyl sulfate (SDS), and magnetic nanoparticle fillers have been reported for improving MW absorption. However, carbonaceous material are more favorable for

use as dielectric susceptors due to their exceptional dielectric loss factor.<sup>23,24</sup> Wu et al. investigated the effect of reduced graphene oxide (RGO) addition on the electromagnetic absorption of polypyrrole. They showed that even a trace content of RGO (0.43 wt% in aerogel) can significantly increase the electromagnetic absorption of the aerogel without affecting its solvent absorption capacity.<sup>25</sup> Wang et al. prepared multiwall carbon nanotubes/poly vinylidene fluoride composites by simple physical blending. They investigated the effect of untreated multiwall carbon nanotubes (MWCNT) on the dielectric constant of composite. Experimental results demonstrate that the dielectric constant of composite increased by more than 30 times with about 2.0 vol % of MWCNT.<sup>26</sup> Chen et al. investigated the MW absorption performance of silicone rubber using five different graphene products at a very low loading of 1 wt %. They found that among all graphene types highly exfoliated RGO is capable of delivering excellent MW absorption at very low loading.<sup>27</sup> Vadivel et al. studied the effect of sodium dodecyl sulfate (SDS) surfactant on the structural, morphological, and dielectric properties of  $\text{CoFe}_2\text{O}_4$ .<sup>28</sup> More recently, Qing et al. reported the effect of MWCNT and ceramic particle on improving the complex permittivity and MW absorption of epoxy composites.<sup>29</sup> These studies showed that the addition of MAM particles to MW transparent material is an effective way for enhancing MW absorption.

#### **1.1.4 MW Sensing**

Recently, planar MW resonators emerged as potential candidates for sensing applications due to their simple and low-cost fabrication process, easy integration with complementary metal-oxide semiconductor (CMOS), lab-on-chip compatibility, and flexible design. They have been utilized for a wide range of applications, including biomedical detection<sup>30-34</sup>, chemical solutions sensing

<sup>30,35–38</sup>, and environmental monitoring<sup>32,39–41</sup>. Integration of MW planar sensors with adsorbents greatly enhances their sensitivity and selectivity, making them capable of gas/VOC detection and concentration monitoring.<sup>42–44</sup> The operation principle of MW planar split-ring resonator based sensors is based on the variation in electromagnetic (EM) field around the sensor due to the changes in the dielectric properties of the surrounding medium. Specifically, during VOC adsorption/desorption process, any change in the VOC loading capacity of the adsorbent can be translated into a change in their dielectric properties, resulting in a change in their resonance profile.

## 1.2 Problem Statement and Hypothesis

Studies on MW heating of adsorbents showed that MW can be effective if either of adsorbent and/or adsorbates can absorb MW energy and dissipate it into heat. Therefore, using MW transparent adsorbents, complete regeneration would be challenging particularly when it is loaded with nonpolar (MW transparent) adsorbates. In this case, the adsorbent bed either cannot be heated, or high MW energy would be needed for a complete regeneration. To overcome this problem, improving the MW absorption ability of the adsorbent bed by adding a MAM is considered here. In this approach, the heat necessary for desorption can be provided through the MAM's ability to absorb and convert MW to heat.

In the thermal regeneration process design, regeneration time is a key parameter used to determine the number of beds required for a continuous cyclic VOC adsorption/desorption operation.<sup>45</sup> Determining the regeneration time can be challenging as the amount of adsorbate load in the adsorbent bed may vary by the properties of the polluted gas stream, such as the number of

compounds and their concentration. Direct measurement of the effluent concentration during regeneration is typically used to determine the regeneration time. While direct measurement is the only way to accurately determine the time needed for complete adsorbent regeneration, it adds other challenges such as the exposure of detector to hazardous, high boiling point, or corrosive compounds. Besides, the current VOC detection technologies (e.g., flame ionization detector, mass spectrometer) are expensive and need regular calibration and preventive maintenance. Alternatively, MW sensors can be used to monitor the dielectric property variation of adsorbent bed during VOCs adsorption/desorption. These changes in dielectric property of the bed can be correlated to the VOC load on the adsorbent from which regeneration time can be determined.

### **1.3 Goal and Objectives**

The ultimate goal of this study is to improve VOC recovery from polluted air streams using adsorption, MW regeneration, and MW sensing. To achieve this goal, four objectives were established to improve MW regeneration of MW transparent adsorbents. An additional fifth objective was considered to monitor VOC desorption process by a newly designed MW sensor and to determine the required time for a complete adsorbent regeneration. Figure 1-1 illustrates the approaches used to achieve the overall goal of this study.

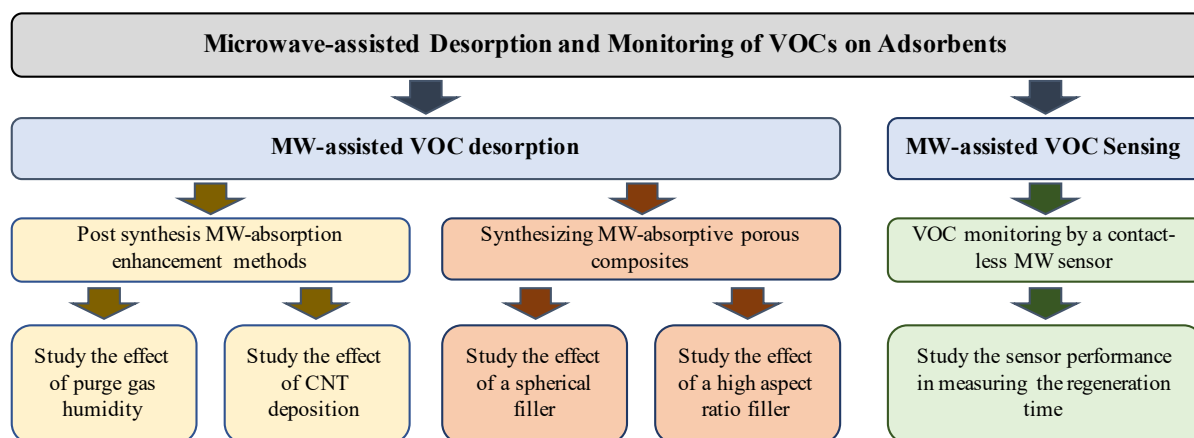


Figure 1-1. Overall approach used to attain the goal of this study.

Based on the research goal and the abovementioned hypotheses, these objectives can be summarized as follows:

**Objective 1:** To investigate the effect of purge gas humidity on the MW-assisted regeneration of MW-transparent adsorbents

**Objective 2:** To investigate the effect of carbon nanotube deposition on the surface of a polymeric adsorbent to enhance its MW regeneration

**Objective 3:** To synthesize a carbon black (CB) filled nanocomposite with large surface area and tunable MW absorption property.

**Objective 4:** To synthesize a GO filled nanocomposites with enhanced MW absorption performance.

**Objective 5:** To introduce a MW resonator sensor as a fast device for monitoring high temperature desorption process.

### **1.4 Research Significance**

Since MW-transparent adsorbents limit the application of MW energy for adsorbent regeneration purposes, this study can be a considerable step for improving MW absorption of MW transparent adsorbents. The project success will provide a notable reduction in the energy consumption associated with MW regeneration of adsorbents. Besides, by demonstrating the use of MW sensors in high temperature desorption process, this study could pave the way towards the use of MW sensors in harsh environment applications. Therefore, this study promotes environmental sustainability by lowering energy consumption and recovering VOCs for recycle and reuse.

### **1.5 Thesis Outline**

This thesis is written in paper-based format. Chapter 1 provides a brief background a on the topics discussed in the thesis and research objectives. Chapter 2 provides a review of the literature and theories related to adsorption, desorption, MW heating principles and nanocomposite preparation methods, and MW sensing. The above-mentioned objectives are met in chapter 3 to 7, individually. Finally, chapter 8 summarizes the main findings, key conclusions of this study and proposes recommendations for future studies.

## 1.6 References

- (1) Srivastava, A.; Mazumdar, D. Monitoring and Reporting VOCs in Ambient Air. In *Air Quality Monitoring, Assessment and Management*; InTech, 2011. <https://doi.org/10.5772/16774>.
- (2) Wang, H.; Nie, L.; Li, J.; Wang, Y.; Wang, G.; Wang, J.; Hao, Z. Characterization and Assessment of Volatile Organic Compounds (VOCs) Emissions from Typical Industries. *Chinese Science Bulletin* **2013**, *58* (7), 724–730. <https://doi.org/10.1007/s11434-012-5345-2>.
- (3) Khan, F. I.; Kr. Ghoshal, A. Removal of Volatile Organic Compounds from Polluted Air. *Journal of Loss Prevention in the Process Industries* **2000**. [https://doi.org/10.1016/S0950-4230\(00\)00007-3](https://doi.org/10.1016/S0950-4230(00)00007-3).
- (4) Shao, M.; Lu, S.; Liu, Y.; Xie, X.; Chang, C.; Huang, S.; Chen, Z. Volatile Organic Compounds Measured in Summer in Beijing and Their Role in Ground-level Ozone Formation. *Journal of Geophysical Research* **2009**, *114* (7), D00G06. <https://doi.org/10.1029/2008JD010863>.
- (5) Ma, L.; He, M.; Fu, P.; Jiang, X.; Lv, W.; Huang, Y.; Liu, Y.; Wang, H. Adsorption of Volatile Organic Compounds on Modified Spherical Activated Carbon in a New Cyclonic Fluidized Bed. *Separation and Purification Technology* **2020**. <https://doi.org/10.1016/j.seppur.2019.116146>.
- (6) Dunn, R. F.; El-Halwagi, M. M. Optimal Design of Multicomponent VOC Condensation Systems. *Journal of Hazardous Materials* **1994**, *38* (1), 187–206. [https://doi.org/10.1016/0304-3894\(94\)00014-X](https://doi.org/10.1016/0304-3894(94)00014-X).
- (7) Wang, J.; Yoshida, A.; Wang, P.; Yu, T.; Wang, Z.; Hao, X.; Abudula, A.; Guan, G. Catalytic Oxidation of Volatile Organic Compound over Cerium Modified Cobalt-Based

- Mixed Oxide Catalysts Synthesized by Electrodeposition Method. *Applied Catalysis B: Environmental* **2020**, *271*, 118941. <https://doi.org/10.1016/j.apcatb.2020.118941>.
- (8) Kirkby, N. Gas Separation by Adsorption Processes. *Gas Separation & Purification* **1988**, *2* (1), 41. [https://doi.org/10.1016/0950-4214\(88\)80042-2](https://doi.org/10.1016/0950-4214(88)80042-2).
- (9) Fuertes, A. .; Marbán, G.; Nevskaia, D. . Adsorption of Volatile Organic Compounds by Means of Activated Carbon Fibre-Based Monoliths. *Carbon* **2003**, *41* (1), 87–96. [https://doi.org/10.1016/S0008-6223\(02\)00274-9](https://doi.org/10.1016/S0008-6223(02)00274-9).
- (10) Pezolt, D. J.; Collick, S. J.; Johnson, H. A.; Robbins, L. A. Pressure Swing Adsorption for VOC Recovery at Gasoline Loading Terminals. *Environmental Progress* **1997**, *16* (1), 16–19. <https://doi.org/10.1002/ep.3300160115>.
- (11) Xiu, G.; Li, P.; E. Rodrigues, A. Sorption-Enhanced Reaction Process with Reactive Regeneration. *Chemical Engineering Science* **2002**, *57* (18), 3893–3908. [https://doi.org/10.1016/S0009-2509\(02\)00245-2](https://doi.org/10.1016/S0009-2509(02)00245-2).
- (12) Price, D. W.; Schmidt, P. S. VOC Recovery through Microwave Regeneration of Adsorbents: Process Design Studies. *Journal of the Air & Waste Management Association* **1998**, *48* (12), 1135–1145. <https://doi.org/10.1080/10473289.1998.10463758>.
- (13) Ondon, B. S.; Sun, B.; Yan, Z. Y.; Zhu, X. M.; Liu, H. Effect of Microwave Heating on the Regeneration of Modified Activated Carbons Saturated with Phenol. *Applied Water Science* **2014**, *4* (4), 333–339. <https://doi.org/10.1007/s13201-013-0147-5>.
- (14) Cherbański, R. Regeneration of Granular Activated Carbon Loaded with Toluene – Comparison of Microwave and Conductive Heating at the Same Active Powers. *Chemical Engineering and Processing - Process Intensification* **2018**, *123*, 148–157. <https://doi.org/10.1016/j.cep.2017.11.008>.

- (15) Fayaz, M.; Shariaty, P.; Atkinson, J. D.; Hashisho, Z.; Phillips, J. H.; Anderson, J. E.; Nichols, M. Using Microwave Heating To Improve the Desorption Efficiency of High Molecular Weight VOC from Beaded Activated Carbon. *Environmental Science & Technology* **2015**, *49* (7), 4536–4542. <https://doi.org/10.1021/es505953c>.
- (16) Chowdhury, T.; Shi, M.; Hashisho, Z.; Sawada, J. A.; Kuznicki, S. M. Regeneration of Na-ETS-10 Using Microwave and Conductive Heating. *Chemical Engineering Science* **2012**, *75*, 282–288. <https://doi.org/10.1016/j.ces.2012.03.039>.
- (17) Roussy, G.; Zoulalian, A.; Charreyre, M.; Thiebaut, J. M. How Microwaves Dehydrate Zeolites. *The Journal of Physical Chemistry* **1984**, *88* (23), 5702–5708. <https://doi.org/10.1021/j150667a049>.
- (18) Burkholder, H. R.; Fanslow, G. E.; Bluhm, D. D. Recovery of Ethanol from a Molecular Sieve by Using Dielectric Heating. *Industrial and Engineering Chemistry Fundamentals* **1986**, *25* (3). <https://doi.org/10.1021/i100023a019>.
- (19) Gibson, C.; Matthews, I.; Samuel, A. Microwave Enhanced Diffusion in Polymeric Materials. *Journal of Microwave Power and Electromagnetic Energy* **1988**, *23* (1), 17–28. <https://doi.org/10.1080/08327823.1988.11688033>.
- (20) Hashisho, Z.; Rood, M. J.; Barot, S.; Bernhard, J. Role of Functional Groups on the Microwave Attenuation and Electric Resistivity of Activated Carbon Fiber Cloth. *Carbon* **2009**, *47* (7), 1814–1823. <https://doi.org/10.1016/j.carbon.2009.03.006>.
- (21) Shariaty, P.; Jahandar Lashaki, M.; Hashisho, Z.; Sawada, J.; Kuznicki, S.; Hutcheon, R. Effect of ETS-10 Ion Exchange on Its Dielectric Properties and Adsorption/Microwave Regeneration. *Separation and Purification Technology* **2017**, *179*, 420–427. <https://doi.org/10.1016/j.seppur.2017.02.016>.
- (22) Meng, Q. B.; Yang, G.-S.; Lee, Y.-S. Sulfonation of a Hypercrosslinked Polymer Adsorbent for Microwave-Assisted Desorption of Adsorbed Benzene. *Journal of Industrial*

- and Engineering Chemistry* **2014**, *20* (4), 2484–2489.  
<https://doi.org/10.1016/j.jiec.2013.10.030>.
- (23) Oh, J.-H.; Oh, K.-S.; Kim, C.-G.; Hong, C.-S. Design of Radar Absorbing Structures Using Glass/Epoxy Composite Containing Carbon Black in X-Band Frequency Ranges. *Composites Part B: Engineering* **2004**, *35* (1), 49–56.  
<https://doi.org/10.1016/j.compositesb.2003.08.011>.
- (24) Chin, W. S.; Lee, D. G. Development of the Composite RAS (Radar Absorbing Structure) for the X-Band Frequency Range. *Composite Structures* **2007**, *77* (4), 457–465.  
<https://doi.org/10.1016/j.compstruct.2005.07.021>.
- (25) Wu, F.; Xie, A.; Sun, M.; Wang, Y.; Wang, M. Reduced Graphene Oxide (RGO) Modified Spongelike Polypyrrole (PPy) Aerogel for Excellent Electromagnetic Absorption. *Journal of Materials Chemistry A* **2015**, *3* (27), 14358–14369.  
<https://doi.org/10.1039/C5TA01577D>.
- (26) Wang, L.; Dang, Z.-M. Carbon Nanotube Composites with High Dielectric Constant at Low Percolation Threshold. *Applied Physics Letters* **2005**, *87* (4), 042903.  
<https://doi.org/10.1063/1.1996842>.
- (27) Chen, C.-Y.; Pu, N.-W.; Liu, Y.-M.; Huang, S.-Y.; Wu, C.-H.; Ger, M.-D.; Gong, Y.-J.; Chou, Y.-C. Remarkable Microwave Absorption Performance of Graphene at a Very Low Loading Ratio. *Composites Part B: Engineering* **2017**, *114*, 395–403.  
<https://doi.org/10.1016/j.compositesb.2017.02.016>.
- (28) Vadivel, M.; Babu, R. R.; Arivanandhan, M.; Ramamurthi, K.; Hayakawa, Y. Role of SDS Surfactant Concentrations on the Structural, Morphological, Dielectric and Magnetic Properties of CoFe<sub>2</sub>O<sub>4</sub> Nanoparticles. *RSC Advances* **2015**, *5* (34), 27060–27068.  
<https://doi.org/10.1039/C5RA01162K>.

- (29) Qing, Y.; Wang, X.; Zhou, Y.; Huang, Z.; Luo, F.; Zhou, W. Enhanced Microwave Absorption of Multi-Walled Carbon Nanotubes/Epoxy Composites Incorporated with Ceramic Particles. *Composites Science and Technology* **2014**, *102*, 161–168. <https://doi.org/10.1016/j.compscitech.2014.08.006>.
- (30) Abbasi, Z.; Daneshmand, M. Contactless PH Measurement Based on High Resolution Enhanced Q Microwave Resonator. In *2018 IEEE/MTT-S International Microwave Symposium-IMS*; IEEE, 2018; pp 1156–1159.
- (31) Kazemi, N.; Schofield, K.; Musilek, P. A High-Resolution Reflective Microwave Planar Sensor for Sensing of Vanadium Electrolyte. *Sensors* **2021**, *21* (11), 3759.
- (32) Kazemi, N.; Abdolrazzaghi, M.; Musilek, P. Comparative Analysis of Machine Learning Techniques for Temperature Compensation in Microwave Sensors. *IEEE Transactions on Microwave Theory and Techniques* **2021**.
- (33) Vélez, P.; Muñoz-Enano, J.; Ebrahimi, A.; Herrojo, C.; Paredes, F.; Scott, J.; Ghorbani, K.; Martín, F. Single-Frequency Amplitude-Modulation Sensor for Dielectric Characterization of Solids and Microfluidics. *IEEE Sensors Journal* **2021**, *21* (10), 12189–12201.
- (34) Abdolrazzaghi, M.; Member, S.; Daneshmand, M.; Member, S. Dual Active Resonator for Dispersion Coefficient Measurement of Asphaltene Nano-Particles. **2017**, *17* (22), 7248–7256.
- (35) Baghelani, M.; Abbasi, Z.; Daneshmand, M. Noncontact High Sensitivity Chipless Tag Microwave Resonator for Bitumen Concentration Measurement at High Temperatures. *Fuel* **2020**, *265*. <https://doi.org/10.1016/j.fuel.2019.116916>.
- (36) Ebrahimi, A.; Withayachumnankul, W.; Al-Sarawi, S. F.; Abbott, D. Microwave Microfluidic Sensor for Determination of Glucose Concentration in Water. In *Microwave Symposium (MMS), 2015 IEEE 15th Mediterranean*; IEEE, 2015; pp 1–3.

- (37) Abbasi, Z.; Baghelani, M.; Daneshmand, M. High-Resolution Chipless Tag RF Sensor. *IEEE Transactions on Microwave Theory and Techniques* **2020**.
- (38) Kazemi, N.; Abdolrazzaghi, M.; Musilek, P.; Daneshmand, M. A Temperature-Compensated High-Resolution Microwave Sensor Using Artificial Neural Network. *IEEE Microwave and Wireless Components Letters* **2020**.
- (39) Jang, C.; Park, J.-K.; Lee, H.-J.; Yun, G.-H.; Yook, J.-G. Non-Invasive Fluidic Glucose Detection Based on Dual Microwave Complementary Split Ring Resonators with a Switching Circuit for Environmental Effect Elimination. *IEEE Sensors Journal* **2020**, *20* (15), 8520–8527.
- (40) Albishi, A. M.; El Badawe, M. K.; Nayyeri, V.; Ramahi, O. M. Enhancing the Sensitivity of Dielectric Sensors with Multiple Coupled Complementary Split-Ring Resonators. *IEEE Transactions on Microwave Theory and Techniques* **2020**, *68* (10), 4340–4347.
- (41) Salim, A.; Naqvi, A. H.; Pham, A. D.; Lim, S. Complementary Split-Ring Resonator (CSRR)-Loaded Sensor Array to Detect Multiple Cracks: Shapes, Sizes, and Positions on Metallic Surface. *IEEE Access* **2020**, *8*, 151804–151816.
- (42) Abbasi, Z.; Shariaty, P.; Hashisho, Z.; Daneshmand, M. SilicaGel-Integrated Chipless RF Tag for Humidity Sensing. In *2018 18th International Symposium on Antenna Technology and Applied Electromagnetics (ANTEM)*; IEEE, 2018; pp 1–2.
- (43) Abbasi, Z.; Zarifi, M. H.; Shariati, P.; Hashisho, Z.; Daneshmand, M. Flexible Coupled Microwave Ring Resonators for Contactless Microbead Assisted Volatile Organic Compound Detection. *IEEE MTT-S International Microwave Symposium Digest* **2017**, *2*, 1228–1231. <https://doi.org/10.1109/MWSYM.2017.8058827>.
- (44) Zarifi, M. H.; Shariaty, P.; Hashisho, Z.; Daneshmand, M. A Non-Contact Microwave Sensor for Monitoring the Interaction of Zeolite 13X with CO<sub>2</sub> and CH<sub>4</sub> in Gaseous

- Streams. *Sensors and Actuators B: Chemical* **2017**, 238, 1240–1247.  
<https://doi.org/10.1016/j.snb.2016.09.047>.
- (45) Schork, J. M.; Fair, J. R. Parametric Analysis of Thermal Regeneration of Adsorption Beds. *Industrial & Engineering Chemistry Research* **1988**, 27 (3), 457–469.  
<https://doi.org/10.1021/ie00075a016>.

## CHAPTER 2: LITERATURE REVIEW

### 2.1 Adsorption

Adsorption is a commonly used method for VOC separation/recovery due to its low cost and high removal efficiency.<sup>1,2</sup> There are many parameters governing the adsorption of VOCs such as adsorbent type, VOC properties and operating conditions. The comprehensive effects of these factors control the affinity of adsorbate molecules to the adsorbent surface and change the adsorption rate and capacity.<sup>1,2</sup>

#### 2.1.1 Adsorbent Materials

There are many adsorbents used for VOC adsorption; however, only a few of them are suitable for practical applications. Some of conventional adsorbents are:

- *Activated carbon* (AC) is typically prepared by thermal decomposition of carbonaceous materials followed by activation with carbon dioxide/steam at elevated temperature.<sup>3</sup> ACs have been widely used in adsorption to recover many types of VOCs such as alcohols, alkanes, ketones, etc.<sup>4,5</sup> ACs are typically nonpolar which limits their adsorption performance in separation of polar VOCs. Besides, the porous structure of ACs used in VOC adsorption is usually in the micropore range (pore size less than 20 Å) which limits the diffusion of large molecules into the pores and prolongs the adsorption equilibrium.<sup>2,6</sup>
- *Zeolites* are porous crystalline aluminosilicates. Zeolite framework consists of  $\text{SiO}_4$  and  $\text{AlO}_4$  tetrahedra, joined together through oxygen atoms to form organized arrangements of pores.<sup>7</sup> Since the structure is precisely determined by the crystal lattice,

pore size distribution of zeolites is usually centralized on a single pore size.<sup>8</sup> For this reason, zeolites are suitable for the separation of molecules based on the molecular size differences. Zeolites are typically polar which makes them suitable adsorbents for the separation of polar compounds.<sup>9</sup> However, compared to other adsorbents, zeolites have a smaller surface area and lower VOC adsorption capacity.<sup>10</sup>

- *Silica Gel* is a partially dehydrated form of polymeric colloidal silicic acid and can be expressed as  $\text{SiO}_2 \cdot n\text{H}_2\text{O}$ . This amorphous material consists of spherical particles 2-25 nm in size which agglomerates to form the adsorbent.<sup>11</sup> Silica gel surface typically has SiOH and SiOSi groups and, being polar, it is conventionally used to adsorb water and polar VOCs by hydrogen bonding mechanisms.<sup>12</sup>

In addition to the mentioned conventional adsorbents, there are other novel porous materials such as metal organic frameworks<sup>13,14</sup>, covalent organic polymers<sup>15,16</sup>, and hypercrosslinked polymers (HCPs)<sup>17,18</sup> used in VOC adsorption process. Among these adsorbents, HCPs exhibit desirable properties such as physicochemical stability, large surface area, adjustable surface chemical groups, high selectivity, and tunable pore structure. HCPs are typically synthesized by post-cross-linking of precursor polymers in a solvent. Cross-linking of polymer chains prevents structural collapse into a non-porous state upon solvent removal and creates microporosity.<sup>19</sup> HCP porosity can be tuned through the degree of cross-linking, the temperature during cross-linking, the solvent, and the catalyst.<sup>20-22</sup> The ability to tailor HCP porosity allows it to be a suitable alternative to conventional adsorbents used in chromatography, water treatment, and gas purification.<sup>23-26</sup> Long et al.<sup>27</sup> prepared a novel HCP (HY-1) with high specific surface area (1244  $\text{m}^2/\text{g}$ ) and showed its

higher adsorption capacity compared to activated carbon for the adsorption of benzene. Shi et al.<sup>18</sup> studied the performance of a microporous HCP and a macroporous polymeric resin for the adsorption of gasoline vapors. Their results showed superior adsorption performance of HCP in treating gasoline vapor compared to the macroporous polymer without hypercrosslinking. Similarly, Zhang et al.<sup>28</sup> and Wang et al.<sup>29</sup> synthesized HCPs with high surface area (1300 m<sup>2</sup>/g and 1606 m<sup>2</sup>/g, respectively) and compared their adsorption performance to commercial HCPs. In both studies, large pore volume and surface area of newly synthesized HCPs lead to better performance compared to commercial polymeric adsorbents for VOC adsorption. Recent works by Long et al.<sup>30</sup> and Zhou et al.<sup>31</sup> developed HCPs with highly hydrophobic nature up to 60% and 80% relative humidity, respectively. Similarly, Wang et al.<sup>32</sup> synthesized a HCP with high surface area (1345 m<sup>2</sup>/g) using new external cross-linkers via one-step Friedel-Crafts reaction. The prepared HCP showed excellent hydrophobicity and adsorption capacity for benzene. Adsorbent hydrophobicity is a particularly important feature as the presence of water vapor in many air streams reduces its adsorption performance for VOCs due to competitive adsorption by water molecules.<sup>33</sup>

## 2.2 Regeneration of Adsorbents

The progressive adsorption of adsorbate molecules on the surface of the adsorbent leads to a gradual reduction in the adsorption capacity until adsorption is no longer achievable. In majority of industrial applications, adsorbent disposal as a waste is not economical and therefore adsorbent regeneration is carried out. Regeneration can be performed through different pathways including heating, depressurization, pH variation, or changing the medium surrounding the adsorbent to a

fluid (e.g., super critical CO<sub>2</sub>) that extracts the adsorbate.<sup>34-37</sup> Chemical reactions can also be used to convert adsorbate into easily removeable products.<sup>36</sup> Among the aforementioned techniques, heating is the most common method of adsorbent regeneration.<sup>38,39</sup> This method typically requires time to heat, desorb, and cool down the adsorbent bed, and is often the time-limiting step in the adsorption/desorption cycle. During thermal regeneration, the temperature of the spent adsorbent is increased, which provides enough energy for adsorbate molecules to escape from the pores. Thus, the surface area and pores of the spent adsorbent are regenerated for the next adsorption cycle. Heating typically is carried out by using steam/hot gas which provides enough thermal energy to break the adsorbent–adsorbate interactions without degrading the adsorbates. However, large volumes of hot purge gas have to be used in these methods to heat the adsorbent to sufficiently high temperatures due to the low heat capacity of the hot purge gas. Using large volumes of purge gas also dilutes the desorbed VOCs, thus a concentration step is usually needed for VOC recovery. Moreover, with steam desorption, the adsorbent bed requires a drying step after each desorption cycle. These shortcomings in conventional thermal regeneration increases the energy consumption and operating cost, which leads to the need for alternative methods of thermal regeneration.

### **2.3 Microwave-assisted Regeneration**

Recently, researchers have shown an increased interest in MW-assisted regeneration of adsorbents due to its molecular level heating, which leads to instant increase in the temperature and VOC desorption rate.<sup>40-43</sup> The main difference between MW-assisted regeneration and conventional thermal methods is in the way heat is transferred to adsorbent/adsorbate system. In conventional

heating methods, the heat source is located outside the adsorbent bed and heat is transferred by conduction and/or convection. Adequate temperature difference between the heating media (e.g., steam, hot gas) and adsorbent bed is necessary for an effective conduction/convection heating. However, in MW-assisted regeneration, heat is directly transferred to the adsorbent bed by radiation. Compared to conventional thermal regeneration methods, MW heating offers many advantages such as rapid heating, shorter regeneration time, and energy savings.<sup>44,45</sup>

Mao et al. studied MW-assisted regeneration of VOC loaded ACs prepared from pine and wheat straw. In particular, they investigated the effect of MW applied power on the regeneration of these adsorbents and compared the energy consumption for three regeneration techniques including constant power, constant temperature, and conductive heating. They found that conductive heating required  $60.8 \left( \frac{\text{kJ}}{\text{g}_{\text{adsorbent}}} \right)$  to achieve 99% regeneration efficiency. However, using MW heating, required energy to achieve 99% regeneration efficiency was reduced by more than 55 %. Moreover, desorption rate was improved by more than 20 times by MW heating compared to conductive heating.<sup>42</sup> Similarly, Fayaz et al. compared MW heating and conductive heating for the regeneration of spent ACs. The total energy needed to achieve 99% desorption efficiency with MW heating and conductive heating was 56 and 972 kJ, and the corresponding heating time was 5 and 90 min, respectively.<sup>40</sup> Similar results were also obtained from Ania et al. studies on the regeneration of ACs loaded with phenol using a MW heating system and an electric furnace.<sup>46,47</sup> Both regeneration methods were performed at a temperature of 850 °C. The sample temperature was reached to 850 °C after 4–6 and 10–13 min by MW heating and furnace, respectively.

Harikoshi et al. study on MW processing of materials demonstrate that 70 to 80 % of power is usually lost in conventional heating method while the lost power is less than 30 % in MW heating process.<sup>48</sup> Table 1 compares MW heating to other heating sources in terms of heating efficiency, temperature control, environmental impact, and heating location.

Table 2-1. Comparison of properties of various heat sources, adopted from Harikoshi et al.<sup>48</sup>

Properties	Gas	Steam	Microwaves
Heating Efficiency	Low	Low	High
Temperature Control	High	Low	High
Environmental Impact	Medium	High (A fossil fuel is used mainly)	Low
Heating Location	Surface	Surface	Whole

MW regeneration can also improve the performance of adsorbents in terms of adsorption rate and capacity compared to conventional thermal regeneration techniques.<sup>49,50</sup> It has been demonstrated that under MW regeneration, AC can be used in more adsorption/desorption cycles compared to conventional thermal methods.<sup>46</sup>

Even though MW heating appears to be very successful, and apparently can improve adsorbents regeneration, its applications is still limited to adsorbents with high level of MW absorption such as ACs. Other types of adsorbents like porous polymers, which are transparent to MW, cannot be heated effectively with MW.<sup>17,51</sup> Unfortunately, there is limited information in the literature on improving MW absorption of these adsorbents. Therefore, an overview of MW heating principles,

presented in the next section, provides needed information to propose potential solutions for improving MW absorption of such adsorbents.

## **2.4 Microwave Heating Principles**

### **2.4.1 Microwave Heating Mechanisms**

MWs are a form of electromagnetic (EM) waves with frequencies in the range of 300 MHz to 300 GHz. To reduce the MW interference with other EM frequencies used for other purposes, the frequency of 915 MHz and 2.45 GHz were selected for heating.<sup>52</sup> MW can be converted to heat due to reorientation and movement of dipoles and free electrons inside the irradiated material. Based on these interactions, two heating mechanisms of conduction loss and dipole moment reorientation are usually considered (Figure 2-1). Conduction losses is the main heating mechanism in conductive materials whereas dipole moment reorientation is the dominant mechanism in materials with polar molecules.<sup>53</sup> In conduction loss, MW induces electric current inside the conductive material which is converted to heat due to ohmic heating. In dipole moment reorientation, dipoles reorient themselves to be aligned with the oscillating electric field. However, frictions and molecular interaction forces resist these rapid changes in orientations of molecules which increases molecular kinetic energy and temperature.<sup>53</sup>

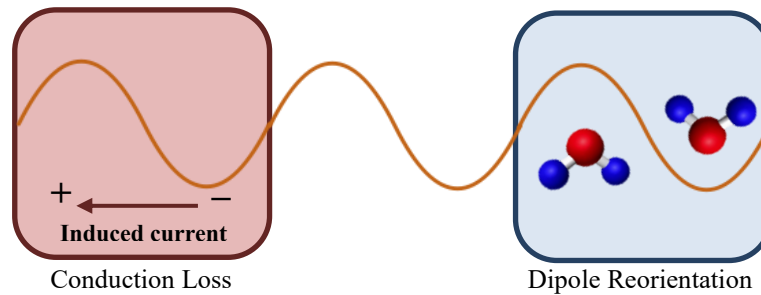


Figure 2-1. MW heating mechanisms.

### 2.4.2 Materials Behavior in Microwave Field

Different materials exhibit different MW absorbing characteristics in MW field. Typically, MW absorption by a material is characterized by the dielectric constant,  $\epsilon'$ , and loss factor,  $\epsilon''$  of the material.<sup>54,55</sup> The dielectric constant expresses the capacity of a molecule to be polarized by an electric field and dielectric loss factor describes the efficiency of electromagnetic energy conversion into heat. Therefore, materials can be selectively heated by MW energy according to their dielectric properties. The amount of absorbed MW energy per unit volume of a material is a function of frequency, material dielectric loss factor, and MW electric field. In case of thin materials (typically less than the wavelength), there is a linear relation between the variation of the MW absorption per unit volume with loss factor which is governed by Eq.1.<sup>56</sup>

$$Q_{\text{avg}} = \omega \epsilon_0 \epsilon'' E_{\text{rms}}^2 \quad \text{Eq. 1}$$

where  $Q_{\text{avg}}$  is the average MW power absorption in  $\text{W/m}^3$ ;  $\omega$  is the MW angular frequency,  $\text{rd/s}$ ;  $\epsilon_0$  is the free space permittivity,  $8.85 \times 10^{-12} \text{ F/m}$ ;  $\epsilon''$  is the dielectric loss factor of the irradiated material, dimensionless; and  $E_{\text{rms}}$  is the root-mean-square electric field intensity in  $\text{V/m}$ .

However, in thick materials (typically longer than the wavelength), electric field strength decreases by transmitting through the material and the concept of MW penetration depth becomes important. MW penetration depth is defined as the depth from the surface into the irradiated material at which the MW power drops to 1/e of its value at the surface.<sup>57</sup> Eq. 2 shows the MW penetration depth as a function of the free space wavelength of the incident radiation,  $\lambda$ , and the dielectric properties of irradiated material.<sup>58</sup>

$$D_p = \frac{\lambda}{2\pi\sqrt{2\epsilon'}} \left[ \left( 1 + \left( \frac{\epsilon''}{\epsilon'} \right)^2 \right)^{\frac{1}{2}} - 1 \right]^{-\frac{1}{2}} \quad \text{Eq. 2}$$

Table 2 presents dielectric constant, dielectric loss factor, and penetration depth of some common materials and adsorbents.

Table 2-2. Microwave properties some selected materials.

Materials	Material Properties (at 2.45 GHz)			
	$\epsilon'$	$\epsilon''$	$D_p$ (mm)	Ref.
Polystyrene (25 °C)	2.55	0.0008	76,193	59
PVC (20 °C)	2.85	0.016	4028	59
Natural Rubber (20 °C)	2.2	0.01	5777	59
Teflon (20 °C)	2.1	0.001	56,444	59
Quartz (25 °C)	4.0	0.001	77,900	59
Alumina (25 °C)	8.9	0.009	12,563	59
Water (25 °C)	78.4	12.5	2	60
Copper	-	-	$1.3 \times 10^{-3}$	61

Iron	-	-	$< 4 \times 10^{-3}$	62
Zeolite HSZ980 (22 °C)	3.0	0.05	670	This work
Dowex Optipore V503 (22 °C)	2.2	0.04	720	This work
HCP-CB composite	11	1.2	54	This work

In materials such as natural rubber and polystyrene, which have very low loss factors, MW can be transmitted for a longer distance with negligible energy loss due to the high MW penetration depth. Further increase in the loss factor increases the absorption of MW and reduces the MW penetration depth. Most of the MW absorbers such as water fall in this category. The highest value of dielectric loss factor belongs to metals (e.g., copper, iron) which reflect MW due to the small value of penetration depth (known as skin depth). In this case, the amount of power absorption becomes negligible due to the reflection of MW from the surface of material. Based on the ability of irradiated material in the absorption of MW, materials are typically categorized into three groups.

- I. MW transparent: MWs can pass through this type of material (e.g., Teflon, polystyrene, quartz) without being absorbed.
- II. MW absorber: Materials (e.g., water, carbon black, graphene) in which MW get totally absorbed based on conduction loss and/or dipole moment reorientation.
- III. MW reflector: Materials (e.g., metals) in which MW get reflected with negligible energy absorption.

In addition to the above-mentioned categories, advanced MW absorbers such as nanocomposites are typically made from at least a MW transparent and a MW absorber material (MAM) to tune the extent of MW absorption. In these materials, the necessary heat is provided through the MAM's ability to absorb and convert MW to heat. Different forms of MAMs such as graphene oxides

(GO), reduced graphene oxide (RGO), carbon nanotubes (CNTs), sodium dodecyl sulfate (SDS), and magnetic nano-particle fillers have been reported to produce MW absorptive composites.<sup>63–68</sup>

### **2.4.3 Measurement of Dielectric Properties**

Many studies have reported the dielectric properties of pure materials; however, when using a mixed MW absorber (i.e., adsorbent mixed with MAMs) it is best to directly measure dielectric properties in the actual sample. There are many techniques for measuring the dielectric properties of samples. Each method is typically restricted to specific MW frequency range, materials, and applications. Venkatesh and Raghavan provided an overview of the various dielectric measurement methods.<sup>69</sup> This section briefly describes the open-ended coaxial probe method used in this research to measure the dielectric properties.

The open-ended coaxial probe method has been used in several studies as a non-destructive measurement technique and is the most often used procedure in MW processing field.<sup>70,71</sup> Using this method, dielectric properties of liquids and solids can be measured at different temperatures. This method uses a dielectric probe coupled to a vector network analyzer (VNA) and a data acquisition software. The probe is usually pressed against a solid specimen or immersed into a liquid/powder sample, followed by measuring the reflection coefficient by VNA in a range of frequencies (e.g., 50 MHz-10GHz). Measured reflection coefficients are subsequently used to calculate the sample dielectric properties. Prior to each experiment, the probe needs to be calibrated using a short, open and standard sample termination. Uncertainties in the measurement are usually due to errors in the characterization of the standard sample, and to the selection of standard sample

for the calibration.<sup>69</sup> The standard sample must be a liquid/solid with known dielectric properties such as water, methanol, and Teflon.

## **2.5 Nanocomposite Preparation Methods**

Polymer nanocomposites are highly demanded materials for various applications (e.g., thermal/microwave/electrical insulator) due to their improved physiochemical properties.<sup>72</sup> Designing a single general composite preparation method is impossible due to the physical and chemical differences among various types of polymers and fillers. Each nanocomposite system requires specific preparation conditions based on the targeted polymer, filler type, filler size and desired properties in the final product. However, the interfacial interaction between fillers and matrix, as well as the homogeneous filler dispersion in the matrix, has a crucial role on the quality of a nanocomposite.<sup>73</sup> These interrelated factors determine the morphology, surface property, dielectric property, thermal stability, shape memory, and self-healing features of the final composite.<sup>74-76</sup> Based on the filler dispersion techniques in the polymer composite, preparation techniques are typically categorized into in situ polymerization, solution mixing, and melt processing.<sup>77-79</sup>

### **2.5.1.1 *In-situ polymerization***

In-situ polymerization is the most widely used method of nanocomposite preparation which offers many advantages such as simplicity, good reproducibility, and easier scale-up of the process.<sup>77,80</sup> This method includes the dispersion of nanofiller into the monomer and/or solvent which is usually

followed by standard polymerization technique. In situ polymerization provides good interaction between filler and polymer due to grafting of polymer molecules from the filler surface.<sup>77,80</sup>

### 2.5.1.2 *Solution mixing*

Solution mixing is the simplest technique of nanocomposite preparation. In this method, polymer and filler are mixed with a solvent which evaporates in a controlled condition to form the nanocomposite.<sup>78</sup> To achieve better dispersion of fillers in the matrix, many techniques have been suggested by researchers. Ultrasonic agitation is widely used for mixing polymer and filler in solvent. Due to solubility issues of polymer/filler in a solvent, other methods such as functionalization of filler surface and surfactant addition to the solvent have been suggested as new variants of this method.

### 2.5.1.3 *Melt processing*

In this method, filler particles are blended with polymer matrices in the molten state without using any solvent.<sup>79</sup> Many thermoplastic polymers (e.g., polypropylene, polystyrene, polycarbonate, etc.) can be used in this technique. The dispersion of filler can be improved by proper shear mixing using extrusion and injection molding techniques. However, filler dispersion is usually poor due to high viscosity of polymers in molten state.

## **2.6 Previous Works on the Preparation of Microwave Absorptive Composites**

MW absorption technique has been used since 1950 for commercial and military applications to reduce undesirable reflections from devices or certain parts of vehicles (e.g., aircrafts, tanks,

etc.).<sup>81</sup> One of the materials extensively studied for MW absorption is nanocomposite. These nanocomposites are usually filled with carbonaceous materials due to their high dielectric loss factor.<sup>82,83</sup>

Wu et al. investigated the effect of RGO addition on the electromagnetic absorption of polypyrrole aerogel. Different loadings of RGO in aerogel was prepared through in-situ polymerization. They showed that the addition of even a trace content of RGO (0.43 wt%) to aerogel can significantly increase its MW absorption without affecting its solvent absorption capacity.<sup>67</sup>

Bhattacharya et al. prepared graphene/CNT filled thermoplastic polyurethane using solution mixing method. Composites with 10 wt% filler content prepared and MW absorption study was performed. Obtained results confirmed higher MW absorption capability of graphene compared to CNT.<sup>68</sup>

Wang et al. investigated the effect of multiwall carbon-nanotubes (MWCNT) in composites with poly vinylidene fluoride prepared by simple physical blending. They found that the dielectric constant of the composite was increased by more than 30 times with about 2.0 vol % of MWCNT.<sup>84</sup>

Chen et al. investigated the MW absorption performance of silicone rubber using five different graphene products at a loading of 1 wt %. They found that among all graphene types, highly exfoliated RGO is capable of delivering excellent MW absorption at very low loading.<sup>85</sup>

Vadivel et al. studied the effect of SDS surfactant on the structural, morphological, and dielectric properties of  $\text{CoFe}_2\text{O}_4$ . Dielectric measurement results showed that both dielectric constant and loss factor of SDS-amended  $\text{CoFe}_2\text{O}_4$  nanoparticles are higher than the pure  $\text{CoFe}_2\text{O}_4$ .<sup>63</sup>

Renukappa et al, studied the effect of CB content on the dielectric properties of styrene–butadiene rubber (SBR) based composites.<sup>86</sup> A series of CB/SBR composites were prepared with different CB contents. They reported that tensile strength and tensile modulus were enhanced by increase in CB content of the composites. Dielectric property measurements of SBR/CB composites revealed that the conductivity does not change until a critical volume fraction of the CB (~ 60 phr). Beyond this critical volume fraction, a steep increase in the dielectric properties was observed which is attributed to the formation of long chains of conductive CB particles in the composite. Similarly, Arief et al. showed that interconnected conductive network of CNTs enhances electrical conductivity of composite which is necessary for effective MW absorption.<sup>87</sup>

Qing et al. investigated the influences of ceramic particle and temperature on the dielectric properties of CNTs/ceramic particle/epoxy composites.<sup>88</sup> Compared to CNT-filled composites, the hybrid filler made from CNTs/ceramic particle enhanced the electrical conductivity and dielectric properties of composite.

Li et al. studied the effect of hybrid nanofillers, prepared from polyaniline decorated RGO, on the MW absorption of poly(methyl methacrylate) nanocomposites.<sup>89</sup> Hybrid nanofillers were synthesized through in-situ polymerization of aniline on GO nanosheets followed by reduction with hydrazine. Obtained results showed that using RGO as a filler increases the loss factor by more than 10,000 times in the poly (methyl methacrylate) nanocomposites compared to the hybrid filler at the same filler content of 6 wt%.

Zhang et al. prepared hybrid fillers of RGO-polystyrene by in-situ polymerization.<sup>90</sup> Subsequently a series of polystyrene-based composites containing different loading of hybrid fillers were

synthesized by solution mixing method using dimethylformamide as solvent. They reported that the interfacial polarization induced by the prepared polystyrene between RGO and matrix improved the composite's dielectric constant and suppressed its dielectric loss factor due to restricted conduction loss.

Singh et al. designed a hybrid filler by growing CNT on carbon fibers through catalytic chemical vapor deposition method.<sup>91</sup> Subsequently, the filler was used in the preparation of epoxy-based composites. The electromagnetic characteristics of synthesized nanocomposites were studied using a VNA. The synthesized nanocomposites, containing 0.35 and 0.50 wt % CNT-carbon fibers, showed substantial MW absorption ability, which were related to the high dielectric losses of fillers.

Weng et al. selected titanium carbide (MXene) as a filler to enhance the dielectric properties of polyimide composites.<sup>92</sup> A series of polyimide/titanium carbide composites were prepared by in-situ polymerization. Atomic force microscopy and SEM images confirmed the homogenous dispersion of titanium carbide particles in filler contents of less than 10 Vol %. Dielectric measurement showed that the dielectric constant and loss factor of synthesized composites were enhanced with the increase of the volume fraction of titanium carbide.

Makeiff et al. prepared conductive thermoplastic composites containing CNTs and polyaniline doped with para-toluene sulfonic acid using two different methods.<sup>93</sup> In the first method, CNT was coated with polyaniline/para-toluene sulfonic acid and subsequently used into the matrix. The second method used mechanical mixing of non-coated fillers into the matrix. MW absorption

measurements results indicated that the non-coated fillers resulted in stronger, and more effective MW absorber compared to the coated fillers.

## **2.7 Microwave Sensing**

In recent years, there has been an increasing interest in the application of electromagnetic (EM) waves in sensing.<sup>94-97</sup> Particularly, EM resonator devices have demonstrated excellent potential for sensing applications including moisture detection, biomolecule detection, pH sensing, VOC detection, and water quality control. Recently, planar MW resonators emerged as potential candidates for sensing applications due to their simple and low-cost fabrication process, easy integration with complementary metal-oxide semiconductor, lab-on-chip compatibility, and flexible design. They have been utilized for a wide range of applications, including biomedical detection<sup>97-101</sup>, chemical solutions sensing<sup>98,102-105</sup>, and environmental monitoring<sup>94-97</sup>. Integration of MW planar sensors with adsorbents markedly enhances their sensitivity and selectivity, making them capable of gas/VOC detection and concentration monitoring.<sup>106-108</sup> In the MW sensing, MW irradiated object alters the velocity of the signal, attenuates or reflects it. These interactions result in changes in transmitted and reflected MW powers at different frequencies which can be correlated with the composition of the irradiated object.<sup>109</sup>

### **2.7.1 Microwave sensing applications in gas phase concentration monitoring**

Bernou et al. developed a gas sensor working at ultra-high frequency formed with a MW structure.<sup>110</sup> The sensor consisted of a MW resonator to which a sensitive material was coated. The EM perturbation was detected through the frequency measurements when the sensor used as

the detecting element in humidity detection. Obtained results showed high sensitivity of the sensor to humidity at MW frequency of 1 GHz. Fonseca et al. designed a MW sensor using zeolite layers as the sensitive material for toluene concentration measurement.<sup>111</sup> The developed sensor showed promising ability for toluene concentration measurements down to 50 ppm. Barochi et al. designed a coplanar grounded wave guide with a gas sensitive material to detect ammonia in argon flux.<sup>112</sup> The effect of sensitive material on the response of the MW sensor was studied in presence of ammonia gas. The ratio of the reflected wave on the incident wave at each frequency was used as the sensor response. They showed that there is a correlation between ammonia concentration and the reflected MW power from the sensitive material. More recently, Zarifi et al. developed a microbead-assisted planar MW resonator for VOC sensing applications.<sup>109</sup> Two types of microbeads, activated carbon and polymer, were studied as the sensitive materials in the gas sensing device. Different concentrations of 2-Butoxyethanol were prepared to evaluate the sensitivity of the sensor, and the transmitted power of the two-port resonator was measured at each experiment. Obtained results showed a minimum resonance frequency shift of 10 kHz for a 35-ppm concentration of 2-Butoxyethanol exposure to activated carbon and 160 kHz for the polymer-based adsorbent at the same concentration. The high-quality factor showed a great potential for real time monitoring of adsorbents behaviour in adsorption process.

## 2.8 References

- (1) Yang, R. T. *Adsorbents: Fundamentals and Applications*; 2003. <https://doi.org/10.1002/047144409x>.
- (2) Zhang, X.; Gao, B.; Creamer, A. E.; Cao, C.; Li, Y. Adsorption of VOCs onto Engineered Carbon Materials: A Review. *Journal of Hazardous Materials*. 2017. <https://doi.org/10.1016/j.jhazmat.2017.05.013>.
- (3) Yuen, F. K.; Hameed, B. H. Recent Developments in the Preparation and Regeneration of Activated Carbons by Microwaves. *Advances in Colloid and Interface Science* 2009, 149 (1–2), 19–27. <https://doi.org/10.1016/j.cis.2008.12.005>.
- (4) RUHL, M. Recover VOCs via Adsorption on Activated Carbon. *Chemical engineering progress* 1993, 89 (7).
- (5) Yi, F. Y.; Lin, X. D.; Chen, S. X.; Wei, X. Q. Adsorption of VOC on Modified Activated Carbon Fiber. *Journal of Porous Materials* 2009, 16 (5). <https://doi.org/10.1007/s10934-008-9228-5>.
- (6) Chiang, Y. C.; Chiang, P. C.; Huang, C. P. Effects of Pore Structure and Temperature on VOC Adsorption on Activated Carbon. *Carbon* 2001, 39 (4). [https://doi.org/10.1016/S0008-6223\(00\)00161-5](https://doi.org/10.1016/S0008-6223(00)00161-5).
- (7) Xiao, F. S.; Meng, X. *Zeolites in Sustainable Chemistry*; 2016.
- (8) Ramesh, K.; Reddy, K. S.; Rashmi, I.; Biswas, A. K. Nanostructured Natural Zeolite: Surface Area, Meso-Pore and Volume Distribution, and Morphology. *Communications in Soil Science and Plant Analysis* 2014, 45 (22). <https://doi.org/10.1080/00103624.2014.956934>.

- (9) Kraus, M.; Trommler, U.; Holzer, F.; Kopinke, F. D.; Roland, U. Competing Adsorption of Toluene and Water on Various Zeolites. *Chemical Engineering Journal* 2018, 351. <https://doi.org/10.1016/j.cej.2018.06.128>.
- (10) Li, X.; Zhang, L.; Yang, Z.; Wang, P.; Yan, Y.; Ran, J. Adsorption Materials for Volatile Organic Compounds (VOCs) and the Key Factors for VOCs Adsorption Process: A Review. *Separation and Purification Technology* 2020, 235. <https://doi.org/10.1016/j.seppur.2019.116213>.
- (11) Facile and Economic Synthesis of Silica Nanoparticles. *Journal of Ovonic Research* 2009, 5 (5).
- (12) Kutluay, S.; Temel, F. Silica Gel Based New Adsorbent Having Enhanced VOC Dynamic Adsorption/Desorption Performance. *Colloids and Surfaces A: Physicochemical and Engineering Aspects* 2021, 609. <https://doi.org/10.1016/j.colsurfa.2020.125848>.
- (13) Lai, C.; Wang, Z.; Qin, L.; Fu, Y.; Li, B.; Zhang, M.; Liu, S.; Li, L.; Yi, H.; Liu, X.; Zhou, X.; An, N.; An, Z.; Shi, X.; Feng, C. Metal-Organic Frameworks as Burgeoning Materials for the Capture and Sensing of Indoor VOCs and Radon Gases. *Coordination Chemistry Reviews* 2021, 427, 213565. <https://doi.org/10.1016/j.ccr.2020.213565>.
- (14) Sudan, S.; Gładysiak, A.; Valizadeh, B.; Lee, J.-H.; Stylianou, K. C. Sustainable Capture of Aromatic Volatile Organic Compounds by a Pyrene-Based Metal–Organic Framework under Humid Conditions. *Inorganic Chemistry* 2020, 59 (13), 9029–9036. <https://doi.org/10.1021/acs.inorgchem.0c00883>.
- (15) Maitlo, H. A.; Kim, K.-H.; Khan, A.; Szulejko, J. E.; Kim, J. C.; Song, H. N.; Ahn, W.-S. Competitive Adsorption of Gaseous Aromatic Hydrocarbons in a Binary Mixture on Nanoporous Covalent Organic Polymers at Various Partial Pressures. *Environmental research* 2019, 173, 1–11. <https://doi.org/10.1016/j.envres.2019.03.028>.

- (16) Vikrant, K.; Qu, Y.; Kim, K.-H.; Boukhvalov, D. W.; Ahn, W.-S. Amine-Functionalized Microporous Covalent Organic Polymers for Adsorptive Removal of a Gaseous Aliphatic Aldehyde Mixture. *Environmental Science: Nano* 2020, 7 (11), 3447–3468. <https://doi.org/10.1039/D0EN00537A>.
- (17) Meng, Q. B.; Yang, G.-S.; Lee, Y.-S. Sulfonation of a Hypercrosslinked Polymer Adsorbent for Microwave-Assisted Desorption of Adsorbed Benzene. *Journal of Industrial and Engineering Chemistry* 2014, 20 (4), 2484–2489. <https://doi.org/10.1016/j.jiec.2013.10.030>.
- (18) Shi, Q.; Yang, X.; Wu, L.; Liu, H.; Zhang, J.; Zhang, F.; Long, C. Binary Adsorption Equilibrium and Breakthrough of Toluene and Cyclohexane on Macroporous and Hypercrosslinked Polymeric Resins. *Microporous and Mesoporous Materials* 2018, 271, 73–82. <https://doi.org/10.1016/j.micromeso.2018.05.034>.
- (19) Xu, S.; Luo, Y.; Tan, B. Recent Development of Hypercrosslinked Microporous Organic Polymers. *Macromolecular Rapid Communications* 2013, 34 (6), 471–484. <https://doi.org/10.1002/marc.201200788>.
- (20) Zeng, S. Z.; Guo, L.; He, Q.; Chen, Y.; Jiang, P.; Shi, J. Facile One-Pot Synthesis of Nanoporous Hypercrosslinked Hydroxybenzene Formaldehyde Resins with High Surface Area and Adjustable Pore Texture. *Microporous and Mesoporous Materials* 2010, 131 (1–3), 141–147. <https://doi.org/10.1016/j.micromeso.2009.12.014>.
- (21) Urban, J.; Svec, F.; Fréchet, J. M. J. Hypercrosslinking: New Approach to Porous Polymer Monolithic Capillary Columns with Large Surface Area for the Highly Efficient Separation of Small Molecules. *Journal of Chromatography A* 2010, 1217 (52), 8212–8221. <https://doi.org/10.1016/j.chroma.2010.10.100>.
- (22) Germain, J.; Svec, F.; Fréchet, J. M. J. Preparation of Size-Selective Nanoporous Polymer Networks of Aromatic Rings: Potential Adsorbents for Hydrogen Storage. *Chemistry of Materials* 2008, 20 (22), 7069–7076. <https://doi.org/10.1021/cm802157r>.

- (23) Ramezanipour Penchah, H.; Ghanadzadeh Gilani, H.; Ghaemi, A. CO<sub>2</sub>, N<sub>2</sub>, and H<sub>2</sub> Adsorption by Hyper-Cross-Linked Polymers and Their Selectivity Evaluation by Gas-Solid Equilibrium. *Journal of Chemical and Engineering Data* 2020, *65* (10), 4905–4913. <https://doi.org/10.1021/acs.jced.0c00541>.
- (24) James, A. M.; Harding, S.; Robshaw, T.; Bramall, N.; Ogden, M. D.; Dawson, R. Selective Environmental Remediation of Strontium and Cesium Using Sulfonated Hyper-Cross-Linked Polymers (SHCPs). *ACS Applied Materials & Interfaces* 2019, *11* (25), 22464–22473. <https://doi.org/10.1021/acsami.9b06295>.
- (25) Wang, X.; Ou, H.; Huang, J. One-Pot Synthesis of Hyper-Cross-Linked Polymers Chemically Modified with Pyrrole, Furan, and Thiophene for Phenol Adsorption from Aqueous Solution. *Journal of Colloid and Interface Science* 2019, *538*, 499–506. <https://doi.org/10.1016/j.jcis.2018.12.021>.
- (26) Penner, N. A.; Nesterenko, P. N.; Hyin, M. M.; Tsyurupa, M. P.; Davankov, V. A. Investigation of the Properties of Hypercrosslinked Polystyrene as a Stationary Phase for High-Performance Liquid Chromatography. *Chromatographia* 1999, *50* (9–10), 611–620. <https://doi.org/10.1007/BF02493669>.
- (27) Long, C.; Li, Y.; Yu, W.; Li, A. Removal of Benzene and Methyl Ethyl Ketone Vapor: Comparison of Hypercrosslinked Polymeric Adsorbent with Activated Carbon. *Journal of Hazardous Materials* 2012. <https://doi.org/10.1016/j.jhazmat.2011.12.010>.
- (28) Zhang, L.; Song, X.; Wu, J.; Long, C.; Li, A.; Zhang, Q. Preparation and Characterization of Micro-Mesoporous Hypercrosslinked Polymeric Adsorbent and Its Application for the Removal of VOCs. *Chemical Engineering Journal* 2012. <https://doi.org/10.1016/j.cej.2012.03.071>.
- (29) Wang, S.; Zhang, L.; Long, C.; Li, A. Enhanced Adsorption and Desorption of VOCs Vapor on Novel Micro-Mesoporous Polymeric Adsorbents. *Journal of Colloid and Interface Science* 2014, *428*, 185–190. <https://doi.org/10.1016/j.jcis.2014.04.055>.

- (30) Long, C.; Li, Y.; Yu, W.; Li, A. Adsorption Characteristics of Water Vapor on the Hypercrosslinked Polymeric Adsorbent. *Chemical Engineering Journal* 2012. <https://doi.org/10.1016/j.cej.2011.11.019>.
- (31) Zhou, B.; Sun, B.; Qiu, W.; Zhou, Y.; He, J.; Lu, X.; Lu, H. Adsorption/Desorption of Toluene on a Hypercrosslinked Polymeric Resin in a Highly Humid Gas Stream. *Chinese Journal of Chemical Engineering* 2019. <https://doi.org/10.1016/j.cjche.2018.09.027>.
- (32) Wang, J.; Wang, W.-Q.; Hao, Z.; Wang, G.; Li, Y.; Chen, J.-G.; Li, M.; Cheng, J.; Liu, Z.-T. A Superhydrophobic Hyper-Cross-Linked Polymer Synthesized at Room Temperature Used as an Efficient Adsorbent for Volatile Organic Compounds. *RSC Advances* 2016, 6 (99), 97048–97054. <https://doi.org/10.1039/C6RA18687D>.
- (33) Águeda, V. I.; Crittenden, B. D.; Delgado, J. A.; Tennison, S. R. Effect of Channel Geometry, Degree of Activation, Relative Humidity and Temperature on the Performance of Binderless Activated Carbon Monoliths in the Removal of Dichloromethane from Air. *Separation and Purification Technology* 2011, 78 (2), 154–163. <https://doi.org/10.1016/j.seppur.2011.01.036>.
- (34) Pezolt, D. J.; Collick, S. J.; Johnson, H. A.; Robbins, L. A. Pressure Swing Adsorption for VOC Recovery at Gasoline Loading Terminals. *Environmental Progress* 1997, 16 (1), 16–19. <https://doi.org/10.1002/ep.3300160115>.
- (35) Xiu, G.; Li, P.; E. Rodrigues, A. Sorption-Enhanced Reaction Process with Reactive Regeneration. *Chemical Engineering Science* 2002, 57 (18), 3893–3908. [https://doi.org/10.1016/S0009-2509\(02\)00245-2](https://doi.org/10.1016/S0009-2509(02)00245-2).
- (36) Leng, C. C.; Pinto, N. G. An Investigation of the Mechanisms of Chemical Regeneration of Activated Carbon. *Industrial and Engineering Chemistry Research* 1996, 35 (6). <https://doi.org/10.1021/ie950576a>.

- (37) Chihara, K.; Oomori, K.; Oono, T.; Mochizuki, Y. Supercritical CO<sub>2</sub> Regeneration of Activated Carbon Loaded with Organic Adsorbates. *Water Science and Technology* 1997, 35 (7). [https://doi.org/10.1016/S0273-1223\(97\)00139-X](https://doi.org/10.1016/S0273-1223(97)00139-X).
- (38) Hwang, K. S.; Choi, D. K.; Gong, S. Y.; Cho, S. Y. Adsorption and Thermal Regeneration of Methylene Chloride Vapor on an Activated Carbon Bed. *Chemical Engineering Science* 1997. [https://doi.org/10.1016/S0009-2509\(96\)00470-8](https://doi.org/10.1016/S0009-2509(96)00470-8).
- (39) Kulkarni, S.; Kaware, J. Regeneration and Recovery in Adsorption- a Review. *International Journal of Innovative Science, Engineering & Technology(IJISSET)* 2014, 1 (8).
- (40) Fayaz, M.; Shariaty, P.; Atkinson, J. D.; Hashisho, Z.; Phillips, J. H.; Anderson, J. E.; Nichols, M. Using Microwave Heating To Improve the Desorption Efficiency of High Molecular Weight VOC from Beaded Activated Carbon. *Environmental Science & Technology* 2015, 49 (7), 4536–4542. <https://doi.org/10.1021/es505953c>.
- (41) Hashisho, Z.; Rood, M. J.; Barot, S.; Bernhard, J. Role of Functional Groups on the Microwave Attenuation and Electric Resistivity of Activated Carbon Fiber Cloth. *Carbon* 2009, 47 (7), 1814–1823. <https://doi.org/10.1016/j.carbon.2009.03.006>.
- (42) Mao, H.; Zhou, D.; Hashisho, Z.; Wang, S.; Chen, H.; Wang, H. H. Constant Power and Constant Temperature Microwave Regeneration of Toluene and Acetone Loaded on Microporous Activated Carbon from Agricultural Residue. *Journal of Industrial and Engineering Chemistry* 2015, 21, 516–525. <https://doi.org/10.1016/j.jiec.2014.03.014>.
- (43) Chowdhury, T.; Shi, M.; Hashisho, Z.; Sawada, J. A.; Kuznicki, S. M. Regeneration of Na-ETS-10 Using Microwave and Conductive Heating. *Chemical Engineering Science* 2012, 75, 282–288. <https://doi.org/10.1016/j.ces.2012.03.039>.
- (44) Shariaty, P.; Jahandar Lashaki, M.; Hashisho, Z.; Sawada, J.; Kuznicki, S.; Hutcheon, R. Effect of ETS-10 Ion Exchange on Its Dielectric Properties and Adsorption/Microwave

- Regeneration. *Separation and Purification Technology* 2017, 179, 420–427. <https://doi.org/10.1016/j.seppur.2017.02.016>.
- (45) Polaert, I.; Estel, L.; Huyghe, R.; Thomas, M. Adsorbents Regeneration under Microwave Irradiation for Dehydration and Volatile Organic Compounds Gas Treatment. *Chemical Engineering Journal* 2010, 162, 941–948. <https://doi.org/10.1016/j.cej.2010.06.047>.
- (46) Ania, C. O.; Parra, J. B.; Menéndez, J. A.; Pis, J. J. Effect of Microwave and Conventional Regeneration on the Microporous and Mesoporous Network and on the Adsorptive Capacity of Activated Carbons. *Microporous and Mesoporous Materials* 2005, 85 (1–2), 7–15. <https://doi.org/10.1016/j.micromeso.2005.06.013>.
- (47) Ania, C. O.; Menéndez, J. A.; Parra, J. B.; Pis, J. J. Microwave-Induced Regeneration of Activated Carbons Polluted with Phenol. A Comparison with Conventional Thermal Regeneration. In *Carbon*; 2004; Vol. 42. <https://doi.org/10.1016/j.carbon.2004.01.010>.
- (48) Horikoshi, S.; Schiffmann, R. F.; Fukushima, J.; Serpone, N. *Microwave Chemical and Materials Processing: A Tutorial*; 2017. <https://doi.org/10.1007/978-981-10-6466-1>.
- (49) Cha, C. Y.; Carlisle, C. T. Microwave Process for Volatile Organic Compound Abatement. *Journal of the Air and Waste Management Association* 2001, 51 (12), 1628–1641. <https://doi.org/10.1080/10473289.2001.10464389>.
- (50) Coss, P. M.; Cha, C. Y. Microwave Regeneration of Activated Carbon Used for Removal of Solvents from Vented Air. *Journal of the Air and Waste Management Association* 2000, 50 (4), 529–535. <https://doi.org/10.1080/10473289.2000.10464038>.
- (51) Meng, Q. B.; Yang, G.-S.; Lee, Y.-S. Preparation of Highly Porous Hypercrosslinked Polystyrene Adsorbents: Effects of Hydrophilicity on the Adsorption and Microwave-Assisted Desorption Behavior toward Benzene. *Microporous and Mesoporous Materials* 2013, 181, 222–227. <https://doi.org/10.1016/j.micromeso.2013.07.027>.

- (52) Kostas, E. T.; Beneroso, D.; Robinson, J. P. The Application of Microwave Heating in Bioenergy: A Review on the Microwave Pre-Treatment and Upgrading Technologies for Biomass. *Renewable and Sustainable Energy Reviews*. Elsevier Ltd September 1, 2017, pp 12–27. <https://doi.org/10.1016/j.rser.2017.03.135>.
- (53) Mishra, R. R.; Sharma, A. K. Microwave–Material Interaction Phenomena: Heating Mechanisms, Challenges and Opportunities in Material Processing. *Composites Part A: Applied Science and Manufacturing* 2016, 81, 78–97. <https://doi.org/10.1016/j.compositesa.2015.10.035>.
- (54) Falciglia, P. P.; Roccaro, P.; Bonanno, L.; De Guidi, G.; Vagliasindi, F. G. A.; Romano, S. A Review on the Microwave Heating as a Sustainable Technique for Environmental Remediation/Detoxification Applications. *Renewable and Sustainable Energy Reviews* 2018, 95, 147–170. <https://doi.org/10.1016/j.rser.2018.07.031>.
- (55) Clark, D. E.; Sutton, W. H. Microwave Processing of Materials. *Annual Review of Materials Science* 1996, 26 (1), 299–331. <https://doi.org/10.1146/annurev.ms.26.080196.001503>.
- (56) Metaxas, A. C.; Meredith, R. J. Book Review: Industrial Microwave Heating. *Journal of Microwave Power and Electromagnetic Energy* 1989, 24 (2), 108–108. <https://doi.org/10.1080/08327823.1989.11688082>.
- (57) Chandrasekaran, S.; Ramanathan, S.; Basak, T. Microwave Material Processing-a Review. *AIChE Journal* 2012, 58 (2), 330–363. <https://doi.org/10.1002/aic.12766>.
- (58) Bradshaw, S. M.; Van Wyk, E. J.; De Swardt, J. B. Microwave Heating Principles and the Application to the Regeneration of Granular Activated Carbon. *Journal of The South African Institute of Mining and Metallurgy* 1998, 98 (4), 201–210.
- (59) Gupta, M.; Wai Leong Eugene, W. *Microwaves and Metals*; John Wiley & Sons (Asia) Pte Ltd: Singapore, 2007. <https://doi.org/10.1002/9780470822746>.

- (60) Moldoveanu, S. C.; David, V. Mobile Phases and Their Properties. In *Essentials in Modern HPLC Separations*; 2013. <https://doi.org/10.1016/b978-0-12-385013-3.00007-0>.
- (61) Mondal, A.; Agrawal, D.; Upadhyaya, A. Microwave Heating of Pure Copper Powder with Varying Particle Size and Porosity. *Journal of Microwave Power and Electromagnetic Energy* 2009, 43 (1). <https://doi.org/10.1080/08327823.2008.11688599>.
- (62) Wu, L. Z.; Ding, J.; Jiang, H. B.; Chen, L. F.; Ong, C. K. Particle Size Influence to the Microwave Properties of Iron Based Magnetic Particulate Composites. *Journal of Magnetism and Magnetic Materials* 2005, 285 (1–2). <https://doi.org/10.1016/j.jmmm.2004.07.045>.
- (63) Vadivel, M.; Babu, R. R.; Arivanandhan, M.; Ramamurthi, K.; Hayakawa, Y. Role of SDS Surfactant Concentrations on the Structural, Morphological, Dielectric and Magnetic Properties of CoFe<sub>2</sub>O<sub>4</sub> Nanoparticles. *RSC Advances* 2015, 5 (34), 27060–27068. <https://doi.org/10.1039/C5RA01162K>.
- (64) Wang, L.; Jia, X.; Li, Y.; Yang, F.; Zhang, L.; Liu, L.; Ren, X.; Yang, H. Synthesis and Microwave Absorption Property of Flexible Magnetic Film Based on Graphene Oxide/Carbon Nanotubes and Fe<sub>3</sub>O<sub>4</sub> Nanoparticles. *Journal of Materials Chemistry A* 2014, 2 (36), 14940. <https://doi.org/10.1039/C4TA02815E>.
- (65) Sun, G.; Dong, B.; Cao, M.; Wei, B.; Hu, C. Hierarchical Dendrite-Like Magnetic Materials of Fe<sub>3</sub>O<sub>4</sub>,  $\gamma$ -Fe<sub>2</sub>O<sub>3</sub>, and Fe with High Performance of Microwave Absorption. *Chemistry of Materials* 2011, 23 (6), 1587–1593. <https://doi.org/10.1021/cm103441u>.
- (66) Che, R. C.; Peng, L.-M.; Duan, X. F.; Chen, Q.; Liang, X. L. Microwave Absorption Enhancement and Complex Permittivity and Permeability of Fe Encapsulated within Carbon Nanotubes. *Advanced Materials* 2004, 16 (5), 401–405. <https://doi.org/10.1002/adma.200306460>.

- (67) Wu, F.; Xie, A.; Sun, M.; Wang, Y.; Wang, M. Reduced Graphene Oxide (RGO) Modified Spongelike Polypyrrole (PPy) Aerogel for Excellent Electromagnetic Absorption. *Journal of Materials Chemistry A* 2015, 3 (27), 14358–14369. <https://doi.org/10.1039/C5TA01577D>.
- (68) Das, C. K.; Bhattacharya, P.; Kalra, S. S. Graphene and MWCNT: Potential Candidate for Microwave Absorbing Materials. *Journal of Materials Science Research* 2012, 1 (2). <https://doi.org/10.5539/jmsr.v1n2p126>.
- (69) Venkatesh, M. S.; Raghavan, G. S. V. An Overview of Dielectric Properties Measuring Techniques. *Canadian Biosystems Engineering / Le Genie des biosystems au Canada*. 2005.
- (70) Marsland, T. P.; Evans, S. Dielectric Measurements with an Open-Ended Coaxial Probe. *IEE Proceedings H: Microwaves, Antennas and Propagation* 1987, 134 (4). <https://doi.org/10.1049/ip-h-2.1987.0068>.
- (71) Aimoto, A.; Matsumoto, T. Noninvasive Method for Measuring the Electrical Properties of Deep Tissues Using an Open-Ended Coaxial Probe. *Medical Engineering and Physics* 1996, 18 (8). [https://doi.org/10.1016/S1350-4533\(96\)00026-4](https://doi.org/10.1016/S1350-4533(96)00026-4).
- (72) Mittal, G.; Dhand, V.; Rhee, K. Y.; Park, S.-J.; Lee, W. R. A Review on Carbon Nanotubes and Graphene as Fillers in Reinforced Polymer Nanocomposites. *Journal of Industrial and Engineering Chemistry* 2015, 21, 11–25. <https://doi.org/10.1016/j.jiec.2014.03.022>.
- (73) Zhang, Y.; Choi, J. R.; Park, S. J. Interlayer Polymerization in Amine-Terminated Macromolecular Chain-Grafted Expanded Graphite for Fabricating Highly Thermal Conductive and Physically Strong Thermoset Composites for Thermal Management Applications. *Composites Part A: Applied Science and Manufacturing* 2018, 109. <https://doi.org/10.1016/j.compositesa.2018.04.001>.

- (74) Thakur, V. K.; Kessler, M. R. Self-Healing Polymer Nanocomposite Materials: A Review. *Polymer* 2015, 69. <https://doi.org/10.1016/j.polymer.2015.04.086>.
- (75) Deshmukh, K.; Ahamed, M. B.; Pasha, S. K. K.; Deshmukh, R. R.; Bhagat, P. R. Highly Dispersible Graphene Oxide Reinforced Polypyrrole/Polyvinyl Alcohol Blend Nanocomposites with High Dielectric Constant and Low Dielectric Loss. *RSC Advances* 2015, 5 (76), 61933–61945. <https://doi.org/10.1039/C5RA11242G>.
- (76) Norkhairunnisa, M.; Azizan, A.; Mariatti, M.; Ismail, H.; Sim, L. Thermal Stability and Electrical Behavior of Polydimethylsiloxane Nanocomposites with Carbon Nanotubes and Carbon Black Fillers. *Journal of Composite Materials* 2012, 46 (8), 903–910. <https://doi.org/10.1177/0021998311412985>.
- (77) Funck, A.; Kaminsky, W. Polypropylene Carbon Nanotube Composites by in Situ Polymerization. *Composites Science and Technology* 2007, 67 (5). <https://doi.org/10.1016/j.compscitech.2006.01.034>.
- (78) Kuila, T.; Bose, S.; Hong, C. E.; Uddin, M. E.; Khanra, P.; Kim, N. H.; Lee, J. H. Preparation of Functionalized Graphene/Linear Low Density Polyethylene Composites by a Solution Mixing Method. *Carbon*. 2011. <https://doi.org/10.1016/j.carbon.2010.10.031>.
- (79) Haggenueller, R.; Gommans, H. H.; Rinzler, A. G.; Fischer, J. E.; Winey, K. I. Aligned Single-Wall Carbon Nanotubes in Composites by Melt Processing Methods. *Chemical Physics Letters* 2000, 330 (3–4). [https://doi.org/10.1016/S0009-2614\(00\)01013-7](https://doi.org/10.1016/S0009-2614(00)01013-7).
- (80) Amorim, S. M.; Steffen, G.; de S Junior, J. M. N.; Brusamarello, C. Z.; Romio, A. P.; Domenico, M. D. Synthesis, Characterization, and Application of Polypyrrole/TiO<sub>2</sub> Composites in Photocatalytic Processes: A Review. *Polymers and Polymer Composites*. 2020. <https://doi.org/10.1177/0967391120949489>.

- (81) Das, C. K.; Mandal, A. Microwave Absorbing Properties of DBSA-Doped Polyaniline/BaTiO<sub>3</sub>-Ni<sub>0.5</sub>Zn<sub>0.5</sub>Fe<sub>2</sub>O<sub>4</sub> Nanocomposites. *Journal of Materials Science Research* 2011, *1* (1). <https://doi.org/10.5539/jmsr.v1n1p45>.
- (82) Oh, J.-H.; Oh, K.-S.; Kim, C.-G.; Hong, C.-S. Design of Radar Absorbing Structures Using Glass/Epoxy Composite Containing Carbon Black in X-Band Frequency Ranges. *Composites Part B: Engineering* 2004, *35* (1), 49–56. <https://doi.org/10.1016/j.compositesb.2003.08.011>.
- (83) Chin, W. S.; Lee, D. G. Development of the Composite RAS (Radar Absorbing Structure) for the X-Band Frequency Range. *Composite Structures* 2007, *77* (4), 457–465. <https://doi.org/10.1016/j.compstruct.2005.07.021>.
- (84) Wang, L.; Dang, Z.-M. Carbon Nanotube Composites with High Dielectric Constant at Low Percolation Threshold. *Applied Physics Letters* 2005, *87* (4), 042903. <https://doi.org/10.1063/1.1996842>.
- (85) Chen, C.-Y.; Pu, N.-W.; Liu, Y.-M.; Huang, S.-Y.; Wu, C.-H.; Ger, M.-D.; Gong, Y.-J.; Chou, Y.-C. Remarkable Microwave Absorption Performance of Graphene at a Very Low Loading Ratio. *Composites Part B: Engineering* 2017, *114*, 395–403. <https://doi.org/10.1016/j.compositesb.2017.02.016>.
- (86) Renukappa, N. M.; Siddaramaiah; Sudhaker Samuel, R. D.; Sundara Rajan, J.; Lee, J. H. Dielectric Properties of Carbon Black: SBR Composites. *Journal of Materials Science: Materials in Electronics* 2009, *20* (7). <https://doi.org/10.1007/s10854-008-9780-4>.
- (87) Arief, I.; Biswas, S.; Bose, S. FeCo-Anchored Reduced Graphene Oxide Framework-Based Soft Composites Containing Carbon Nanotubes as Highly Efficient Microwave Absorbers with Excellent Heat Dissipation Ability. *ACS Applied Materials and Interfaces* 2017, *9* (22). <https://doi.org/10.1021/acsami.7b04053>.

- (88) Qing, Y.; Wang, X.; Zhou, Y.; Huang, Z.; Luo, F.; Zhou, W. Enhanced Microwave Absorption of Multi-Walled Carbon Nanotubes/Epoxy Composites Incorporated with Ceramic Particles. *Composites Science and Technology* 2014, *102*, 161–168. <https://doi.org/10.1016/j.compscitech.2014.08.006>.
- (89) Li, M.; Huang, X.; Wu, C.; Xu, H.; Jiang, P.; Tanaka, T. Fabrication of Two-Dimensional Hybrid Sheets by Decorating Insulating PANI on Reduced Graphene Oxide for Polymer Nanocomposites with Low Dielectric Loss and High Dielectric Constant. *Journal of Materials Chemistry* 2012, *22* (44). <https://doi.org/10.1039/c2jm34683d>.
- (90) Zhang, T.; Huang, W.; Zhang, N.; Huang, T.; Yang, J.; Wang, Y. Grafting of Polystyrene onto Reduced Graphene Oxide by Emulsion Polymerization for Dielectric Polymer Composites: High Dielectric Constant and Low Dielectric Loss Tuned by Varied Grafting Amount of Polystyrene. *European Polymer Journal* 2017, *94* (111), 196–207. <https://doi.org/10.1016/j.eurpolymj.2017.07.008>.
- (91) Singh, S. K.; Akhtar, M. J.; Kar, K. K. Hierarchical Carbon Nanotube-Coated Carbon Fiber: Ultra Lightweight, Thin, and Highly Efficient Microwave Absorber. *ACS Applied Materials and Interfaces* 2018, *10* (29). <https://doi.org/10.1021/acsami.8b06673>.
- (92) Weng, L.; Xia, Q. S.; Yan, L. W.; Liu, L. Z.; Sun, Z. In Situ Preparation of Polyimide/Titanium Carbide Composites with Enhanced Dielectric Constant. *Polymer Composites* 2016, *37* (1). <https://doi.org/10.1002/pc.23162>.
- (93) Makeiff, D. A.; Huber, T. Microwave Absorption by Polyaniline-Carbon Nanotube Composites. *Synthetic Metals* 2006, *156* (7–8). <https://doi.org/10.1016/j.synthmet.2005.05.019>.
- (94) Jang, C.; Park, J.-K.; Lee, H.-J.; Yun, G.-H.; Yook, J.-G. Non-Invasive Fluidic Glucose Detection Based on Dual Microwave Complementary Split Ring Resonators with a Switching Circuit for Environmental Effect Elimination. *IEEE Sensors Journal* **2020**, *20* (15), 8520–8527.

- (95) Albishi, A. M.; El Badawe, M. K.; Nayyeri, V.; Ramahi, O. M. Enhancing the Sensitivity of Dielectric Sensors with Multiple Coupled Complementary Split-Ring Resonators. *IEEE Transactions on Microwave Theory and Techniques* **2020**, *68* (10), 4340–4347.
- (96) Salim, A.; Naqvi, A. H.; Pham, A. D.; Lim, S. Complementary Split-Ring Resonator (CSRR)-Loaded Sensor Array to Detect Multiple Cracks: Shapes, Sizes, and Positions on Metallic Surface. *IEEE Access* **2020**, *8*, 151804–151816.
- (97) Kazemi, N.; Abdolrazzagh, M.; Musilek, P. Comparative Analysis of Machine Learning Techniques for Temperature Compensation in Microwave Sensors. *IEEE Transactions on Microwave Theory and Techniques* **2021**.
- (98) Abbasi, Z.; Daneshmand, M. Contactless PH Measurement Based on High Resolution Enhanced Q Microwave Resonator. In *2018 IEEE/MTT-S International Microwave Symposium-IMS*; IEEE, 2018; pp 1156–1159.
- (99) Kazemi, N.; Schofield, K.; Musilek, P. A High-Resolution Reflective Microwave Planar Sensor for Sensing of Vanadium Electrolyte. *Sensors* **2021**, *21* (11), 3759.
- (100) Vélez, P.; Muñoz-Enano, J.; Ebrahimi, A.; Herrojo, C.; Paredes, F.; Scott, J.; Ghorbani, K.; Martín, F. Single-Frequency Amplitude-Modulation Sensor for Dielectric Characterization of Solids and Microfluidics. *IEEE Sensors Journal* **2021**, *21* (10), 12189–12201.
- (101) Abdolrazzagh, M.; Member, S.; Daneshmand, M.; Member, S. Dual Active Resonator for Dispersion Coefficient Measurement of Asphaltene Nano-Particles. **2017**, *17* (22), 7248–7256.
- (102) Baghelani, M.; Abbasi, Z.; Daneshmand, M. Noncontact High Sensitivity Chipless Tag Microwave Resonator for Bitumen Concentration Measurement at High Temperatures. *Fuel* **2020**, *265*. <https://doi.org/10.1016/j.fuel.2019.116916>.

- (103) Ebrahimi, A.; Withayachumnankul, W.; Al-Sarawi, S. F.; Abbott, D. Microwave Microfluidic Sensor for Determination of Glucose Concentration in Water. In *Microwave Symposium (MMS), 2015 IEEE 15th Mediterranean*; IEEE, 2015; pp 1–3.
- (104) Abbasi, Z.; Baghelani, M.; Daneshmand, M. High-Resolution Chipless Tag RF Sensor. *IEEE Transactions on Microwave Theory and Techniques* **2020**.
- (105) Kazemi, N.; Abdolrazzagli, M.; Musilek, P.; Daneshmand, M. A Temperature-Compensated High-Resolution Microwave Sensor Using Artificial Neural Network. *IEEE Microwave and Wireless Components Letters* **2020**.
- (106) Abbasi, Z.; Shariaty, P.; Hashisho, Z.; Daneshmand, M. SilicaGel-Integrated Chipless RF Tag for Humidity Sensing. In *2018 18th International Symposium on Antenna Technology and Applied Electromagnetics (ANTEM)*; IEEE, 2018; pp 1–2.
- (107) Abbasi, Z.; Zarifi, M. H.; Shariati, P.; Hashisho, Z.; Daneshmand, M. Flexible Coupled Microwave Ring Resonators for Contactless Microbead Assisted Volatile Organic Compound Detection. *IEEE MTT-S International Microwave Symposium Digest* **2017**, 2, 1228–1231. <https://doi.org/10.1109/MWSYM.2017.8058827>.
- (108) Zarifi, M. H.; Shariaty, P.; Hashisho, Z.; Daneshmand, M. A Non-Contact Microwave Sensor for Monitoring the Interaction of Zeolite 13X with CO<sub>2</sub> and CH<sub>4</sub> in Gaseous Streams. *Sensors and Actuators, B: Chemical* **2017**, 238, 1240–1247. <https://doi.org/10.1016/j.snb.2016.09.047>.
- (109) Zarifi, M. H.; Fayaz, M.; Goldthorp, J.; Abdolrazzagli, M.; Hashisho, Z.; Daneshmand, M. Microbead-Assisted High Resolution Microwave Planar Ring Resonator for Organic-Vapor Sensing. *Applied Physics Letters* **2015**, 106 (6), 062903. <https://doi.org/10.1063/1.4907944>.

- (110) Bernou, C.; Rebière, D.; Pistré, J. Microwave Sensors: A New Sensing Principle. Application to Humidity Detection. *Sensors and Actuators B: Chemical* **2000**, *68* (1–3), 88–93. [https://doi.org/10.1016/S0925-4005\(00\)00466-4](https://doi.org/10.1016/S0925-4005(00)00466-4).
- (111) De Fonseca, B.; Rossignol, J.; Bezverkhy, I.; Bellat, J. P.; Stuerger, D.; Pribetich, P. VOCs Detection by Microwave Transduction Using Zeolites as Sensitive Material. *Procedia Engineering* **2014**, *87*, 1019–1022. <https://doi.org/10.1016/J.PROENG.2014.11.334>.
- (112) Barochi, G.; Rossignol, J.; Bouvet, M. Development of Microwave Gas Sensors. *Sensors and Actuators B: Chemical* **2011**, *157* (2), 374–379. <https://doi.org/10.1016/j.snb.2011.04.059>.

# **CHAPTER 3: PURGE GAS HUMIDITY IMPROVES MICROWAVE ABSORPTION OF POLYMERIC AND ZEOLITE ADSORBENTS**

## **3.1 Chapter Overview**

In this chapter, two commercially available MW transparent adsorbents (a beta type zeolite and a hypercrosslinked polystyrene resin) were regenerated using MW heating to study the effect of purge gas humidity on MW absorption. Dielectric properties and water adsorption capacity of each adsorbent were measured at different purge gas RH and applied MW power. Additionally, MW heating was used to desorb polar and non-polar adsorbates from adsorbents in both dry and humid purge gases. Finally, complete desorption of selected adsorbates in both dry and humid conditions was compared in terms of regeneration time and energy consumption.

### 3.2 Introduction

Microwave (MW) heating has potential for effective regeneration of adsorbents.<sup>1-3</sup> A number of advantages offered by MW regeneration such as fast and volumetric heating of adsorbent, and energy-efficient surpassing other regeneration techniques.<sup>4-6</sup> Moreover, MW heating is selective, depending on the dielectric properties of the material, which reduces energy losses that heat unnecessary parts in hot gas/steam regeneration methods. MW heating principles and its applications in environmental remediation has been discussed in detail by Jones and Falciglia.<sup>7,8</sup> They showed that the ability of a material to be heated by MW depends on its dielectric properties, namely the dielectric constant ( $\epsilon'$ ) and the dielectric loss factor ( $\epsilon''$ ). The dielectric constant describes the material ability to be polarized in an electromagnetic field, while the dielectric loss factor describes the material's ability to convert electromagnetic energy into heat.<sup>9</sup>

MW heating has been employed for the adsorbent regeneration since 1980s.<sup>10</sup> Several review papers summarize these studies.<sup>11,12</sup> While most studies concern MW regeneration of adsorbents with large dielectric loss factor, only some of them focused on MW regeneration of adsorbents with low dielectric loss factor. For effective MW regeneration, the adsorbent should have a large dielectric loss factor to effectively absorb MW. However, there are many adsorbents such as porous polymers and zeolites that are transparent to MW due to their poor dielectric loss factor.

Meng et al. studied the effect of sulfonation on MW absorption properties of a hypercrosslinked polymer. They showed that sulfonated samples become hydrophilic and MW absorptive compare to as-received polymer.<sup>13</sup> Shariaty et al. studied the effect of ion exchange on the dielectric properties of Engelhard Titanosilicate molecular sieve (ETS-10).<sup>14</sup> They demonstrated that using

monovalent and divalent cations in the ion exchanging of ETS-10 increases its water adsorption capacity and decreases its dielectric properties which can be useful during the regeneration of polar compounds from the adsorbent. Hashisho et al. investigated the effect of activated fiber cloth (ACFC) functional groups on its MW absorption performance.<sup>15</sup> The density of functional groups on ACFCs surface were controlled through acid and hydrogen treatments and their effect on MW absorption was studied. They showed that hydrogen-treatment increases MW attenuation by 50 %, while acid treatment reduces MW attenuation by 89 %.

Other studies investigated the addition of MW susceptors to improve the dielectric properties.<sup>16,17</sup> Zhang-Steenwinkel et al. investigated MW heating of a cordierite monoliths coated with a  $\text{La}_{0.8}\text{Ce}_{0.2}\text{MnO}_3$  perovskite.<sup>18</sup> Enhanced MW absorption was reported for the coated cordierites and attributed to the dielectric properties of coating substance. Lv et al. reported MW absorption enhancement of NaY zeolite through the addition of activated carbon as a MW absorptive material. Their results showed improved cyclic VOC adsorption/MW assisted desorption for the mixed adsorbent compared to NaY zeolite.<sup>19</sup>

So far post synthesis process of MW transparent adsorbents has been predominantly used for improving the dielectric properties and MW absorption. In the present study, the effect of purge gas relative humidity (RH) on MW absorption of two commercially available adsorbents is investigated. Dielectric properties and water adsorption capacity of each adsorbent were measured at different purge gas RH and applied MW power. Furthermore, polar and nonpolar adsorbates were used to investigate VOC adsorption and MW assisted desorption under dry and humid conditions. Finally, complete desorption of selected adsorbates in both dry and humid conditions was compared in terms of regeneration time and energy consumption.

### 3.3 Experimental Section

#### 3.3.1 Adsorbents and Adsorbates

A beta type zeolite (HSZ980, Tosoh Corp.) and beaded hypercrosslinked polystyrene (Optipore V503, Dow Chemical Co.) were selected as adsorbents and used in adsorption and regeneration experiments. Table 1 shows BET surface area, total pore volume, average pore size, and dielectric loss factor of selected adsorbents. Due to their low dielectric loss factor (Table 1), both adsorbents are transparent to MW and cannot be heated in the MW field. Adsorbates used in this study were Cyclohexane (Cyhex) (99%, fisher scientific) and Isopropyl Alcohol (IPA) (99%, Fisher Scientific). Both compounds have similar boiling point but contrasting polarity and dielectric properties which allows better investigation of the effect of purge gas RH on adsorbent regeneration with MW. Table 2 presents physical properties of selected adsorbates and water.

Table 3-1. Physical properties of selected adsorbents

Adsorbent	Optipore V503	Zeolite HSZ980
BET surface area, $\left(\frac{\text{m}^2}{\text{g}}\right)$	1111	496
Total Pore volume, $\left(\frac{\text{cc}}{\text{g}}\right)$	0.9	0.3
Average pore diameter, ( $\text{\AA}$ )	34	6.5
Dielectric loss factor, $\epsilon''$	0.04	0.05

Table 3-2. Physical properties of tested adsorbates

Adsorbate	Cyhex	IPA	Water	Ref.
Boiling Point (°C)	81	82	100	
Dipole moment (D)	0.55	1.66	1.85	20
Relative Polarity	0.006	0.546	1	21
Dielectric loss factor, $\epsilon''$	0.01	3.00	12.50	22–24

### 3.3.2 Methods

#### 3.3.2.1 *Microwave heating*

A MW heating system (Figure 3-1) was used to investigate the effect of purge gas humidity on MW heating and VOC desorption from the selected adsorbents. The details of the MW heating setup are described elsewhere.<sup>2</sup> In brief, it consists of a 2.45 GHz variable power MW generator an isolator (National Electronics), a three-stub tuner (National Electronics), a single mode waveguide applicator, a quartz sample holder, a dual channel MW power meter (E4419B, Agilent), and a fiberoptic thermometer (Reflex, Neoptix). A sliding short was used to maximize MW energy transfer to the sample. A flame ionization detector (FID, Baseline- Mocon Inc., series 9000) was used to measure the concentration of adsorbate in the effluent stream. A data acquisition system equipped with LabVIEW software recorded the effluent concentration, temperature, and forward/reverse power. A 1 SLPM flow of N<sub>2</sub> (99.99 %) with different RH at 22 °C was used to purge the adsorbent bed during the MW heating. Two mass flow controllers, a humidifier, and a RH meter were used to control the purge gas humidity (Figure 3-1). MW heating experiments were

carried out by placing 4 grams of adsorbent into the sample holder followed by exposing the adsorbent bed to the desired MW power.

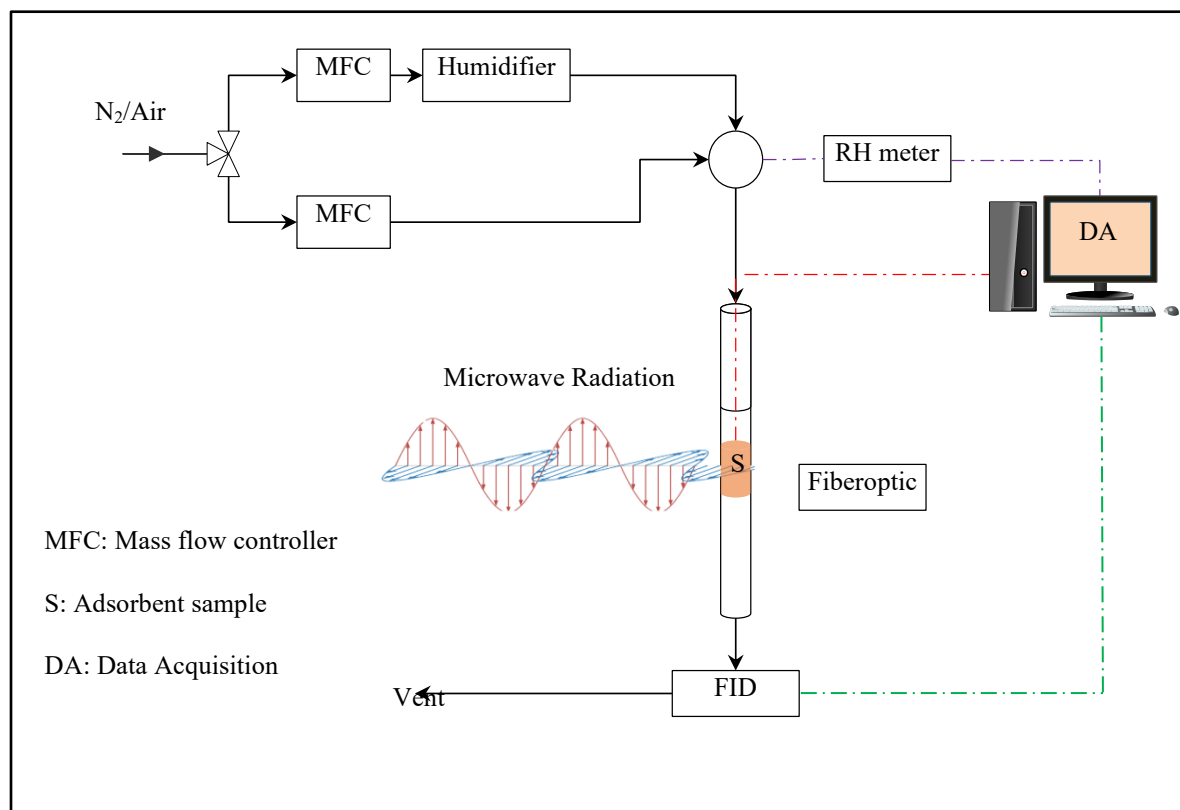


Figure 3-1. Schematic diagram of MW assisted regeneration setup.

### 3.3.2.2 Dielectric permittivity measurement

The complex permittivity of the adsorbents at 2.45 GHz was measured by a vector network analyzer (VNA, supplied by Rohde and Schwarz) and open ended probe method.<sup>25</sup> Samples were placed in a quartz tube and reflection coefficients of electromagnetic waves from the samples were determined at room temperature, and atmospheric pressure. Adsorbent changes the phase and

magnitude of the reflected power observed by the VNA, from which dimensionless complex permittivity values are obtained. Before each measurement, the probe was calibrated using different terminations including short, open and standard sample.

### 3.3.2.3 *Water adsorption under microwave irradiation*

Water vapor adsorption experiments were performed while the adsorbent bed was exposed to select MW power levels (0-400 W). Adsorbent exposure to MW and humid purge stream was continued till adsorbent temperature reached a steady state level (i.e.,  $<0.1^{\circ}\text{C}$  change in 2 min). Then, samples were cooled to room temperature. Water adsorption amount ( $g_{\text{water}}/g_{\text{adsorbent}}$ , %) and dielectric properties of each sample were measured at room temperature to investigate the potential effect of purge gas humidity on the adsorption capacity and dielectric properties of adsorbents.

### 3.3.2.4 *VOC adsorption & desorption*

VOC adsorption experiments were conducted at  $22^{\circ}\text{C}$  on 4 g of each adsorbent. For adsorption tests, 500 ppm of Cyhex/IPA vapor obtained by injecting liquid organic solvent (Cyhex or IPA) into 10 SLPM air stream. After the organic vapor concentration reached a stable level for 20 minutes, adsorption was started by flowing the gas into a quartz tube that holds adsorbent beads. The organic vapor concentration in the outlet stream was measured using a FID every 30 seconds until it stably reached the inlet concentration. FID was calibrated for each adsorbate with the vapor generation system prior to each test. The adsorption capacity was determined gravimetrically, using Eq. 1.

$$\text{Adsorption Capacity} \left( \frac{\text{mg}}{\text{g}} \right) = \frac{(W_{AA} - W_{BA}) * 1000}{W_{BA}} \quad \text{Eq. 1}$$

where  $W_{AA}$  and  $W_{BA}$  are the adsorbent weight after and before the adsorption process, respectively.

VOC desorption experiments were initiated by placing the VOC loaded adsorbent into the sample holder followed by setting the reactor to the desired MW power. Time based desorption efficiency was calculated based on the effluent VOC concentration and Eq. 2. Since the desorption rate is not constant during the desorption time, time-based desorption efficiency can illustrate the effect of purge gas humidity on the desorption rate.

$$\eta_t(\%) = \frac{\sum_0^t (C_{\text{VOC}} PQ\Delta t M_w)}{RT(W_{AA} - W_{BA})} \times 100 \quad \text{Eq. 2}$$

where  $\eta_t$  is the desorption efficiency at time  $t$ ,  $C_{\text{VOC}}$  is effluent VOC concentration,  $P$  is the pressure,  $Q$  is the purge gas flow rate,  $\Delta t$  is the time period between the two recorded concentrations,  $R$  is the ideal gas constant, and  $T$  is the room temperature.

### 3.4 Results and Discussion

#### 3.4.1 Effect of Microwave Applied Power

The effect of MW applied power levels on the adsorbent temperature was investigated in dry and humid purge gas conditions. The temperature of Optipore V503 and zeolite HSZ980 increased with increasing applied power for dry and humid purge gas conditions (Figure 3-2.a). However, there is a clear difference between the adsorbent temperature profile in humid and dry conditions, particularly for zeolite. Previous studies on MW absorption of mordenites showed that pre-

adsorption of water vapor onto the adsorbent can improve its MW absorption.<sup>26,27</sup> Therefore, a possible explanation for the temperature difference may be due to water vapor adsorption.

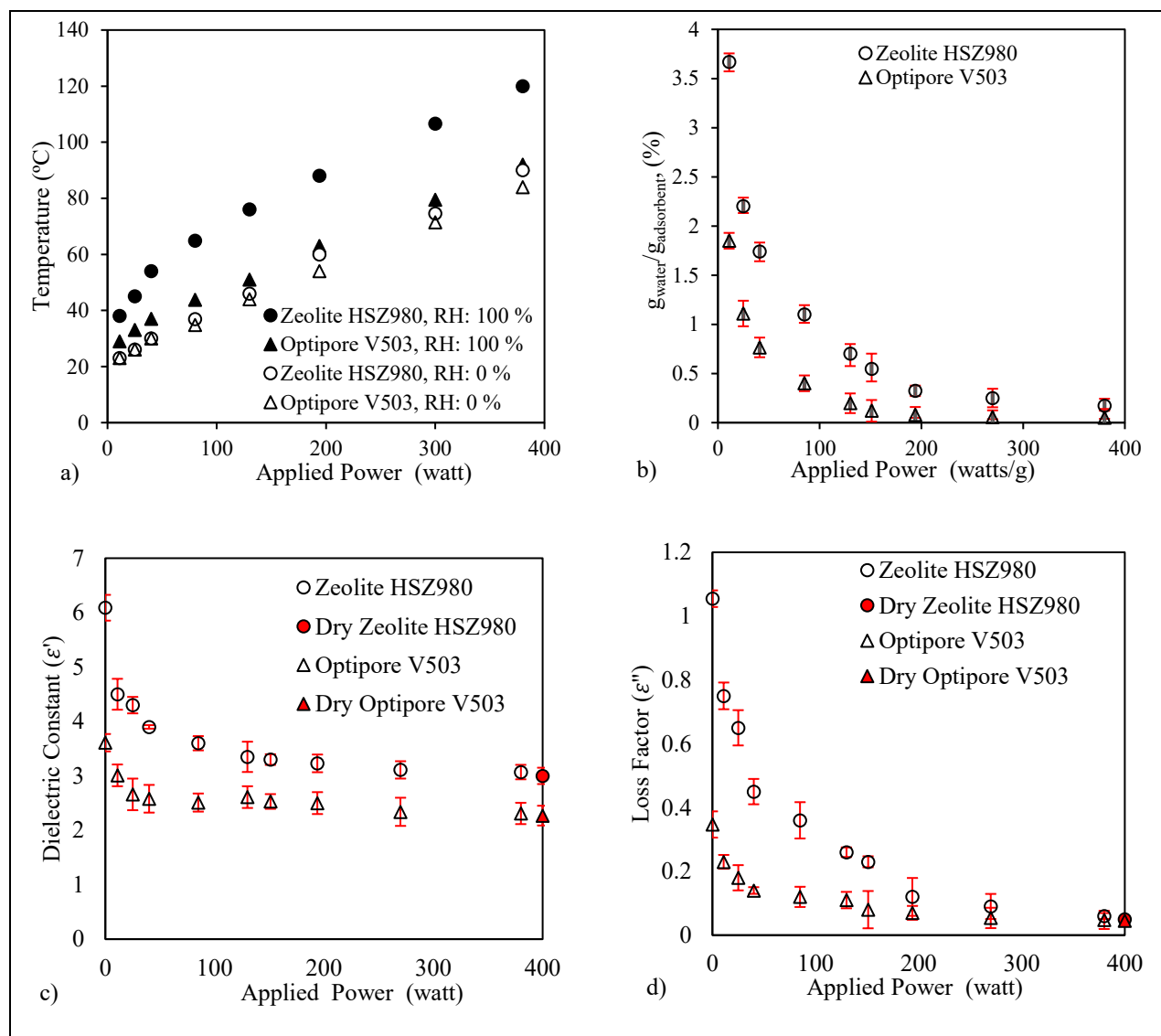


Figure 3-2. MW heating effect on Optipore V503 and Zeolite HSZ980: a) temperature evolution, b) Water vapour adsorption c) dielectric constant, and d) dielectric loss factor. The error bars represent standard deviations calculated based on three rounds of experiments.

Figure 3-2.b presents water adsorption amount of adsorbents after simultaneous exposure to water saturated purge gas and select MW powers. As expected, water adsorption capacity of Optipore

V503 and zeolite HSZ980 dropped to less than  $0.0017 \left( \frac{g_{water}}{g_{Adsorbent}} \right)$  by increasing the applied power to 380 watts. Comparing this water adsorption amount to the Optipore V503 and zeolite HSZ980 water adsorption isotherms (Appendix A, Figure A-1) demonstrate more than 99 % reduction in the water adsorption capacity due to MW heating. As a result of intense reduction in water adsorption, dielectric constants and loss factors of Optipore V503/zeolite HSZ980 approached values for dry adsorbents (Figures 3-2.c and 3-2.d). Nevertheless, Figure 3-2.a shows that the temperature difference between humid and dry heating didn't change at high applied powers. To better explain the additional heat generation in the case of humid MW heating, we attribute the effect of MW on water molecules inside the adsorbent bed to two parts: (i) the effect of MW on water vapor molecules in the bulk gas phase, and (ii) the effect of MW on water molecules inside the adsorbent pores. In the first part, water molecules in the gas phase have negligible contribution to MW absorption since the dielectric permittivity of gases is extremely low. In fact, water molecules in the gas phase are no longer bound to each other to convert MW energy into heat by rotational polarization.<sup>28</sup> Uematsu and Frank study on the dielectric properties of steam at different temperatures and pressures shows that the dielectric constant of water in gas phase at low pressure (less than 5 bar) and temperatures between 0 to 240 °C is 1.0.<sup>29</sup> This is equal to the dielectric constant of dry air reported by Hughes and Armstrong.<sup>30</sup> On the other hand, water adsorption amount of tested adsorbents is less than  $0.0017 \left( \frac{g_{water}}{g_{Adsorbent}} \right)$  when adsorbent bed is irradiated with MW at 380 watts (Figures 3-2.c and 3-2.d). Therefore, it is reasonable to presume that water molecules in the vicinity of adsorbent surface is responsible for enhancing MW heating due to the molecular interaction between water and adsorbent surface. This is also consistent with Roussy et al. theoretical and experimental study on the dehydration of zeolite 13X.<sup>6</sup> They demonstrated that

water molecules in zeolite 13X pores interact with each other and the zeolite surface by reorientations in a MW field. Therefore, different behavior of zeolite and Optipore V503 in humid MW heating can be explained by the difference in the interaction of water molecules with zeolite and Optipore V503 surface. Molecular interactions between water and zeolite surface is attributed mostly to the surface exchangeable cations and the oxygen atoms and is higher than water molecule interaction with the hydrophobic surface of Optipore V503.<sup>27</sup>

### 3.4.2 Relative Humidity Effect

In order to investigate the effect of purge gas RH on MW absorption by Optipore V503 and zeolite, a humid nitrogen stream was used during MW heating. The purge stream was generated at 22 °C by passing 1 SLPM dry nitrogen through a bubble column. The temperature difference between humid and dry MW heating is presented in Figure 3-3. The maximum temperature difference between humid and dry heating for both adsorbents occurred at the water saturation point at 22 °C which is equal to 0.019 g<sub>water</sub>/l in the purge gas. These results indicate that the concentration of water molecules in the purge gas governs the extent of additional heat dissipation in the adsorbent bed. In fact, higher water concentration increases the interaction between the adsorbent surface and water molecules during polarization which leads to higher heat generation inside the bed. Therefore, higher heat generation rates are expected in case of using water saturated purge gas at high temperatures.

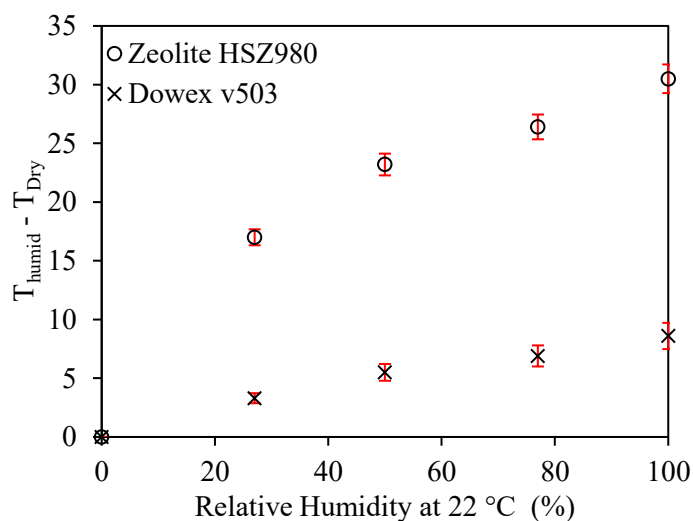


Figure 3-3. Temperature difference between humid and dry MW heating at constant applied power of 380 W and purge gas flow rate of 1 l/min. The error bars represent standard deviations calculated based on three rounds of experiments.

### 3.4.3 VOC Adsorption and Desorption

To study the effect of humid purge gas on adsorbent regeneration, IPA and Cyhex were adsorbed on zeolite (Figures 3-4) and Optipore V503 (Figures 3-5) and then regeneration was carried out using dry and water saturated purge gas. For both adsorbents, the required time for complete desorption is shorter in humid MW heating. However, the reduction in the regeneration time is more notable for Cyhex desorption than IPA desorption. IPA, having a large dipole moment, can be efficiently polarized in a MW field. Therefore, compared to Cyhex, IPA molecules absorb more MW energy resulting in an immediate rise in the temperature and desorption rate (Figures 3-4.a, 3-4.b, 3-5.a, and 3-5.b). However, the adsorbent bed gradually loses its IPA molecules, thereby its ability to absorb MW energy, which results in a decrease in the desorption temperature (Figures 3-4.b and 3-5.b). Kim et al. reported similar observations during their study on MW heating of

mordenites. They reported that NaMOR (sodium type mordenite) initial water content can change the maximum achievable temperature during MW heating which decreases as NaMOR loses its water content during MW heating.<sup>26</sup>

On the other hand, Cyhex is transparent to MW owing to its very low polarity and zero dipole moment. Consequently, water saturated purge gas is more effective on the desorption of Cyhex leading to larger increase in Cyhex desorption rate by humid purge gas compared to IPA (Appendix A, Figure A-2). Similar observation can be seen from Mao et al. investigations on MW regeneration of agricultural based activated carbon saturated with toluene and acetone.<sup>31</sup> They reported higher desorption rate enhancement for toluene (nonpolar) than acetone (polar) using humidified purge gas. It can be seen also from Figures 3-4.a and 3-4.b that using water saturated purge gas during MW heating of zeolite increases the effluent concentration of Cyhex and IPA by 86% and 9%, respectively. Similarly, Figures 3-5.a and 3-5.b demonstrate 34 % and 22 % enhancement in the Cyhex and IPA concentration, respectively, during MW heating of Optipore V503. Higher desorption temperature due to addition of water vapor provides heat needed to overcome heat of adsorption. Moreover, adsorbates molecules reorientation and agitation in the MW field can facilitate diffusion into the gas phase and thus reducing the regeneration time. Antonio and Deam study on water diffusion coefficient in MW field shows that MW effect on molecules can lead to an increase of 75 to 100% in the diffusion coefficient over conventional heating technique at the same temperature.<sup>32</sup>

Second cycle IPA/Cyhex adsorption were carried out on all regenerated adsorbents to illustrate the effect of purge gas humidity on zeolite/Optipore V503 adsorption capacity. Adsorption capacity of each adsorbent was measured and compared to corresponding values in the first cycle. Table 3

summarizes adsorption capacity results and shows that MW regeneration with humidified purge gas has a negligible effect on the adsorption capacity of zeolite and Optipore V503 as water molecules barely adsorbed on the adsorbents during MW heating (Figure 3-2.b).

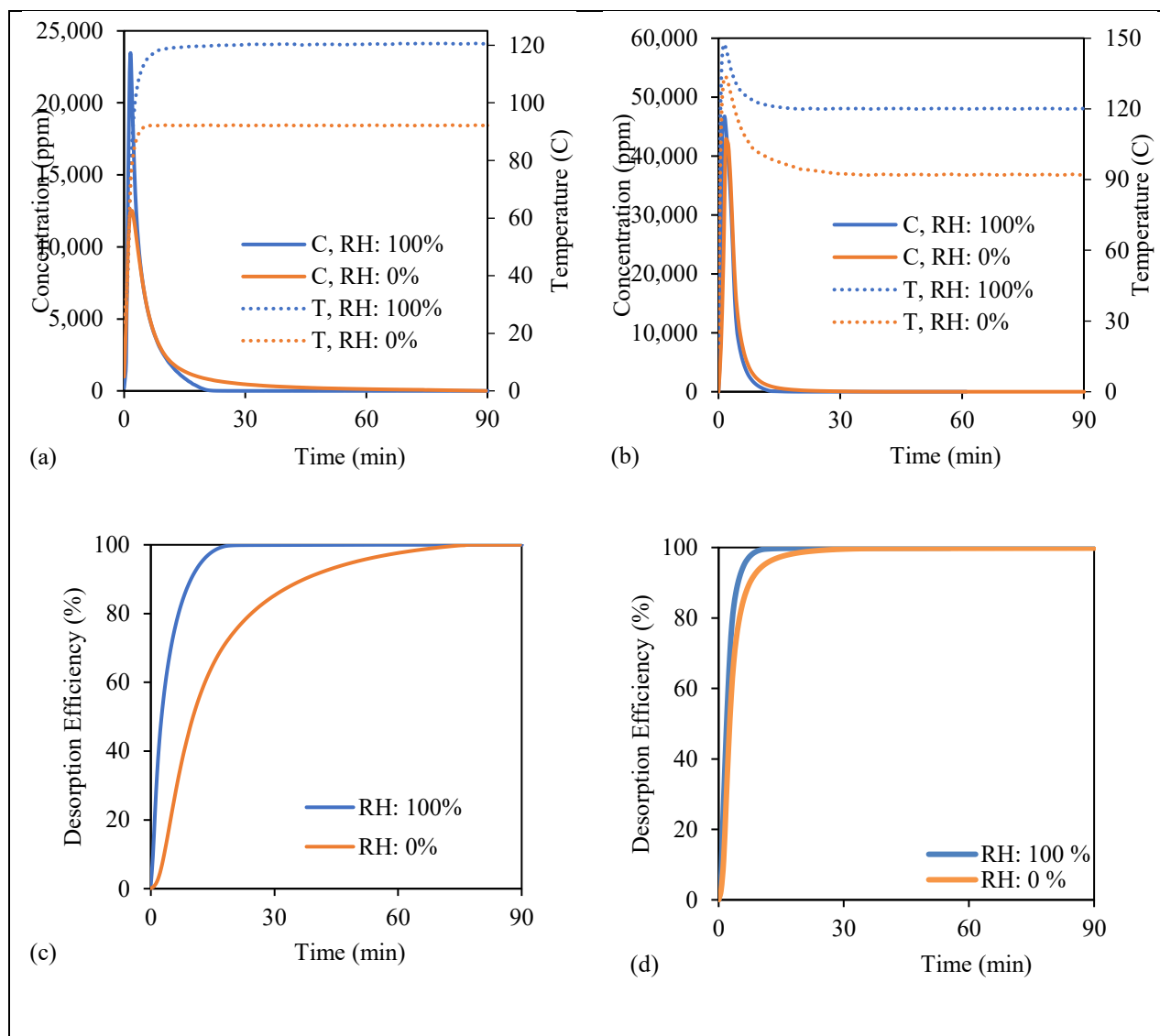


Figure 3-4. Desorption of Cyhex and IPA off Zeolite HSZ980. Effluent concentration and Zeolite HSZ980 temperature profiles during desorption of Cyhex (a) and IPA (b); Desorption efficiency of Cyhex (c) and IPA (d) at 0 and 100 % RH and constant applied power of 380 W.

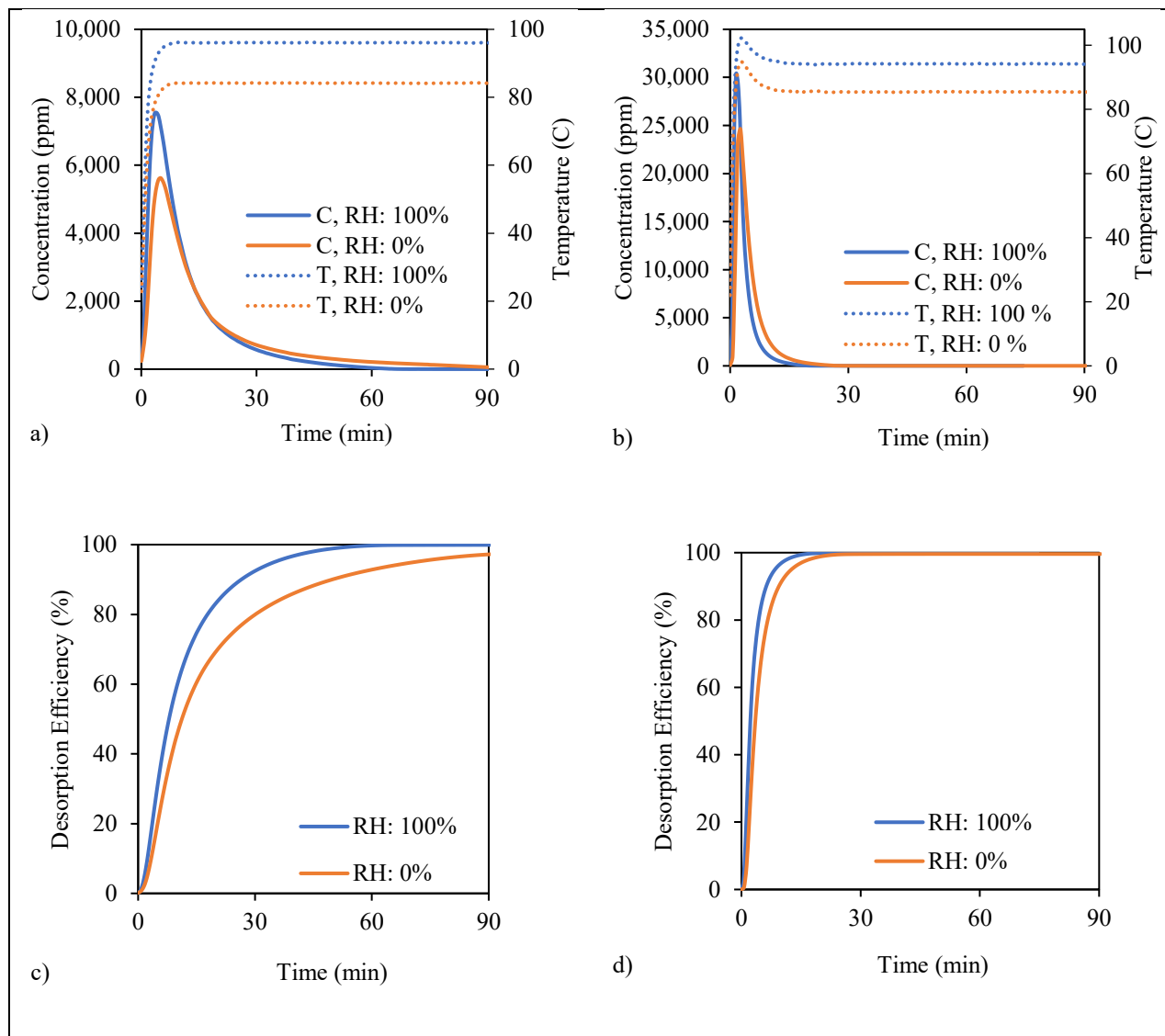


Figure 3-5. Desorption of Cyhex and IPA off Optipore V503. Effluent concentration and Optipore V503 temperature profiles during desorption of Cyhex (a) and IPA (b); Desorption efficiency of Cyhex (c) and IPA (d) at 0 and 100 % RH and constant applied power of 380 W.

Table 3-3. The results of Cyhex and IPA adsorption on Optipore V503 and Zeolite HSZ980.

Values are reported as mean  $\pm$  standard deviation of three rounds of measurement

Adsorbent	Adsorption Capacity at equilibrium state and 22 °C ( $\frac{\text{mg}_{\text{adsorbate}}}{\text{g}_{\text{adsorbent}}}) \pm \text{SD}^a$							
	Optipore v503				Zeolite HSZ980			
Adsorbate	Cyhex		IPA		Cyhex		IPA	
Before MW regeneration	102 $\pm$ 4		64 $\pm$ 2		95 $\pm$ 3		103 $\pm$ 2	
Desorption condition	Dry	Humid	Dry	Humid	Dry	Humid	Dry	Humid
After MW regeneration	97 $\pm$ 2	99 $\pm$ 2	61 $\pm$ 3	63 $\pm$ 1	95 $\pm$ 2	94 $\pm$ 3	102 $\pm$ 3	98 $\pm$ 2

### 3.4.4 Energy Consumption

The energy consumed during the regeneration of Optipore and zeolite was calculated using MW applied power and time needed to reach 99% desorption efficiency for each adsorbate. The results depicted in Figure 3-6 shows that using humid purge gas instead of dry purge gas decreases the energy required to desorb Cyhex and IPA on zeolite by 73 % and 61 %, respectively. Similarly, for Optipore V503, energy needed to desorb Cyhex and IPA decreased by 33 % and 25 %, respectively.

Comparing the energy required during dry regenerations indicates that energy consumption during the desorption of Cyhex on Optipore V503 is more than on zeolite which is attributed to the higher affinity of Optipore V503 to nonpolar VOCs (Table 3) and lower desorption temperature during MW-assisted regeneration compared to zeolite (Figures 3-4.a and 3-5.a). In contrast, both adsorbents showed similar energy requirement for the desorption of IPA in dry condition. Although zeolite showed higher IPA adsorption capacity compared to Optipore V503 (Table 3), it

reached higher desorption temperature in dry condition which reduced the desorption time and total energy required for its complete desorption.

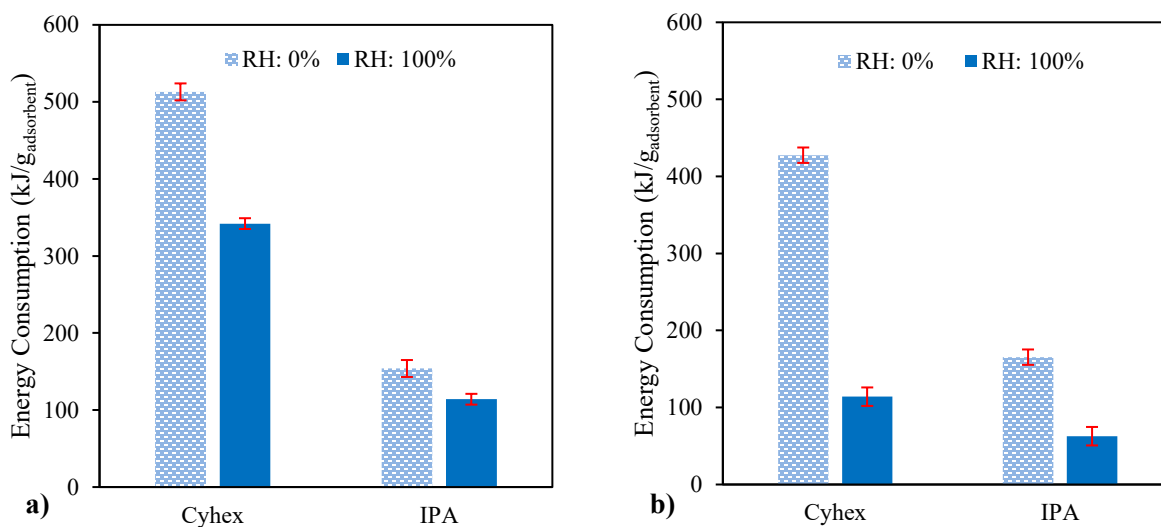


Figure 3-6. Energy consumption during the desorption of Cyhex and IPA on a) Optipore v503 and b) Zeolite HSZ980. The error bars represent standard deviations calculated based on three rounds of experiments.

### 3.5 Conclusions

In this study, the effect of purge gas relative humidity on MW absorption of Zeolite/Optipore V503 was investigated at a range of MW applied power. Higher temperature is achieved when adsorbents were purged with humid purge gas compared to dry purge gas. To elucidate the reason behind this, water vapor adsorption experiments were performed on both adsorbents under MW irradiation (0-400 W). After each adsorption test, the adsorption capacity and dielectric properties of the adsorbent samples were measured. Dielectric property measurements showed that the dielectric constant and loss factor of the adsorbents decreased with increasing MW applied power. This trend is attributed to the water adsorption capacity of zeolite and Optipore V503 which was reduced by

more than 93 % and 97 %, respectively, due to the MW irradiation and corresponding adsorbent temperature increase. Further investigation revealed that water vapor concentration in the purge gas and the interaction of water molecules with the adsorbent surface are two major factors governing the extent of MW heating at constant applied power. Additionally, VOC adsorption on /MW assisted desorption of zeolite/Optipore V503 was performed to study the effect of purge gas humidity on the regeneration of adsorbents. Using humidified purge gas in the MW-assisted regeneration of zeolite increased desorption rates leading to 86% and 9% increase in the effluent concentration of Cyhex and IPA, respectively. Similarly, 34% and 22% enhancement were obtained in the Cyhex and IPA effluent concentration, respectively, during MW heating of Optipore V503.

All in all, using humid purge gas during MW assisted desorption shows faster heating, higher desorption rate, and lower energy requirement compared to dry regeneration. In addition, this method doesn't affect VOC adsorption capacity of adsorbents and doesn't need a drying step unlike the case of conventional steam regeneration.

### 3.6 References

- (1) Kim, K.-J.; Ahn, H.-G. The Effect of Pore Structure of Zeolite on the Adsorption of VOCs and Their Desorption Properties by Microwave Heating. *Microporous and Mesoporous Materials* **2012**, *152*, 78–83. <https://doi.org/10.1016/j.micromeso.2011.11.051>.
- (2) Fayaz, M.; Shariaty, P.; Atkinson, J. D.; Hashisho, Z.; Phillips, J. H.; Anderson, J. E.; Nichols, M. Using Microwave Heating To Improve the Desorption Efficiency of High Molecular Weight VOC from Beaded Activated Carbon. *Environmental Science & Technology* **2015**, *49* (7), 4536–4542. <https://doi.org/10.1021/es505953c>.
- (3) Lv, Y.; Sun, J.; Yu, G.; Wang, W.; Song, Z.; Zhao, X.; Mao, Y. Hydrophobic Design of Adsorbent for VOC Removal in Humid Environment and Quick Regeneration by Microwave. *Microporous and Mesoporous Materials* **2020**, *294*, 109869. <https://doi.org/10.1016/j.micromeso.2019.109869>.
- (4) Fayaz, M.; Shariaty, P.; Atkinson, J. D.; Hashisho, Z.; Phillips, J. H.; Anderson, J. E.; Nichols, M. Using Microwave Heating To Improve the Desorption Efficiency of High Molecular Weight VOC from Beaded Activated Carbon. *Environmental Science & Technology* **2015**, *49* (7), 4536–4542. <https://doi.org/10.1021/es505953c>.
- (5) Chowdhury, T.; Shi, M.; Hashisho, Z.; Sawada, J. A.; Kuznicki, S. M. Regeneration of Na-ETS-10 Using Microwave and Conductive Heating. *Chemical Engineering Science* **2012**, *75*, 282–288. <https://doi.org/10.1016/j.ces.2012.03.039>.
- (6) Roussy, G.; Zoulalian, A.; Charreyre, M.; Thiebaut, J. M. How Microwaves Dehydrate Zeolites. *The Journal of Physical Chemistry* **1984**, *88* (23), 5702–5708. <https://doi.org/10.1021/j150667a049>.
- (7) Jones, D. A.; Lelyveld, T. P.; Mavrofidis, S. D.; Kingman, S. W.; Miles, N. J. Microwave Heating Applications in Environmental Engineering—a Review. *Resources, Conservation and Recycling* **2002**, *34* (2), 75–90. [https://doi.org/10.1016/S0921-3449\(01\)00088-X](https://doi.org/10.1016/S0921-3449(01)00088-X).

- (8) Falciglia, P. P.; Roccaro, P.; Bonanno, L.; De Guidi, G.; Vagliasindi, F. G. A.; Romano, S. A Review on the Microwave Heating as a Sustainable Technique for Environmental Remediation/Detoxification Applications. *Renewable and Sustainable Energy Reviews* **2018**, *95*, 147–170. <https://doi.org/10.1016/j.rser.2018.07.031>.
- (9) Clark, D. E.; Sutton, W. H. Microwave Processing of Materials. *Annual Review of Materials Science* **1996**, *26* (1), 299–331. <https://doi.org/10.1146/annurev.ms.26.080196.001503>.
- (10) Gibson, C.; Matthews, I.; Samuel, A. Microwave Enhanced Diffusion in Polymeric Materials. *Journal of Microwave Power and Electromagnetic Energy* **1988**, *23* (1), 17–28. <https://doi.org/10.1080/08327823.1988.11688033>.
- (11) Yuen, F. K.; Hameed, B. H. Recent Developments in the Preparation and Regeneration of Activated Carbons by Microwaves. *Advances in Colloid and Interface Science* **2009**, *149* (1–2), 19–27. <https://doi.org/10.1016/j.cis.2008.12.005>.
- (12) Cherbański, R.; Molga, E. Intensification of Desorption Processes by Use of Microwaves- An Overview of Possible Applications and Industrial Perspectives. *Chemical Engineering and Processing: Process Intensification* **2009**. <https://doi.org/10.1016/j.cep.2008.01.004>.
- (13) Meng, Q. B.; Yang, G.-S.; Lee, Y.-S. Preparation of Highly Porous Hypercrosslinked Polystyrene Adsorbents: Effects of Hydrophilicity on the Adsorption and Microwave-Assisted Desorption Behavior toward Benzene. *Microporous and Mesoporous Materials* **2013**, *181*, 222–227. <https://doi.org/10.1016/j.micromeso.2013.07.027>.
- (14) Shariaty, P.; Jahandar Lashaki, M.; Hashisho, Z.; Sawada, J.; Kuznicki, S.; Hutcheon, R. Effect of ETS-10 Ion Exchange on Its Dielectric Properties and Adsorption/Microwave Regeneration. *Separation and Purification Technology* **2017**, *179*, 420–427. <https://doi.org/10.1016/j.seppur.2017.02.016>.

- (15) Hashisho, Z.; Rood, M. J.; Barot, S.; Bernhard, J. Role of Functional Groups on the Microwave Attenuation and Electric Resistivity of Activated Carbon Fiber Cloth. *Carbon* **2009**, *47* (7), 1814–1823. <https://doi.org/10.1016/j.carbon.2009.03.006>.
- (16) Zhao, P.; Wang, S.; Kadlec, A.; Li, Z.; Wang, X. Properties of Cement–Sand-Based Piezoelectric Composites with Carbon Nanotubes Modification. *Ceramics International* **2016**, *42* (13), 15030–15034. <https://doi.org/10.1016/j.ceramint.2016.06.153>.
- (17) Qing, Y.; Wang, X.; Zhou, Y.; Huang, Z.; Luo, F.; Zhou, W. Enhanced Microwave Absorption of Multi-Walled Carbon Nanotubes/Epoxy Composites Incorporated with Ceramic Particles. *Composites Science and Technology* **2014**, *102*, 161–168. <https://doi.org/10.1016/j.compscitech.2014.08.006>.
- (18) Zhang-Steenwinkel, Y.; van der Zande, L. M.; Castricum, H. L.; Blik, A.; van den Brink, R. W.; Elzinga, G. D. Microwave-Assisted in-Situ Regeneration of a Perovskite Coated Diesel Soot Filter. *Chemical Engineering Science* **2005**, *60* (3), 797–804. <https://doi.org/10.1016/j.ces.2004.09.042>.
- (19) Lv, Y.; Sun, J.; Yu, G.; Wang, W.; Song, Z.; Zhao, X.; Mao, Y. Hydrophobic Design of Adsorbent for VOC Removal in Humid Environment and Quick Regeneration by Microwave. *Microporous and Mesoporous Materials* **2020**, *294*, 109869. <https://doi.org/10.1016/j.micromeso.2019.109869>.
- (20) Nelson, R. D.; Lide, D. R.; Maryott, A. A. Selected Values of Electric Dipole Moments for Molecules in the Gas Phase. *National Standard Reference Series - National Bureau of Standards 10*; United States Department of Commerce, 1967; pp 1–49.
- (21) Reichardt, C.; Welton, T. *Solvents and Solvent Effects in Organic Chemistry*; Wiley-VCH Verlag GmbH & Co. KGaA: Weinheim, Germany, 2010. <https://doi.org/10.1002/9783527632220>.

- (22) Jogdand, A. P.; Kadam, D. P. L. Dielectric Behavior of Acetonitrile + Methanol Binary Mixtures at Microwave Frequency. *IOSR Journal of Applied Physics* **2014**, *6* (1), 14–22. <https://doi.org/10.9790/4861-06121422>.
- (23) Jia, G.-Z.; Jie, Q.; Feng, W. Hydrogen Bond Analysis in Alcohol (1-Propanol, 2-Propanol and Glycerol)-DMF Mixtures Based on Dielectric Spectroscopy. *Journal of Molecular Structure* **2015**, *1100*, 354–358. <https://doi.org/10.1016/j.molstruc.2015.07.065>.
- (24) Komarov, V.; Wang, S.; Tang, J. Permittivity and Measurements. In *Encyclopedia of RF and Microwave Engineering*; John Wiley & Sons, Inc.: Hoboken, NJ, USA, 2005. <https://doi.org/10.1002/0471654507.eme308>.
- (25) Brodie, G.; Jacob, M. V.; Farrell, P. 6 Techniques for Measuring Dielectric Properties. In *Microwave and Radio-Frequency Technologies in Agriculture*; De Gruyter Open Poland, 2015; pp 52–77. <https://doi.org/10.1515/9783110455403-007>.
- (26) Kim, S.-I.; Aida, T.; Niiyama, H. Binary Adsorption of Very Low Concentration Ethylene and Water Vapor on Mordenites and Desorption by Microwave Heating. *Separation and Purification Technology* **2005**, *45* (3), 174–182. <https://doi.org/10.1016/j.seppur.2005.03.006>.
- (27) Legras, B.; Polaert, I.; Estel, L.; Thomas, M. Mechanisms Responsible for Dielectric Properties of Various Faujasites and Linde Type A Zeolites in the Microwave Frequency Range. *The Journal of Physical Chemistry C* **2011**, *115* (7), 3090–3098. <https://doi.org/10.1021/jp111423z>.
- (28) Horikoshi, S.; Serpone, N. *RF Power Semiconductor Generator Application in Heating and Energy Utilization*; Horikoshi, S., Serpone, N., Eds.; Springer Singapore: Singapore, 2020. <https://doi.org/10.1007/978-981-15-3548-2>.
- (29) Uematsu, M.; Frank, E. U. Static Dielectric Constant of Water and Steam. *Journal of Physical and Chemical Reference Data* **1980**, *9* (4), 1291–1306. <https://doi.org/10.1063/1.555632>.

- (30) Hughes, J. V.; Armstrong, H. L. The Dielectric Constant of Dry Air. *Journal of Applied Physics* **1952**, *23* (5), 501–504. <https://doi.org/10.1063/1.1702240>.
- (31) Mao, H.; Zhou, D.; Hashisho, Z.; Wang, S.; Chen, H.; Wang, H. H. Constant Power and Constant Temperature Microwave Regeneration of Toluene and Acetone Loaded on Microporous Activated Carbon from Agricultural Residue. *Journal of Industrial and Engineering Chemistry* **2015**, *21*, 516–525. <https://doi.org/10.1016/j.jiec.2014.03.014>.
- (32) Antonio, C.; Deam, R. T. Can “Microwave Effects” Be Explained by Enhanced Diffusion? *Physical Chemistry Chemical Physics* **2007**, *9* (23), 2976–2982. <https://doi.org/10.1039/b617358f>.

# **CHAPTER 4: ENHANCED MICROWAVE REGENERATION OF A POLYMERIC ADSORBENT THROUGH CARBON NANOTUBES DEPOSITION**

## **4.1 Chapter Overview**

The previous chapter demonstrated that microwave (MW) absorption of MW-transparent adsorbents can be improved using humid purge gas. However, the extent of improvement was limited to the water vapor concentration in the purge gas and the interactions of water molecules with the adsorbent surface. This chapter aimed to develop a new method to tune MW absorption of MW-transparent adsorbents for any desired MW absorption requirements. In this regard, the influence of carbon nanotube (CNT) addition to a commercially available styrene-divinylbenzene porous adsorbent resin beads, Optipore V503, was studied. CNTs were selected as a MW absorptive material due to their large loss factor and electrical conductivity. Different levels of CNT (0-0.3 wt%) were deposited on the adsorbent surface using a physical deposition method. CNT-coated samples were characterized using helium ion microscopy, Raman spectroscopy, thermal gravimetry analysis, dielectric property analysis, and N<sub>2</sub> and n-heptane adsorption isotherms. In addition, cyclic adsorption/MW-assisted desorption of heptane on pristine and CNT-coated samples was carried out to study the effect of CNT addition on adsorption capacity and MW-assisted regeneration efficiency.

## 4.2 Introduction

Adsorption is a widely used method for abatement of volatile organic compound (VOC) emissions due to its high efficiency and relatively low operating cost. Following adsorption, desorption is used to regenerate the adsorbent. Different techniques are used to regenerate used adsorbents. These techniques are typically categorized into pressure swing regeneration, temperature swing regeneration, and reactive regeneration.<sup>1,2</sup> Among the aforementioned techniques, temperature swing regeneration, using hot purge gas or superheated steam, is the most commonly used method. However, large volumes of hot purge gas have to be used in these methods to heat the adsorbent to sufficiently high temperatures due to the low heat capacity of the hot purge gas. Using large volumes of purge gas also dilutes the desorbed VOCs, thus a concentration step is usually needed for VOC recovery. Moreover, with steam desorption, the adsorbent bed requires a drying step after each desorption cycle. Each of these shortcomings for conventional thermal regeneration increase the energy penalty and operating cost, which leads to the need for alternative methods of thermal regeneration.

In recent years, microwave (MW) regeneration has been proposed as a potential alternative to conventional thermal regeneration.<sup>3-5</sup> MW regeneration has several advantages over conventional thermal regeneration including faster heating, higher recovered adsorbate concentration due to lower purge gas consumption, and ability to heat the bed to higher temperatures as there is no temperature limitation associated with a purge gas. Furthermore, the energy efficiency of MW heating is substantially greater than conventional heating, as the latter involves additional heat loss in hot gas/steam generation and conveyance equipment.<sup>6-8</sup> Despite these advantages, widespread

application of MW regeneration has been limited by obstacles such as the lack of adsorbent/adsorbate dielectric data and the inability to heat adsorbents that are MW-transparent.<sup>9</sup>

Many factors can affect MW heating of adsorbents, with dielectric properties and penetration depth playing important roles. In general, heat generation inside the MW-irradiated material is governed by the material's dielectric constant and dielectric loss factor. The dielectric constant expresses the capacity of a molecule to be polarised by an electric field. The dielectric loss factor describes the efficiency of electromagnetic energy conversion into heat. Therefore, materials can be selectively heated by MW energy according to their dielectric properties. Eq. 1 shows the heating potential of MW power per unit volume as a function of dielectric loss factor.<sup>10</sup>

$$Q_{\text{avg}} = \omega \varepsilon_0 \varepsilon'' E_{\text{rms}}^2 \quad \text{Eq. 2}$$

where  $Q_{\text{avg}}$  is the average MW power absorption in  $\text{W/m}^3$ ;  $\omega$  is the MW angular frequency,  $\text{rd/s}$ ;  $\varepsilon_0$  is the free space permittivity,  $8.85 \times 10^{-12} \text{ F/m}$ ;  $\varepsilon''$  is the dielectric loss factor of the irradiated material, dimensionless; and  $E_{\text{rms}}$  is the root-mean-square electric field intensity in  $\text{V/m}$ . The MW heating rate ( $\frac{dT}{dt}$ ) is consequently given in Eq. 2:<sup>9</sup>

$$\frac{dT}{dt} = \frac{Q_{\text{avg}}}{C_p \rho} = \frac{\omega \varepsilon_0 \varepsilon'' E_{\text{rms}}^2}{C_p \rho} \quad \text{Eq. 2}$$

where  $C_p$  and  $\rho$  are the heat capacity and the density of the heated material, respectively. Another important parameter that needs to be considered in designing a MW heating system is the penetration depth of MW into the irradiated material. The penetration depth is defined as the depth from the surface into the irradiated material at which the MW power drops to  $1/e$  of its value at

the surface.<sup>11</sup> Eq. 3 shows the MW penetration depth as a function of the free space wavelength of the incident radiation,  $\lambda$ , and the dielectric properties of irradiated material.<sup>12</sup>

$$D_p = \frac{\lambda}{2\pi\sqrt{2\varepsilon'}} \left[ \left( 1 + \left( \frac{\varepsilon''}{\varepsilon'} \right)^2 \right)^{\frac{1}{2}} - 1 \right]^{-\frac{1}{2}} \quad \text{Eq. 3}$$

In objects smaller than the penetration depth, materials cannot be heated effectively.<sup>13</sup> On the other hand, for material larger than penetration depth, the rapid drop of incident wave power nearest the surface is the main cause of non-uniform heating.<sup>13</sup> Consequently, the dimensions of the irradiated material determine the penetration depth needed for suitable and uniform MW heating. To accomplish the MW-assisted regeneration of an adsorbent bed, the adsorbent material should have a dielectric loss factor and MW penetration depth that is appropriate to provide efficient and uniform heating.

MW heating of various types of adsorbent/adsorbate systems has been studied previously, including desorption of polar and non-polar adsorbate on silica gel, zeolites, activated carbon, and polymeric adsorbents.<sup>15-19</sup> These studies revealed that MW heating can be effective if either the adsorbate or the adsorbent can absorb and dissipate MW energy into heat. Conversely, regeneration would be challenging if the adsorbent is MW-transparent and the adsorbate is nonpolar.<sup>19</sup> To overcome this problem, improving the dielectric properties of the adsorbent bed by doping with a secondary MW absorptive material (MAM) is considered here. In this approach, the necessary desorption heat can be provided through the MAM's ability to absorb and convert MW to heat.

Different forms of MAMs such as graphene oxide (GO), carbon nanotubes (CNTs), sodium dodecyl sulfate (SDS), and magnetic nano-particle fillers have been reported.<sup>20-23</sup> Carbonaceous materials are favorable for this application due to their high dielectric loss factor.<sup>24,25</sup> Wu et al. investigated the effect of reduced graphene oxide (RGO) addition on the electromagnetic absorption of polypyrrole aerogel. They showed that the addition of even a trace content of RGO (0.43 wt%) to aerogel can significantly increase the electromagnetic absorption of the aerogel without affecting its solvent absorption capacity.<sup>26</sup> Wang et al. investigated the effect of multiwall carbon nanotubes (MWCNT) in composites with poly vinylidene fluoride prepared by simple physical blending. They found that the dielectric constant of the composite was increased by more than 30 times with about 2.0 vol % of MWCNT.<sup>27</sup> Chen et al. investigated the MW absorption performance of silicone rubber using five different graphene products at a loading of 1 wt %. They found that among all graphene types, highly exfoliated RGO is capable of delivering excellent MW absorption at very low loading.<sup>28</sup> Vadivel et al. studied the effect of SDS surfactant on the structural, morphological, and dielectric properties of  $\text{CoFe}_2\text{O}_4$ . Dielectric measurement results showed that the both dielectric constant and loss factor of SDS-amended  $\text{CoFe}_2\text{O}_4$  nanoparticles are higher than the pure  $\text{CoFe}_2\text{O}_4$ .<sup>20</sup> More recently, Qing et al. reported the improving effect of MWCNT and ceramic particles on the complex permittivity and MW absorption of epoxy composites.<sup>29</sup> These studies showed that the addition of high dielectric loss factor MAMs to MW-transparent adsorbents is an effective way of enhancing their MW absorption.

As mentioned earlier, the dielectric loss factor and penetration depth of an adsorbent are key factors in determining the suitability of adsorbent for effective and uniform MW regeneration. These properties have also been shown to be quite challenging to control. Therefore, the aim of this work

was to develop a simple way to alter dielectric loss factor and penetration depth of MW transparent adsorbents. In this regard, the influence of CNT addition to a commercially available styrene-divinylbenzene porous adsorbent resin beads, Optipore V503, was studied. CNTs were selected as a MAM due to their large loss factor and electrical conductivity. Different levels of CNT (0-0.3 wt%) were deposited on the adsorbent surface using a physical deposition method. CNT-coated samples were characterized using helium ion microscopy (HIM), Raman spectroscopy, thermal gravimetry analysis, dielectric property analysis, and N<sub>2</sub> and n-heptane adsorption isotherms. In addition, cyclic adsorption/MW-assisted desorption of heptane on pristine and CNT-coated samples was carried out to study the effect of CNT addition on adsorption capacity and MW-assisted regeneration efficiency.

### **4.3 Experimental Section**

#### **4.3.1 Material**

Porous styrene-divinylbenzene resin (Dowex Optipore V503, Dow Chemicals) was used as the base polymeric adsorbent to which CNT was added. Multiwalled CNTs (US Research Nanomaterials) with a purity of 95%, outer diameter of less than 7 nm, aspect ratio of 1100 and specific surface area of 500 m<sup>2</sup>/g, were used as received. Sodium dodecyl sulfate (SDS, Sigma Aldrich, 99% purity) was used as the dispersion detergent of CNT in deionized (DI) water. The critical micelle concentration of SDS in water is 8 mmol/l.<sup>30</sup> In this study, n-heptane (99%, Fisher Scientific, hereafter “heptane”) was used as a nonpolar and MW-transparent adsorbate to better investigate the effect of deposited CNTs on the MW-assisted regeneration of Optipore V503.

### 4.3.2 Sample Preparation

To uniformly deposit CNTs on the surface of Optipore V503, CNTs were first dispersed and stabilized in deionized (DI) water. Shear-mixing and ultrasonication are usually employed to disperse CNTs in aqueous solutions; however, high van der Waals force, surface area, and aspect ratio of CNTs inevitably cause self-aggregation.<sup>31</sup> Surfactants such as SDS are an effective way to overcome this self-aggregation and improve the stability of the dispersion.<sup>32,33</sup> The hydrophobic group,  $-\text{CH}_3$ , of the SDS molecule adsorbs on the surface of a CNT tube, while the hydrophilic head,  $-\text{SO}_4$ , links with water. In other words, SDS molecules provide steric hinderance and static charge repulsion which increases the stability of the surfactant/CNT complex in the solution.<sup>34</sup> In this study, different concentrations of CNT in DI water were produced using SDS as a surfactant. CNT-water suspensions were produced at different SDS:CNT ratios, by 1 hr mechanical stirring and 1 hr sonication in an ultrasonic bath. The dispersion stability of the CNT solutions with different SDS:CNT ratios was evaluated over 8 hours by ultraviolet-visible (UV-vis) spectroscopy, as described elsewhere.<sup>35</sup> The degree of CNT sedimentation is reversely proportional to the concentration of CNT in the solution so that it can denote the dispersion stability of the CNTs in the solution. A 10:1 SDS:CNT ratio was sufficient to effectively disperse CNTs in aqueous solution (Appendix A, Figure A-3), which is consistent with results from Sun et al.<sup>34</sup> and Richard et al.<sup>36</sup> Using the SDS:CNT ratio of 10:1, different concentrations of CNT were produced in DI water. Then CNT were coated on the adsorbent by placing 2 grams of the adsorbent beads into a sample tube containing 10 ml stabilized CNT solutions and heating to 120 °C using MW irradiation. A stream of 0.5 SLPM  $\text{N}_2$  (99%) was used to purge the sample tube and carry evaporated water from the sample.

### 4.3.3 Characterizations and Measurements

#### 4.3.3.1 *Raman spectroscopy*

All Raman spectra were acquired at room temperature using a Raman microscope system (DXR2, Thermo Scientific). In this study, the photon source was a powerful monochromatic visible light at the 532 nm wavelength. The detector scans for the scattered photons at the wavelength range of 500 to 3000  $\text{cm}^{-1}$ . Maximum power and exposure time were set to 1 mW and 10 s, respectively.

#### 4.3.3.2 *Scanning helium ion microscopy*

The morphology of deposited CNTs on the adsorbent surface was obtained using HIM (Zeiss Orion Nanofab). Unlike scanning electron microscopy, imaging of nonconductive samples (such as Optipore V503) with HIM results in a net surface positive charge on the sample, which is neutralized by an in situ electron flood gun.<sup>37</sup> The difference in conduction properties between CNTs and polymer were exploited to gain enhanced contrast images with high spatial resolution. The images were acquired using  $\text{He}^+$  ions with an accelerating voltage of 27 kV, working distance of 8.5 mm, scan dwell time of 5  $\mu\text{s}$ , and resolution of 200 nm.

#### 4.3.3.3 *Micropore surface analysis*

The specific surface area, total pore volume and pore size distribution of samples were calculated from  $\text{N}_2$  adsorption isotherms obtained using micropore surface analysis (iQ2MP, Quantachrome). The  $\text{N}_2$  adsorption isotherms were measured at  $-196\text{ }^\circ\text{C}$ , maintained using a liquid nitrogen bath. All samples were outgassed at  $120\text{ }^\circ\text{C}$  for 5h before adsorption measurements. The specific surface area was calculated based on the Brunauer–Emmett–Teller (BET) method within the relative

pressure values of  $10^{-3}$  to 0.04. Micropore volume was calculated based on the Dubinin Astakhov method within the relative pressure values of  $10^{-7}$  to 0.02. The pore size distribution (PSD) was calculated by the density function theory method within the relative pressure values of  $10^{-7}$  to 0.98. Finally, total pore volume was calculated based on the volume of adsorbed nitrogen at a relative pressure of 0.98.

#### 4.3.3.4 *Heptane adsorption isotherm*

A gravimetric sorption analyzer (TA Instruments, model VTI-SA) was used to measure heptane adsorption in ultra-pure N<sub>2</sub> (99.998%) at 25 °C and a relative pressure range of 0.02–0.9. Typically,  $10.0 \pm 0.5$  mg of adsorbent was oven dried for at least 24 h at 120 °C before heptane adsorption. Adsorption at each relative pressure continued until a stable mass was achieved ( $< 0.01$  wt% change in 5 min) indicating an equilibrium state. Mass changes were logged to calculate adsorption capacity at each relative pressure.

#### 4.3.3.5 *Derivative thermo-gravimetric analysis*

Derivative thermo-gravimetric analysis (DTG) was performed on a thermo-gravimetric analyzer (TGA/DSC 1, Mettler Toledo) to analyze thermal stability of the samples. Samples of approximately 20 mg were weighed and heated from room temperature to 220 °C at a heating rate of 5 °C/min under a 50 ml/min flow of N<sub>2</sub> (99.998%). Prior to each experiment, samples were dried in an oven at 120 °C for at least 24 hr.

#### 4.3.3.6 *Dielectric properties measurement*

Dielectric properties of CNT-coated and as-received Optipore V503 beads were measured using the open ended probe method.<sup>38</sup> The method uses a dielectric probe (Keycom) coupled to a vector network analyzer (VNA, Rohde and Schwarz), and a data acquisition software. A quartz tube was used to hold the sample. Reflection coefficients of electromagnetic waves were determined at 2.45 GHz, room temperature, and atmospheric pressure. The VNA analyzes the reflected radiation from the adsorbents from which the complex permittivity is calculated. Prior to each experiment, the probe was calibrated by short, open and standard sample termination.

#### 4.3.3.7 *Heating rate and microwave heating capacity*

Previous studies showed the importance of MW heating rate in desorption experiments.<sup>39</sup> In this study, heating rates were experimentally measured at different MW power densities, as calculated in Eq. 4.

$$\text{Heating rate} = \frac{T_{\text{final}} - T_{\text{initial}}}{\Delta t} \quad \text{Eq. 4}$$

where  $T_{\text{final}}$  is the sample temperature at the steady state condition after MW irradiation,  $T_{\text{initial}}$  is the sample temperature before MW irradiation, and  $\Delta t$  is the heating time needed to reach the final temperature. MW heating capacity was also defined and calculated as the amount of MW energy required to increase the temperature of 1 gram of adsorbent by 1 °C.

### **4.3.4 Cyclic Heptane Adsorption and Microwave-assisted Desorption**

#### **4.3.4.1 *Adsorption setup***

Adsorption experiments were conducted at 25 °C using 4 g samples contained in a quartz tube. A stream of 500 ppm of heptane in air was generated by injecting liquid heptane into a 10 SLPM stream of air using a syringe pump (KD Scientific, model 200). Heptane concentration in air was measured by a flame ionization detector (FID, Baseline-Mocon Inc., series 9000). After the heptane concentration reached a stable value, adsorption was initiated by flowing the heptane-containing air stream through the quartz tube. Adsorption continued until the heptane concentration at the tube's exit reached the inlet concentration.

#### **4.3.4.2 *Microwave regeneration setup***

The MW-assisted regeneration setup (Figure 4-1) consisted of a MW generator equipped with a 2.45 GHz magnetron, an isolator (National Electronics), a three-stub tuner (National Electronics), and a single mode waveguide applicator. A dual channel MW power meter (E4419B, Agilent) and directional coupler with 60 dB attenuation (Mega Industries) were employed to measure forward and reverse power. A fibreoptic sensor (Reflex, Neoptix), known for its transparency to electromagnetic fields, was used to measure the bed temperature. A sliding short was also used before each set of experiments to maximize MW energy transfer to the sample. A data acquisition and control (DAC) system equipped with LabVIEW software recorded temperature, and forward and reverse power. All MW heating experiments were carried out at constant MW applied power.

During regeneration, the adsorbent bed was continuously irradiated with 15 W MW power and purged with 1 SLPM N<sub>2</sub> (99%) for 60 minutes. The FID was used to measure the effluent heptane concentration. Cumulative desorption efficiency as a function of elapsed desorption time was calculated based on the amount of heptane desorbed relative to the total amount adsorbed, as indicated in Eq. 5.

$$\eta_t(\%) = \frac{\sum_0^t C P Q \Delta t M_w}{RT(W_{AA} - W_{BA})} \times 100 \quad \text{Eq. 5}$$

where  $\eta_t$  is the desorption efficiency at time  $t$ ,  $C$  is effluent heptane concentration,  $P$  is the pressure,  $Q$  is the purge gas flow rate,  $\Delta t$  is the time period between two recorded concentrations,  $R$  is the ideal gas constant,  $T$  is the room temperature,  $W_{AA}$  is the adsorbent weight after adsorption, and  $W_{BA}$  is the adsorbent weight before adsorption.

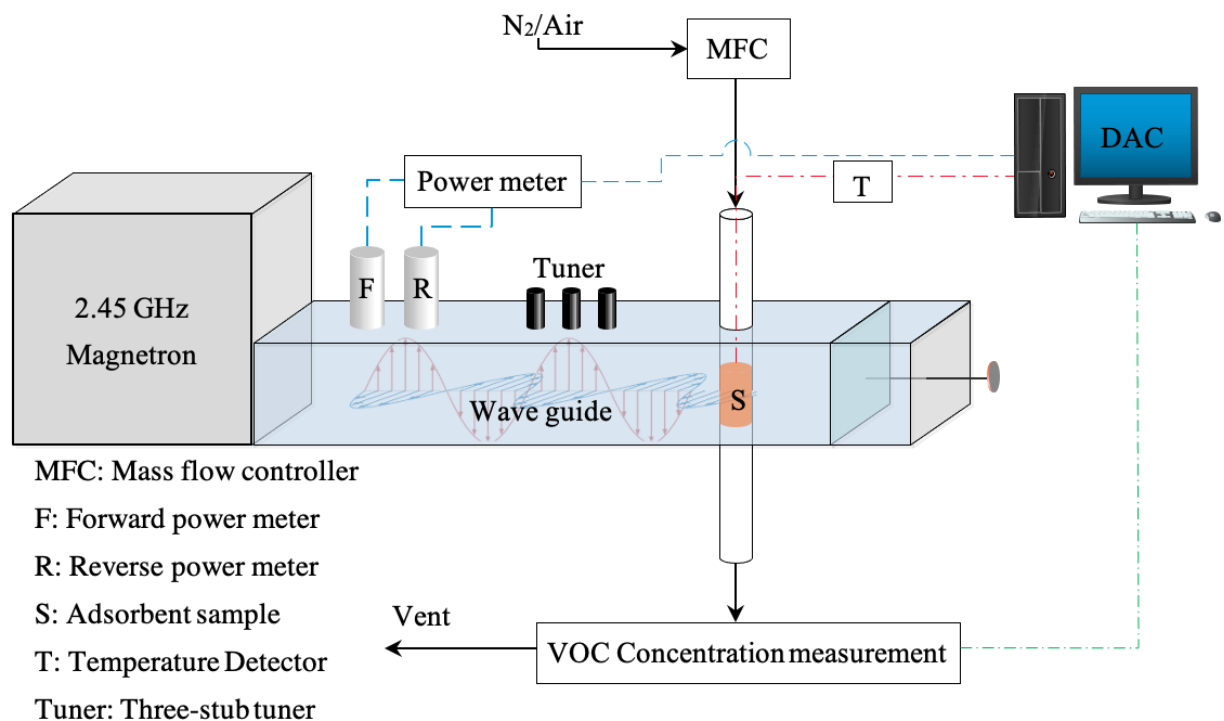


Figure 4-1. Schematic diagram of MW-assisted regeneration setup.

## 4.4 Results and Discussion

### 4.4.1 Raman Spectroscopy and HIM

The physical deposition of CNT on the adsorbent surface was characterized by Raman spectroscopy and HIM micrographs (Figures 4-2 and 4-3). CNTs have Raman spectra that can be distinguished from the adsorbent background. The Raman spectrum of a CNT sample typically has three main characteristic peaks at  $1350\text{ cm}^{-1}$ ,  $1600\text{ cm}^{-1}$  and  $2700\text{ cm}^{-1}$ .<sup>40</sup> Figure 4-2 depicts Raman spectra of the CNT-coated and as-received adsorbent samples. The CNT-coated samples

have three prominent peaks at  $1350\text{ cm}^{-1}$ ,  $1570\text{ cm}^{-1}$  and  $2690\text{ cm}^{-1}$ . The first peak (at  $1350\text{ cm}^{-1}$ ), called D band, emerges from the disordered  $\text{sp}^2$  bonding in C-C bonds. This peak is seen for all types of  $\text{sp}^2$  carbon materials such as carbon black, amorphous carbons and graphite.<sup>41</sup> The second peak (at  $1570\text{ cm}^{-1}$ ) called G band, arises due to the stretching of  $\text{sp}^2$  bonding in C-C bonds. The third peak (at  $2700\text{ cm}^{-1}$ ) is the second order harmonic of the D band and is called G' band.<sup>42</sup> The intensity of the D, G and G' bands of CNT-coated adsorbent follows the CNT loading on the adsorbent surface.

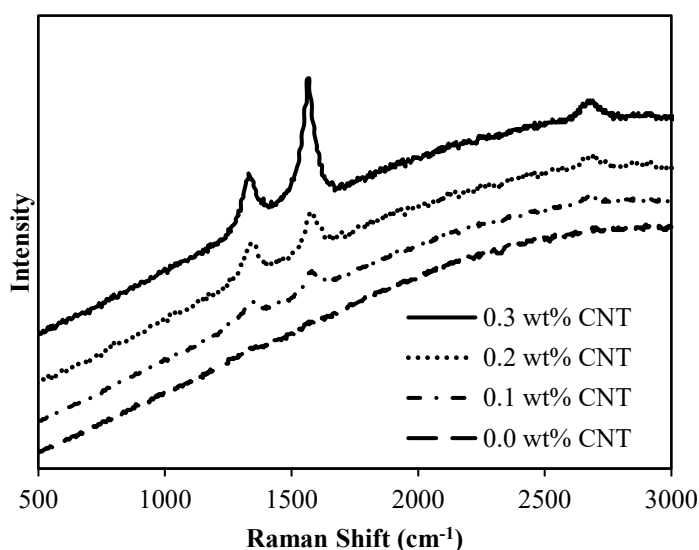


Figure 4-2. Raman spectra of CNT-coated and as-received Optipore V503 samples.

HIM analysis was done to examine the effect of CNT deposition on the adsorbent surface morphology and to investigate the uniformity of CNT distribution over the adsorbent surface (Figure 4-3). For CNT-coated samples, nanotube bundles are visible on the porous adsorbent surface. The surface was gradually and uniformly covered with nanotubes as the CNT loading

increased to 0.3 wt %. Uniform CNT distribution on the adsorbent surface is needed for uniform MW heating, but can increase mass transfer resistance for VOC diffusion into the adsorbent pores.

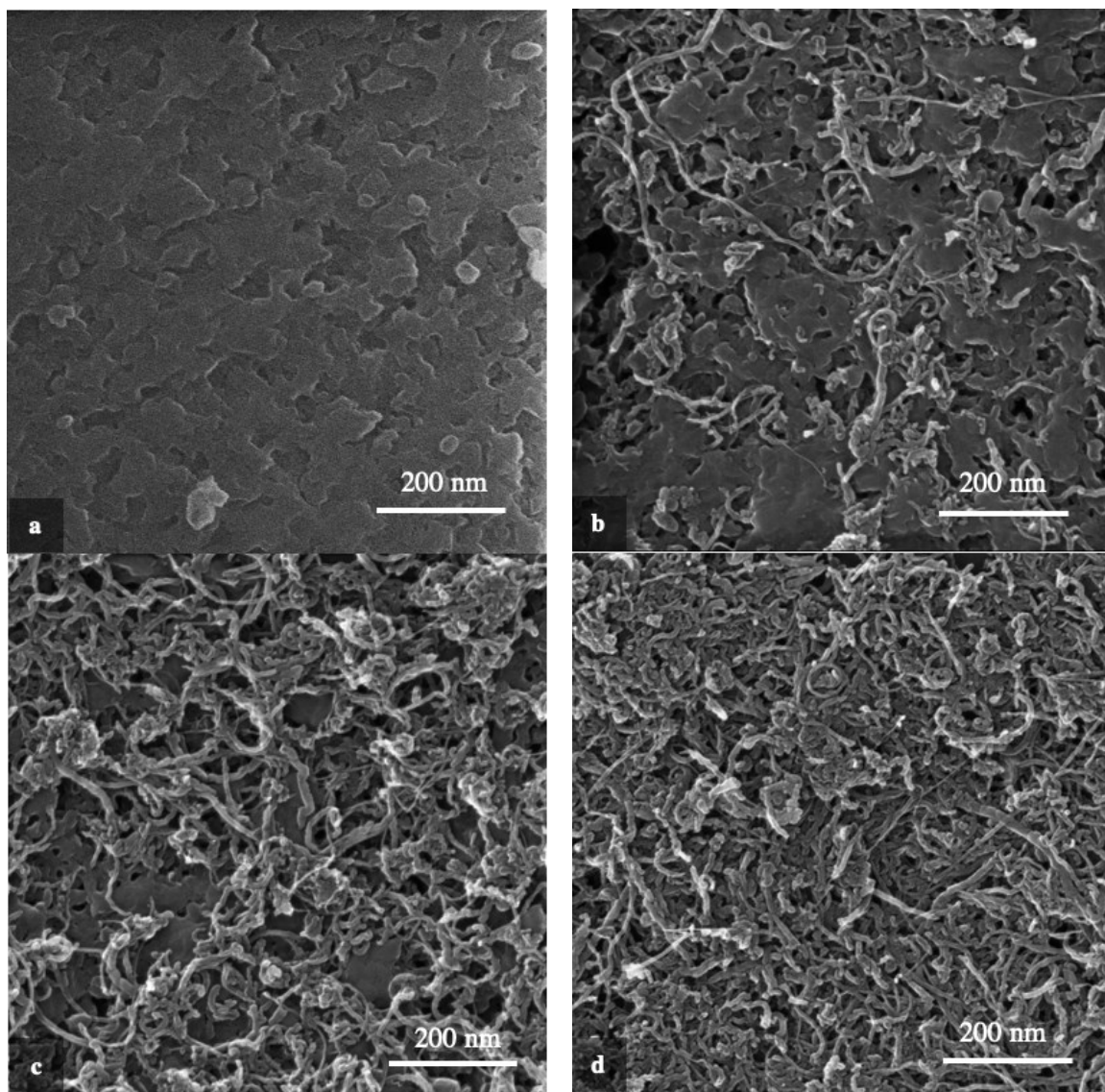


Figure 4-3. HIM images obtained for a) 0.0 wt%, b) 0.1 wt%, c) 0.2 wt%, and d) 0.3 wt% of CNT on Optipore V503.

#### 4.4.2 Surface Property Measurement

The effect of CNT loading on the total pore volume, micropore volume, BET surface area, and pore size distribution was investigated using N<sub>2</sub> adsorption (Figure 4-4 and 4-5). The total pore volume and micro pore volume are highest in the as-received adsorbent and decreased by 28% as CNT content increased from 0 to 0.3 wt% (Figure 4-4.a). Similarly, the BET surface area decreased by 25 % (Figure 4-4.b). The effect of the SDS surfactant on the adsorbent surface properties was also investigated by coating the adsorbent with an amount of SDS similar to that used in the CNT dispersions. Comparison of the surface properties of SDS- and CNT-coated samples reveals that the SDS in the coating solution is the main contributor to the reduction in BET surface area, micropore volume and total pore volume. According to the molecular dynamics simulation by Bruce et al., the effective radius of a SDS micelle in water is around 22 Å<sup>43</sup>, which is sufficiently small to be able to contribute to blockage of the adsorbent's micropores during CNT deposition. In addition, the SDS concentration in the CNT solution is less than the critical micelle concentration, therefore individual SDS molecules may be diffusing into the adsorbent pores. As expected, CNT-coated samples show a clear reduction in the micropore region of the pore size distributions (Figure 4-5). The micropore region is particularly important for VOC adsorption since their kinetic diameters are usually less than 20 Å.

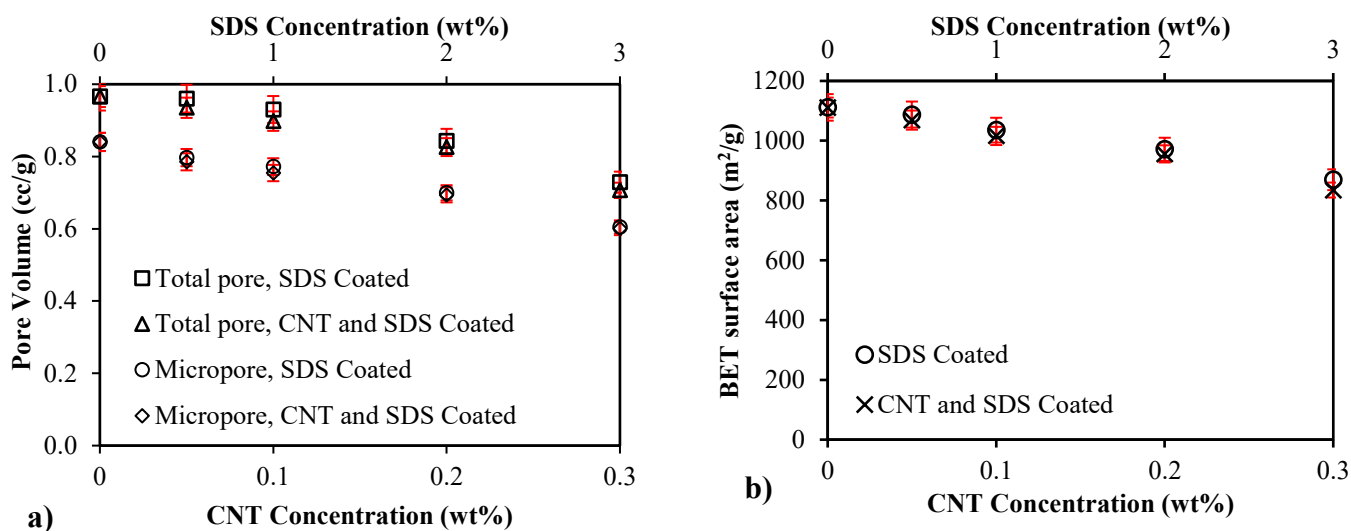


Figure 4-4. Effect of SDS and CNT deposition on a) pore volume and b) BET surface area of Optipore V503.

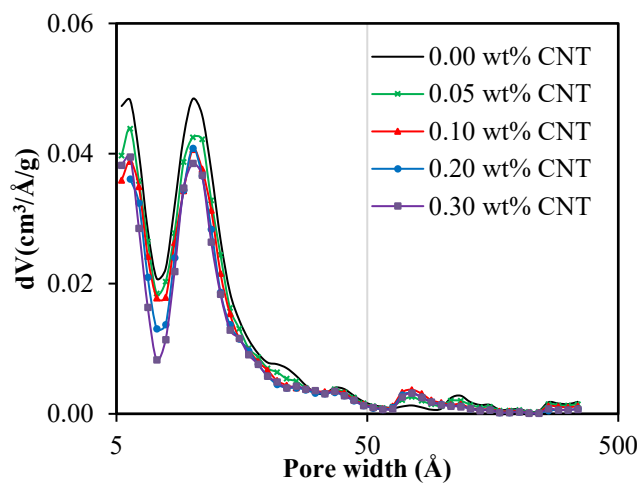


Figure 4-5. Pore size distribution of the CNT and SDS coated Optipore V503.

#### 4.4.3 Heptane Adsorption Isotherms

Since the porosity of the adsorbent was changed during CNT coating (Figure 4-4), additional investigation was completed to quantify the VOC adsorption performance of CNT-coated samples. Adsorption isotherms of CNT-coated and as-received adsorbent were measured using a

gravimetric sorption analyzer (Figure 4-6). Heptane with a kinetic diameter of 4.3 Å was used as adsorbate to determine the CNT-coating effect on adsorption.<sup>44</sup> Heptane's linear structure and small kinetic diameter permits diffusion into irregular pores with narrow throats. As suggested by the porosity analysis, heptane adsorption capacity decreased by up to 19 % with CNT loading of 0.3 wt%. For comparison, Figure 4-6 also depicts the heptane adsorption capacity of CNT at different relative pressures. The adsorption contribution of the deposited CNT is negligible due to the low concentration deposited (less than 0.3wt%) and lower adsorption capacity compared to the as-received adsorbent.

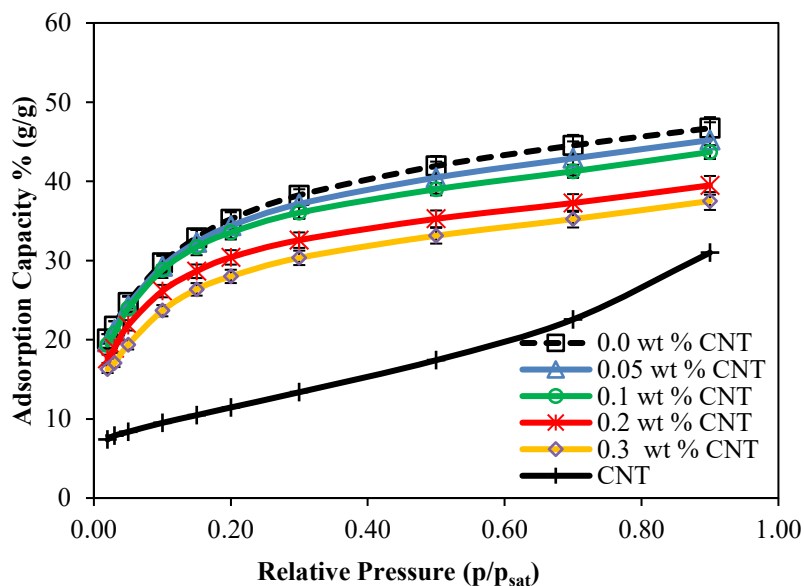


Figure 4-6. Heptane adsorption isotherms of virgin Optipore V503, CNT-coated Optipore V503, and CNT. The error bars represent standard deviations of two runs.

#### 4.4.4 DTG Analysis

DTG analysis was carried out to investigate the effect of CNT addition on the adsorbent thermal stability up to 220 °C (the Optipore V503 material significantly degrades above this temperature). The DTG profiles for CNT-coated and as-received adsorbent samples (Figure 4-7) show the rate of mass loss from the sample as the temperature was steadily increased. For all samples, a DTG peak around 40 °C is attributed to desorption of water vapor adsorbed from air<sup>45</sup>. No additional mass loss occurred until about 220 °C. All as-received and CNT-coated samples showed similar thermal stability.

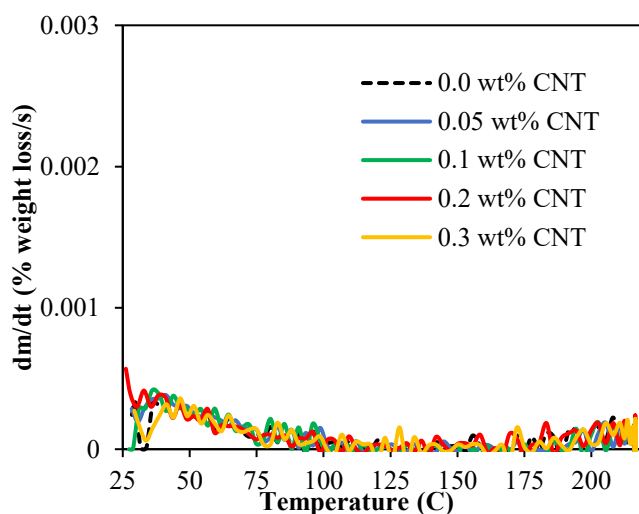


Figure 4-7. Thermograms of virgin adsorbent and CNT-coated Optipore V503

#### 4.4.5 Dielectric Property Analysis

The effect of CNT and SDS contents on the complex permittivity of Optipore V503 and MW penetration depth (at 2.45 GHz and room temperature) are presented in Figure 4-8. Increases of 160% and 2790% in the dielectric constant and loss factor were obtained with a CNT loading of

0.3 wt %, respectively. The observed nonlinear increase in the dielectric property values with the addition of trace amount of CNT can be due to exceeding the percolation threshold of CNT. Percolation threshold is defined as the minimum nanoparticle concentration that forms a continuous network in a composite. Previous studies showed significant change in the electrical conductivity and dielectric properties of polymers around the percolation threshold.<sup>46-48</sup> Therefore, this suggests that the CNT percolation threshold is less than 0.3 wt%. This is consistent with Qin et al.'s study of MW absorption of polymeric composites filled with carbonaceous particles, who estimated that the percolation threshold of a CNT with an aspect ratio of 1100 is between 0.1 to 0.2 wt%.<sup>49</sup> Figure 4-8.a also shows that SDS content has a negligible effect on both dielectric constant and loss factor of the adsorbent. Vadivel et al. similarly showed that SDS can considerably increase the dielectric loss factor of  $\text{CoFe}_2\text{O}_4$  at low frequencies (less than 1000 Hz), but not at higher frequencies.<sup>20</sup> This can be explained by the fact that dielectric properties of many materials decline with increasing electromagnetic field frequency. Therefore, SDS dielectric constant and loss factor at the 2.45 GHz used in the present study may not be large enough to change the adsorbent's dielectric properties. Figure 4-8.b presents the penetration depth of CNT- and SDS-coated adsorbent samples which were calculated based on Eq. 3 and the measured dielectric property values. The penetration depth decreased from 69 cm to 4 cm as the CNT content increased from 0 to 0.3 wt%. This reduction in penetration depth (>94 %) can significantly improve the MW absorption efficiency in the adsorbent bed. Further CNT deposition would be expected to decrease the penetration depth to less than the reactor diameter which could detrimentally increase the temperature gradient inside the bed.

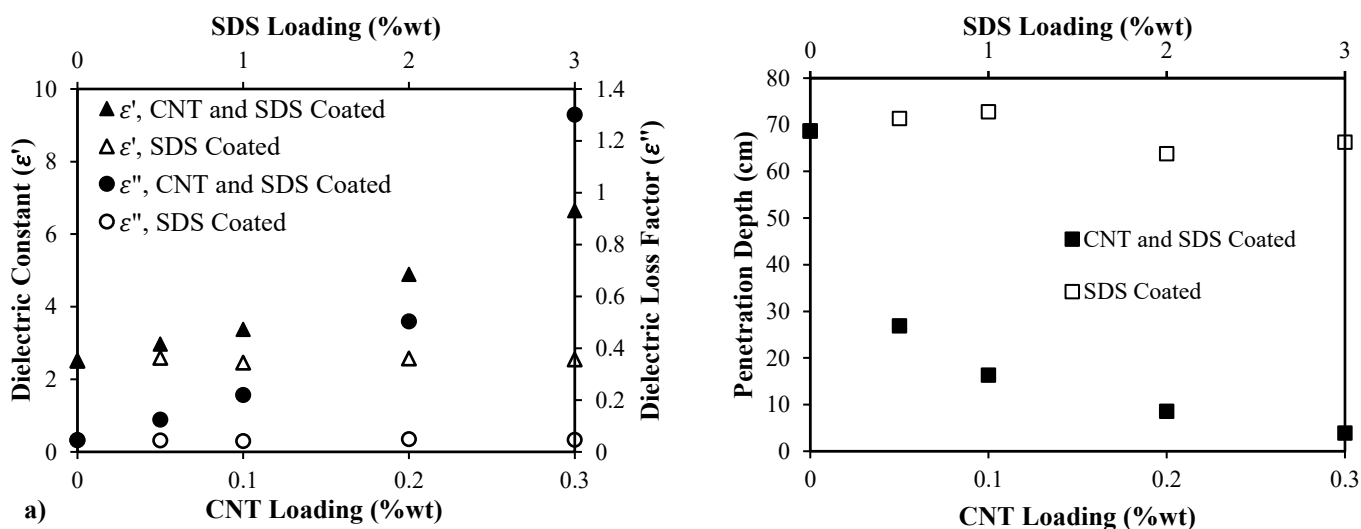


Figure 4-8. Effect of CNT and SDS loading on a) dielectric properties and b) penetration depth of virgin adsorbent and CNT-coated adsorbent.

#### 4.4.6 Heating Rate and Microwave Heating Capacity

To evaluate the effectiveness of MW heating for CNT-coated adsorbent samples, 4 grams samples were irradiated at different power densities in the MW applicator while monitoring sample temperatures (Figure 4-9.a). The calculated heating rates were greatly increased by adding small amounts of high loss factor CNT. In other words, the MW energy required to reach a particular temperature was greatly reduced by adding CNT.

MW heating capacity, defined as the amount of applied MW energy needed to raise the temperature of 1 gram of adsorbent by  $1^{\circ}\text{C}$ , was determined based on energy consumption. Figure 4-9.b shows measured MW heating capacity values at each CNT content. These results show that the MW heating capacity is reduced from 722 J/g-C for the as-received adsorbent to 13 J/g-C with 0.3 wt % of CNT, a 98 % reduction in applied MW energy. This reduction stems from the highly

MW-absorptive nature of CNTs compared to the adsorbent porous resin. These results are consistent with Eq. 2 that shows the dielectric loss factor and the specific heat of the irradiated adsorbent determine the heating rate.

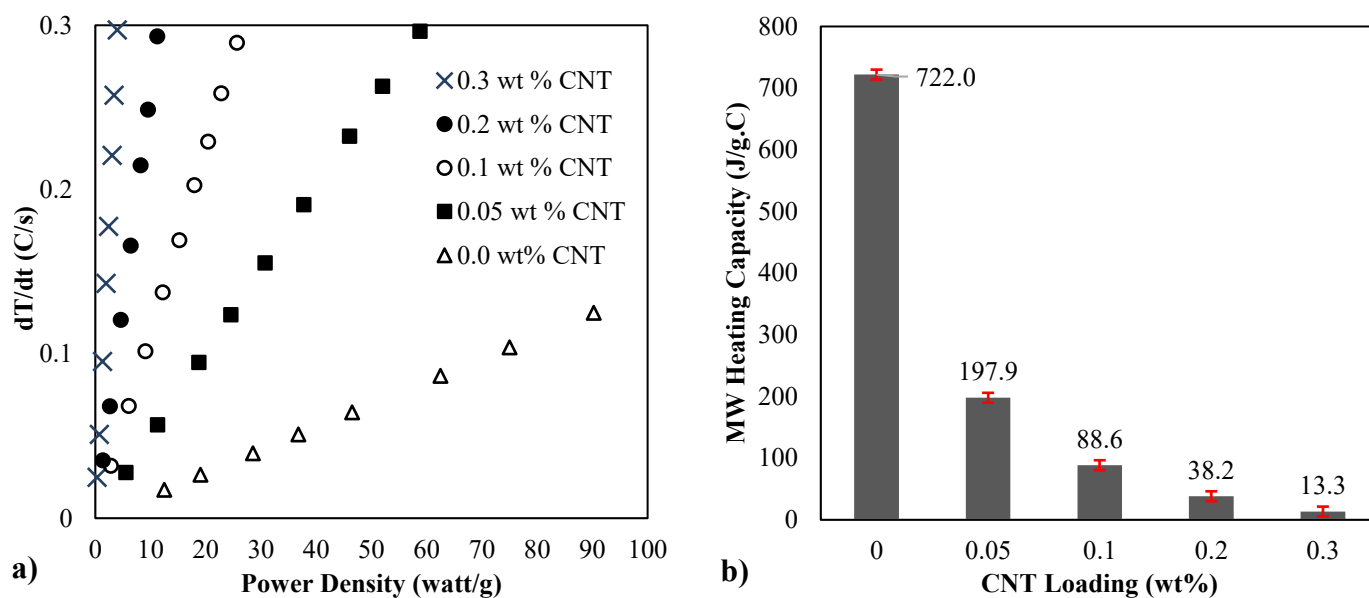


Figure 4-9. a) Effect of MW power level on the heating rate; b) Effect of CNT loading on the MW heating capacity. The error bars represent standard deviations calculated based on three rounds of experiments.

#### 4.4.7 Microwave-assisted Desorption

Successive cycles of heptane adsorption and MW-assisted desorption were carried out 5 times to determine the effectiveness of MW heating as a means to regenerate the spent adsorbents. MW-assisted regeneration was conducted at a constant power density of  $3.75 \frac{W}{g_{adsorbent}}$  for 60 min.

Figure 4-10 depicts the 5-cycle breakthrough profiles for the CNT-coated and as-received adsorbent samples. In the first adsorption cycle (black dashed lines), higher CNT content on the adsorbent gradually decreased the breakthrough times and slopes. These impacts are consistent

with the effect of SDS on the textural properties of CNT-coated samples and the effect of CNT layer on the mass transfer inside the bed. With the exception of the 0.3 wt% sample, all subsequent adsorption/regeneration cycles (2 through 5) showed further breakthrough time reduction. This reduction is due to non-desorbed heptane (incomplete regeneration) during the previous regeneration cycle which reduces the adsorption capacity of the bed. However, increasing the CNT content to 0.3 wt% improved MW heating to the extent that adsorption capacity of adsorbent was completely restored at each cycle.

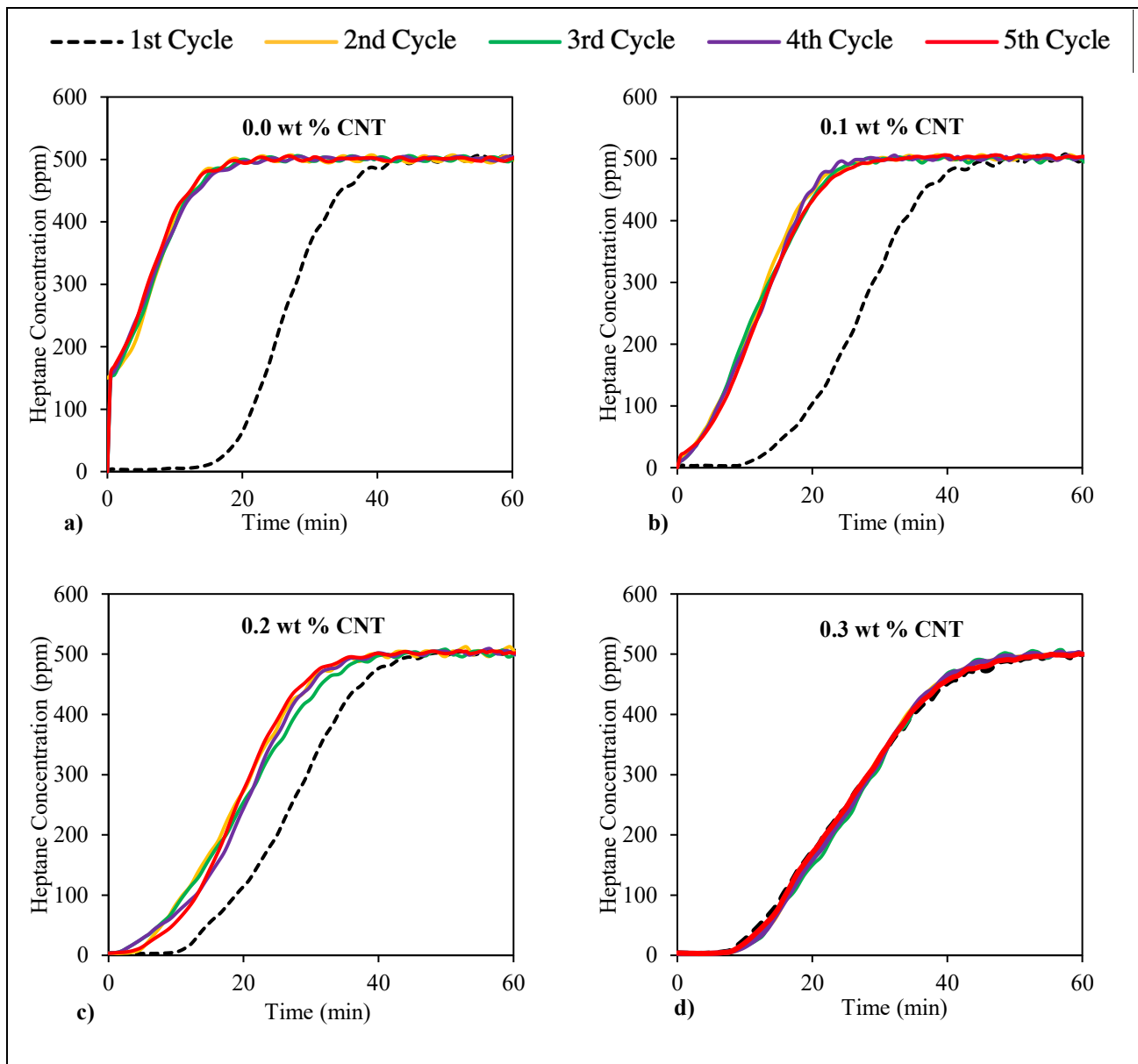
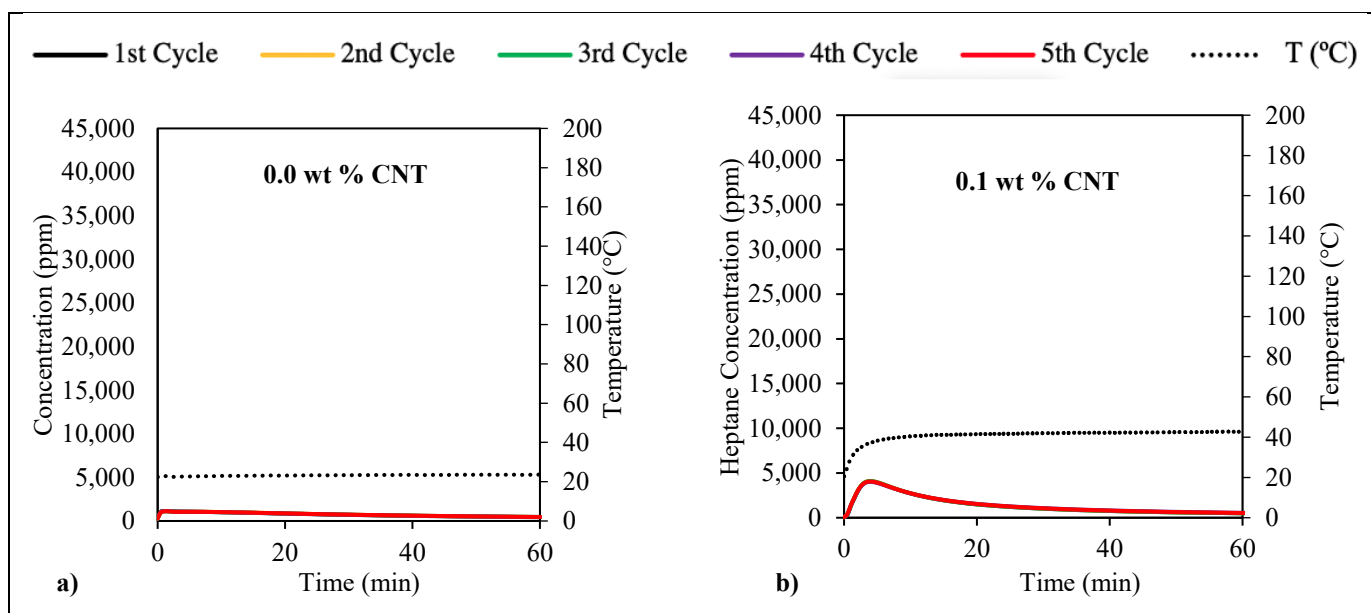


Figure 4-10. Adsorption breakthrough curves of heptane on a) 0 wt% CNT, b) 0.1 wt% CNT, c) 0.2 wt% CNT, and d) 0.3 wt% CNT-coated adsorbent.

Figure 4-11 shows the temperature and heptane concentration profiles during the regeneration of CNT-coated and as-received adsorbent samples. These results indicate that for the applied MW power density of  $3.75 \frac{W}{g_{adsorbent}}$ , the as-received adsorbent sample only reached 26 °C even after

60 minutes of MW heating while the 0.3 wt% CNT-coated sample reached 200 °C in 20 minutes. Lower CNT loading gave intermediate temperatures (42 °C for 0.1% and 75 °C for 0.2%). Higher temperature, ideally above the solvent boiling point (98 °C for n-heptane), is particularly important for effective regeneration of a VOC-laden adsorbent. Higher temperature during desorption also increases the diffusivity of VOCs in the adsorbent’s pores and thus reduces the energy needed to complete the regeneration.<sup>50</sup> As a result, the maximum heptane concentration in the effluent stream increased more than 40 times by increasing the CNT loading compared to the as-received adsorbent. This higher VOC concentration and shorter duration can be exploited for enhanced VOC recovery.



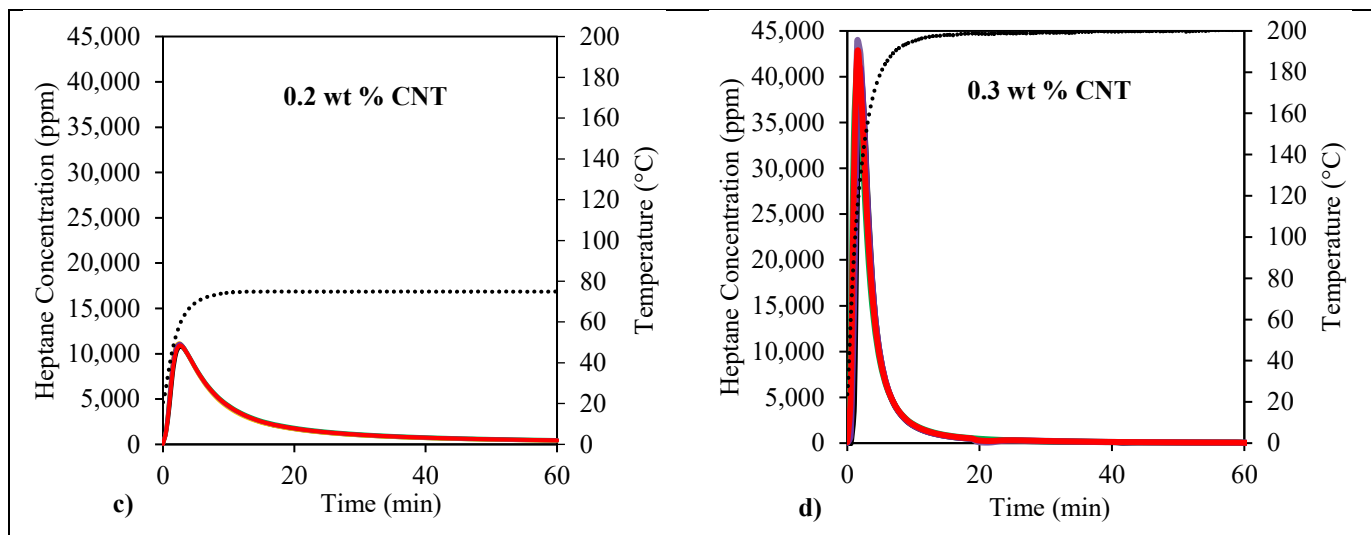
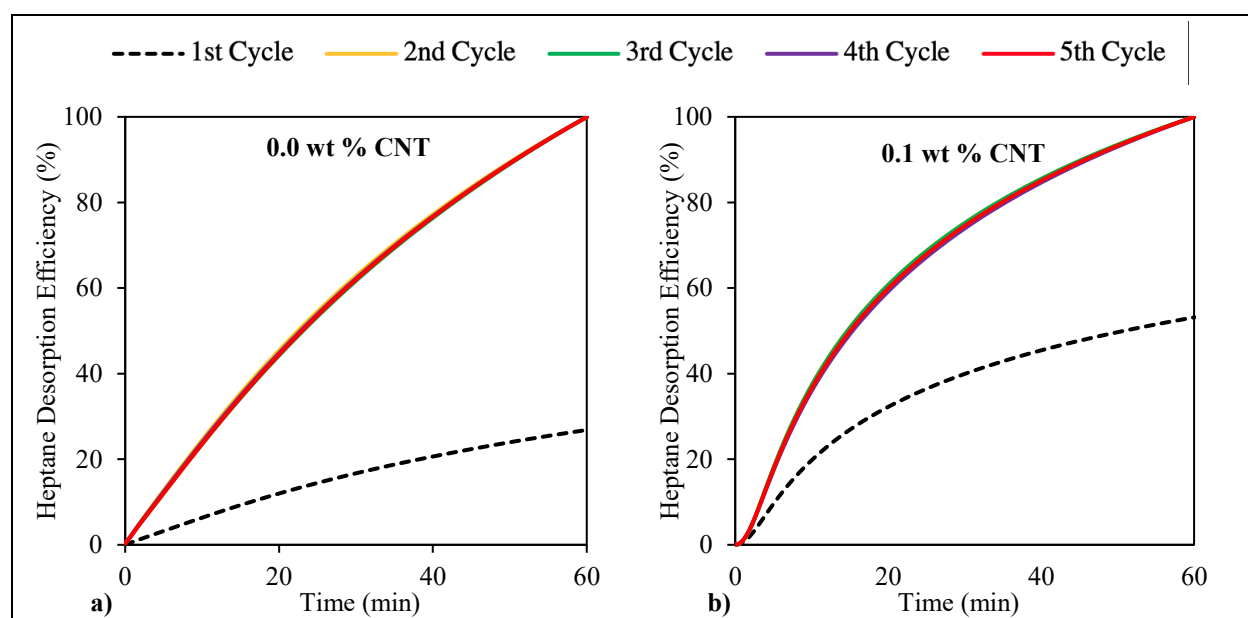


Figure 4-11. Heptane concentration and bed temperature during the regeneration of a) 0 wt% CNT, b) 0.1 wt% CNT, c) 0.2 wt% CNT, and d) 0.3 wt% CNT-coated adsorbent.

Desorption efficiency (Eq. 5) is shown versus regeneration time in Figure 4-12. Comparison of the first cycle desorption efficiency profiles (black dashed lines) again indicates the large improvements due to the addition of CNT to the adsorbent. After 10 minutes of MW heating, the 0.3 wt % CNT samples had lost more than 90 % of the adsorbed heptane while the next highest CNT content sample had lost only 45 %. The first cycle desorption efficiency profiles also show that 0.3 wt % CNT loading allowed complete regeneration in 60 min while the other samples still had undesorbed heptane that carried over to the next adsorption cycle. Desorption efficiency profiles for the 2<sup>nd</sup> to 5<sup>th</sup> cycles are overlapping and all reached 99 % or more after 60 minutes of MW heating. In the case of the 0-0.2 wt% samples, this occurs because the desorption efficiency of each cycle (as defined here) is expressed relative to the amount of heptane adsorbed in the previous adsorption cycle. After the first cycle, the adsorption capacities of these samples were reduced which led to higher calculated values for the desorption efficiency despite the lower

amounts of heptane removed. The subsequent adsorption steps are fully restoring the heptane removed in each prior MW regeneration step. We see no indication of non-desorbable heel accumulation in these results, as expected. Our prior studies have shown that certain VOCs, such as 1,2,4-trimethylbenzene, are prone to forming heel that is not fully removed during desorption and progressively decreases the adsorption capacity.<sup>51</sup> Heptane is much less susceptible to this issue. Finally, desorption efficiency profiles revealed that coating adsorbent with CNT at 0.1, 0.2 and 0.3 wt % improves the overall desorption efficiency by 103%, 211% and 284%, relative to the uncoated adsorbent.



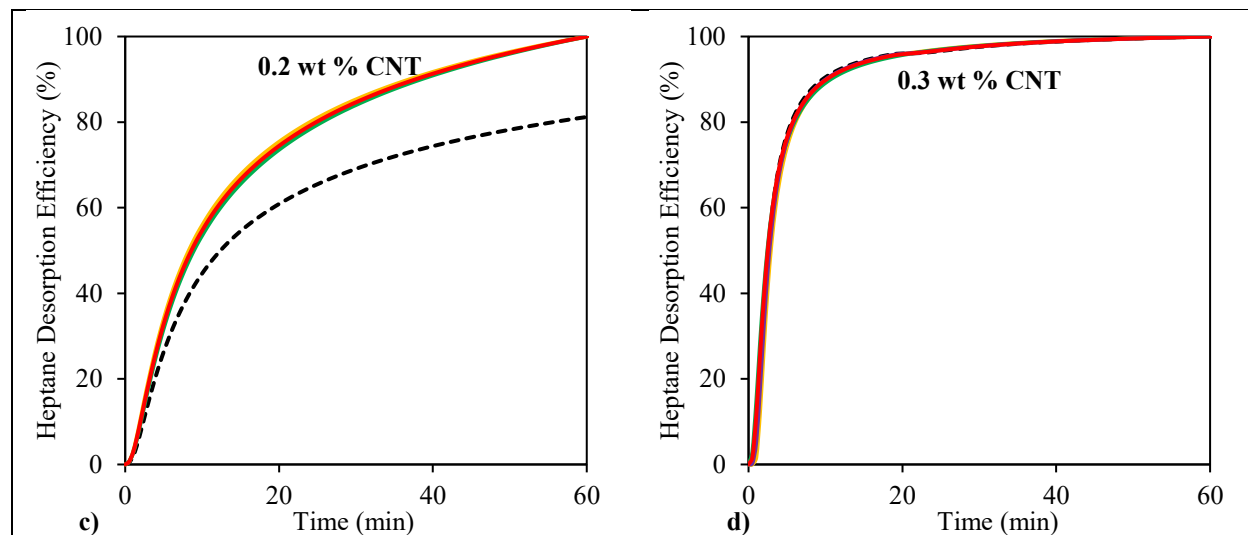


Figure 4-12. Heptane desorption efficiency of a) 0 wt% CNT, b) 0.1 wt% CNT, c) 0.2 wt% CNT, and d) 0.3 wt% CNT coated adsorbent.

Heptane adsorption capacity (measured after each cycle by the gravimetric method) is shown in Figure 4-13. As expected from the surface property analysis and breakthrough profiles (Figures 4-4 and 4-10), the first cycle adsorption capacity decreased with successive increase in CNT loading. As shown earlier (Figure 4-4), this reduction in the adsorption performance is mainly due to the SDS diffusion during the coating process. However, having a larger CNT loading on the adsorbent, a notable increase ( $> 240\%$ ) in the 5<sup>th</sup> cycle adsorption capacity was achieved. This improvement in the 5<sup>th</sup> cycle adsorption capacity is attributed to the enhanced MW-assisted regeneration of adsorbents with higher CNT loadings (Figures 4-11 and 4-12).

To evaluate the performance of an adsorbent in a cyclic process, the working capacity of the adsorbent is often used. Working capacity can be calculated as the difference between the amount of VOC adsorbed in the adsorption step and the amount of VOC that remains adsorbed on the following regeneration step.<sup>52</sup> In this study, the working capacity is equal to the 5<sup>th</sup> cycle adsorption capacity as the amount of undesorbed heptane was constant between 2<sup>nd</sup> to 5<sup>th</sup> cycle. Figure 4-13

shows that working capacities of the 0.3 wt% CNT-coated samples were 240 % greater than the as-received adsorbent. Higher working capacity for a certain regeneration condition means smaller amount of adsorbent would be needed to reach a specific VOC removal efficiency.

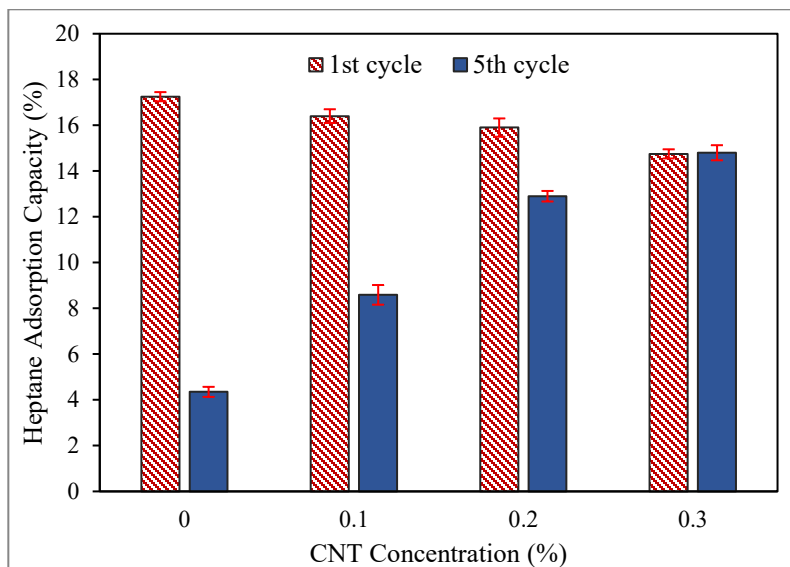


Figure 4-13. 1st and 5th cycle adsorption capacity of CNT coated and as-received Optipore V503. Error bars represent standard deviation of two runs.

#### 4.5 Conclusions

In this study, CNT was deposited on a porous polymeric resin adsorbent (Optipore V503) to enhance its regeneration by MW heating. Based on the results and discussion, the following conclusions can be obtained:

- Polymeric adsorbent beads can be successfully coated with CNT using SDS/CNT suspension as confirmed by HIM imaging and Raman spectroscopy.

- BET surface area and adsorption performance of the polymeric adsorbent decreased due to SDS diffusion into the microporous during CNT coating.
- CNT-coated and as received adsorbent samples demonstrated similar thermal stability based on TGA analysis.
- Coating Optipore with 0.3 wt% of CNT enhanced its dielectric constant and loss factor by 160% and 2790%, respectively.
- Needed MW energy to heat the bed for 1 °C was reduced by 98% with CNT coating in MW heating experiments.
- More than 284% improvement in the desorption efficiency of CNT coated samples was achieved in cyclic heptane adsorption/MW regeneration experiments.
- Up to 14 % reduction in the first cycle adsorption capacity and up to 237 % improvement in the working capacity for CNT-coated samples were obtained in cyclic adsorption capacity tests.

#### 4.6 References

- (1) Pezolt, D. J.; Collick, S. J.; Johnson, H. A.; Robbins, L. A. Pressure Swing Adsorption for VOC Recovery at Gasoline Loading Terminals. *Environmental Progress* **1997**, *16* (1), 16–19. <https://doi.org/10.1002/ep.3300160115>.
- (2) Xiu, G.; Li, P.; E. Rodrigues, A. Sorption-Enhanced Reaction Process with Reactive Regeneration. *Chemical Engineering Science* **2002**, *57* (18), 3893–3908. [https://doi.org/10.1016/S0009-2509\(02\)00245-2](https://doi.org/10.1016/S0009-2509(02)00245-2).
- (3) Price, D. W.; Schmidt, P. S. VOC Recovery through Microwave Regeneration of Adsorbents: Process Design Studies. *Journal of the Air & Waste Management Association* **1998**, *48* (12), 1135–1145. <https://doi.org/10.1080/10473289.1998.10463758>.
- (4) Ondon, B. S.; Sun, B.; Yan, Z. Y.; Zhu, X. M.; Liu, H. Effect of Microwave Heating on the Regeneration of Modified Activated Carbons Saturated with Phenol. *Applied Water Science* **2014**, *4* (4), 333–339. <https://doi.org/10.1007/s13201-013-0147-5>.
- (5) Cherbański, R. Regeneration of Granular Activated Carbon Loaded with Toluene – Comparison of Microwave and Conductive Heating at the Same Active Powers. *Chemical Engineering and Processing - Process Intensification* **2018**, *123*, 148–157. <https://doi.org/10.1016/j.cep.2017.11.008>.
- (6) Fayaz, M.; Shariaty, P.; Atkinson, J. D.; Hashisho, Z.; Phillips, J. H.; Anderson, J. E.; Nichols, M. Using Microwave Heating To Improve the Desorption Efficiency of High Molecular Weight VOC from Beaded Activated Carbon. *Environmental Science & Technology* **2015**, *49* (7), 4536–4542. <https://doi.org/10.1021/es505953c>.
- (7) Chowdhury, T.; Shi, M.; Hashisho, Z.; Sawada, J. A.; Kuznicki, S. M. Regeneration of Na-ETS-10 Using Microwave and Conductive Heating. *Chemical Engineering Science* **2012**, *75*, 282–288. <https://doi.org/10.1016/j.ces.2012.03.039>.

- (8) Roussy, G.; Zoulalian, A.; Charreyre, M.; Thiebaut, J. M. How Microwaves Dehydrate Zeolites. *The Journal of Physical Chemistry* **1984**, *88* (23), 5702–5708. <https://doi.org/10.1021/j150667a049>.
- (9) Clark, D. E.; Folz, D. C.; West, J. K. Processing Materials with Microwave Energy. *Materials Science and Engineering: A* **2000**, *287* (2), 153–158. [https://doi.org/10.1016/S0921-5093\(00\)00768-1](https://doi.org/10.1016/S0921-5093(00)00768-1).
- (10) Metaxas, A. C.; Meredith, R. J. Book Review: Industrial Microwave Heating. *Journal of Microwave Power and Electromagnetic Energy* **1989**, *24* (2), 108–108. <https://doi.org/10.1080/08327823.1989.11688082>.
- (11) Chandrasekaran, S.; Ramanathan, S.; Basak, T. Microwave Material Processing-a Review. *AIChE Journal* **2012**, *58* (2), 330–363. <https://doi.org/10.1002/aic.12766>.
- (12) Bradshaw, S. M.; Van Wyk, E. J.; De Swardt, J. B. Microwave Heating Principles and the Application to the Regeneration of Granular Activated Carbon. *Journal of The South African Institute of Mining and Metallurgy* **1998**, *98* (4), 201–210.
- (13) Funawatashi, Y.; Suzuki, T. Numerical Analysis of Microwave Heating of a Dielectric. *Heat Transfer - Asian Research* **2003**, *32* (3), 227–236. <https://doi.org/10.1002/htj.10087>.
- (14) Shariaty, P.; Jahandar Lashaki, M.; Hashisho, Z.; Sawada, J.; Kuznicki, S.; Hutcheon, R. Effect of ETS-10 Ion Exchange on Its Dielectric Properties and Adsorption/Microwave Regeneration. *Separation and Purification Technology* **2017**, *179*, 420–427. <https://doi.org/10.1016/j.seppur.2017.02.016>.
- (15) Yuen, F. K.; Hameed, B. H. Recent Developments in the Preparation and Regeneration of Activated Carbons by Microwaves. *Advances in Colloid and Interface Science* **2009**, *149* (1–2), 19–27. <https://doi.org/10.1016/j.cis.2008.12.005>.

- (16) Meier, M.; Turner, M.; Vallee, S.; Conner, W. C.; Lee, K. H.; Yngvesson, K. S. Microwave Regeneration of Zeolites in a 1 Meter Column. *AIChE Journal* **2009**, *55* (7), 1906–1913. <https://doi.org/10.1002/aic.11793>.
- (17) Yang, H.; Shan, J.; Li, J.; Jiang, S. Microwave Desorption and Regeneration Methods for Activated Carbon with Adsorbed Radon. *Adsorption* **2019**, *25* (2), 173–185. <https://doi.org/10.1007/s10450-019-00019-3>.
- (18) Nigar, H.; Navascués, N.; de la Iglesia, O.; Mallada, R.; Santamaría, J. Removal of VOCs at Trace Concentration Levels from Humid Air by Microwave Swing Adsorption, Kinetics and Proper Sorbent Selection. *Separation and Purification Technology* **2015**, *151*, 193–200. <https://doi.org/10.1016/j.seppur.2015.07.019>.
- (19) Meng, Q. B.; Yang, G.-S.; Lee, Y.-S. Preparation of Highly Porous Hypercrosslinked Polystyrene Adsorbents: Effects of Hydrophilicity on the Adsorption and Microwave-Assisted Desorption Behavior toward Benzene. *Microporous and Mesoporous Materials* **2013**, *181*, 222–227. <https://doi.org/10.1016/j.micromeso.2013.07.027>.
- (20) Vadivel, M.; Babu, R. R.; Arivanandhan, M.; Ramamurthi, K.; Hayakawa, Y. Role of SDS Surfactant Concentrations on the Structural, Morphological, Dielectric and Magnetic Properties of CoFe<sub>2</sub>O<sub>4</sub> Nanoparticles. *RSC Advances* **2015**, *5* (34), 27060–27068. <https://doi.org/10.1039/C5RA01162K>.
- (21) Wang, L.; Jia, X.; Li, Y.; Yang, F.; Zhang, L.; Liu, L.; Ren, X.; Yang, H. Synthesis and Microwave Absorption Property of Flexible Magnetic Film Based on Graphene Oxide/Carbon Nanotubes and Fe<sub>3</sub>O<sub>4</sub> Nanoparticles. *Journal of Materials Chemistry A* **2014**, *2* (36), 14940. <https://doi.org/10.1039/C4TA02815E>.
- (22) Sun, G.; Dong, B.; Cao, M.; Wei, B.; Hu, C. Hierarchical Dendrite-Like Magnetic Materials of Fe<sub>3</sub>O<sub>4</sub>,  $\gamma$ -Fe<sub>2</sub>O<sub>3</sub>, and Fe with High Performance of Microwave Absorption. *Chemistry of Materials* **2011**, *23* (6), 1587–1593. <https://doi.org/10.1021/cm103441u>.

- (23) Che, R. C.; Peng, L.-M.; Duan, X. F.; Chen, Q.; Liang, X. L. Microwave Absorption Enhancement and Complex Permittivity and Permeability of Fe Encapsulated within Carbon Nanotubes. *Advanced Materials* **2004**, *16* (5), 401–405. <https://doi.org/10.1002/adma.200306460>.
- (24) Oh, J.-H.; Oh, K.-S.; Kim, C.-G.; Hong, C.-S. Design of Radar Absorbing Structures Using Glass/Epoxy Composite Containing Carbon Black in X-Band Frequency Ranges. *Composites Part B: Engineering* **2004**, *35* (1), 49–56. <https://doi.org/10.1016/j.compositesb.2003.08.011>.
- (25) Chin, W. S.; Lee, D. G. Development of the Composite RAS (Radar Absorbing Structure) for the X-Band Frequency Range. *Composite Structures* **2007**, *77* (4), 457–465. <https://doi.org/10.1016/j.compstruct.2005.07.021>.
- (26) Wu, F.; Xie, A.; Sun, M.; Wang, Y.; Wang, M. Reduced Graphene Oxide (RGO) Modified Spongelike Polypyrrole (PPy) Aerogel for Excellent Electromagnetic Absorption. *Journal of Materials Chemistry A* **2015**, *3* (27), 14358–14369. <https://doi.org/10.1039/C5TA01577D>.
- (27) Wang, L.; Dang, Z.-M. Carbon Nanotube Composites with High Dielectric Constant at Low Percolation Threshold. *Applied Physics Letters* **2005**, *87* (4), 042903. <https://doi.org/10.1063/1.1996842>.
- (28) Chen, C. Y.; Pu, N. W.; Liu, Y. M.; Huang, S. Y.; Wu, C. H.; Ger, M. Der; Gong, Y. J.; Chou, Y. C. Remarkable Microwave Absorption Performance of Graphene at a Very Low Loading Ratio. *Composites Part B: Engineering* **2017**, *114*, 395–403. <https://doi.org/10.1016/j.compositesb.2017.02.016>.
- (29) Qing, Y.; Wang, X.; Zhou, Y.; Huang, Z.; Luo, F.; Zhou, W. Enhanced Microwave Absorption of Multi-Walled Carbon Nanotubes/Epoxy Composites Incorporated with Ceramic Particles. *Composites Science and Technology* **2014**, *102*, 161–168. <https://doi.org/10.1016/j.compscitech.2014.08.006>.

- (30) Dominguez, A.; Fernandez, A.; Gonzalez, N.; Iglesias, E.; Montenegro, L. Determination of Critical Micelle Concentration of Some Surfactants by Three Techniques. *Journal of Chemical Education* **1997**, *74* (10), 1227. <https://doi.org/10.1021/ed074p1227>.
- (31) Huang, Y. Y.; Terentjev, E. M. Dispersion of Carbon Nanotubes: Mixing, Sonication, Stabilization, and Composite Properties. *Polymers* **2012**, *4* (1), 275–295. <https://doi.org/10.3390/polym4010275>.
- (32) Duan, W. H.; Wang, Q.; Collins, F. Dispersion of Carbon Nanotubes with SDS Surfactants: A Study from a Binding Energy Perspective. *Chemical Science* **2011**, *2* (7), 1407. <https://doi.org/10.1039/c0sc00616e>.
- (33) Wusiman, K.; Jeong, H.; Tulugan, K.; Afrianto, H.; Chung, H. Thermal Performance of Multi-Walled Carbon Nanotubes (MWCNTs) in Aqueous Suspensions with Surfactants SDBS and SDS. *International Communications in Heat and Mass Transfer* **2013**, *41*, 28–33. <https://doi.org/10.1016/j.icheatmasstransfer.2012.12.002>.
- (34) Sun, Z.; Nicolosi, V.; Rickard, D.; Bergin, S. D.; Aherne, D.; Coleman, J. N. Quantitative Evaluation of Surfactant-Stabilized Single-Walled Carbon Nanotubes: Dispersion Quality and Its Correlation with Zeta Potential. *The Journal of Physical Chemistry C* **2008**, *112* (29), 10692–10699. <https://doi.org/10.1021/jp8021634>.
- (35) Peyravi, A.; Keshavarz, P.; Mowla, D. Experimental Investigation on the Absorption Enhancement of CO<sub>2</sub> by Various Nanofluids in Hollow Fiber Membrane Contactors. *Energy and Fuels* **2015**. <https://doi.org/10.1021/acs.energyfuels.5b01956>.
- (36) Richard, C. Supramolecular Self-Assembly of Lipid Derivatives on Carbon Nanotubes. *Science* **2003**, *300* (5620), 775–778. <https://doi.org/10.1126/science.1080848>.
- (37) Dykas, M. M.; Poddar, K.; Yoong, S. L.; Viswanathan, V.; Mathew, S.; Patra, A.; Saha, S.; Pastorin, G.; Venkatesan, T. Enhancing Image Contrast of Carbon Nanotubes on Cellular Background Using Helium Ion Microscope by Varying Helium Ion Fluence. *Journal of microscopy* **2018**, *269* (1), 14–22. <https://doi.org/10.1111/jmi.12604>.

- (38) Brodie, G.; Jacob, M. V.; Farrell, P. 6 Techniques for Measuring Dielectric Properties. In *Microwave and Radio-Frequency Technologies in Agriculture*; De Gruyter Open Poland, 2015; pp 52–77. <https://doi.org/10.1515/9783110455403-007>.
- (39) Mao, H.; Zhou, D.; Hashisho, Z.; Wang, S.; Chen, H.; Wang, H. H. Constant Power and Constant Temperature Microwave Regeneration of Toluene and Acetone Loaded on Microporous Activated Carbon from Agricultural Residue. *Journal of Industrial and Engineering Chemistry* **2015**, *21*, 516–525. <https://doi.org/10.1016/j.jiec.2014.03.014>.
- (40) Hiura, H.; Ebbesen, T. W.; Tanigaki, K.; Takahashi, H. Raman Studies of Carbon Nanotubes. *Chemical Physics Letters* **1993**. [https://doi.org/10.1016/0009-2614\(93\)90040-8](https://doi.org/10.1016/0009-2614(93)90040-8).
- (41) Brown, S. D. M.; Jorio, A.; Dresselhaus, M. S.; Dresselhaus, G. Observations of the D - Band Feature in the Raman Spectra of Carbon Nanotubes. *Physical Review B* **2001**, *64* (7), 073403. <https://doi.org/10.1103/PhysRevB.64.073403>.
- (42) Koyuncu, F.; Güzel, F.; Saygılı, H. Role of Optimization Parameters in the Production of Nanoporous Carbon from Mandarin Shells by Microwave-Assisted Chemical Activation and Utilization as Dye Adsorbent. *Advanced Powder Technology* **2018**, *29* (9), 2108–2118. <https://doi.org/10.1016/j.appt.2018.05.019>.
- (43) Bruce, C. D.; Berkowitz, M. L.; Perera, L.; Forbes, M. D. E. Molecular Dynamics Simulation of Sodium Dodecyl Sulfate Micelle in Water: Micellar Structural Characteristics and Counterion Distribution. *The Journal of Physical Chemistry B* **2002**, *106* (15), 3788–3793. <https://doi.org/10.1021/jp013616z>.
- (44) Funke, H. H.; Argo, A. M.; Baertsch, C. D.; Falconer, J. L.; Noble, R. D. Separation of Close-Boiling Hydrocarbons with Silicalite Zeolite Membranes. *Journal of the Chemical Society, Faraday Transactions* **1996**, *92* (13), 2499. <https://doi.org/10.1039/ft9969202499>.
- (45) Jahandar Lashaki, M.; Atkinson, J. D.; Hashisho, Z.; Phillips, J. H.; Anderson, J. E.; Nichols, M. The Role of Beaded Activated Carbon's Pore Size Distribution on Heel

- Formation during Cyclic Adsorption/Desorption of Organic Vapors. *Journal of Hazardous Materials* **2016**, *315*, 42–51. <https://doi.org/10.1016/j.jhazmat.2016.04.071>.
- (46) Chen, C.; Pan, L.; Jiang, S.; Yin, S.; Li, X.; Zhang, J.; Feng, Y.; Yang, J. Electrical Conductivity, Dielectric and Microwave Absorption Properties of Graphene Nanosheets/Magnesia Composites. *Journal of the European Ceramic Society* **2018**, *38* (4), 1639–1646. <https://doi.org/10.1016/j.jeurceramsoc.2017.11.052>.
- (47) Moulart, A.; Marrett, C.; Colton, J. Polymeric Composites for Use in Electronic and Microwave Devices. *Polymer Engineering and Science* **2004**, *44* (3), 588–597. <https://doi.org/10.1002/pen.20053>.
- (48) Shi, S.-L.; Zhang, L.-Z.; Li, J.-S. Electrical and Dielectric Properties of Multiwall Carbon Nanotube/Polyaniline Composites. *Journal of Polymer Research* **2009**, *16* (4), 395–399. <https://doi.org/10.1007/s10965-008-9241-z>.
- (49) Qin, F.; Brosseau, C. A Review and Analysis of Microwave Absorption in Polymer Composites Filled with Carbonaceous Particles. *Journal of Applied Physics* **2012**, *111* (6), 061301. <https://doi.org/10.1063/1.3688435>.
- (50) Cherbański, R.; Komorowska-Durka, M.; Stefanidis, G. D.; Stankiewicz, A. I. Microwave Swing Regeneration vs Temperature Swing Regeneration—Comparison of Desorption Kinetics. *Industrial & Engineering Chemistry Research* **2011**, *50* (14), 8632–8644. <https://doi.org/10.1021/ie102490v>.
- (51) Niknaddaf, S.; Atkinson, J. D.; Shariaty, P.; Jahandar Lashaki, M.; Hashisho, Z.; Phillips, J. H.; Anderson, J. E.; Nichols, M. Heel Formation during Volatile Organic Compound Desorption from Activated Carbon Fiber Cloth. *Carbon* **2016**, *96*, 131–138. <https://doi.org/10.1016/j.carbon.2015.09.049>.
- (52) Raganati, F.; Chirone, R.; Ammendola, P. CO<sub>2</sub> Capture by Temperature Swing Adsorption: Working Capacity As Affected by Temperature and CO<sub>2</sub> Partial Pressure.

*Industrial & Engineering Chemistry Research* **2020**, *59* (8), 3593–3605.  
<https://doi.org/10.1021/acs.iecr.9b04901>.

# **CHAPTER 5: POROUS CARBON BLACK/POLYMER COMPOSITES FOR VOC ADSORPTION AND EFFICIENT MICROWAVE-ASSISTED DESORPTION**

## **5.1 Chapter Overview**

The previous chapter demonstrated that the deposition of small amounts of CNT on a polymeric adsorbent substantially enhances its regeneration with microwave (MW) heating. However, BET surface area and adsorption performance of the polymeric adsorbent decreased due to SDS diffusion into the micropores during CNT coating. In this chapter, carbon black (CB) was selected as an inexpensive MW absorptive material (MAM) to be incorporated into the structure of a porous hypercrosslinked polymer (HCP) through in-situ polymerization. Combining the MW absorptive ability of CB particles with the excellent VOC adsorption performance of HCPs can provide a lightweight composite adsorbent for use in cyclic VOC adsorption/MW regeneration systems. CB filled composites were synthesized from (4, 4'-bis ((chloromethyl)-1, 1'-biphenyl) + (benzyl chloride)) via Friedel-Crafts reaction. Fourier-transform infrared spectroscopy and helium ion microscopy were employed to confirm the synthesis of the HCP and CB/HCPs composites. Synthesized composites were characterized using thermo-gravimetric analysis, dielectric property measurement, BET analysis and gravimetric sorption analysis. In addition, adsorption and MW-assisted desorption of hexane was carried out on HCP and CB/HCPs and MW regeneration efficiencies were compared.

## 5.2 Introduction

Adsorption on activated carbon has been widely used for capture and recovery of volatile organic compounds (VOCs). Recently, novel types of porous materials such as metal organic frameworks<sup>1,2</sup>, covalent organic polymers<sup>3,4</sup>, and hypercrosslinked polymers (HCPs)<sup>5,6</sup> have shown promising performance in the adsorption of VOCs. Among these adsorbents, HCPs exhibit desirable properties such as physicochemical stability, large surface area, adjustable surface chemical groups, high selectivity, and tunable pore structure. HCPs are typically synthesized by the post-cross-linking of precursor polymers in a solvent. Cross-linking of polymer chains prevents structural collapsing into non-porous state upon solvent removal and creates microporosity.<sup>7</sup> HCP porosity can be tuned by the degree of cross-linking, the temperature during cross-linking, the solvent, and the catalyst.<sup>8-10</sup> Ability to tailor HCP porosity allows it to be a suitable alternative to conventional sorbents used in chromatography, water treatment, and gas purification.<sup>11-14</sup> Long et al.<sup>15</sup> prepared a novel HCP (HY-1) with high specific surface area (1244 m<sup>2</sup>/g) and showed its higher adsorption capacity compared to activated carbon for the adsorption of benzene. Shi et al.<sup>6</sup> studied the performance of a microporous HCP and a microporous polymeric resin for the adsorption of gasoline vapors. Their results showed superior adsorption performance of HCP in treating gasoline vapor compared to the macroporous polymer without hypercrosslinking. Similarly, Zhang et al.<sup>16</sup> and Wang et al.<sup>17</sup> synthesized HCPs with high surface area (1300 m<sup>2</sup>/g and 1606 m<sup>2</sup>/g, respectively) and compared their adsorption performance with commercial HCPs. In both studies, large pore volume and surface area of newly synthesized HCPs lead to better performance compared to commercial polymeric adsorbents for VOC adsorption. Recent works by Long et al.<sup>18</sup> and Zhou et al.<sup>19</sup> developed HCPs with highly hydrophobic nature up to 60% and

80% relative humidity, respectively. Similarly, Wang et al.<sup>20</sup> synthesized a HCP with high surface area (1345 m<sup>2</sup>/g) using new external cross-linkers via one-step Friedel-Crafts reaction. The prepared HCP showed excellent hydrophobicity and adsorption capacity for benzene. Adsorbent hydrophobicity is a particularly important feature as the presence of water vapor in many air streams reduces its adsorption performance for VOCs due to competitive adsorption by water molecules.<sup>21</sup> Adsorbent regenerability is another important attribute, allowing recovery of the adsorbate and reuse of the adsorbent.

The use of microwave (MW) heating has emerged as an attractive technique for regenerating used adsorbents.<sup>22–24</sup> Using MW heating for adsorbent regeneration has several advantages over traditional convection/conduction heating including faster heating which enables heating to high temperatures, and higher desorption concentration with lower purge gas consumption. Moreover, the transfer of MW energy through radiation can heat the target material with lower energy loss compared to conventional thermal techniques.<sup>25–27</sup> MW heating principles have been discussed in detail by Jones and Falciglia.<sup>28,29</sup> The absorption of MW energy by a material depends on the material's complex permittivity,  $\epsilon$ , which consists of dielectric constant,  $\epsilon'$ , and dielectric loss factor,  $\epsilon''$  (Eq. 1).

$$\epsilon = \epsilon' - j\epsilon'' \quad \text{Eq. 1}$$

The dielectric constant accounts for the ability of a molecule to be polarized by the MW, while the dielectric loss factor accounts for MW dissipation in the medium as heat. The relation between the average power dissipated per unit volume of a material to its dielectric loss factor can be given using Poynting's Theorem (Eq. 2).<sup>30</sup>

$$Q_{ave} = \omega \epsilon_0 \epsilon'' E_{rms}^2 \quad \text{Eq. 2}$$

where  $Q_{ave}$  is the average absorption of MW power per unit volume in  $W/m^3$ ;  $\omega$  is the angular frequency in  $rd/s$ ;  $\epsilon_0$  is the free space permittivity;  $\epsilon''$  is the loss factor of the irradiated material; and  $E_{rms}$  is the root-mean-square electric field intensity in  $V/m$ .

Eq. 2 indicates that a large dielectric loss factor increases the rate of MW heating inside the irradiated material. However, a large dielectric loss factor can also cause a larger temperature gradient inside the irradiated material. This phenomenon can be characterized using the concept of penetration depth, which is defined as the distance from the surface into the irradiated material at which the MW power drops to  $1/e$  of its value at the surface.<sup>31</sup> Very low ( $<1$  cm) or very high ( $> 1$  m) penetration depths are unfavorable in industrial processes.<sup>32</sup> MW penetration depth can be calculated based on the free space wavelength of the MW and the dielectric properties of the irradiated material (Eq. 3).<sup>33</sup>

$$D_p = \frac{\lambda}{2\pi\sqrt{2\epsilon'}} \left[ \left( 1 + \left( \frac{\epsilon''}{\epsilon'} \right)^2 \right)^{\frac{1}{2}} - 1 \right]^{-\frac{1}{2}} \quad \text{Eq. 3}$$

where  $\lambda$  is the free space wavelength of incident MW.

Considering the above parameters, HCPs need to have high dielectric loss factor and suitable penetration depth in order for MW assisted regeneration to be effective. However, most HCPs have a low dielectric constant and loss factor. Therefore, a key enabler for practical application of

MW to regenerate spent HCPs is to improve their dielectric properties while retaining other excellent properties.

There is limited information in the literature on improving MW absorption by polymers, particularly for adsorption applications. Meng et al. used sulfonation to improve the MW absorption of polymeric adsorbents. They showed that the sulfonated samples have lower adsorption capacities, but higher desorption efficiencies during MW-assisted regeneration, compared to the as-synthesized polymer without sulfonation.<sup>34</sup> The addition of MW absorptive material (MAM) to nonporous polymers has been used to improve their MW shielding properties for stealth operations.<sup>35-37</sup> The synthesis of composites filled with MAMs such as metal particles, carbon black (CB), carbon nano tubes (CNTs), and graphite nano particles at percolation threshold, considerably enhances the MW absorption of the polymer.<sup>38-41</sup> Percolation threshold can be defined as the minimum filler fraction that creates a continuous network in the nanocomposites.<sup>42</sup> Percolative approach requires only a small amount of MAM (typically less than 2 vol%) to raise the dielectric properties substantially above that of polymer.<sup>43,44</sup> Therefore, the dielectric properties of HCPs can be tailored by the filler content in the matrix.

As described above, VOC adsorption on porous HCPs and VOC desorption by MW heating has been shown to be a promising technique for VOC capture and recovery from polluted air streams. The experimental work presented here provides one of the first investigations into the enhancement of MW absorption of polymeric adsorbents by synthesizing percolative composites filled with a MAM. Combining the MW absorptive ability of CB particles with the excellent VOC adsorption performance of HCPs can provide a lightweight composite adsorbent for use in cyclic VOC adsorption/MW regeneration systems. CB filled composites were synthesized for the first time

from (4, 4'-bis ((chloromethyl)-1, 1'-biphenyl) + (benzyl chloride)) via Friedel-Crafts reaction. CB was selected as a filler due to its low cost, low density, high dielectric values and thermal stability.<sup>45,46</sup> Fourier transform infrared spectroscopy (FTIR) and helium ion microscopy (HIM) were employed to confirm the synthesis of the HCP and CB/HCPs composites. Synthesized composites were characterized using thermo-gravimetric analysis, dielectric property measurement, Bruner–Emmett-Teller (BET) analysis and gravimetric sorption analysis. In addition, adsorption and MW-assisted desorption of hexane was carried out on HCP and CB/HCPs and MW regeneration efficiencies were compared.

### **5.3 Experimental Section**

#### **5.3.1 Materials**

The following reagents were used in the polymer synthesis and characterization: 4, 4'-bis(chloromethyl)-1, 1'-biphenyl (95.0 %, BCMB), dimethoxy methane (99.0 %, DMM), 1, 2-dichloroethane (99.8 %, DCE), Iron (III) chloride (98.0 %, FC), benzyl chloride (99 %, BCH), hydrochloric acid (1 M), methanol (99.0 %), acetone (99.5 %), hexane (99.0 %) and toluene (99.0 %). CB (99.9%) with specific surface area of 75 m<sup>2</sup>/g was used as the source of carbon.

#### **5.3.2 Synthesis of Hypercrosslinked Polymer**

The synthesizing method of HCP was adopted from Vinodh et al. with a minor modification to meet the aim of this study.<sup>47</sup> In brief, 50 ml of 1, 2-dichloroethane was placed in a 100-ml round bottom flask with a mechanical stirrer. To ensure uniform heating during polymerization, the flask was submerged in an ethylene glycol bath. To the flask was added 1.1 g of 4, 40-bis

(chloromethyl)-1, 10-biphenyl, 2.5 ml of dimethoxy methane, and 3.5 g of ferric chloride and the mixture was stirred at 500 rpm for 10 minutes. Then, over a 5 minute period, 10 ml of a benzyl chloride:1,2-dichloroethane mixture (1:10 v:v) was added drop-wise using a syringe pump to the flask with 200 rpm mechanical stirring. After 20 minutes, the reaction temperature was raised and remained at 40 °C for 4 hours. Then, the temperature was raised to 80 °C for 20 hours. After 24 hours from starting the synthesis, the flask was cooled to room temperature and the solid product was filtered and consecutively washed with methanol, 5 % HCl in acetone water mixture (1:1), and acetone. The recovered polymers were then dried in air at 120 °C.

#### 5.3.2.1 *Preparation of carbon black/polymer composites*

To uniformly disperse them in the polymer matrix, CB particles (0.2 to 2.4 g/L) were first dispersed and stabilized in DCE. All CB suspensions were mixed and stabilized by 15 min stirring and 1 hr ultrasonication. CB solutions were then incorporated in the polymer synthesis procedure to produce polymer composites containing 0.5 to 6 wt % CB. The stability of the CB-DCE mixtures against agglomeration and sedimentation was evaluated by monitoring absorption at 266 nm using a UV-Vis spectrometer. Figure 5-1 summarizes the synthesis steps of CB/HCP composites.

### 5.3.3 Characterizations and Measurements

#### 5.3.3.1 *FTIR analysis*

Fourier transform infrared (FTIR) spectra were obtained in transmission mode using a Nicolet iS50 spectrometer, under ambient conditions and with 4 cm<sup>-1</sup> resolution over a wave number range of 4000–400 cm<sup>-1</sup>.

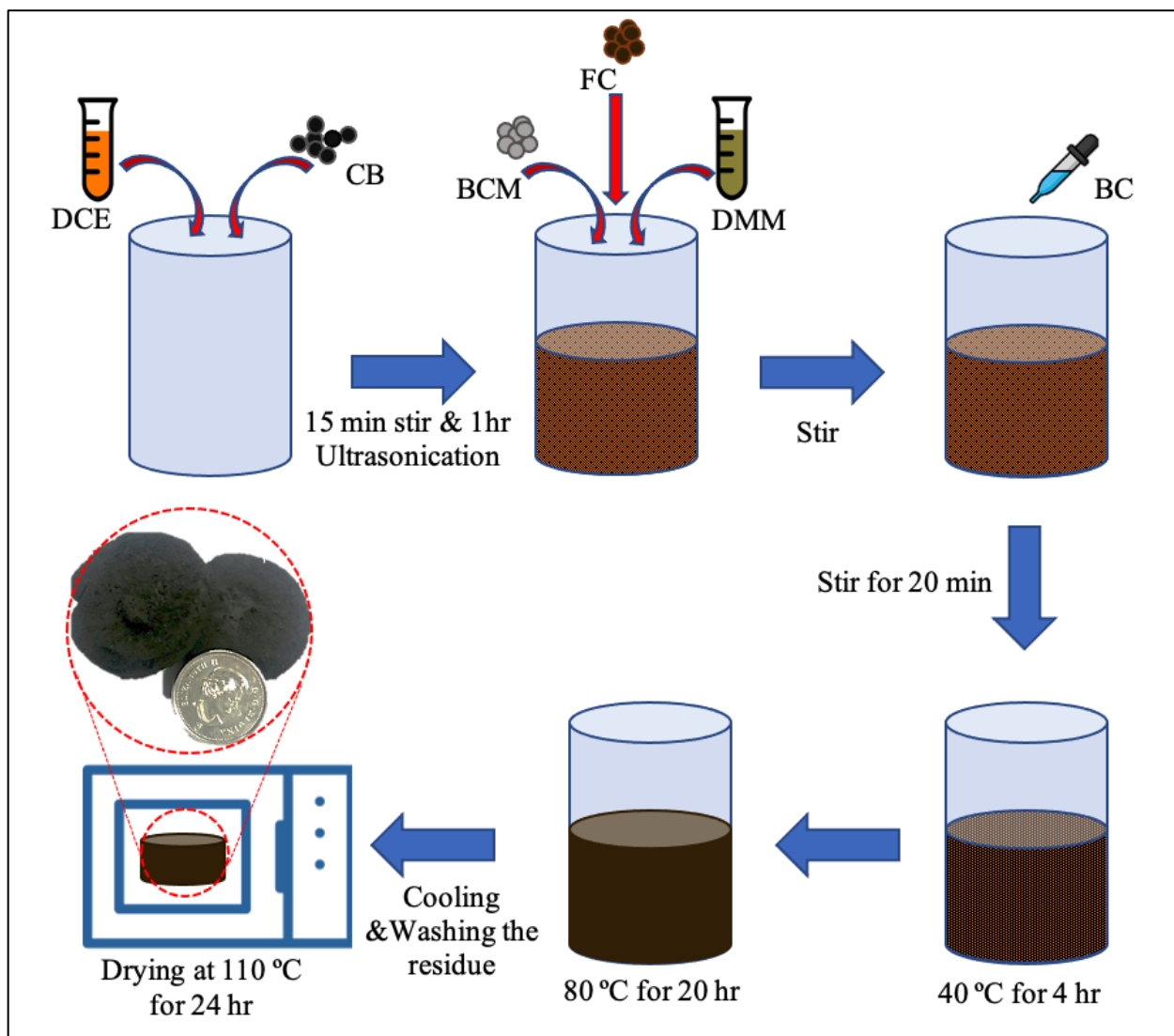


Figure 5-1. CB/HCP composite synthesis steps.

### 5.3.3.2 HIM analysis

The morphology of CB in HCPs was obtained using a Zeiss Orion Nanofab helium ion microscope. HIM was selected primarily because of its advantages over scanning electron microscopy in neutralizing the sample surface by an in situ electron flood gun.<sup>48</sup> This feature allows HIM to visualize carbonaceous particles on high resistivity HCP. In addition, unlike scanning electron

microscopy, a conductive coating is not needed in HIM analysis. In this study, HIM analysis was carried out on the HCPs at 35 kV, working distance of 8.5 mm, scan dwell time of 0.2  $\mu$ s, and resolution of 1  $\mu$ m.

#### 5.3.3.3 *TGA analysis*

TGA of CB/HCP composites was carried out on a thermogravimetric analyzer (TGA/DSC 1, Mettler Toledo) in the temperature range 30 to 900  $^{\circ}$ C, at a heating rate of 10  $^{\circ}$ C/min under nitrogen purge gas for a sample size of 7–9 mg. Prior to analyses, samples were ground to less than 1 mm using a porcelain mortar and pestle to ensure fast temperature equilibrium.

#### 5.3.3.4 *Micropore surface analysis*

To investigate the surface area, pore volume and pore size distribution,  $50 \pm 5$  mg of CB/HCP composites were analyzed with the  $N_2$  (99.9 %) adsorption at -196  $^{\circ}$ C in a micropore surface analyzer (iQ2MP, Quantachrome). Samples were outgassed in the instrument at 120  $^{\circ}$ C for 5h before adsorption experiments. The analysis temperature of -196  $^{\circ}$ C was obtained using liquid nitrogen. The BET surface area was calculated within the relative pressure values of 0.001 to 0.02. The pore size distribution (PSD) was calculated using the quenched solid density function theory method,<sup>49</sup> assuming slit-shaped pores, within the relative pressure values of  $10^{-7}$  to 0.99. Micropore volume was calculated based on the statistical thickness method (t-method) within the relative pressure values of 0.05 to 0.4. The total pore volume was measured based on the volume of adsorbed nitrogen at  $P/P_0 = 0.99$ . All the calculations were performed using the instrument's built-in software.

#### 5.3.3.5 *VOC adsorption isotherm*

VOC adsorption performance of synthesized composites was evaluated gravimetrically in an automated vapor sorption analyzer (TA Instruments, VTI-SA). Toluene was selected as a model adsorbate for VOC adsorption isotherm analysis. Toluene is a common VOC emitted from chemical processes and has been widely studied to evaluate the adsorption performance of adsorbents, including synthesized HCPs.<sup>47,50-54</sup> Typically,  $10 \pm 2$  mg of each sample was inserted into a sample holder of the instrument and dried at 100 °C for 2 hr before toluene exposure. All adsorption experiments were performed by increasing the relative saturation pressure from 0.02 to 0.9 at 25 °C. Adsorption continued until a stable mass was achieved (i.e. <0.01 wt% change in 5 min) indicating an equilibrium state was reached. Weight changes at each equilibrium state were recorded to determine adsorption capacity. The total time to complete the toluene adsorption isotherm on each sample was 16 to 20 hours.

#### 5.3.3.6 *Dielectric properties*

The dielectric properties of CB/HCP composites were measured at 2.45 GHz, room temperature, and atmospheric pressure using a vector network analyzer (VNA, supplied by Rohde and Schwarz) with an open-ended probe method.<sup>55</sup>

#### 5.3.3.7 *Microwave heating rate and capacity*

MW heating rates of CB/HCP composites were experimentally measured at different applied powers to study the effect of CB content. The obtained temperature increases were used to calculate heating rate via Eq. 4.

$$\text{Heating rate} = \frac{T_{\text{final}} - T_{\text{initial}}}{\Delta t} \quad \text{Eq. 4}$$

where  $T_{\text{final}}$  is the sample temperature at the steady state heated condition,  $T_{\text{initial}}$  is the sample temperature before heating, and  $\Delta t$  is the time to reach the steady state temperature (i.e.  $<0.1^{\circ}\text{C}$  change in 2 min). MW heating capacity was also defined and calculated as the amount of absorbed MW energy to increase the temperature of 1 gram of sample by  $1^{\circ}\text{C}$ .

#### 5.3.3.8 *Hexane adsorption and microwave-assisted desorption*

Hexane adsorption experiments were conducted at  $25^{\circ}\text{C}$  using 2 g of each CB/HCP composite. Hexane, as a MW transparent adsorbate, was selected to evaluate the effect of CB content on the MW regeneration of HCPs. For the adsorption tests, 500 ppm of hexane in air was generated using a syringe pump injecting liquid hexane into 5 SLPM of air. After the concentration of hexane in air reached a stable level for 20 minutes, the adsorption test was started by flowing the hexane-laden air into a quartz tube containing the adsorbent. Hexane concentration in the outlet stream was measured using a flame ionization detector (FID, Baseline- Mocon Inc., series 9000) until it reached the inlet concentration and remained constant with time.

Following adsorption, the adsorbent was regenerated using MW heating at 2.45 GHz. The regeneration setup consisted of a single mode MW applicator equipped with a rectangular waveguide connected to a magnetron that was controlled by a switching power supply. A three-stub tuner (National Electronics) and a sliding short were used to maximize MW energy transfer to the sample. A dual channel MW power meter (E4419B, Agilent) and directional coupler (Mega Industries) with 60 db nominal attenuation were used to measure forward and reverse power. A

fiberoptic sensor (Neoptix, Reflex), which is transparent to electromagnetic fields, was used to measure the bed temperature during MW heating. Regeneration experiments (60 min in duration) were conducted by applying a constant applied power of 30 W to the quartz tube containing 2 grams of adsorbent in the MW applicator while purging with 1 SLPM of ultrapure N<sub>2</sub> (99.9 %). Hexane effluent concentration was measured by FID and used to calculate time-resolved desorption efficiency (Eq. 5). This approach is better than a gravimetric approach (weight gain at discrete intervals over time) since the desorption rate is not constant over the desorption cycle. The time-resolved desorption efficiency is calculated as:

$$\eta_t(\%) = \frac{\sum_0^t (C_{\text{Hexane}} \cdot P \cdot Q \cdot \Delta t \cdot M_w)}{R \cdot T \cdot (W_{AA} - W_{BA})} \times 100 \quad \text{Eq. 5}$$

where  $\eta_t$  is the desorption efficiency at time  $t$ ,  $C_{\text{Hexane}}$  is effluent hexane concentration during desorption,  $P$  is the atmospheric pressure,  $Q$  is the purge gas flow rate,  $\Delta t$  is the time period between the two recorded concentrations,  $R$  is the ideal gas constant,  $T$  is the room temperature,  $W_{AA}$  and  $W_{BA}$  are the sample weight after and before the adsorption process, respectively.

## 5.4 Results and Discussion

### 5.4.1 CB Dispersion Stability in 1, 2-dichloroethane

Shear mixing using a magnetic stirrer and ultrasonication was used to stabilize CB particles in DCE; however, high van der Waals forces between CB particles can inevitably cause self-aggregation. In addition, rising temperature during the polymer synthesis increases self-aggregation and subsequent sedimentation due to Brownian motion of CB particles. Therefore, UV-vis spectroscopy was used to evaluate the stability of dispersed CB/DCE suspensions. Since

most of the polymerization is completed in the first 4 hr (at 40 °C), an 8 hr duration and 40 °C were selected for the dispersion stability experiments. Figure 5-2 presents the UV–vis absorption spectra of CB, a calibration curve, and the resulting carbon black concentrations versus time. UV–vis analysis shows CB dispersions were fairly stable up to at least 1 hour in all samples but that self-aggregation and sedimentation eventually occurred for CB concentrations above 0.4 g/l. Therefore, agglomerated CB particles are expected to be present in the synthesized composites when higher CB concentrations are used.

### 5.4.2 FTIR

FTIR spectra of the synthesized HCP and CB/HCP composites are shown in Figure 5-3. The broad band at  $3444\text{ cm}^{-1}$  is attributed to the O–H stretching vibration due to water adsorption from air during sample handling. The bands at  $3014\text{ cm}^{-1}$  and  $2918\text{ cm}^{-1}$  are attributed to aromatic C–H stretching vibration and –CH<sub>2</sub>– vibrations, respectively. Bands at  $1439\text{ cm}^{-1}$  and  $1603\text{ cm}^{-1}$  are due to aromatic ring vibrations. Bands at 1089, 886, 809, and  $607\text{ cm}^{-1}$  are attributed to aromatic C–H bending modes. The spectra of HCP and CB/HCPs illustrate similar features and verified the synthesis of HCP based on the published FTIRs for this polymer.<sup>47</sup>

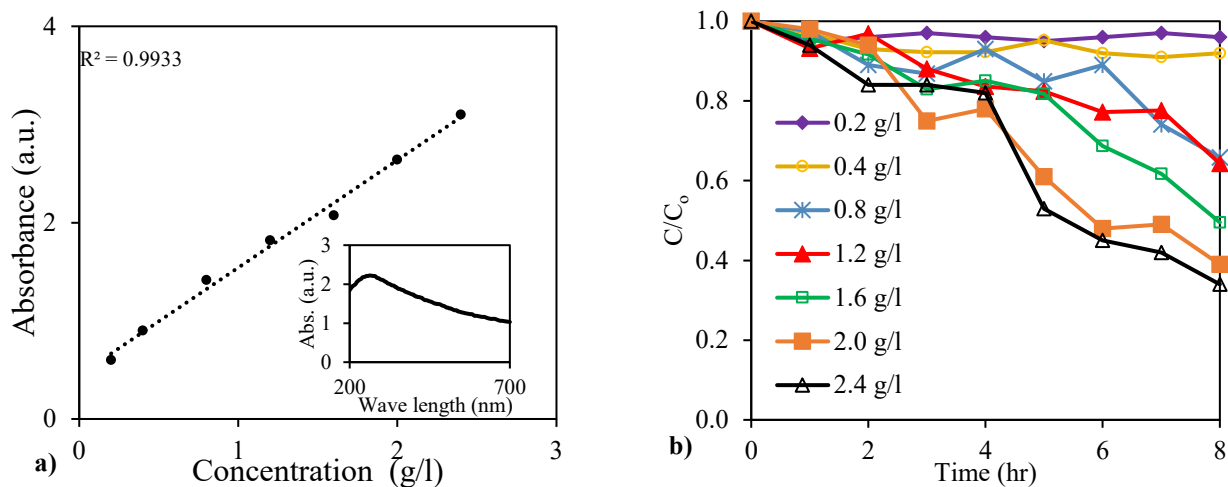


Figure 5-2. a) CB UV-vis absorbance; b) Change in CB concentration in DCE with time.

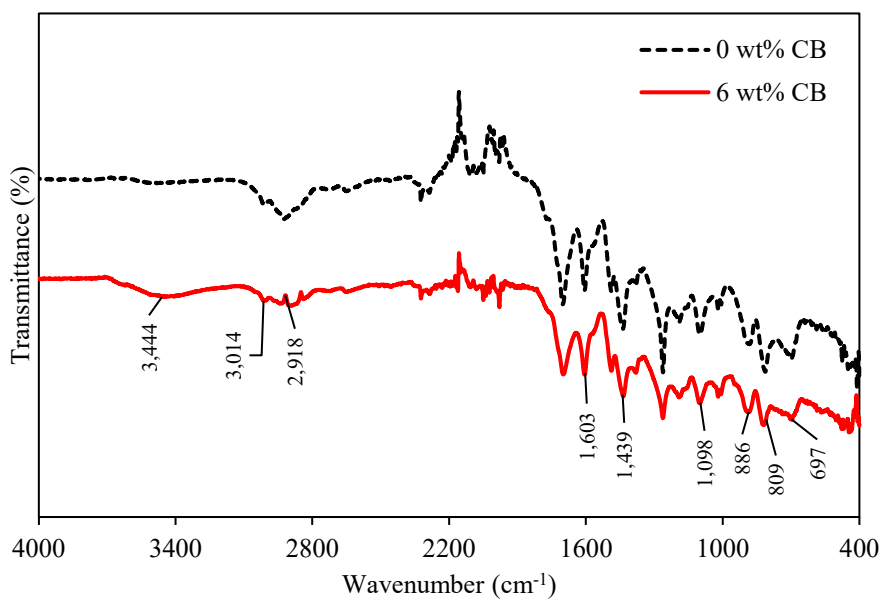


Figure 5-3. FTIR spectra acquired for 0 wt% and 6 wt% CB/HCP.

### 5.4.3 HIM

Figure 5-4 presents the microstructure of synthesized HCP and CB/HCP obtained using HIM.

HIM micrographs show that CB particles are of submicron size, and there is a certain degree of

agglomeration of CB in the CB/HCP composite. The surface of the CB/HCP (Figure 5-4.b) shows a fluffy morphology and reduced uniformity compared to pristine polymer (Figure 5-4.a). The dispersed CB particles are completely connected to the polymer matrix to form a local conductive network structure. This morphological structure can play an important role in terms of enhancing the dielectric loss factor, which will be discussed later.

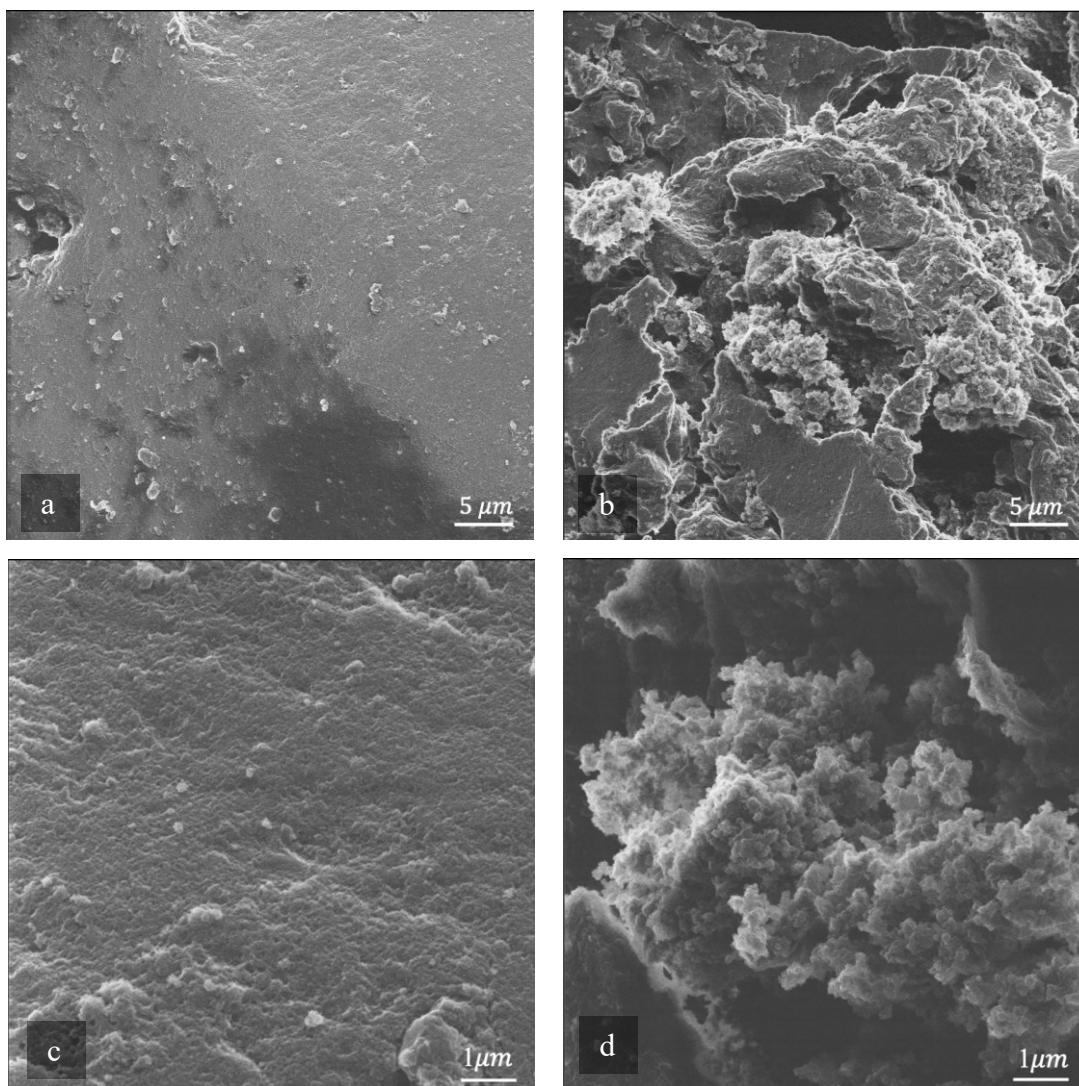


Figure 5-4. HIM micrographs of synthesized HCPs with 0 wt% CB (a & c) and 4 wt% CB (b & d).

#### 5.4.4 TGA

TGA was used to investigate the degradation behavior and the thermal stability of the CB/HCP composites at elevated temperatures (Figure 5-5). The weight loss during the initial stage of heating was attributed to the presence of moisture and the volatile substances adsorbed in HCP pores. After ramping the temperature to 887 °C, the residual weight was 1% (of the original weight) for HCP and 63% for the CB/HCP composites (Figure 5-5.a). Derivative thermogravimetry results show that the initial degradation temperature, defined here as the temperature at which a sample loses 1 percent of its weight, decreased from 270 °C for HCP to 220 °C for the CB/HCP composites (Figure 5-5.b). The study by Levchik et al.<sup>56</sup> of cross-linking and thermal stability of polystyrenes and polymethacrylates at 900 °C showed that decreases in a polymer's decomposition temperature and residual mass remaining at high temperature are indicative of a lower degree of cross-linking. Since CB addition to HCP reduces the degradation temperature and increases the residual at 887 °C, TGA analysis cannot provide a definitive conclusion on the degree of hypercrosslinking. Previous studies on thermal stability of nanocomposites show that aggregates of filler can function as a barrier, preventing the diffusion of degraded products from the composite into the gas phase which results in a greater residual.<sup>57,58</sup> Moreover, entrapment of polymer in the filler network can delay its thermal degradation, which reduces its chain mobility and enhances the apparent composite thermal stability at elevated temperatures.<sup>57,58</sup>

The variation of the weight loss percent at 887 °C with the composite's CB content is presented in Figure 5-5.c. Comparing the weight loss percent among different CB/HCP composites show that there is an optimum content of CB, between 3 wt% to 5 wt%, which results in less than 30 % weight loss.

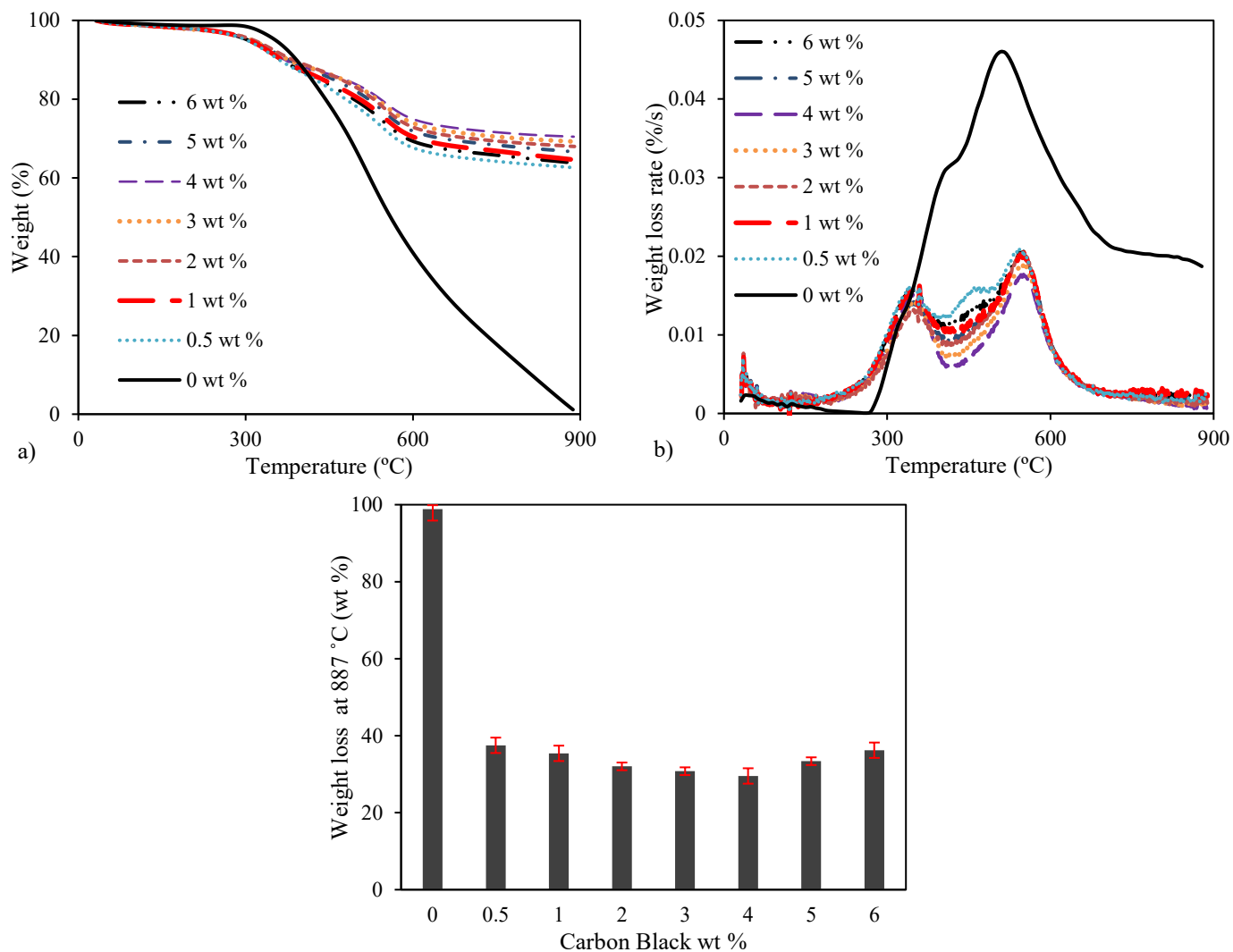


Figure 5-5. a) Weight percent, b) weight loss rate versus temperature, and c) weight loss of composites with different CB content at 887 °C. The error bars represent the maximum based on three rounds of analysis.

#### 5.4.5 Textural Analysis

BET surface area, pore volume and pore size distribution of CB/HCPs were determined using  $N_2$  adsorption (Figure 5-6). Increasing the CB content in the composite to 4 wt % reduces BET surface area, total pore volume, and micropore volume by 10 %, 13 %, and 9 % respectively (Figures 5-6.a and 5-6.b). This adverse effect nonlinearly increases with CB content. Further reduction led to

proportionally greater impacts (6 wt % CB resulted in 38 %, 26 %, and 24 % reductions in BET surface area, total pore volume and micropore volume, respectively). This greater impact on surface properties may be due to the percolation threshold of CB in the matrix and the tendency of CB particles to create agglomerates in the composite at high CB content. Agglomeration and nonuniform dispersion of CB in the matrix can affect the internal porosity of the composite. Pore size distribution results showed minimal change in the distribution of pores among samples with different CB content (Figure 5-6.c); however, there is a clear reduction in the micropore region volume with higher CB content in the matrix. Additionally, pore size distribution results show mesoporous ( $2 \text{ nm} < \text{pore diameter} < 50 \text{ nm}$ ) structure for the synthesized composites. The presence of mesopores plays a particularly important role in both VOC adsorption capacities and desorption efficiencies.<sup>59</sup> Materials with mesoporous structure have been shown to be ideal candidates for catalysts and adsorbents due to convenient diffusion of adsorbate molecules in the pores during both adsorption and desorption.<sup>60,61</sup> Overall, these results indicate that the prepared composites have well-developed micro-mesopore structure although increasing CB content degraded that structure somewhat.

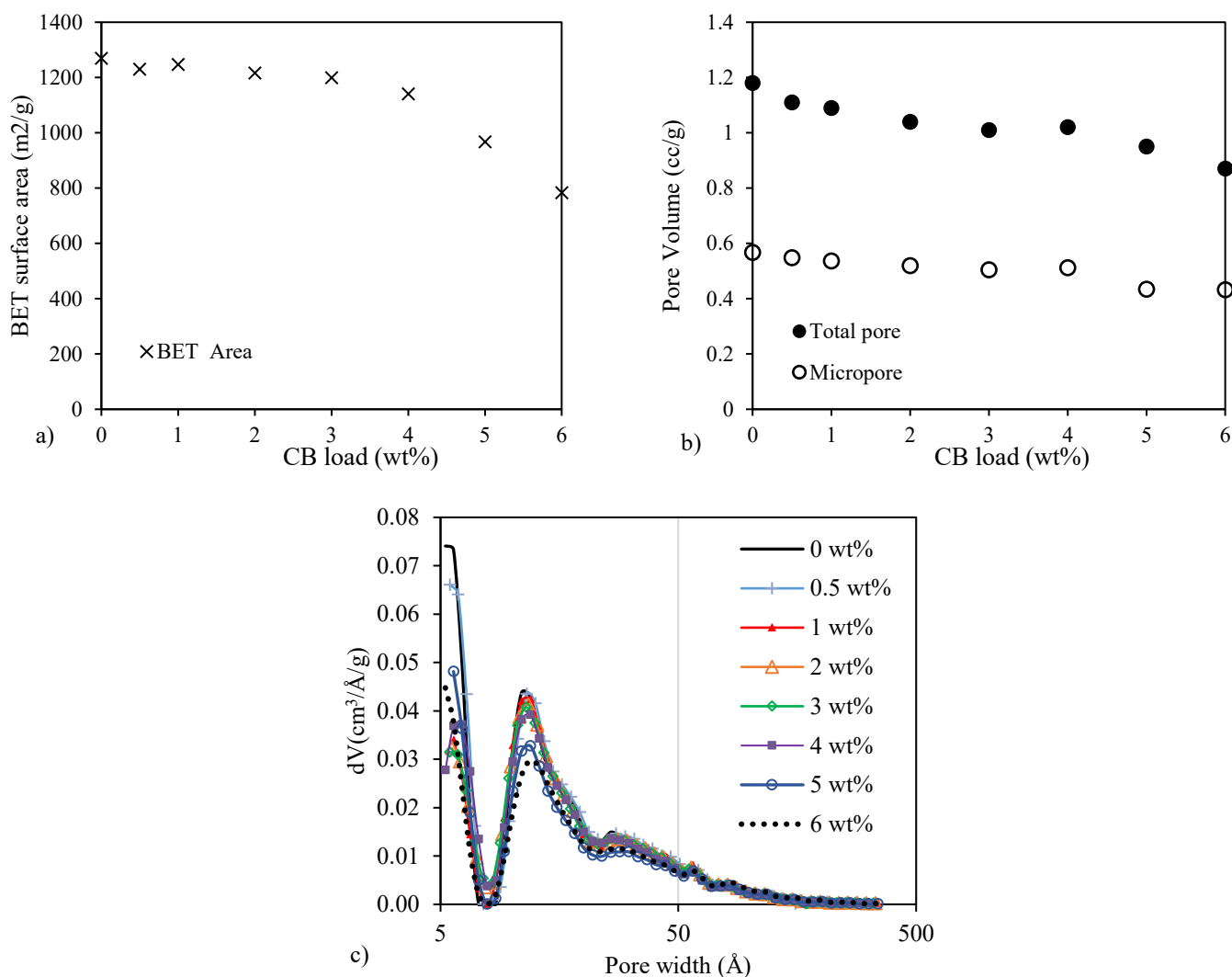


Figure 5-6. a) BET surface area, b) Pore volume, and c) Pore size distribution of synthesized composites.

#### 5.4.6 Toluene Adsorption Isotherm

Since the pore structure of HCP was changed by the CB filler (Figure 5-6), additional investigation was completed to evaluate the VOC adsorption performance of CB/HCP composites. Toluene, one of the most studied VOCs for adsorption processes, was utilized to examine the effect of the adsorbent pore structure on adsorption performance. Toluene adsorption isotherms of the

CB/HCPs are shown in Figure 5-7.a. As expected, the adsorption capacity for toluene decreased with increasing filler content; however, this effect is aggravated above 4 wt% CB in the composite. Figure 5-7.b compares the adsorption capacities of toluene on CB/HCP composites at  $p/p_0 = 0.02$  and  $p/p_0 = 0.9$ . Adsorption at  $p/p_0 = 0.02$  is attributed mainly to micropores, whereas the high adsorption capacity at  $p/p_0 = 0.9$  is attributed to the presence of mesopores. It can be seen from Figure 5-7.b that increasing CB content from 0 to 4 wt% reduces the toluene adsorption capacity by 8 % and 5 % at relative pressures of 0.02 and 0.9, respectively. Further increase in CB content to 6 wt% reduces toluene adsorption capacity at both relative pressures by more than 34%, which is consistent with the porosity analysis results in Figure 5-6.

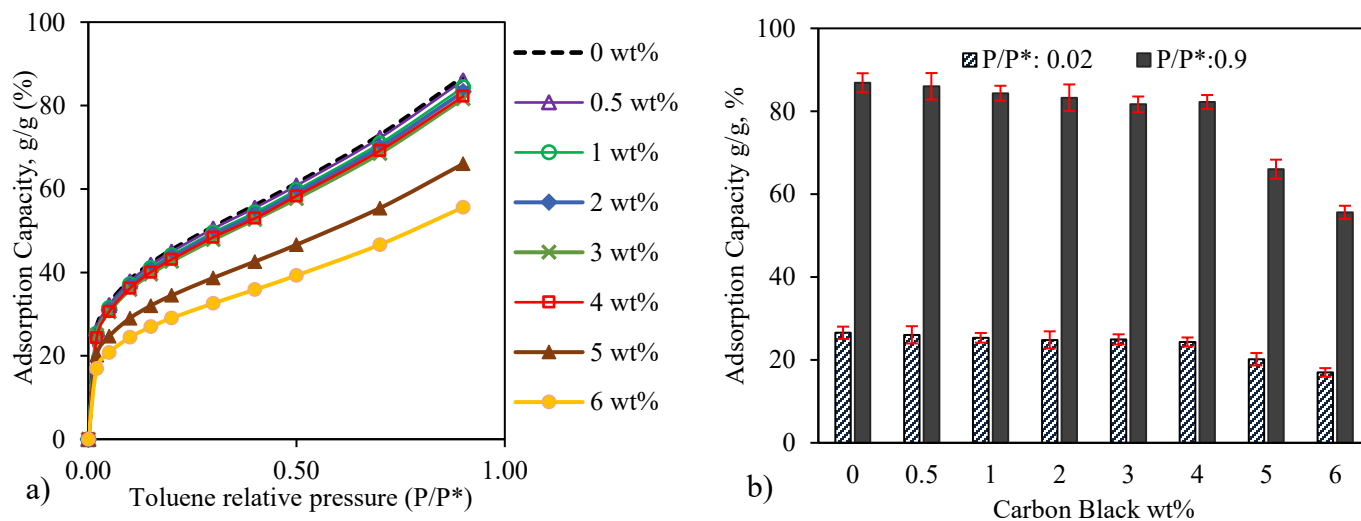


Figure 5-7. a) Toluene adsorption isotherms of CB/HCPs at 25 °C; b) Toluene adsorption capacity of CB/HCPs at 0.02 and 0.9 toluene relative vapor pressures. The error bars represent standard deviations calculated based on three rounds of analysis.

Table 5-1 compares the surface properties and toluene adsorption capacity of the HCP samples as well as other adsorbents reported in previous studies. Synthesized HCP in this study demonstrates better pore properties than most of the other adsorbents, including zeolites, silica gel, metal-

organic frameworks (MOF), activated carbons (AC) and polymeric adsorbents that were previously investigated for toluene adsorption. Notably, HCP and BC/HCP composites showed higher toluene adsorption capacity than all but one of the other adsorbents at the same toluene relative pressure, which is mainly due to the large micropore volume of synthesized HCP, higher than even the total pore volume of some of the adsorbents (Table 5-1).

Table 5-1. Surface property and toluene adsorption capacities of various adsorbents as compared to that of synthesized HCP and CB/HCP composites.

Adsorbent	Previous studies				This study		
	S <sub>BET</sub> , m <sup>2</sup> /g	V <sub>Total</sub> , cc/g	$\frac{g_{Toluene}}{g_{Adsorbent}}$ , % <sup>a</sup>	Ref.	$\frac{g_{Toluene}}{g_{HCP}}$ , % <sup>b</sup>	$\frac{g_{Toluene}}{g_{CB-HCP}}$ , % <sup>c</sup>	$\frac{P_{Toluene}}{P^{Sat.}_{Toluene}}$
Activated Carbon	1030	0.67	20	50	27	24	0.02
	1339	0.56	40	51	44	42	0.2
MOFs	470	–	26	62	44	42	0.2
	–	–	51	63	87	82	0.9
	1335	0.83	15	52	31	28	0.04
	1183	0.79	39	52	31	28	0.04
Silica Gel	765.6	0.44	43	53	51	48	0.32
Zeolite (USY)	676	0.30	21	54	44	42	0.2
Zeolite (DAY)	704	–	14	64	27	24	0.02
Polymer	1077	0.63	55 (at 30 °C)	6	62	57	0.5
	1134	0.53	23	47	39	37	0.13

<sup>a</sup> Toluene adsorption capacity of conventional adsorbents at 25 °C.

<sup>b</sup> Toluene adsorption capacity of the synthesized HCP at the same relative pressure as the previous works and 25 °C.

<sup>c</sup> Toluene adsorption capacity of the synthesized HCP with 4 wt % of CB at the same relative pressure as the previous works and 25 °C.

### 5.4.7 Dielectric Properties Measurement

The effect of CB filler on the complex permittivity of HCP and MW penetration depth was investigated at 2.45 GHz and room temperature. Figure 5-8.a presents the complex permittivity of CB/HCP composites with the seven different filler loadings (0-6 wt%) at 2.45 GHz. The value of dielectric constant ( $\epsilon'$ ) and the dielectric loss factor ( $\epsilon''$ ) nonlinearly increased by more than 2 and 21 times, respectively, with increasing CB content to 4 wt%. Further CB addition to 6 wt % in the matrix increased both  $\epsilon'$  and  $\epsilon''$  by more than 5 and 91 times compared to HCP. This large enhancement in the dielectric properties is attributed to the formation of local conductive networks by CB particles inside the composites. Tang et al. reported that CB agglomerates can form a network inside the polymer that provides more conductive paths for charge carriers and enhances conduction loss.<sup>40</sup>

Figure 5-8.a demonstrates a sharp increase in the dielectric constant and loss factor values for CB content above 3 wt%. This critical content of filler in composites is known as the percolation threshold. The actual value of the percolation threshold depends mainly on the filler physiochemical properties, size, shape, structure and on its distribution throughout the composite.<sup>65</sup>

Figure 5-8.b presents the penetration depth of CB/HCPs which were calculated based on Eq. 3 and measured dielectric properties. The penetration depth decreased from 77 cm to 2 cm as the CB content increased from 0 to 6 wt%. This drop in the penetration depth (>97 %) can considerably improve the MW absorption efficiency in the adsorbent bed. It should be pointed out that further CB deposition would drop the penetration depth to less than the reactor diameter which can increase the temperature gradient inside the bed.

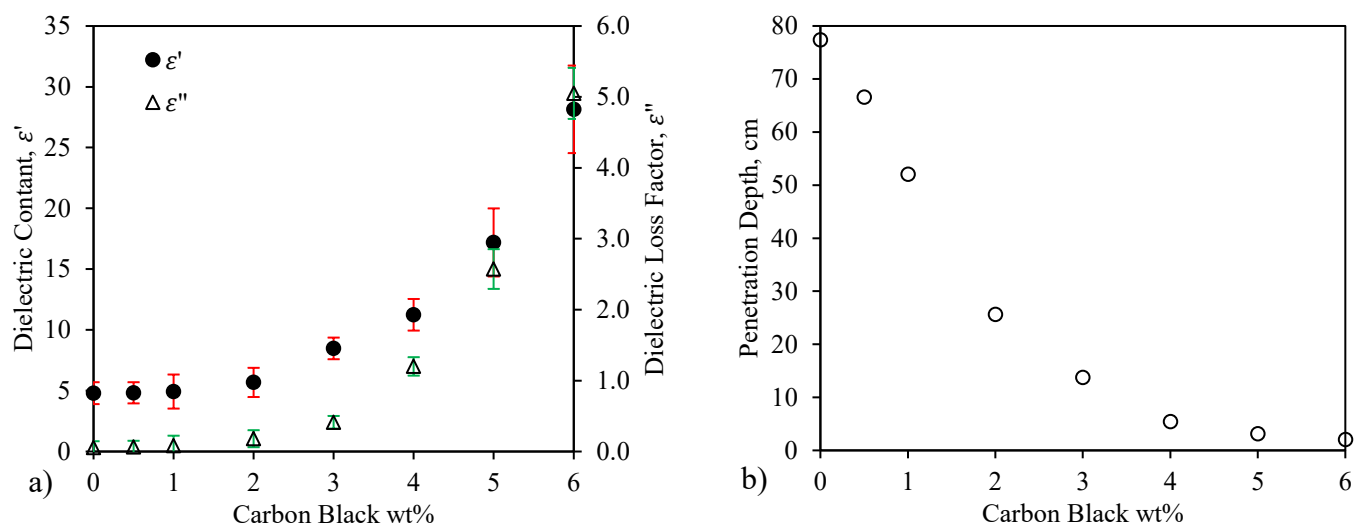


Figure 5-8. Effect of CB loading on a) dielectric properties and b) MW penetration depth. The error bars represent standard deviations calculated based on three rounds of measurements.

#### 5.4.8 Microwave Heating

To investigate the effect of CB addition to HCP on MW heating, heating rates were determined for 2-gram samples irradiated in the MW heating apparatus. Heating rates were determined using measured temperatures versus time at each applied power density (Figure 5-9.a). Obtained results show that the heating rate can be greatly increased by increasing the CB content in the composite.

MW heating capacity, defined as the amount of MW energy needed to raise the temperature of 1 gram of sample by 1°C, was determined based on energy consumption. Figure 5-9.b presents measured MW heating capacity values at each CB content in composite. MW heating capacity decreased by 99 % as the CB content was increased from 0 to 6 wt%. In other words, the energy needed to heat 1 gram of composite by 1°C is reduced by 99 % when 6 wt % CB is added to the HCP.

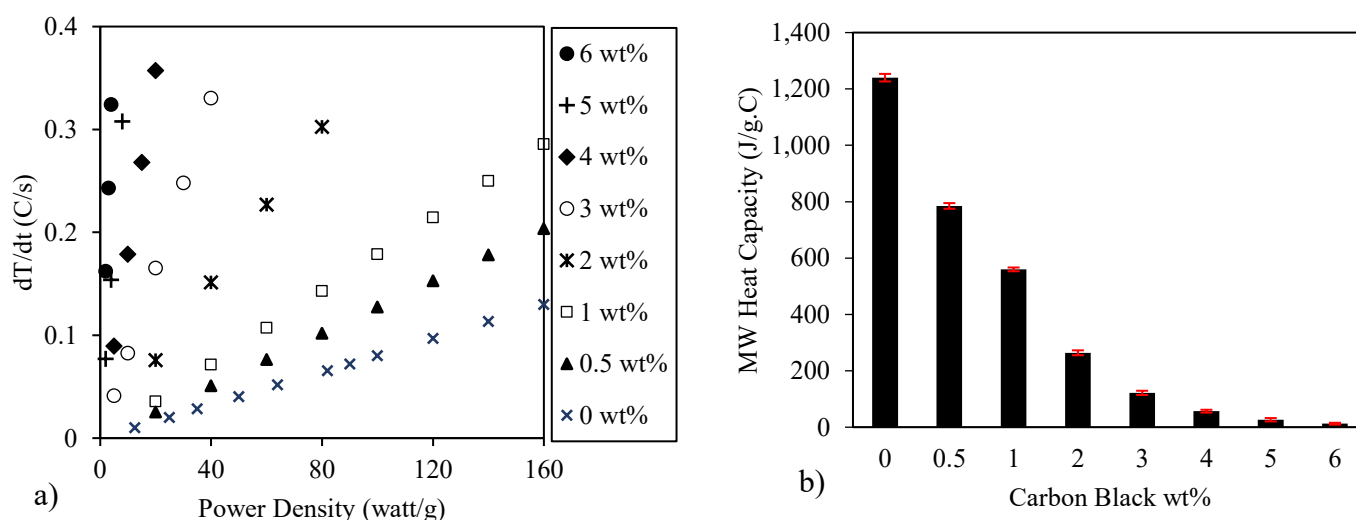
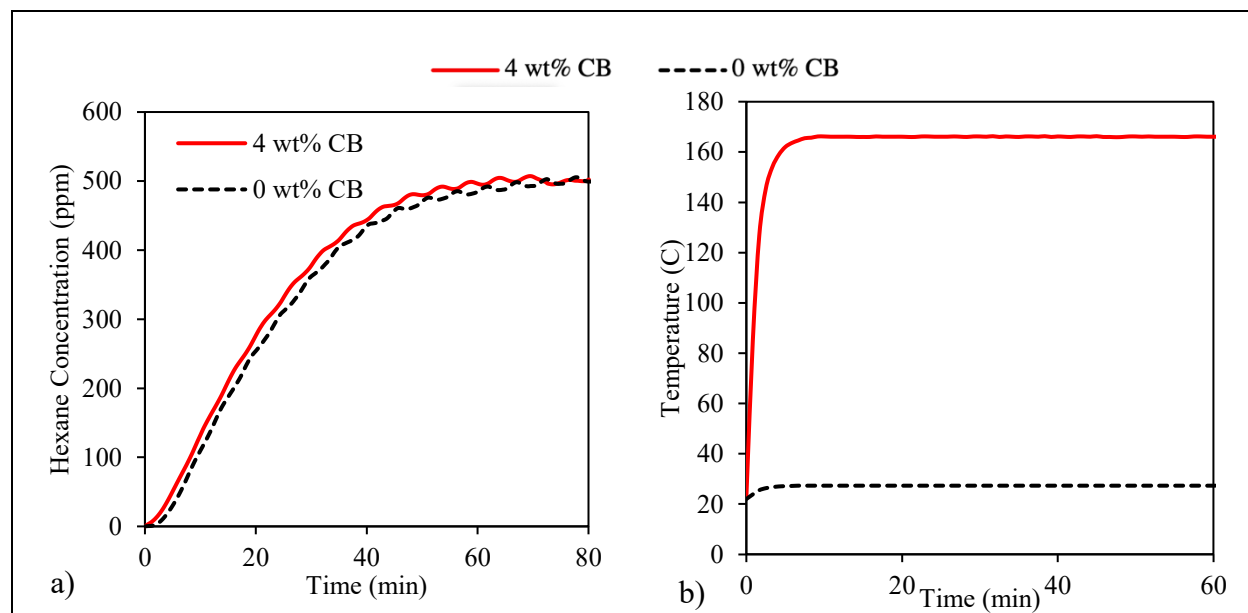


Figure 5-9. Effect of CB loading on a) heat up rate and b) MW heating capacity. The error bars represent standard deviations calculated based on three rounds of analysis.

#### 5.4.9 Microwave-assisted Desorption

MW-assisted desorption was carried out to study the effect of CB addition on the desorption of hexane from HCP and CB/HCP. HCP with 4 wt % CB was compared with HCP, because of the former's desirable pore properties (surface area, micro/total pore volume, pore size distribution), thermal stability, VOC adsorption capacity, and MW absorption performance. Figure 5-10 depicts the breakthrough profiles, desorption temperature, hexane effluent concentration during

regeneration, and desorption efficiency. The breakthrough curves show that addition of CB to the polymer matrix slightly shifts the breakthrough curve to the left due to the negative effect of CB on the pore properties of HCP (Figure 5-5.a). Figure 5-10.b shows that after 60 mins of MW heating, the HCP barely reached 27 °C, while CB/HCP reached 166 °C in 10 mins. A higher regeneration temperature provides needed energy to overcome the heat of adsorption and increases the diffusivity of adsorbates in the adsorbent's pores.<sup>66</sup> As a result, maximum hexane concentration in the effluent for the CB/HCP increased to a maximum of 12,000 ppm whereas the HCP reached only 420 ppm. Higher desorption concentration in the effluent stream is important for efficient VOC recovery and reuse. The desorption efficiency versus time (Figure 5-10.d) shows that 99% of adsorbed hexane was desorbed from CB/HCP in less than 35 minutes while the HCP reached only 27 % desorption efficiency after 60 min of MW heating.



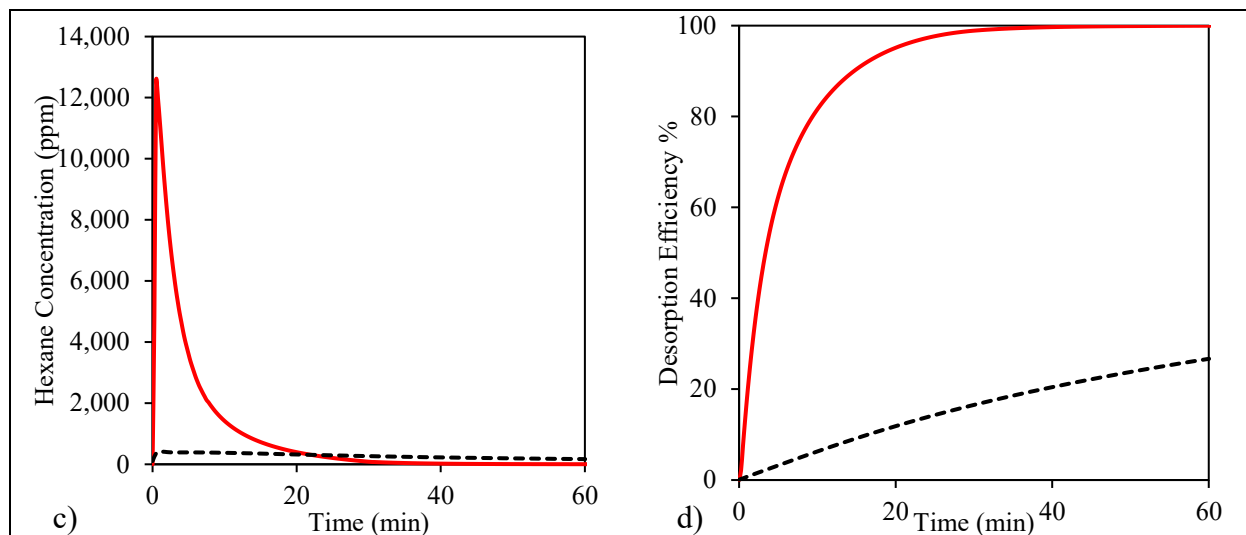


Figure 5-10. Hexane adsorption/MW assisted regeneration of HCPs with 0 and 4 wt% CB; a) hexane adsorption breakthrough curves, b) desorption temperature, c) effluent hexane concentration during the desorption, and d) desorption efficiency versus desorption time.

## 5.5 Conclusions

In this study, a series of CB/HCP composites of different CB contents were prepared via Friedel-Crafts polymerization. FTIR analysis and HIM images confirmed the synthesis of HCP and CB/HCP, respectively. The HIM images showed formation of CB agglomerates that can act as a conductive network within the matrix. TGA analysis showed more than 60 percent increase in the residual weight at 880 °C in CB filled polymers that shows higher thermal stability of CB-filled composites. This is particularly important feature since adsorbent can undergo elevated temperatures in MW-heating. Nitrogen and toluene adsorption analysis indicated that the composites have well-developed micropore and mesopore structures. The CB content of 4 wt% was found to be optimum as disproportionally larger reductions in pore volumes and adsorption capacity were observed above this filler content. Dielectric property measurement of HCP with 4

wt % CB showed more than 2 and 21-times enhancement in dielectric constant and loss factor, respectively. These increases are attributed to the formation of a conductive CB network inside the polymer structure which provided more paths for electron migration and therefore conduction loss inside the composite. MW-assisted desorption of HCP with 4 wt% CB showed 139 °C increase in the desorption temperature compared to pristine HCP at the same applied MW power. The higher desorption temperature resulted in more than a 450 % enhancement in the desorption efficiency after 35 minutes of MW irradiation.

In summary, this study showed the critical impact of filler content on the performance of MW-absorptive HCPs. While the presence of a MAM in the matrix is needed for efficient MW heating, it reduces pore volume and surface of the composite. An optimum filler content of 4 wt % CB provided HCP with suitable thermal stability, enhanced MW absorption, and minimal effect on the VOC adsorption. Future research could usefully explore the effect of other fillers such as graphene oxides, carbon nanotubes and magnetic nano particles as MAMs which could potentially result in better VOC adsorption and MW assisted regeneration of adsorbents.

## 5.6 References

- (1) Lai, C.; Wang, Z.; Qin, L.; Fu, Y.; Li, B.; Zhang, M.; Liu, S.; Li, L.; Yi, H.; Liu, X.; Zhou, X.; An, N.; An, Z.; Shi, X.; Feng, C. Metal-Organic Frameworks as Burgeoning Materials for the Capture and Sensing of Indoor VOCs and Radon Gases. *Coordination Chemistry Reviews* **2021**, *427*, 213565. <https://doi.org/10.1016/j.ccr.2020.213565>.
- (2) Sudan, S.; Gładysiak, A.; Valizadeh, B.; Lee, J.-H.; Stylianou, K. C. Sustainable Capture of Aromatic Volatile Organic Compounds by a Pyrene-Based Metal–Organic Framework under Humid Conditions. *Inorganic Chemistry* **2020**, *59* (13), 9029–9036. <https://doi.org/10.1021/acs.inorgchem.0c00883>.
- (3) Maitlo, H. A.; Kim, K.-H.; Khan, A.; Szulejko, J. E.; Kim, J. C.; Song, H. N.; Ahn, W.-S. Competitive Adsorption of Gaseous Aromatic Hydrocarbons in a Binary Mixture on Nanoporous Covalent Organic Polymers at Various Partial Pressures. *Environmental research* **2019**, *173*, 1–11. <https://doi.org/10.1016/j.envres.2019.03.028>.
- (4) Vikrant, K.; Qu, Y.; Kim, K.-H.; Boukhvalov, D. W.; Ahn, W.-S. Amine-Functionalized Microporous Covalent Organic Polymers for Adsorptive Removal of a Gaseous Aliphatic Aldehyde Mixture. *Environmental Science: Nano* **2020**, *7* (11), 3447–3468. <https://doi.org/10.1039/D0EN00537A>.
- (5) Meng, Q. B.; Yang, G.-S.; Lee, Y.-S. Sulfonation of a Hypercrosslinked Polymer Adsorbent for Microwave-Assisted Desorption of Adsorbed Benzene. *Journal of Industrial and Engineering Chemistry* **2014**, *20* (4), 2484–2489. <https://doi.org/10.1016/j.jiec.2013.10.030>.
- (6) Shi, Q.; Yang, X.; Wu, L.; Liu, H.; Zhang, J.; Zhang, F.; Long, C. Binary Adsorption Equilibrium and Breakthrough of Toluene and Cyclohexane on Macroporous and Hypercrosslinked Polymeric Resins. *Microporous and Mesoporous Materials* **2018**, *271*, 73–82. <https://doi.org/10.1016/j.micromeso.2018.05.034>.

- (7) Xu, S.; Luo, Y.; Tan, B. Recent Development of Hypercrosslinked Microporous Organic Polymers. *Macromolecular Rapid Communications* **2013**, *34* (6), 471–484. <https://doi.org/10.1002/marc.201200788>.
- (8) Zeng, S. Z.; Guo, L.; He, Q.; Chen, Y.; Jiang, P.; Shi, J. Facile One-Pot Synthesis of Nanoporous Hypercrosslinked Hydroxybenzene Formaldehyde Resins with High Surface Area and Adjustable Pore Texture. *Microporous and Mesoporous Materials* **2010**, *131* (1–3), 141–147. <https://doi.org/10.1016/j.micromeso.2009.12.014>.
- (9) Urban, J.; Svec, F.; Fréchet, J. M. J. Hypercrosslinking: New Approach to Porous Polymer Monolithic Capillary Columns with Large Surface Area for the Highly Efficient Separation of Small Molecules. *Journal of Chromatography A* **2010**, *1217* (52), 8212–8221. <https://doi.org/10.1016/j.chroma.2010.10.100>.
- (10) Germain, J.; Svec, F.; Fréchet, J. M. J. Preparation of Size-Selective Nanoporous Polymer Networks of Aromatic Rings: Potential Adsorbents for Hydrogen Storage. *Chemistry of Materials* **2008**, *20* (22), 7069–7076. <https://doi.org/10.1021/cm802157r>.
- (11) Ramezanipour Penchah, H.; Ghanadzadeh Gilani, H.; Ghaemi, A. CO<sub>2</sub>, N<sub>2</sub>, and H<sub>2</sub> Adsorption by Hyper-Cross-Linked Polymers and Their Selectivity Evaluation by Gas-Solid Equilibrium. *Journal of Chemical and Engineering Data* **2020**, *65* (10), 4905–4913. <https://doi.org/10.1021/acs.jced.0c00541>.
- (12) James, A. M.; Harding, S.; Robshaw, T.; Bramall, N.; Ogden, M. D.; Dawson, R. Selective Environmental Remediation of Strontium and Cesium Using Sulfonated Hyper-Cross-Linked Polymers (SHCPs). *ACS Applied Materials & Interfaces* **2019**, *11* (25), 22464–22473. <https://doi.org/10.1021/acsami.9b06295>.
- (13) Wang, X.; Ou, H.; Huang, J. One-Pot Synthesis of Hyper-Cross-Linked Polymers Chemically Modified with Pyrrole, Furan, and Thiophene for Phenol Adsorption from Aqueous Solution. *Journal of Colloid and Interface Science* **2019**, *538*, 499–506. <https://doi.org/10.1016/j.jcis.2018.12.021>.

- (14) Penner, N. A.; Nesterenko, P. N.; Hyin, M. M.; Tsyurupa, M. P.; Davankov, V. A. Investigation of the Properties of Hypercrosslinked Polystyrene as a Stationary Phase for High-Performance Liquid Chromatography. *Chromatographia* **1999**, *50* (9–10), 611–620. <https://doi.org/10.1007/BF02493669>.
- (15) Long, C.; Li, Y.; Yu, W.; Li, A. Removal of Benzene and Methyl Ethyl Ketone Vapor: Comparison of Hypercrosslinked Polymeric Adsorbent with Activated Carbon. *Journal of Hazardous Materials* **2012**. <https://doi.org/10.1016/j.jhazmat.2011.12.010>.
- (16) Zhang, L.; Song, X.; Wu, J.; Long, C.; Li, A.; Zhang, Q. Preparation and Characterization of Micro-Mesoporous Hypercrosslinked Polymeric Adsorbent and Its Application for the Removal of VOCs. *Chemical Engineering Journal* **2012**. <https://doi.org/10.1016/j.cej.2012.03.071>.
- (17) Wang, S.; Zhang, L.; Long, C.; Li, A. Enhanced Adsorption and Desorption of VOCs Vapor on Novel Micro-Mesoporous Polymeric Adsorbents. *Journal of Colloid and Interface Science* **2014**, *428*, 185–190. <https://doi.org/10.1016/j.jcis.2014.04.055>.
- (18) Long, C.; Li, Y.; Yu, W.; Li, A. Adsorption Characteristics of Water Vapor on the Hypercrosslinked Polymeric Adsorbent. *Chemical Engineering Journal* **2012**. <https://doi.org/10.1016/j.cej.2011.11.019>.
- (19) Zhou, B.; Sun, B.; Qiu, W.; Zhou, Y.; He, J.; Lu, X.; Lu, H. Adsorption/Desorption of Toluene on a Hypercrosslinked Polymeric Resin in a Highly Humid Gas Stream. *Chinese Journal of Chemical Engineering* **2019**. <https://doi.org/10.1016/j.cjche.2018.09.027>.
- (20) Wang, J.; Wang, W.-Q.; Hao, Z.; Wang, G.; Li, Y.; Chen, J.-G.; Li, M.; Cheng, J.; Liu, Z.-T. A Superhydrophobic Hyper-Cross-Linked Polymer Synthesized at Room Temperature Used as an Efficient Adsorbent for Volatile Organic Compounds. *RSC Advances* **2016**, *6* (99), 97048–97054. <https://doi.org/10.1039/C6RA18687D>.
- (21) Águeda, V. I.; Crittenden, B. D.; Delgado, J. A.; Tennison, S. R. Effect of Channel Geometry, Degree of Activation, Relative Humidity and Temperature on the Performance

- of Binderless Activated Carbon Monoliths in the Removal of Dichloromethane from Air. *Separation and Purification Technology* **2011**, 78 (2), 154–163. <https://doi.org/10.1016/j.seppur.2011.01.036>.
- (22) Price, D. W.; Schmidt, P. S. VOC Recovery through Microwave Regeneration of Adsorbents: Process Design Studies. *Journal of the Air & Waste Management Association* **1998**, 48 (12), 1135–1145. <https://doi.org/10.1080/10473289.1998.10463758>.
- (23) Ondon, B. S.; Sun, B.; Yan, Z. Y.; Zhu, X. M.; Liu, H. Effect of Microwave Heating on the Regeneration of Modified Activated Carbons Saturated with Phenol. *Applied Water Science* **2014**, 4 (4), 333–339. <https://doi.org/10.1007/s13201-013-0147-5>.
- (24) Cherbański, R. Regeneration of Granular Activated Carbon Loaded with Toluene – Comparison of Microwave and Conductive Heating at the Same Active Powers. *Chemical Engineering and Processing - Process Intensification* **2018**, 123, 148–157. <https://doi.org/10.1016/j.cep.2017.11.008>.
- (25) Fayaz, M.; Shariaty, P.; Atkinson, J. D.; Hashisho, Z.; Phillips, J. H.; Anderson, J. E.; Nichols, M. Using Microwave Heating To Improve the Desorption Efficiency of High Molecular Weight VOC from Beaded Activated Carbon. *Environmental Science & Technology* **2015**, 49 (7), 4536–4542. <https://doi.org/10.1021/es505953c>.
- (26) Chowdhury, T.; Shi, M.; Hashisho, Z.; Sawada, J. A.; Kuznicki, S. M. Regeneration of Na-ETS-10 Using Microwave and Conductive Heating. *Chemical Engineering Science* **2012**, 75, 282–288. <https://doi.org/10.1016/j.ces.2012.03.039>.
- (27) Roussy, G.; Zoulalian, A.; Charreyre, M.; Thiebaut, J. M. How Microwaves Dehydrate Zeolites. *The Journal of Physical Chemistry* **1984**, 88 (23), 5702–5708. <https://doi.org/10.1021/j150667a049>.
- (28) Jones, D. A.; Lelyveld, T. P.; Mavrofidis, S. D.; Kingman, S. W.; Miles, N. J. Microwave Heating Applications in Environmental Engineering—a Review. *Resources, Conservation and Recycling* **2002**, 34 (2), 75–90. [https://doi.org/10.1016/S0921-3449\(01\)00088-X](https://doi.org/10.1016/S0921-3449(01)00088-X).

- (29) Falciglia, P. P.; Roccaro, P.; Bonanno, L.; De Guidi, G.; Vagliasindi, F. G. A.; Romano, S. A Review on the Microwave Heating as a Sustainable Technique for Environmental Remediation/Detoxification Applications. *Renewable and Sustainable Energy Reviews* **2018**, *95*, 147–170. <https://doi.org/10.1016/j.rser.2018.07.031>.
- (30) Pozar, D. M. *Microwave Engineering, 4th Edition*; 2012.
- (31) Chandrasekaran, S.; Ramanathan, S.; Basak, T. Microwave Material Processing-a Review. *AIChE Journal* **2012**, *58* (2), 330–363. <https://doi.org/10.1002/aic.12766>.
- (32) Shariaty, P.; Jahandar Lashaki, M.; Hashisho, Z.; Sawada, J.; Kuznicki, S.; Hutcheon, R. Effect of ETS-10 Ion Exchange on Its Dielectric Properties and Adsorption/Microwave Regeneration. *Separation and Purification Technology* **2017**, *179*, 420–427. <https://doi.org/10.1016/j.seppur.2017.02.016>.
- (33) Bradshaw, S. M.; Van Wyk, E. J.; De Swardt, J. B. Microwave Heating Principles and the Application to the Regeneration of Granular Activated Carbon. *Journal of The South African Institute of Mining and Metallurgy* **1998**, *98* (4), 201–210.
- (34) Meng, Q. B.; Yang, G.-S.; Lee, Y.-S. Preparation of Highly Porous Hypercrosslinked Polystyrene Adsorbents: Effects of Hydrophilicity on the Adsorption and Microwave-Assisted Desorption Behavior toward Benzene. *Microporous and Mesoporous Materials* **2013**, *181*, 222–227. <https://doi.org/10.1016/j.micromeso.2013.07.027>.
- (35) Jayalakshmi, C. G.; Inamdar, A.; Anand, A.; Kandasubramanian, B. Polymer Matrix Composites as Broadband Radar Absorbing Structures for Stealth Aircrafts. *Journal of Applied Polymer Science* **2018**, 47241. <https://doi.org/10.1002/app.47241>.
- (36) Saini, P.; Aror, M. Microwave Absorption and EMI Shielding Behavior of Nanocomposites Based on Intrinsically Conducting Polymers, Graphene and Carbon Nanotubes. In *New Polymers for Special Applications*; InTech, 2012. <https://doi.org/10.5772/48779>.

- (37) Kruželák, J.; Kvasničáková, A.; Hložeková, K.; Hudec, I. Progress in Polymers and Polymer Composites Used as Efficient Materials for EMI Shielding. *Nanoscale Advances*. Royal Society of Chemistry January 7, 2021, pp 123–172. <https://doi.org/10.1039/d0na00760a>.
- (38) Tian, C.; Du, Y.; Cui, C.; Deng, Z.; Xue, J.; Xu, P.; Qiang, R.; Wang, Y.; Han, X. Synthesis and Microwave Absorption Enhancement of Yolk–Shell Fe<sub>3</sub>O<sub>4</sub>@C Microspheres. *Journal of Materials Science* **2017**, *52* (11), 6349–6361. <https://doi.org/10.1007/s10853-017-0866-3>.
- (39) Micheli, D.; Vricella, A.; Pastore, R.; Marchetti, M. Synthesis and Electromagnetic Characterization of Frequency Selective Radar Absorbing Materials Using Carbon Nanopowders. *Carbon* **2014**, *77*, 756–774. <https://doi.org/10.1016/j.carbon.2014.05.080>.
- (40) Tang, J.; Bi, S.; Wang, X.; Hou, G. liang; Su, X. jia; Liu, C. hui; Lin, Y. yang; Li, H. Excellent Microwave Absorption of Carbon Black/Reduced Graphene Oxide Composite with Low Loading. *Journal of Materials Science* **2019**, *54* (22), 13990–14001. <https://doi.org/10.1007/s10853-019-03902-0>.
- (41) He, F.; Lau, S.; Chan, H. L.; Fan, J. High Dielectric Permittivity and Low Percolation Threshold in Nanocomposites Based on Poly(Vinylidene Fluoride) and Exfoliated Graphite Nanoplates. *Advanced Materials* **2009**, *21* (6), 710–715. <https://doi.org/10.1002/adma.200801758>.
- (42) Nikfar, N.; Zare, Y.; Rhee, K. Y. Dependence of Mechanical Performances of Polymer/Carbon Nanotubes Nanocomposites on Percolation Threshold. *Physica B: Condensed Matter* **2018**, *533*, 69–75. <https://doi.org/10.1016/j.physb.2018.01.008>.
- (43) Dang, Z.-M.; Wu, J.-P.; Xu, H.-P.; Yao, S.-H.; Jiang, M.-J.; Bai, J. Dielectric Properties of Upright Carbon Fiber Filled Poly(Vinylidene Fluoride) Composite with Low Percolation Threshold and Weak Temperature Dependence. *Applied Physics Letters* **2007**, *91* (7), 072912. <https://doi.org/10.1063/1.2770664>.

- (44) Wang, L.; Dang, Z.-M. Carbon Nanotube Composites with High Dielectric Constant at Low Percolation Threshold. *Applied Physics Letters* **2005**, *87* (4), 042903. <https://doi.org/10.1063/1.1996842>.
- (45) Shen, X.-Z.; Xie, S.-M.; Guo, J.; Liu, Z.-C. Microwave Absorbing Properties of Ternary Linear Low-Density Polyethylene/Carbonyl Iron Powder/Carbon Black Composites. *Journal of Applied Polymer Science* **2009**, *114* (6), 3434–3439. <https://doi.org/10.1002/app.30666>.
- (46) Min, D.; Zhou, W.; Qing, Y.; Luo, F.; Zhu, D. Enhanced Microwave Absorption Properties of Oriented Carbonyl Iron/Carbon Black Composite Induced by Shear Force. *Journal of Electronic Materials* **2017**, *46* (8), 4903–4911. <https://doi.org/10.1007/s11664-017-5493-x>.
- (47) Vinodh, R.; Jung, E. M.; Ganesh, M.; Peng, M. M.; Abidov, A.; Palanichamy, M.; Cha, W. S.; Jang, H. T. Novel Microporous Hypercross-Linked Polymers as Sorbent for Volatile Organic Compounds and CO<sub>2</sub> Adsorption. *Journal of Industrial and Engineering Chemistry* **2015**, *21*, 1231–1238. <https://doi.org/10.1016/j.jiec.2014.05.039>.
- (48) Dykas, M. M.; Poddar, K.; Yoong, S. L.; Viswanathan, V.; Mathew, S.; Patra, A.; Saha, S.; Pastorin, G.; Venkatesan, T. Enhancing Image Contrast of Carbon Nanotubes on Cellular Background Using Helium Ion Microscope by Varying Helium Ion Fluence. *Journal of microscopy* **2018**, *269* (1), 14–22. <https://doi.org/10.1111/jmi.12604>.
- (49) Neimark, A. V.; Lin, Y.; Ravikovitch, P. I.; Thommes, M. Quenched Solid Density Functional Theory and Pore Size Analysis of Micro-Mesoporous Carbons. *Carbon* **2009**, *47* (7), 1617–1628. <https://doi.org/10.1016/j.carbon.2009.01.050>.
- (50) Chiang, Y.-C.; Chiang, P.-C.; Chang, E.-E. Effects of Surface Characteristics of Activated Carbons on VOC Adsorption. *Journal of Environmental Engineering* **2001**. [https://doi.org/10.1061/\(asce\)0733-9372\(2001\)127:1\(54\)](https://doi.org/10.1061/(asce)0733-9372(2001)127:1(54)).

- (51) Jahandar Lashaki, M.; Fayaz, M.; Niknaddaf, S.; Hashisho, Z. Effect of the Adsorbate Kinetic Diameter on the Accuracy of the Dubinin–Radushkevich Equation for Modeling Adsorption of Organic Vapors on Activated Carbon. *Journal of Hazardous Materials* **2012**, 241–242, 154–163. <https://doi.org/10.1016/j.jhazmat.2012.09.024>.
- (52) Zhang, X.; Yang, Y.; Lv, X.; Wang, Y.; Liu, N.; Chen, D.; Cui, L. Adsorption/Desorption Kinetics and Breakthrough of Gaseous Toluene for Modified Microporous-Mesoporous UiO-66 Metal Organic Framework. *Journal of Hazardous Materials* **2019**. <https://doi.org/10.1016/j.jhazmat.2018.11.099>.
- (53) Sui, H.; Liu, H.; An, P.; He, L.; Li, X.; Cong, S. Application of Silica Gel in Removing High Concentrations Toluene Vapor by Adsorption and Desorption Process. *Journal of the Taiwan Institute of Chemical Engineers* **2017**. <https://doi.org/10.1016/j.jtice.2017.02.019>.
- (54) Feng, A.; Yu, Y.; Mi, L.; Cao, Y.; Yu, Y.; Song, L. Structural, Textural and Toluene Adsorption Properties of NH<sub>4</sub>HF<sub>2</sub> and Alkali Modified USY Zeolite. *Microporous and Mesoporous Materials* **2019**, 290, 109646. <https://doi.org/10.1016/j.micromeso.2019.109646>.
- (55) Brodie, G.; Jacob, M. V.; Farrell, P. 6 Techniques for Measuring Dielectric Properties. In *Microwave and Radio-Frequency Technologies in Agriculture*; De Gruyter Open Poland, 2015; pp 52–77. <https://doi.org/10.1515/9783110455403-007>.
- (56) Levchik, G. F.; Si, K.; Levchik, S. V.; Camino, G.; Wilkie, C. A. Correlation between Cross-Linking and Thermal Stability: Cross-Linked Polystyrenes and Polymethacrylates. *Polymer Degradation and Stability* **1999**. [https://doi.org/10.1016/S0141-3910\(99\)00028-2](https://doi.org/10.1016/S0141-3910(99)00028-2).
- (57) Ismail, H.; Pasbakhsh, P.; Fauzi, M. N. A.; Abu Bakar, A. Morphological, Thermal and Tensile Properties of Halloysite Nanotubes Filled Ethylene Propylene Diene Monomer (EPDM) Nanocomposites. *Polymer Testing* **2008**, 27 (7), 841–850. <https://doi.org/10.1016/j.polymertesting.2008.06.007>.

- (58) Norkhairunnisa, M.; Azizan, A.; Mariatti, M.; Ismail, H.; Sim, L. C. Thermal Stability and Electrical Behavior of Polydimethylsiloxane Nanocomposites with Carbon Nanotubes and Carbon Black Fillers. *Journal of Composite Materials* **2012**. <https://doi.org/10.1177/0021998311412985>.
- (59) Kosuge, K.; Kubo, S.; Kikukawa, N.; Takemori, M. Effect of Pore Structure in Mesoporous Silicas on VOC Dynamic Adsorption/Desorption Performance. *Langmuir* **2007**. <https://doi.org/10.1021/la062616t>.
- (60) Taguchi, A.; Schüth, F. Ordered Mesoporous Materials in Catalysis. *Microporous and Mesoporous Materials*. 2005. <https://doi.org/10.1016/j.micromeso.2004.06.030>.
- (61) Mu, B.; Schoenecker, P. M.; Walton, K. S. Gas Adsorption Study on Mesoporous Metal–Organic Framework UCM-1. *The Journal of Physical Chemistry C* **2010**, *114* (14), 6464–6471. <https://doi.org/10.1021/jp906417z>.
- (62) Ma, F. J.; Liu, S. X.; Liang, D. D.; Ren, G. J.; Wei, F.; Chen, Y. G.; Su, Z. M. Adsorption of Volatile Organic Compounds in Porous Metal-Organic Frameworks Functionalized by Polyoxometalates. *Journal of Solid State Chemistry* **2011**. <https://doi.org/10.1016/j.jssc.2011.09.002>.
- (63) Vermoortele, F.; Bueken, B.; Le Bars, G.; Van de Voorde, B.; Vandichel, M.; Houthoofd, K.; Vimont, A.; Daturi, M.; Waroquier, M.; Van Speybroeck, V.; Kirschhock, C.; De Vos, D. E. Synthesis Modulation as a Tool To Increase the Catalytic Activity of Metal–Organic Frameworks: The Unique Case of UiO-66(Zr). *Journal of the American Chemical Society* **2013**, *135* (31), 11465–11468. <https://doi.org/10.1021/ja405078u>.
- (64) Lee, D.-G.; Kim, J.-H.; Lee, C.-H. Adsorption and Thermal Regeneration of Acetone and Toluene Vapors in Dealuminated Y-Zeolite Bed. *Separation and Purification Technology* **2011**, *77* (3), 312–324. <https://doi.org/10.1016/j.seppur.2010.12.022>.

- (65) Yacubowicz, J.; Narkis, M.; Benguigui, L. Electrical and Dielectric Properties of Segregated Carbon Black-Polyethylene Systems. *Polymer Engineering and Science* **1990**, *30* (8), 459–468. <https://doi.org/10.1002/pen.760300806>.
- (66) Cherbański, R.; Komorowska-Durka, M.; Stefanidis, G. D.; Stankiewicz, A. I. Microwave Swing Regeneration vs Temperature Swing Regeneration—Comparison of Desorption Kinetics. *Industrial & Engineering Chemistry Research* **2011**, *50* (14), 8632–8644. <https://doi.org/10.1021/ie102490v>.

# **CHAPTER 6: VOC ADSORPTION AND MICROWAVE ABSORPTION STUDY OF POROUS GRAPHENE OXIDE/POLYMER NANOCOMPOSITES**

## **6.1 Chapter Overview**

Filler agglomeration during the in-situ polymerization of composites was shown in the previous chapter to negatively impact the pore properties of prepared composites. In this chapter, solution mixing method was selected to minimize the filler agglomeration in the composite. Graphene oxide (GO) was also selected as the microwave (MW) absorptive filler that could potentially have a low percolation threshold due to its large aspect ratio. In this regard, polymers of 4, 4'-bis((chloromethyl)-1, 1'-biphenyl- benzyl chloride) were synthesized through the Friedel-Crafts reactions and GO nano-sheets were synthesized through the Hummer's method. Then, ethanol was selected as the solvent to fabricate a series of nanocomposites with different GO contents (1-8 wt%) by solution mixing method. X-Ray Diffraction (XRD) and Fourier Transform Infrared (FTIR) analysis was performed to study the synthesis of GO, hypercrosslinked polymer, and GO-filled nanocomposite. The morphology of synthesized samples and GO dispersion were characterized by scanning electron microscopy, helium ion microscopy, and transmission electron microscopy analysis. Thermogravimetry analysis and N<sub>2</sub> adsorption at 77 °K were performed to investigate the effect of GO content on the thermal stability and pore properties of nanocomposites, respectively. Finally, dielectric property measurement and MW heating experiments were performed to study the extent of MW absorption enhancement by GO content in the matrix.

## 6.2 Introduction

Hypercrosslinked polymer (HCP), as a type of porous polymers with a micro-mesopore structure, has received much attention in adsorption process due to its lightweight, large specific surface area, high physiochemical stability, and low production cost.<sup>1-4</sup> Besides, compared to traditional VOC adsorbents, HCPs have better chemical stability and adsorption/desorption kinetics. The adsorption properties of HCPs can be controlled by tuning the degree of crosslinking, the temperature during crosslinking, the solvent, the catalyst, and functional group addition.<sup>5,6</sup> Additionally, the hydrophobicity of HCPs can be tailored to enhance adsorption of non-polar VOCs in humid conditions.<sup>7</sup>

The adsorption of VOCs on HCPs progressively decreases the adsorbent's removal efficiency until breakthrough is reached at which point the adsorbent need to be regenerated. Adsorbent regeneration, often known as the most limiting step in the adsorption process, is a time- and energy-consuming stage and is often completed through using hot purge gas or superheated steam.<sup>8,9</sup>

Recently, microwave (MW) heating has emerged as an attractive technique for adsorbent regeneration.<sup>10-12</sup> The considerable advantages offered by MW regeneration such as quick and volumetric heating of adsorbent, lower process temperature, and energy-efficient and repeatable processes surpass other regeneration techniques.<sup>13-15</sup> MW heating is based on conduction loss and dipole moment reorientation.<sup>16</sup> Conduction loss is the dominant heating mechanism in electrical conductors and dipole moment reorientation in the MW field is the main heating mechanism in materials with polar molecules.<sup>16</sup> Therefore, HCPs need to be electrically conductive and/or have

polar molecules for effective MW-assisted regeneration. However, most HCPs are nonconductive and have rigid molecular structures, leading to little or no reorientation of the dipoles in the MW field and poor MW absorption<sup>17,18</sup>

A practical approach to improve MW-assisted regeneration of HCPs is to incorporate MW absorbing materials (MAM) into the polymeric matrix. Magnetic powders like cobalt and nickel and carbon-based powders such as carbon nanotubes, carbon black, and graphite nanoparticles are the most prominent categories of MAMs.<sup>19-24</sup> Among MAMs, graphene oxide (GO), the most robust two-dimensional material with extraordinary features such as superior heat conductivity, lightweight, and easy synthesis, has shown remarkable MW absorption properties.<sup>25-27</sup>

In the current study, graphene oxide was selected as a MAM filler for a hypercrosslinked polymer. GO-filled nanocomposites were synthesized for the first time from (4, 4'-bis ((chloromethyl)-1, 1'-biphenyl) + (benzyl chloride)) via the Friedel-Crafts reaction. The porous GO-nanocomposites hold great promise for gas adsorption. The thermal, chemical structure, morphological features, and pore properties of samples were investigated via X-ray diffraction (XRD), Fourier transform infrared spectroscopy (FTIR), scanning/transmission electron microscopy (SEM/TEM), helium ion microscopy (HIM), thermo-gravimetric analysis (TGA), and nitrogen adsorption isotherm. The toluene adsorption isotherms of the nanocomposites were obtained, and the MW regeneration of samples was comprehensively assessed. To the best of the authors' knowledge, such a systematic study on the VOC adsorption and MW regeneration of these nanocomposites is quite new and cannot be found in the literature.

## 6.3 Experimental Section

### 6.3.1 Materials

All chemicals, including [4, 4'-bis (chloromethyl)-1, 1'-biphenyl] (95 %), dimethoxy methane (99 %), 1, 2-dichloroethane (99 %), Iron (III) chloride (98 %), benzyl chloride (99 %), hydrochloric acid (1 M), methanol (99 %), acetone (99 %), toluene (99 %), graphite powder (99.9), potassium permanganate (KMnO<sub>4</sub>, 99 %), sulfuric acid (H<sub>2</sub>SO<sub>4</sub>, 99 %), and phosphoric acid (H<sub>3</sub>PO<sub>4</sub>, 99 %), were supplied by Sigma-Aldrich. Distilled water was used throughout the synthesis procedure.

### 6.3.2 Synthesis of Graphene Oxide

The graphene oxide was synthesized through a modified Hummer's method.<sup>28,29</sup> Briefly, 5 g of KMnO<sub>4</sub> was reacted with 1 g of graphite powder in 100 ml solution of H<sub>2</sub>SO<sub>4</sub>/H<sub>3</sub>PO<sub>4</sub> (4:1). The synthesized GO was washed several times with distilled water and finally freeze-dried.

### 6.3.3 Synthesis of Hypercrosslinked Polymer

The polymerization was performed based on the reported method by Vinodh et al. in a 100 ml round bottom flask equipped with a mechanical stirrer, heating bath, and thermometer.<sup>30</sup> 50 ml of 1, 2-dichloroethane was added to 2.5 ml of dimethoxy methane and mixed for 5 min. The powdery ingredients, i.e., 1.1 g of [4, 4'-bis (chloromethyl)-1, 1'-biphenyl], and 3.5 g of ferric chloride, were added gradually to the solution and stirred at 550 rpm for an extra 15 min. In the following, a 10 ml mixture of benzyl chloride and 1,2-dichloroethane (1:10) was added dropwise to the solution using a syringe pump. The reaction temperature was raised to 40 °C at a heating rate of 1 °C/min and stirred for four hours. Afterward, the solution was heated up to 80 °C for 20 hours to

complete the polymerization reaction. Finally, the product was filtered and washed several times with methanol, HCl solution, water, and acetone. All the synthesized polymers were dried at 110 °C for a day under vacuum.

#### **6.3.4 Preparation of Graphene Oxide/Polymer Nanocomposites**

Nanocomposites' properties tightly depend on the quality of the nanofiller, such as purity and aspect ratio.<sup>31-33</sup> Besides, the proper dispersion of fillers is a critical factor that governs the physical properties of the nanocomposite. Agglomeration and inappropriate dispersion of nanoparticles could deteriorate the nanocomposite's mechanical, thermal, and dielectric properties.<sup>34</sup> Filler surface modification with proper functionalities has been widely used to improve dispersion and prevent filler aggregation in the polymer matrix.<sup>35</sup> However, the structure of nanofillers could be changed due to the deformation of covalent functionalization upon chemical reactions.<sup>36</sup>

In this study, GO nanosheets were synthesized and used without any modification. The nanosheets were physically dispersed inside the polymer structure. A specified amount of polymer was added to 50 ml ethanol and stirred for half an hour to attain a homogenous solution. The graphene oxide nanoparticle in different weight percentages was added to the solution and mixed for 30 min. After that, the mixture was sonicated for an hour at 25 °C and 100 watts. Subsequently, the suspension was vacuum filtered, and the nanocomposite was dried at 110 °C overnight under vacuum.

### 6.3.5 Characterizations and Measurements

#### 6.3.5.1 XRD analysis

The crystallinity of synthesized GO was studied by XRD analysis on Bruker D8 FOCUS XRD with a Cu Ka radiation source operating at 40 kV and 30 mA in a scanning range of  $2\theta=10-60^\circ$ .

#### 6.3.5.2 FTIR analysis

FTIR spectroscopy was used to confirm the synthesis of GO and polymer. FTIR spectra were performed on a 100-FTIR Spectrometer, Perkin-Elmer, in the scanning spectrum of 400 to 4000 with a resolution of  $4\text{ cm}^{-1}$  to confirm the right synthesis of the graphene oxide nanoparticles and polymer. All spectra were collected in transmission mode, and background absorbance was subtracted from that of samples.

#### 6.3.5.3 Microscopy study

The morphology of synthesized GO was studied by Scanning Electron Microscopy (SEM, MIRA3-TESCAN-3-XMU). However, it was difficult to detect GO sheets in HCP with SEM as both are predominantly made of carbon, which reduced the image contrast. Therefore, a Zeiss Orion Nanofab helium ion microscope (HIM) was used to visualize the state of GO particles in HCP. Unlike SEM, high contrast images can be obtained from nonconductive carbon-rich samples (such as HCP) with HIM due to surface neutralization of the sample by an in situ electron flood gun.<sup>37</sup> HIM analysis was carried out on the selected samples at 35 kV, a working distance of 8.5 mm, a scan dwell time of 0.2  $\mu\text{s}$ , and two resolutions of 1 and 2  $\mu\text{m}$ . The only drawback of HIM analysis is its limitation in studying the nanofillers dispersion in the polymer at the sample surface.

Therefore, transmission electron microscopy (TEM) was used to investigate the dispersion of GO particles in the synthesized nanocomposites. TEM images were taken on a JEOL JEM-ARM200CF S/TEM electron microscope at an accelerating voltage of 200 kV. The TEM images were processed using Gatan Digital Micrograph software. TEM samples were prepared by depositing a droplet of a well-dispersed sample onto an ultra-thin carbon-coated copper grid (obtained from Electron Microscopy Science Inc). The grid was dried at least 24 h before data collection.

#### 6.3.5.4 *TGA analysis*

The temperature of adsorbents could increase to more than 300 °C during the regeneration stage, leading to structural decomposition of the samples.<sup>38</sup> The cyclical performance of the adsorbent has a close relationship to its structural integrity. Hence, assessing the thermal stability behavior of adsorbents at elevated temperatures is of great importance. In this study, a Perkin-Elmer Pyris thermogravimetric analyzer was used to investigate the samples' thermal stability at a temperature range of 40 °C to 900 °C with a heating ramp of 10 °C/min under nitrogen atmosphere.

#### 6.3.5.5 *Micropore surface analysis*

Pore properties of samples were studied using N<sub>2</sub> (99.9 %) adsorption at 77 °K in a micropore surface analyzer (Autosorb iQ, Quantachrome). Samples were degassed at 110 °C for 5 h before the measurements. BET surface area analysis was carried out within the relative pressure values of 0.001 to 0.03. Pore size distribution (PSD) analysis was performed using the density function theory method, assuming slit-shaped pores within the relative pressure values of 10<sup>-7</sup> to 0.99. Total

pore volume was determined based on the adsorbed volume of nitrogen at a relative pressure of 0.99.

#### 6.3.5.6 *VOC adsorption isotherm*

A vapor sorption analyzer (TA instrument, VTI-SA), using ultrapure nitrogen (99.9 %) as the carrier gas, was used to investigate the samples' toluene adsorption performance. Toluene adsorption experiments were performed by increasing the relative saturation pressure from 0.02 to 0.9 at 25 °C. Adsorption continued until equilibrium state was achieved (i.e., < 0.01wt% change in 5 min). Samples' weight changes were recorded to calculate the adsorption capacity at each relative pressure.

#### 6.3.5.7 *Dielectric properties and penetration depth*

Several studies have shown the direct relationship between MW heating and the dielectric loss factor,  $\epsilon''$ , of material.<sup>39,40</sup> Loss factor has a direct correlation with the conduction loss in the material, which can be shown using the Debye Theorem (Eq. 1).<sup>41</sup>

$$\epsilon'' \propto \sigma / \omega \epsilon_0 \quad \text{Eq. 1}$$

where  $\epsilon''$  is the dielectric loss factor;  $\sigma$  is the conductivity;  $\omega$  is the angular frequency in rad/s, and  $\epsilon_0$  is the free space permittivity. Therefore, the dielectric loss factor can be used to evaluate the extent of conduction loss and MW heating inside the irradiated material. In this study, a vector network analyzer (VNA, Rohde and Schwarz) and an open-ended probe (Keycom) were used to measure the samples' dielectric properties at 2.45 GHz and ambient conditions. A quartz tube was

used to hold the sample. The probe was calibrated using a short, open, and standard sample termination before each measurement.

One of the major concerns associated with MW heating is the non-uniform temperature distribution in the irradiated material.<sup>42-44</sup> Penetration depth of MW in the irradiated object has been reported as one of the main parameters that affect the temperature uniformity. MW penetration depth is defined as the distance from the surface of the irradiated object at which the power decays to 1/e of its value at the surface. Therefore, it can be expected to have inefficient heating in objects with a thickness much smaller than the penetration depth and non-uniform MW heating in objects with a thickness much larger than the penetration depth.<sup>45</sup> Penetration depth is inversely proportional to the dielectric loss factor and calculated from the following equation.<sup>46</sup>

$$D_p = \frac{\lambda_0}{2\pi\sqrt{2\varepsilon'}} \left[ \left( 1 + \left( \frac{\varepsilon''}{\varepsilon'} \right)^2 \right)^{\frac{1}{2}} - 1 \right]^{-\frac{1}{2}} \quad \text{Eq. 2}$$

where  $\lambda_0$  is the MW wavelength in free space,  $\varepsilon'$  is the dielectric constant, and  $\varepsilon''$  is the dielectric loss factor.

#### 6.3.5.8 *Microwave heating rate and capacity*

The MW heating rate of synthesized nanocomposites was experimentally measured at different MW applied power using the following equation.

$$\text{Heating rate} = \frac{T_{\text{final}} - T_{\text{initial}}}{\Delta t} \quad \text{Eq. 3}$$

$T_{\text{final}}$  is the sample temperature at the steady-state heated condition,  $T_{\text{initial}}$  is the sample temperature before heating, and  $\Delta t$  is the time to reach the steady-state temperature (i.e.,  $<0.1^{\circ}\text{C}$  change in 2 min). Furthermore, the MW heating capacity was obtained by calculating the required MW energy consumed to increase the temperature of 1 g specimen by one degree Celsius.

#### 6.3.5.9 *Toluene adsorption and microwave-assisted desorption*

VOC adsorption and desorption behavior of synthesized nanocomposites was studied in a lab-scale adsorption setup and a MW heating system, respectively. Adsorption experiments were carried out at  $25^{\circ}\text{C}$  using 2 g samples in a quartz tube with 2.2 cm inner diameter. Each sample was saturated with toluene at 500 ppm. Following adsorption, the toluene-saturated adsorbent was regenerated using MW heating at 2.45 GHz and 20 watts. All MW heating experiments were carried out at a constant MW applied power. The adsorbent bed was continuously purged with 1 SLPM  $\text{N}_2$  (99%) for 60 minutes during the regeneration. A flame ionization detector (FID) was used to measure the effluent toluene concentration. Desorption efficiency of toluene from HCP with and without GO filler were calculated based on toluene concentration in the effluent stream and ideal gas law. The details of VOC adsorption and MW-assisted regeneration setups are reported elsewhere.<sup>47</sup>

## 6.4 Results and Discussion

### 6.4.1 XRD

XRD was used to assess the inter-planar distance between the atomic planes contained in the GO samples. Figure 6-1 shows (001) diffraction peak at  $2\theta=13^\circ$  which indicate a distance between graphene layers of 0.71 nm, based on Bragg's equation. Besides, graphene diffraction peak, typically between  $20^\circ$  to  $30^\circ$ , didn't appear in the XRD spectrum which confirms the successful synthesis of GO. These results are consistent with reported XRD spectra for the synthesized GO by Hummers method.<sup>48,49</sup>

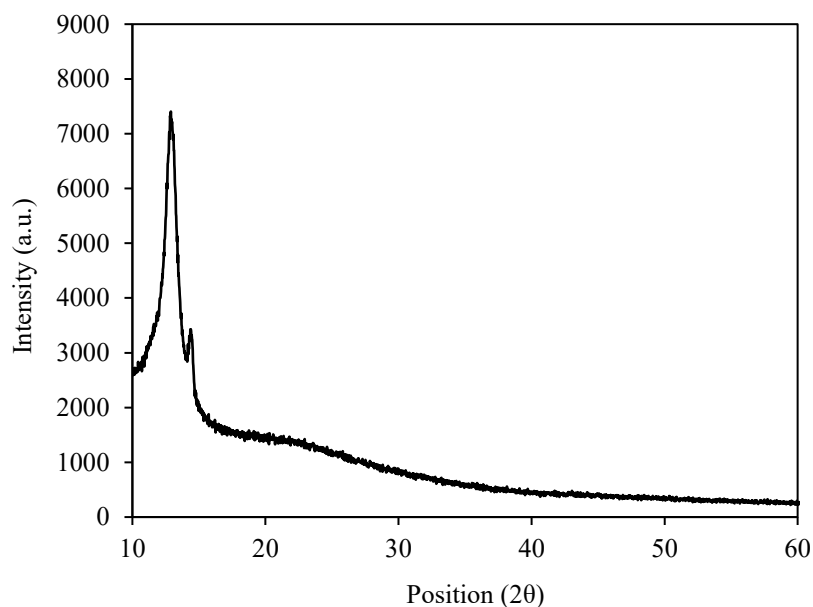


Figure 6-1. XRD spectrum of synthesized GO.

### 6.4.2 FTIR

The FTIR spectra of the synthesized GO, pristine polymer and 8% GO-holding nanocomposite are shown in Figure 6-2. The FTIR spectrum of GO showed various oxygen functionalities, including

hydroxyls, epoxide, and carbonyls. The broad absorption band in 3300-3400  $\text{cm}^{-1}$  is assigned to the O-H stretching vibrations. The bands at 1720  $\text{cm}^{-1}$  and 1610  $\text{cm}^{-1}$  relate to the C=O stretching vibration and C=C from unoxidized  $\text{sp}^2$  C=C bonds. The band around 1240  $\text{cm}^{-1}$  is related to the C-O vibrations. The pristine polymer and GO nanocomposite have almost the same FTIR spectra. The broad band around 2918  $\text{cm}^{-1}$  is related to the aromatic C-H stretching vibrations. The sharp absorption band observed at 1701  $\text{cm}^{-1}$  is assigned to the C-H bending vibration. Bands at 1438 and 1606  $\text{cm}^{-1}$  are ascribed to aromatic ring vibrations. The bands below the wavenumber of 1000  $\text{cm}^{-1}$  originate from aromatic C-H bending modes. These bands occurred in the same wavenumbers for both pristine polymer and the polymer holding 8 wt% GO. No trace of water was observed in the FTIR spectra, indicating successful drying of the samples. These results illustrate the successful synthesis of GO and the HCP based on the published FTIR spectra for GO and HCP.<sup>27,30</sup>

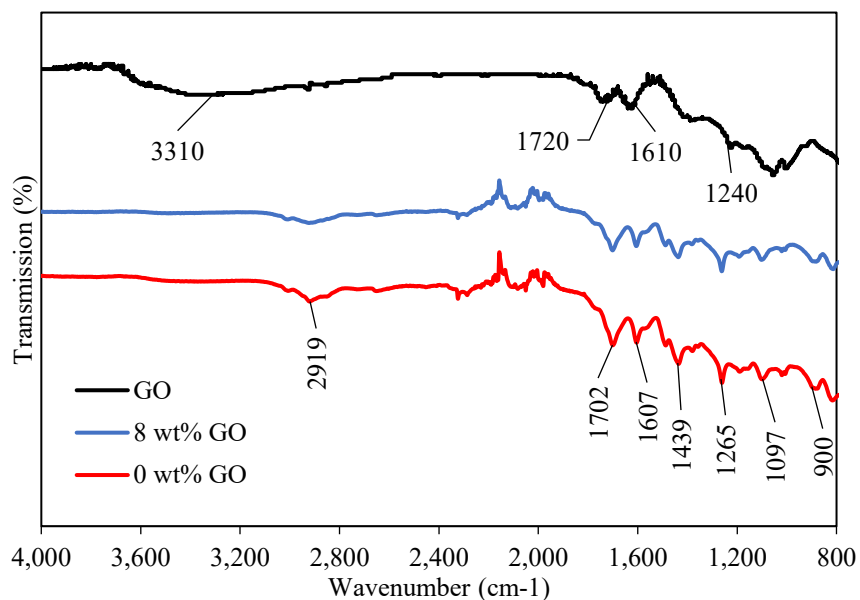


Figure 6-2. FTIR spectra acquired for 0 wt% and 8 wt% GO/HCP.

### 6.4.3 Microscopic Studies

SEM image of synthesized GO shows a sheet-like structure (Figure 6-3). GO shows a randomly aggregated, thin, multi-layer structure. Previous studies reported a similar morphology on GO.<sup>50,51</sup> The SEM image illustrates that GO possesses an ultra-hollow framework constructed with sheets. This particularly contributes to GO's lightweight since sheets are loosely stacked on top of each other.

The morphology of HCP polymer and GO filled polymer was investigated using HIM analysis (Figure 6-4). The porous HCP has a rough surface. The micrograph for the sample containing 8 wt% GO revealed the two-dimensional layer-like structure of GO particles. A similar morphology can be found in a study by Zhang et al. on grafting of polystyrene onto reduced graphene oxide.<sup>52</sup> The size of GO agglomerates in the 8 wt% GO sample varies within 2-6  $\mu\text{m}$ .

The TEM images of pristine HCP and the GO-filled nanocomposite are depicted in Figure 6-5. The presence of the two distinct phases in the TEM image of GO-containing samples, i.e., dark black and light black, confirms the dispersion of GO nanosheets inside the polymer matrix. The TEM images also confirmed the proper dispersion of GO into the HCP.

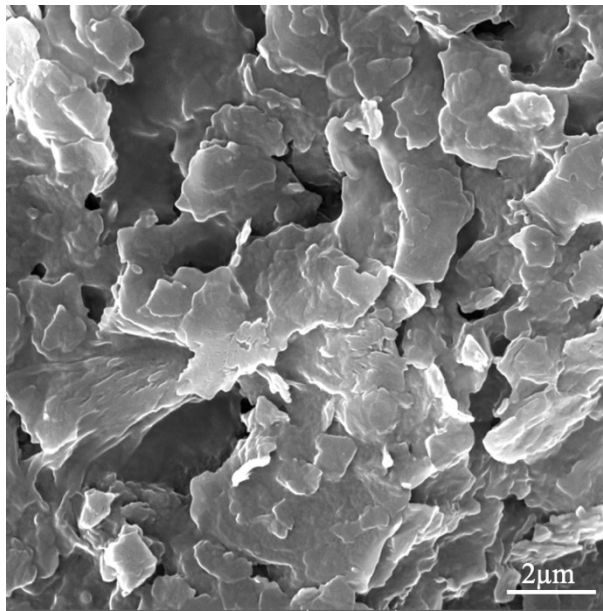
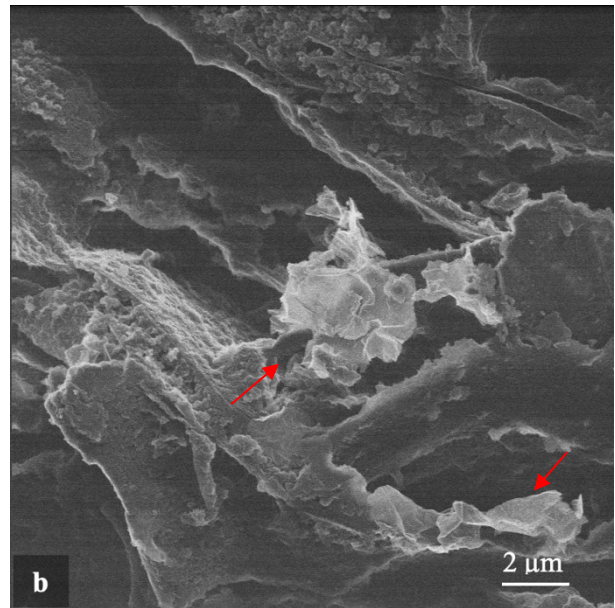
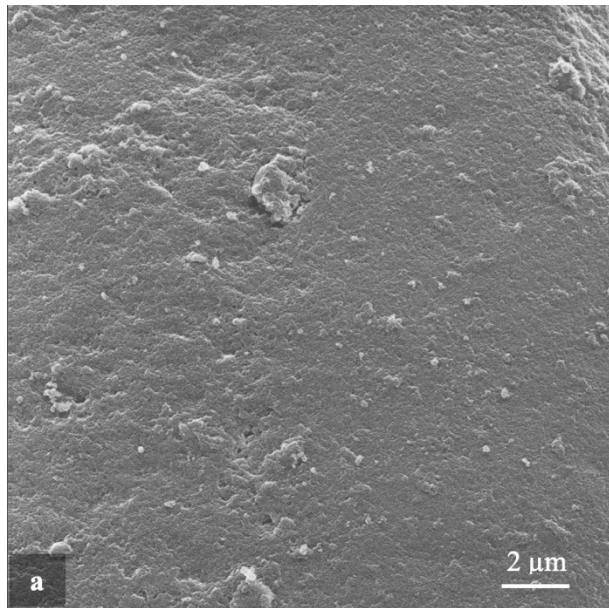


Figure 6-3. SEM image of synthesized GO sheets.



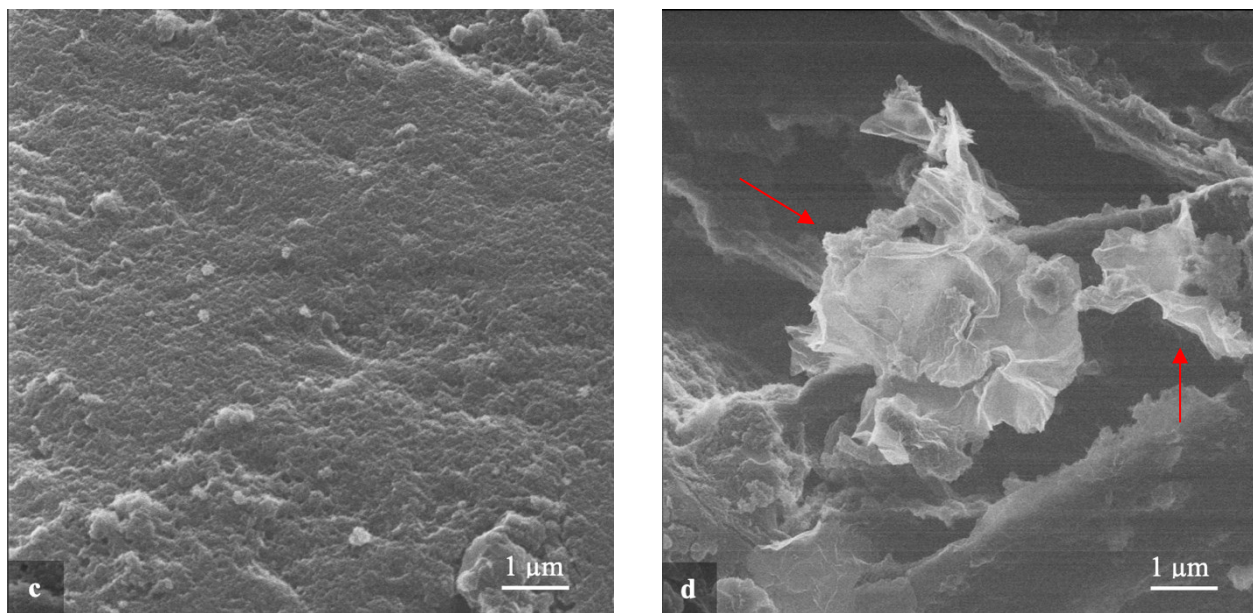


Figure 6-4. HIM images of synthesized HCPs with 0 wt% GO (a & c) and 8 wt% GO (b & d).

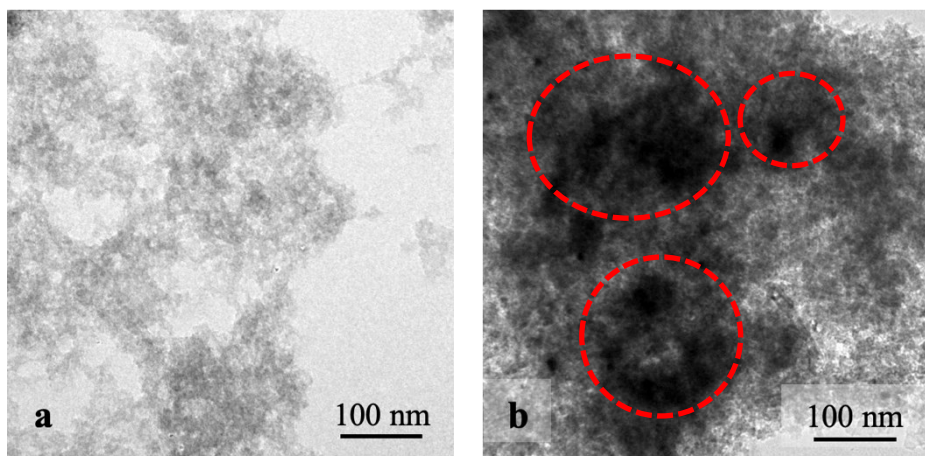


Figure 6-5. TEM images of synthesized HCPs with 0 wt% GO (a) and 8 wt% GO (b). Red circles indicate areas abundant in GO.

#### 6.4.4 Thermal Properties of Adsorbents

The thermal stability of the GO sheets, HCP, and GO filled nanocomposites was studied using TGA analysis. Figure 6-6 illustrates TGA and its first-derivative (DTGA) thermograms of GO, pristine HCP, and GO-filled nanocomposites. As the GO thermogram shows, an initial weight loss of about 10% occurred below 100 °C due to water loss. The second weight loss occurred at a temperature around 220 °C due to the thermal decomposition of oxygen-containing functional groups such as hydroxyl, carbonyl, and carboxylic acid groups, causing a 25 % weight reduction. Finally, at the third stage, at the temperature range of 590 – 710 °C, a weight loss of about 20% emerged due to the decomposition of carbon-carbon bonds of the main structure of GO.<sup>53,54</sup>

The pristine polymer (0 wt% GO) experienced one-step thermal degradation, starting from 280 °C. The polymer was decomposed entirely at a temperature around 887 °C. For the GO-containing samples, a different degradation trend was observed. All samples underwent two-step thermal degradation. The first one started at a temperature around 250 °C, lower than the onset degradation of the pristine polymer, and the second step initiated at a temperature around 400 °C. As an indicator of thermal stability, the remaining sample weight at 887 °C was 65% of the initial weight for the sample holding 1 wt% GO, which is much higher than the pristine polymer (~1 %). This shows the prominent role of GO content, even at a low amount, on the thermal stability of the samples. This observation could be attributed to the good thermal stability of GO and the better heat transfer in nanocomposite due to the high thermal conductivity of GO-filled nanocomposites. Moreover, the proper dispersion of GO in the polymer matrix enhanced the polymer-filler

interactions and reduced the macromolecular motions, boosting the thermal stability of nanocomposites.<sup>55,56</sup> The results revealed that further increase of GO content up to 8 wt% has negligible effect on the thermal stability of the specimens.

The first-derivative TGA (DTGA) was extracted to get more insights into the specimen's degradation. As shown in Figure 6-6.b, the pristine polymer revealed a broad peak at 280 °C to 700 °C. This peak is composed of two peaks, centered at 330 °C and 540 °C. The first inflection point at about 380 °C is related to the evaporation of ferric chloride, and the second one belongs to the degradation of the carbon skeleton of the polymer. The new peak that appeared at around 220 °C in samples containing GO is related to the decomposition of unstable oxygen-containing functional groups on GO structure. Figure 6-6.b illustrated that the addition of GO markedly decreased the degradation peaks intensity of polymer, approving its boosting effect on the thermal stability of the nanocomposite.

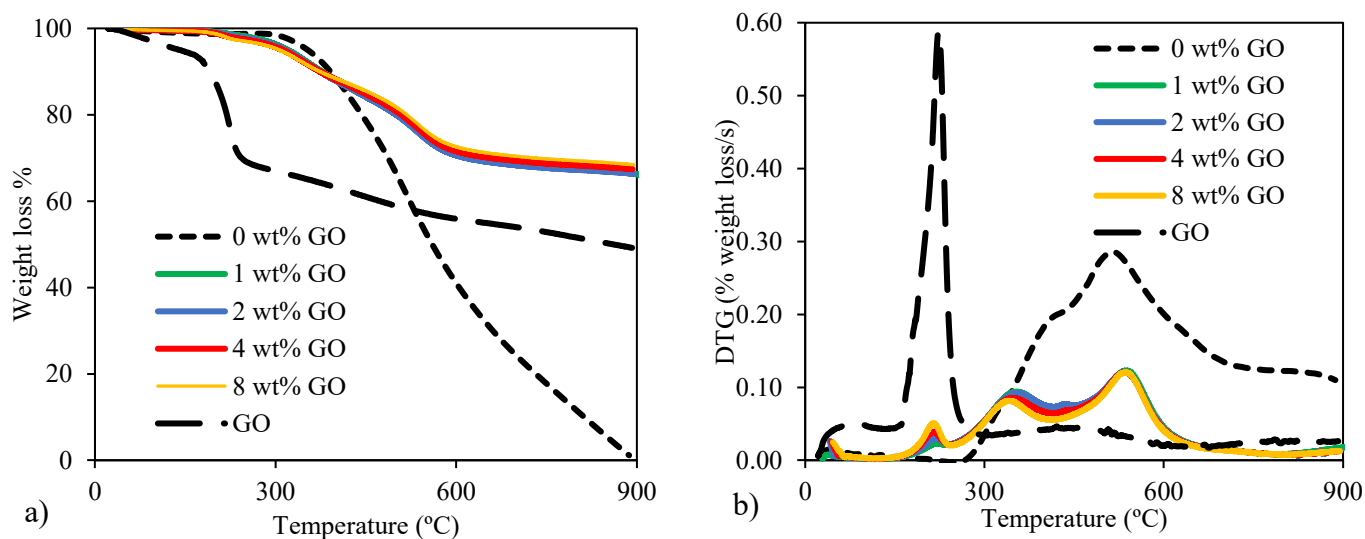


Figure 6-6. a) Percent weight loss, and b) weight loss rate versus temperature of synthesized GO/HCPs.

### 6.4.5 Textural Analysis

Adsorbent pore properties, including surface area, pore volume, and pore size distribution, play a dominant role in VOC adsorption/desorption performance of adsorbents.<sup>57,58</sup> Hence, the effect of GO addition on HCP pore properties was investigated using N<sub>2</sub> adsorption isotherm. Figure 6-7.a shows that the pristine polymer has a surface area of 1269 m<sup>2</sup>/g, with a total pore volume of 1.18 cc/g. The introduction of 8 wt% GO into the polymer negligibly reduced the BET surface area, by about 7%. This reduction is attributed to the nonporous structure of GO nanosheets. The total pore volume decreased to 1.07 cc/g for the sample containing 8 wt% GO. The pore size distribution analysis of the synthesized nanocomposites reveals a mesoporous (2 nm < pore diameter < 50 nm) structure (Figure 6-7.b). Large pore size can potentially reduce the diffusion limitation of adsorbates during adsorption/desorption by providing larger pathways for the molecular transportation inside the adsorbent, unlike fully microporous adsorbents.

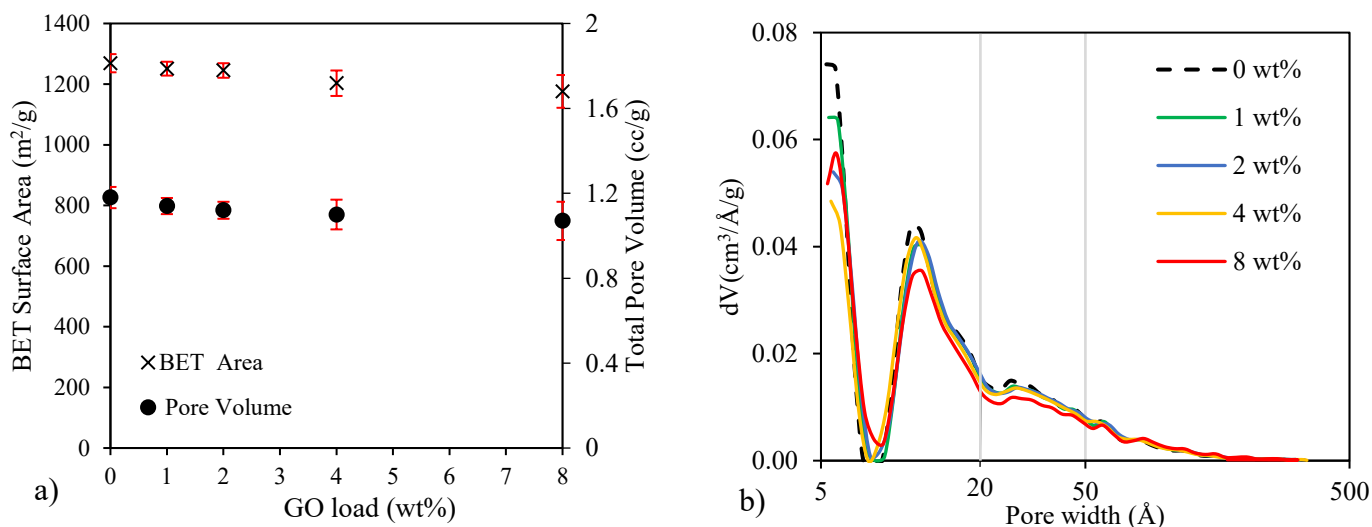


Figure 6-7. a) BET surface area, total pore volume, and b) pore size distribution of synthesized GO/HCPs. Error bars represent the standard deviation of two measurements.

### 6.4.6 Toluene Adsorption Isotherm

Figure 6-8 shows the adsorption isotherms of toluene on pristine HCP and GO-filled nanocomposite samples. For all the samples, the adsorption capacity steeply increases at very low toluene relative pressures but the increase gradually slowed down. The dramatic increase at low pressures could be attributed to the presence of a large available free surface area, responsible for toluene adsorption, which was continuously occupied by toluene molecules with rising pressure. As depicted in Figure 6-8, the introduction of GO into the polymer did not markedly change the adsorption capacity, neither at low nor high relative pressures. The addition of 8 wt % GO decreased the adsorption capacity at low and high relative pressures by 9 % and 8 wt %, respectively.

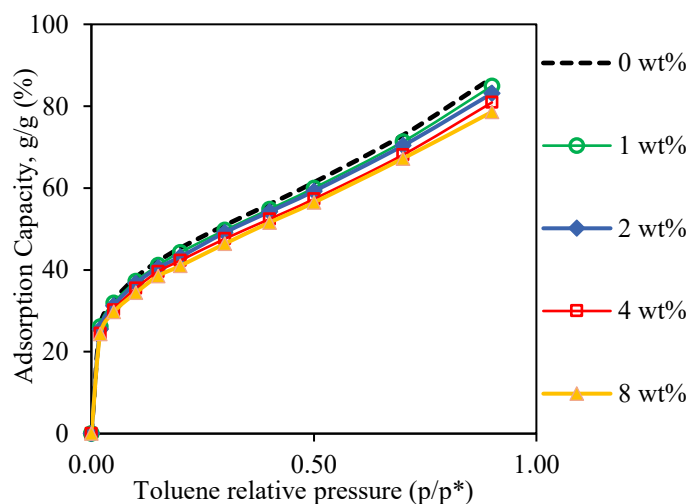


Figure 6-8. Toluene adsorption isotherms of GO/HCPs at 25 °C.

### 6.4.7 Dielectric Properties Measurement

The dielectric properties and penetration depth of the pristine polymer and nanocomposites were studied at 2.45 GHz and room temperature (Figure 6-9a). Both dielectric constant ( $\epsilon'$ ) and loss factor ( $\epsilon''$ ) of nanocomposites were enhanced by the addition of GO. The addition of GO up to 2 wt% showed no considerable effect on  $\epsilon'$  and  $\epsilon''$ . However, further increment of fillers rapidly enhanced the dielectric constant and dielectric loss factor. The addition of 2 and 8 wt% GO to the pristine polymer enhanced dielectric constant by 36 % and 263 %, respectively, illustrating the profound effect of GO on the dielectric constant. The same trend was observed for the effect of GO on the loss factor. More than 29 times improvement in the dielectric loss factor was observed in the nanocomposite with 8 wt% GO. The sharp increase in both parameters at GO contents higher than 2 wt% is attributed to reaching the percolation threshold of GO. Liu et al. showed that dielectric properties improvement in the GO filled nanocomposites is mainly due to the dipolar relaxation and interfacial polarization.<sup>59</sup> In fact, large number of defects such as dangling bonds and vacancies at the polymer-GO interface creates a capacitor-like structure which results in interfacial polarization and loss factor enhancement.<sup>59</sup> Since GO nanosheets have a higher aspect ratio compared to spherical fillers, percolation structure can be produced at a low filler loading such as 4 wt%.<sup>60</sup> Figure 6-9.b presents the calculated penetration depths of synthesized HCP and GO-filled nanocomposites. The addition of 8 wt% GO sharply decreased the penetration depth from 77.4 cm down to 4.9 cm, revealing the boosting effect of GO on the MW absorption efficiency. Based on the MW penetration depth analysis, the sample holding 4 wt % GO was selected as the best filler content that promotes MW heating efficiency and prevents non-uniform

heating. These results demonstrate that GO addition can be used to tune the MW penetration depth inside the material and enhance the MW absorption efficiency inside the adsorbent bed.

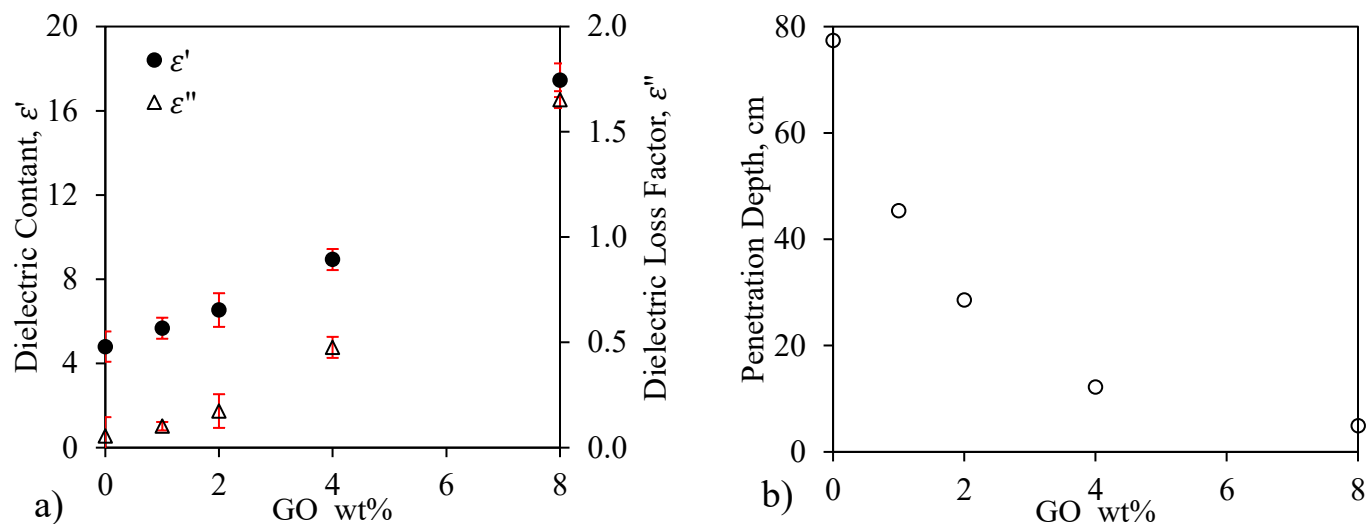


Figure 6-9. Effect of GO on a) dielectric properties and b) MW penetration depth. Error bars represent the standard deviation of two measurements.

#### 6.4.8 Microwave Heating

Synthesized nanocomposites were exposed to a range of MW applied power to study the effect of GO content on MW heating rate. Figure 6-10.a shows the calculated heating rates versus MW applied power. As expected from dielectric properties measurement, the MW absorption performance of the polymer and its heating rate were markedly improved following GO addition. All the samples showed an ascending trend in heating rate with increasing the power density. The introduction of GO into the polymer entirely changed the heating rate of the polymer. The changes in the heating rate of samples can be investigated in terms of the required power density to get a particular heating rate. For instance, the maximum heating rate of pristine polymer is 0.1 ( $^{\circ}\text{C}/\text{s}$ ), obtained at the power density of 160 (watt/g). However, the addition of 8 wt % GO can give three

times higher heating rate (0.3 °C/s) at just 3 (watt/g) power density. These results demonstrate that adding GO to the polymer contributes markedly to the fast and energy-efficient heating of the adsorbent. Figure 6-10.b shows that adding GO to the polymer exponentially decreased the energy required to increase the temperature of 1 gr adsorbent by 1 °C. The inclusion of 8 wt% GO into the polymer reduced the MW heat capacity from 1240 to 10.1 J/ g°C, a 99% decrement. The results showcase the controlling effect of GO content on the MW heating rate and MW heat capacity of the polymer samples.

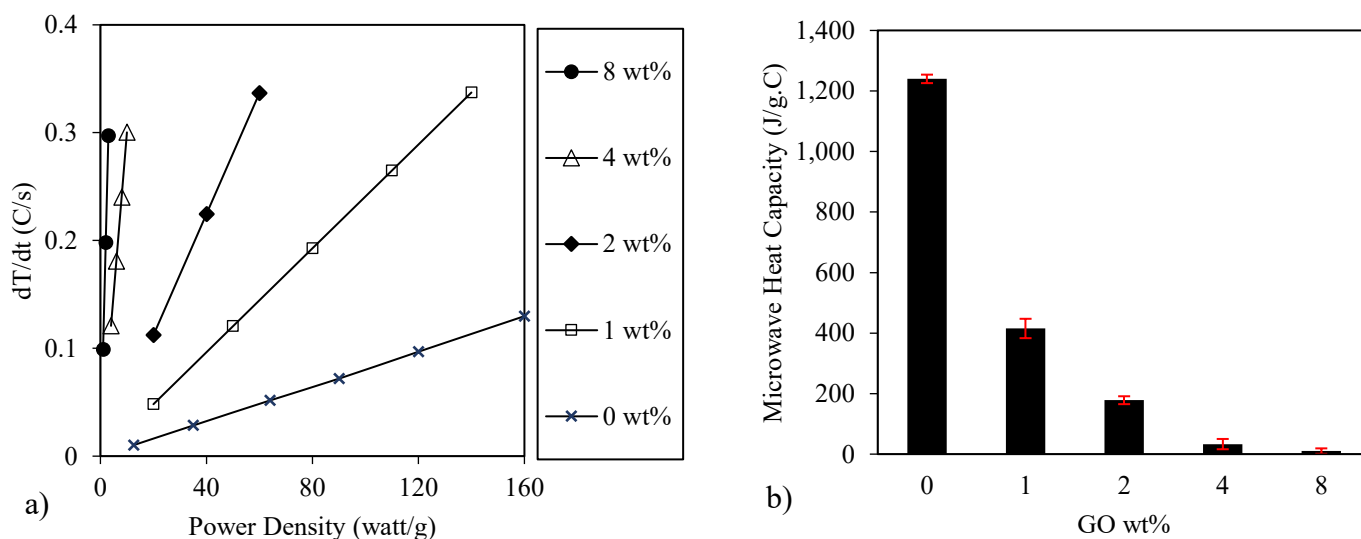


Figure 6-10. Effect of GO content on a) heating rate and b) MW heating capacity. Error bars represent the standard deviation of three measurements.

#### 6.4.9 Microwave-assisted Desorption

Based on the penetration depth results, HCP with 4 wt % GO content was selected for comparison to the pristine polymer in terms of toluene adsorption/desorption. The effluent toluene concentration and desorption temperature during MW heating of GO-filled nanocomposite and pristine polymer were measured (Figure 6-11.a). Figure 6-11.a shows a large temperature

difference (more than 160 °C) between the GO-filled nanocomposite and HCP in the 60 minutes of exposure to 20 watts of MW heating. A strong relationship between temperature and gas-phase molecular diffusivity in porous material has been reported in the literature.<sup>61,62</sup> Higher adsorbate diffusion increases the desorption rate and creates a sharp peak in the toluene concentration profile (Figure 6-11.a). As a result, the toluene desorption efficiency from the GO-filled nanocomposite improved by 4.4 times compared to pristine HCP (Figure 6-11.b).

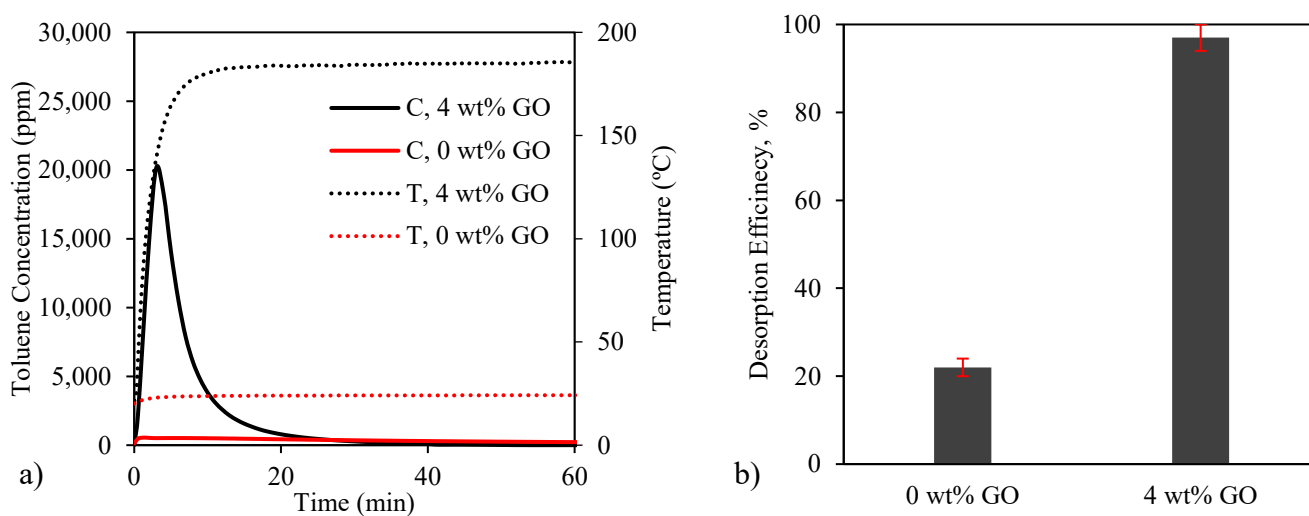


Figure 6-11. a) Effluent concentration and adsorbent temperature profiles during desorption of toluene, and b) Toluene desorption efficiency. Error bars represent the standard deviation of two measurements.

## 6.5 Conclusions

In summary, GO sheets and HCP were synthesized by a modified Hummer's method and Friedel-Crafts reactions. A series of GO-filled nanocomposites were produced by colloidal blending of GO, and HCP. XRD, FTIR, SEM, HIM, and TEM studies showed the successful synthesis of GO and HCPs and the proper dispersion of GO inside the HCP matrix. TGA analysis revealed that

even a small amount of GO (1 wt%) profoundly increases the thermal stability of HCP. The small reduction in BET surface area and total pore volume of nanocomposites by GO content was attributed to the nonporous structure of GO sheets. Dielectric measurement results revealed that filling HCP with 8 wt% of GO enhances the dielectric constant and loss factor by more than 3 and 28 times, respectively. The consumed MW energy to heat the bed for 1 °C was reduced by 99% by using GO filler in the MW heating experiments. More than 160 °C and 4.4 times enhancement in the desorption temperature and toluene desorption efficiency were achieved by addition of 4 wt% of GO to the polymer.

## 6.6 References

- (1) Ghafari, M.; Atkinson, J. D. Impact of Styrenic Polymer One-Step Hyper-Cross-Linking on Volatile Organic Compound Adsorption and Desorption Performance. *Journal of Hazardous Materials* **2018**, *351*, 117–123. <https://doi.org/10.1016/j.jhazmat.2018.02.051>.
- (2) Wang, G.; Dou, B.; Wang, J.; Wang, W.; Hao, Z. Adsorption Properties of Benzene and Water Vapor on Hyper-Cross-Linked Polymers. *RSC Advances* **2013**, *3* (43), 20523–20531. <https://doi.org/10.1039/c3ra41450g>.
- (3) Wang, W.-Q.; Wang, J.; Chen, J.-G.; Fan, X.-S.; Liu, Z.-T.; Liu, Z.-W.; Jiang, J.; Hao, Z. Synthesis of Novel Hyper-Cross-Linked Polymers as Adsorbent for Removing Organic Pollutants from Humid Streams. *Chemical Engineering Journal* **2015**, *281*, 34–41. <https://doi.org/10.1016/j.cej.2015.06.095>.
- (4) Huang, J.; Turner, S. R. Polymer Reviews Hypercrosslinked Polymers: A Review Hypercrosslinked Polymers: A Review. *Polymer Reviews* **2018**, *58* (1), 1–41. <https://doi.org/10.1080/15583724.2017.1344703>.
- (5) Germain, J.; Svec, F.; Fréenet, J. M. J. Preparation of Size-Selective Nanoporous Polymer Networks of Aromatic Rings: Potential Adsorbents for Hydrogen Storage. *Chemistry of Materials* **2008**, *20* (22), 7069–7076. <https://doi.org/10.1021/cm802157r>.
- (6) Macintyre, F. S.; Sherrington, D. C. Control of Porous Morphology in Suspension Polymerized Poly(Divinylbenzene) Resins Using Oligomeric Porogens. *Macromolecules* **2004**, *37* (20), 7628–7636. <https://doi.org/10.1021/ma0491053>.

- (7) Ghafari, M.; Atkinson, J. D. One-Step Hyper-Cross-Linking of Porous Styrenic Polymers Using Dichloroalkane Cross-Linkers to Maintain Hydrophobicity. *Polymer* **2017**, *116*, 278–286. <https://doi.org/10.1016/j.polymer.2017.03.082>.
- (8) Steam Regeneration of Adsorbents: An Experimental and Technical Review. *Chemical Science Transactions* **2013**, *2* (4). <https://doi.org/10.7598/cst2013.545>.
- (9) Salvador, F.; Martin-Sanchez, N.; Sanchez-Hernandez, R.; Sanchez-Montero, M. J.; Izquierdo, C. Regeneration of Carbonaceous Adsorbents. Part I: Thermal Regeneration. *Microporous and Mesoporous Materials* **2015**, *202*, 259–276. <https://doi.org/10.1016/j.micromeso.2014.02.045>.
- (10) Price, D. W.; Schmidt, P. S. VOC Recovery through Microwave Regeneration of Adsorbents: Process Design Studies. *Journal of the Air & Waste Management Association* **1998**, *48* (12), 1135–1145. <https://doi.org/10.1080/10473289.1998.10463758>.
- (11) Ondon, B. S.; Sun, B.; Yan, Z. Y.; Zhu, X. M.; Liu, H. Effect of Microwave Heating on the Regeneration of Modified Activated Carbons Saturated with Phenol. *Applied Water Science* **2014**, *4* (4), 333–339. <https://doi.org/10.1007/s13201-013-0147-5>.
- (12) Cherbański, R. Regeneration of Granular Activated Carbon Loaded with Toluene – Comparison of Microwave and Conductive Heating at the Same Active Powers. *Chemical Engineering and Processing - Process Intensification* **2018**, *123*, 148–157. <https://doi.org/10.1016/j.cep.2017.11.008>.
- (13) Fayaz, M.; Shariaty, P.; Atkinson, J. D.; Hashisho, Z.; Phillips, J. H.; Anderson, J. E.; Nichols, M. Using Microwave Heating To Improve the Desorption Efficiency of High Molecular Weight VOC from Beaded Activated Carbon. *Environmental Science & Technology* **2015**, *49* (7), 4536–4542. <https://doi.org/10.1021/es505953c>.
- (14) Chowdhury, T.; Shi, M.; Hashisho, Z.; Sawada, J. A.; Kuznicki, S. M. Regeneration of Na-ETS-10 Using Microwave and Conductive Heating. *Chemical Engineering Science* **2012**, *75*, 282–288. <https://doi.org/10.1016/j.ces.2012.03.039>.

- (15) Roussy, G.; Zoulalian, A.; Charreyre, M.; Thiebaut, J. M. How Microwaves Dehydrate Zeolites. *The Journal of Physical Chemistry* **1984**, *88* (23), 5702–5708. <https://doi.org/10.1021/j150667a049>.
- (16) Mishra, R. R.; Sharma, A. K. Microwave–Material Interaction Phenomena: Heating Mechanisms, Challenges and Opportunities in Material Processing. *Composites Part A: Applied Science and Manufacturing* **2016**, *81*, 78–97. <https://doi.org/10.1016/j.compositesa.2015.10.035>.
- (17) Meng, Q. B.; Yang, G.-S.; Lee, Y.-S. Preparation of Highly Porous Hypercrosslinked Polystyrene Adsorbents: Effects of Hydrophilicity on the Adsorption and Microwave-Assisted Desorption Behavior toward Benzene. *Microporous and Mesoporous Materials* **2013**, *181*, 222–227. <https://doi.org/10.1016/j.micromeso.2013.07.027>.
- (18) Meng, Q. B.; Yang, G.-S.; Lee, Y.-S. Sulfonation of a Hypercrosslinked Polymer Adsorbent for Microwave-Assisted Desorption of Adsorbed Benzene. *Journal of Industrial and Engineering Chemistry* **2014**, *20* (4), 2484–2489. <https://doi.org/10.1016/j.jiec.2013.10.030>.
- (19) Wang, L.; Jia, X.; Li, Y.; Yang, F.; Zhang, L.; Liu, L.; Ren, X.; Yang, H. Synthesis and Microwave Absorption Property of Flexible Magnetic Film Based on Graphene Oxide/Carbon Nanotubes and Fe<sub>3</sub>O<sub>4</sub> Nanoparticles. *Journal of Materials Chemistry A* **2014**, *2* (36), 14940. <https://doi.org/10.1039/C4TA02815E>.
- (20) Wang, C.; Han, X.; Xu, P.; Zhang, X.; Du, Y.; Hu, S.; Wang, J.; Wang, X. The Electromagnetic Property of Chemically Reduced Graphene Oxide and Its Application as Microwave Absorbing Material. *Applied Physics Letters* **2011**, *98* (7), 1–4. <https://doi.org/10.1063/1.3555436>.
- (21) Tian, C.; Du, Y.; Cui, C.; Deng, Z.; Xue, J.; Xu, P.; Qiang, R.; Wang, Y.; Han, X. Synthesis and Microwave Absorption Enhancement of Yolk–Shell Fe<sub>3</sub>O<sub>4</sub>@C Microspheres. *Journal*

- of Materials Science* **2017**, *52* (11), 6349–6361. <https://doi.org/10.1007/s10853-017-0866-3>.
- (22) Micheli, D.; Vricella, A.; Pastore, R.; Marchetti, M. Synthesis and Electromagnetic Characterization of Frequency Selective Radar Absorbing Materials Using Carbon Nanopowders. *Carbon* **2014**, *77*, 756–774. <https://doi.org/10.1016/j.carbon.2014.05.080>.
- (23) Tang, J.; Bi, S.; Wang, X.; Hou, G. liang; Su, X. jia; Liu, C. hui; Lin, Y. yang; Li, H. Excellent Microwave Absorption of Carbon Black/Reduced Graphene Oxide Composite with Low Loading. *Journal of Materials Science* **2019**, *54* (22), 13990–14001. <https://doi.org/10.1007/s10853-019-03902-0>.
- (24) He, F.; Lau, S.; Chan, H. L.; Fan, J. High Dielectric Permittivity and Low Percolation Threshold in Nanocomposites Based on Poly(Vinylidene Fluoride) and Exfoliated Graphite Nanoplates. *Advanced Materials* **2009**, *21* (6), 710–715. <https://doi.org/10.1002/adma.200801758>.
- (25) Wang, L.; Jia, X.; Li, Y.; Yang, F.; Zhang, L.; Liu, L.; Ren, X.; Yang, H. Synthesis and Microwave Absorption Property of Flexible Magnetic Film Based on Graphene Oxide/Carbon Nanotubes and Fe<sub>3</sub>O<sub>4</sub> Nanoparticles. *Journal of Materials Chemistry A* **2014**, *2* (36), 14940. <https://doi.org/10.1039/C4TA02815E>.
- (26) Deshmukh, K.; Ahamed, M. B.; Pasha, S. K. K.; Deshmukh, R. R.; Bhagat, P. R. Highly Dispersible Graphene Oxide Reinforced Polypyrrole/Polyvinyl Alcohol Blend Nanocomposites with High Dielectric Constant and Low Dielectric Loss. *RSC Advances* **2015**, *5* (76), 61933–61945. <https://doi.org/10.1039/c5ra11242g>.
- (27) Ebrahimi-Tazangi, F.; Hekmatara, S. H.; Seyed-Yazdi, J. Remarkable Microwave Absorption of GO-SiO<sub>2</sub>/Fe<sub>3</sub>O<sub>4</sub> via an Effective Design and Optimized Composition. *Journal of Alloys and Compounds* **2021**, *854*, 157213. <https://doi.org/10.1016/j.jallcom.2020.157213>.

- (28) Marcano, D. C.; Kosynkin, D. V.; Berlin, J. M.; Sinitiskii, A.; Sun, Z.; Slesarev, A.; Alemany, L. B.; Lu, W.; Tour, J. M. Improved Synthesis of Graphene Oxide. *ACS Nano* **2010**, *4* (8), 4806–4814. <https://doi.org/10.1021/nn1006368>.
- (29) Pourjavid, M. R.; Arabieh, M.; Yousefi, S. R.; Jamali, M. R.; Rezaee, M.; Hosseini, M. H.; Sehat, A. A. Study on Column SPE with Synthesized Graphene Oxide and FAAS for Determination of Trace Amount of Co(II) and Ni(II) Ions in Real Samples. *Materials Science and Engineering: C* **2015**, *47*, 114–122. <https://doi.org/10.1016/j.msec.2014.11.028>.
- (30) Vinodh, R.; Jung, E. M.; Ganesh, M.; Peng, M. M.; Abidov, A.; Palanichamy, M.; Cha, W. S.; Jang, H. T. Novel Microporous Hypercross-Linked Polymers as Sorbent for Volatile Organic Compounds and CO<sub>2</sub> Adsorption. *Journal of Industrial and Engineering Chemistry* **2015**, *21*, 1231–1238. <https://doi.org/10.1016/j.jiec.2014.05.039>.
- (31) Bibi, S.; Yasin, T.; Hassan, S.; Riaz, M.; Nawaz, M. Chitosan/CNTs Green Nanocomposite Membrane: Synthesis, Swelling and Polyaromatic Hydrocarbons Removal. *Materials Science and Engineering: C* **2015**, *46*, 359–365. <https://doi.org/10.1016/j.msec.2014.10.057>.
- (32) Morales Mendoza, N.; Goyanes, S.; Chilotte, C.; Bekeris, V.; Rubiolo, G.; Candal, R. Magnetic Binary Nanofillers. *Physica B: Condensed Matter* **2012**, *407* (16), 3203–3205. <https://doi.org/10.1016/j.physb.2011.12.065>.
- (33) Han, Z.; Fina, A. Thermal Conductivity of Carbon Nanotubes and Their Polymer Nanocomposites: A Review. *Progress in Polymer Science* **2011**, *36* (7), 914–944. <https://doi.org/10.1016/j.progpolymsci.2010.11.004>.
- (34) Mittal, G.; Dhand, V.; Rhee, K. Y.; Park, S.-J.; Lee, W. R. A Review on Carbon Nanotubes and Graphene as Fillers in Reinforced Polymer Nanocomposites. *Journal of Industrial and Engineering Chemistry* **2015**, *21*, 11–25. <https://doi.org/10.1016/j.jiec.2014.03.022>.

- (35) Ma, P. C.; Siddiqui, N. A.; Marom, G.; Kim, J. K. Dispersion and Functionalization of Carbon Nanotubes for Polymer-Based Nanocomposites: A Review. *Composites Part A: Applied Science and Manufacturing*. Elsevier Ltd October 1, 2010, pp 1345–1367. <https://doi.org/10.1016/j.compositesa.2010.07.003>.
- (36) Akram, Z.; Kausar, A.; Siddiq, M. Review on Polymer/Carbon Nanotube Composite Focusing Polystyrene Microsphere and Polystyrene Microsphere/Modified CNT Composite: Preparation, Properties, and Significance. *Polymer-Plastics Technology and Engineering* **2016**, *55* (6), 582–603. <https://doi.org/10.1080/03602559.2015.1098696>.
- (37) Dykas, M. M.; Poddar, K.; Yoong, S. L.; Viswanathan, V.; Mathew, S.; Patra, A.; Saha, S.; Pastorin, G.; Venkatesan, T. Enhancing Image Contrast of Carbon Nanotubes on Cellular Background Using Helium Ion Microscope by Varying Helium Ion Fluence. *Journal of microscopy* **2018**, *269* (1), 14–22. <https://doi.org/10.1111/jmi.12604>.
- (38) Lashaki, M. J.; Fayaz, M.; Wang, H. (Helena); Hashisho, Z.; Philips, J. H.; Anderson, J. E.; Nichols, M. Effect of Adsorption and Regeneration Temperature on Irreversible Adsorption of Organic Vapors on Beaded Activated Carbon. *Environmental Science & Technology* **2012**, *46* (7), 4083–4090. <https://doi.org/10.1021/es3000195>.
- (39) Falciglia, P. P.; Roccaro, P.; Bonanno, L.; De Guidi, G.; Vagliasindi, F. G. A.; Romano, S. A Review on the Microwave Heating as a Sustainable Technique for Environmental Remediation/Detoxification Applications. *Renewable and Sustainable Energy Reviews* **2018**, *95*, 147–170. <https://doi.org/10.1016/j.rser.2018.07.031>.
- (40) Clark, D. E.; Sutton, W. H. Microwave Processing of Materials. *Annual Review of Materials Science* **1996**, *26* (1), 299–331. <https://doi.org/10.1146/annurev.ms.26.080196.001503>.
- (41) Luo, J.; Shen, P.; Yao, W.; Jiang, C.; Xu, J. Synthesis, Characterization, and Microwave Absorption Properties of Reduced Graphene Oxide/Strontium Ferrite/Polyaniline

- Nanocomposites. *Nanoscale Research Letters* **2016**, *11* (1), 1–14. <https://doi.org/10.1186/s11671-016-1340-x>.
- (42) Fakhouri, M. O.; Ramaswamy, H. S. Temperature Uniformity of Microwave Heated Foods as Influenced by Product Type and Composition. *Food Research International* **1993**, *26* (2), 89–95. [https://doi.org/10.1016/0963-9969\(93\)90062-N](https://doi.org/10.1016/0963-9969(93)90062-N).
- (43) Manickavasagan, A.; Jayas, D. S.; White, N. D. G. Non-Uniformity of Surface Temperatures of Grain after Microwave Treatment in an Industrial Microwave Dryer. *Drying Technology* **2006**, *24* (12), 1559–1567. <https://doi.org/10.1080/07373930601030796>.
- (44) Geedipalli, S. S. R.; Rakesh, V.; Datta, A. K. Modeling the Heating Uniformity Contributed by a Rotating Turntable in Microwave Ovens. *Journal of Food Engineering* **2007**, *82* (3), 359–368. <https://doi.org/10.1016/j.jfoodeng.2007.02.050>.
- (45) Funawatashi, Y.; Suzuki, T. Numerical Analysis of Microwave Heating of a Dielectric. *Heat Transfer - Asian Research* **2003**, *32* (3), 227–236. <https://doi.org/10.1002/htj.10087>.
- (46) Metaxas, A. C.; Meredith, R. J. Book Review: Industrial Microwave Heating. *Journal of Microwave Power and Electromagnetic Energy* **1989**, *24* (2), 108–108. <https://doi.org/10.1080/08327823.1989.11688082>.
- (47) Fayaz, M.; Shariaty, P.; Atkinson, J. D.; Hashisho, Z.; Phillips, J. H.; Anderson, J. E.; Nichols, M. Using Microwave Heating To Improve the Desorption Efficiency of High Molecular Weight VOC from Beaded Activated Carbon. *Environmental Science & Technology* **2015**, *49* (7), 4536–4542. <https://doi.org/10.1021/es505953c>.
- (48) Stobinski, L.; Lesiak, B.; Malolepszy, A.; Mazurkiewicz, M.; Mierzwa, B.; Zemek, J.; Jiricek, P.; Bieloshapka, I. Graphene Oxide and Reduced Graphene Oxide Studied by the XRD, TEM and Electron Spectroscopy Methods. *Journal of Electron Spectroscopy and Related Phenomena* **2014**, *195*, 145–154. <https://doi.org/10.1016/j.elspec.2014.07.003>.

- (49) Krishnamoorthy, K.; Veerapandian, M.; Yun, K.; Kim, S.-J. The Chemical and Structural Analysis of Graphene Oxide with Different Degrees of Oxidation. *Carbon* **2013**, *53*, 38–49. <https://doi.org/10.1016/j.carbon.2012.10.013>.
- (50) Saleem, H.; Haneef, M.; Abbasi, H. Y. Synthesis Route of Reduced Graphene Oxide via Thermal Reduction of Chemically Exfoliated Graphene Oxide. *Materials Chemistry and Physics* **2018**, *204*, 1–7. <https://doi.org/10.1016/j.matchemphys.2017.10.020>.
- (51) Zhou, X.; Liu, Z. A Scalable, Solution-Phase Processing Route to Graphene Oxide and Graphene Ultralarge Sheets. *Chemical Communications* **2010**, *46* (15), 2611. <https://doi.org/10.1039/b914412a>.
- (52) Zhang, T.; Huang, W.; Zhang, N.; Huang, T.; Yang, J.; Wang, Y. Grafting of Polystyrene onto Reduced Graphene Oxide by Emulsion Polymerization for Dielectric Polymer Composites: High Dielectric Constant and Low Dielectric Loss Tuned by Varied Grafting Amount of Polystyrene. *European Polymer Journal* **2017**, *94* (111), 196–207. <https://doi.org/10.1016/j.eurpolymj.2017.07.008>.
- (53) Justh, N.; Berke, B.; László, K.; Szilágyi, I. M. Thermal Analysis of the Improved Hummers' Synthesis of Graphene Oxide. *Journal of Thermal Analysis and Calorimetry* **2018**, *131* (3), 2267–2272. <https://doi.org/10.1007/s10973-017-6697-2>.
- (54) Li, J.; Gao, M.; Zheng, Y.; Guan, Y.; Yi, D. Effects of Low-Load Boron/Silicon-Based Graphene Oxide on Combustion and Thermal Degradation of Flame-Retardant Unsaturated Polyester Resin. *Macromolecular Materials and Engineering* **2020**, *305* (12), 2000454. <https://doi.org/10.1002/mame.202000454>.
- (55) Ismail, H.; Pasbakhsh, P.; Fauzi, M. N. A.; Abu Bakar, A. Morphological, Thermal and Tensile Properties of Halloysite Nanotubes Filled Ethylene Propylene Diene Monomer (EPDM) Nanocomposites. *Polymer Testing* **2008**, *27* (7), 841–850. <https://doi.org/10.1016/j.polymertesting.2008.06.007>.

- (56) Norkhairunnisa, M.; Azizan, A.; Mariatti, M.; Ismail, H.; Sim, L. Thermal Stability and Electrical Behavior of Polydimethylsiloxane Nanocomposites with Carbon Nanotubes and Carbon Black Fillers. *Journal of Composite Materials* **2012**, *46* (8), 903–910. <https://doi.org/10.1177/0021998311412985>.
- (57) Dou, B.; Hu, Q.; Li, J.; Qiao, S.; Hao, Z. Adsorption Performance of VOCs in Ordered Mesoporous Silicas with Different Pore Structures and Surface Chemistry. *Journal of Hazardous Materials* **2011**, *186* (2–3), 1615–1624. <https://doi.org/10.1016/j.jhazmat.2010.12.051>.
- (58) Jahandar Lashaki, M.; Atkinson, J. D.; Hashisho, Z.; Phillips, J. H.; Anderson, J. E.; Nichols, M. The Role of Beaded Activated Carbon's Pore Size Distribution on Heel Formation during Cyclic Adsorption/Desorption of Organic Vapors. *Journal of Hazardous Materials* **2016**, *315*, 42–51. <https://doi.org/10.1016/j.jhazmat.2016.04.071>.
- (59) Liu, J.; Duan, Y.; Song, L.; Hu, J.; Zeng, Y. Heterogeneous Nucleation Promoting Formation and Enhancing Microwave Absorption Properties in Hierarchical Sandwich-like Polyaniline/Graphene Oxide Induced by Mechanical Agitation. *Composites Science and Technology* **2019**, *182*, 107780. <https://doi.org/10.1016/j.compscitech.2019.107780>.
- (60) Yu, Y.; Song, S.; Bu, Z.; Gu, X.; Song, G.; Sun, L. Influence of Filler Waviness and Aspect Ratio on the Percolation Threshold of Carbon Nanomaterials Reinforced Polymer Nanocomposites. *Journal of Materials Science* **2013**, *48* (17), 5727–5732. <https://doi.org/10.1007/s10853-013-7364-z>.
- (61) Cherbański, R.; Komorowska-Durka, M.; Stefanidis, G. D.; Stankiewicz, A. I. Microwave Swing Regeneration vs Temperature Swing Regeneration—Comparison of Desorption Kinetics. *Industrial & Engineering Chemistry Research* **2011**, *50* (14), 8632–8644. <https://doi.org/10.1021/ie102490v>.

- (62) Deng, Q.; Yang, X.; Zhang, J. Study on a New Correlation between Diffusion Coefficient and Temperature in Porous Building Materials. *Atmospheric Environment* **2009**, *43* (12), 2080–2083. <https://doi.org/10.1016/j.atmosenv.2008.12.052>.

# CHAPTER 7: REAL-TIME NONCONTACT VOC DESORPTION MONITORING SENSOR

## 7.1 Chapter Overview

In this chapter, a contactless microwave (MW) sensor is presented for real-time monitoring of the desorption process. The main sensing element of the proposed desorption monitoring platform is a chipless flexible MW split-ring resonator (SRR), ‘tag’, which is electromagnetically coupled to a read-out circuit, ‘reader’. A styrene-divinylbenzene resin was loaded with heptane (nonpolar) and n-propyl alcohol (polar) at different concentrations to evaluate the use of the sensor for desorption monitoring. After verifying the sensor's temperature stability, the desorption was carried out at 175 °C. The sensor response was compared to effluent adsorbate concentration measured by flame ionization detector (FID), and thereby, adsorbent dielectric properties were related to adsorbate load on the resin. A linear correlation ( $R^2 > 0.95$ ) between the adsorbate load and the measured frequency shift was observed. The saturation time and regeneration time determined based on the non-contact sensor showed more than 95 % and 75 % consistency, respectively, with corresponding values obtained from concentration measurements by FID. The proposed sensor has the potential to be integrated as a low-cost handheld sensing device. The proposed chipless MW resonator sensor demonstrates the capability of real-time distant monitoring and detection, making it suitable for use in harsh environments and high-temperature sensing applications.

## 7.2 Introduction

Thermal regeneration is commonly used for adsorbent regeneration and is operated in a cyclic mode. This step typically requires time to heat, desorb, and cool down the adsorbent bed, and is often the time-limiting step in the temperature swing adsorption cycle. During thermal regeneration, the temperature of the spent adsorbent is increased, which provides enough energy for adsorbate molecules to escape from the pores. Thus, the surface area and pores of the spent adsorbent are regenerated for the next adsorption cycle. In the thermal regeneration process design, regeneration time is a key parameter used to determine the number of beds required for a continuous cyclic VOC adsorption/desorption operation.<sup>1</sup> Besides, regeneration time directly impacts energy consumption, and thus, the operating cost of the air treatment facility. Regeneration time can be defined as when effluent gas concentration from the adsorbent bed reaches 1% of feed gas concentration.<sup>2</sup> Prediction of the regeneration time can be challenging as the amount of adsorbate load in the adsorbent bed may vary by the properties of the polluted gas stream, such as the number of compounds and their concentration. These parameters can change the adsorbate load on the adsorbent and the adsorbent temperature after the adsorption. Besides, the strength of the adsorbate molecule interaction with the adsorbent surface can change the required time for a complete adsorbent regeneration.<sup>3,4</sup> The stronger the interaction is, the longer the regeneration time is.<sup>5</sup> Diffusion of desorbed molecules into the purge gas is controlled by the contact time between the adsorbent and the purge gas.<sup>6</sup> Higher purge gas flow rates result in shorter regeneration times for a given bed length.<sup>7</sup> Considering all the above parameters, prediction of regeneration time using a theoretical approach can be demanding and needs a long computational time. Alternatively, direct measurement of the effluent concentration during regeneration is typically used to determine

the regeneration time. In this method, a volatile organic compound (VOC) detector is used to directly monitor the effluent VOC concentration during desorption, from which regeneration time can be determined.<sup>2</sup> While direct measurement is the only way to accurately determine the time needed for a complete adsorbent regeneration, it adds other challenges such as the exposure of detector to hazardous, high boiling point, or corrosive compounds.

Recently, planar MW resonators emerged as potential candidates for sensing applications due to their simple and low-cost fabrication process, easy integration with complementary metal-oxide semiconductor (CMOS), lab-on-chip compatibility, and flexible design. They have been utilized for a wide range of applications, including biomedical detection<sup>8-12</sup>, chemical solutions sensing<sup>8,13-16</sup>, and environmental monitoring<sup>10,17-19</sup>. Integration of MW planar sensors with adsorbents significantly enhances their sensitivity and selectivity, making them capable of gas/VOC detection and concentration monitoring.<sup>20-22</sup> The operation principle of MW planar split-ring resonator (SRR) based sensors is the result of the variation in electromagnetic (EM) field around the sensor due to the changes in the dielectric properties of the surrounding medium. Specifically, during VOC adsorption/desorption process, any change in the VOC loading capacity of the adsorbents can be translated into a change in their dielectric properties, resulting in a change in their resonance profile. However, VOC desorption process by thermal method is typically carried out at high temperatures (above 100 °C) that is beyond the maximum bearable temperature for any non-linear electronic components integrated with MW sensors and the read-out equipment. To resolve this issue and enable precise VOC sensing in high temperature applications, a new reader-tag based MW sensor is developed.

The proposed design demonstrates distant sensing performance, makes the sensor an exceptional choice for VOC monitoring and detection in harsh environments.<sup>21,23-25</sup> In this study, the application of a MW resonator for real-time distant monitoring of VOC adsorption/desorption process is investigated. The main sensing element of the proposed MW resonator is a chipless flexible tag that can communicate variation in the dielectric properties of the ambient around itself to a reader circuit through electromagnetic coupling when the distance between the reader and the tag is up to 60 mm. During the adsorption/desorption process, the change in the tag's resonant frequency is measured and monitored using a vector network analyzer (VNA). Obtained results from the proposed VOC sensing element were compared with measured values from a flame ionization detector (FID). Finally, the variations in the frequency response are used to determine the saturation and regeneration times.

### **7.3 Experimental set-up and methods**

#### **7.3.1 Material**

Styrene-divinylbenzene porous resin (Dowex Optipore V503) with a BET surface area of 1100 m<sup>2</sup>/g and a total pore volume of 0.9 cc/g was used as the adsorbent. Heptane (99%, Fisher Scientific) and 1-propanol (99%, Fisher Scientific) were selected as adsorbates. These two compounds have similar boiling points; however, heptane is nonpolar, and 1-propanol is polar. Difference in the polarity of adsorbates indicates a difference in their dielectric properties which allows the sensor to be assessed in the detection of a wide range of VOCs. Table 1 shows some physical properties of selected adsorbates.

Table 7-1. Physical properties of tested adsorbates

Adsorbate	Heptane	1-Propanol	Ref.
Boiling Point (°C)	98	97	
Dipole moment (D)	0.1	1.6	26
Relative Polarity	0.01	0.61	27
Dielectric Constant at 25 °C	1.92	20.40	28,29

### 7.3.2 VOC Adsorption and Desorption

The adsorption apparatus consisted of a quartz tube, an adsorbate vapor generation system, and an adsorbate concentration detection system. A quartz tube with 2.2 cm inner diameter and 35 cm length was used to hold 2 grams of adsorbent beads. The adsorbate vapor generation system consisted of a syringe pump (KD Scientific, KDS-220) to inject liquid VOC into a 1 standard liter per minute (SLPM) dry air which is controlled by a mass flow controller to reach the target concentration at room temperature. A FID (Baseline- Mocon Inc., series 9000) was used to record the adsorbate concentration in the inlet and outlet air streams. FID was calibrated, using the manufacturer calibration procedure, for each adsorbate prior to each test. Before each experiment, adsorbent beads were outgassed in a vacuum oven by heating at 110 °C for 24 hours. The outgassed adsorbents were weighed and placed into the quartz tube, then adsorption started. The concentration of adsorbate in the effluent stream was continuously recorded every 30 seconds until it reached the inlet concentration and remained constant with time.

The experimental apparatus used for adsorbent regeneration experiments included a mass flow controller, a FID detector, a heating loop, heating jackets, and insulation tapes. A constant flow of nitrogen at 175 °C was produced in a copper heating loop and used to regenerate the spent

adsorbents. A fiber optic sensor (Reflex, Neoptix) was used to measure the temperature of the adsorbent bed during the regeneration. Figure 7-1.a depicts a schematic diagram of the adsorption/desorption experimental setup.

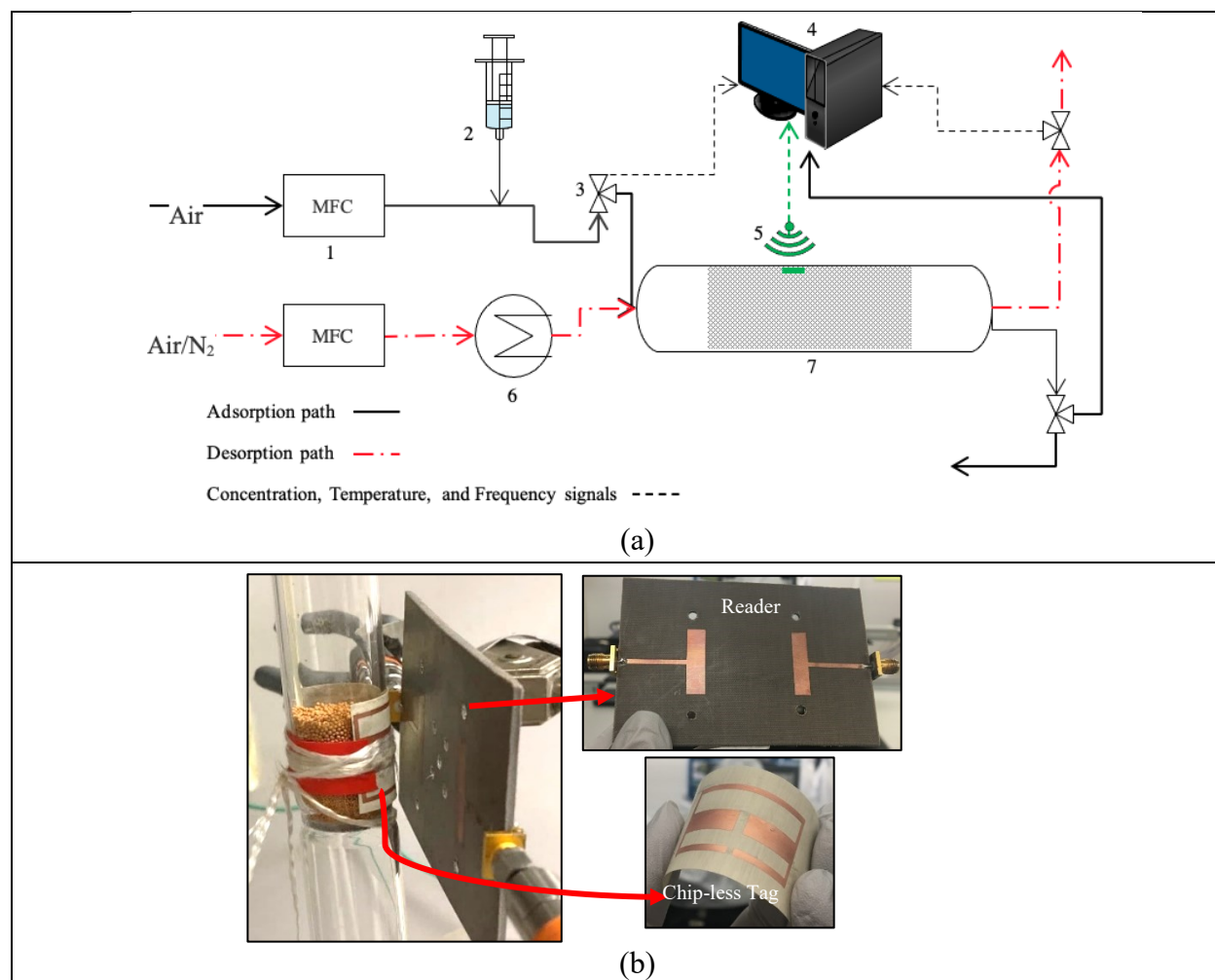


Figure 7-1. (a) Schematic diagram of the adsorption and desorption process. (1) Mass flow controller; (2) Syringe pump; (3) Tee; (4) FID & Data acquisition; (5) Sensing tag and reader; (6) Heating loop; (7) Adsorbent Bed. (b) Picture of MW reader-tag sensor used for distant desorption monitoring.

### 7.3.3 Dielectric Property Measurement

Variation in the dielectric properties of the adsorbent during the adsorption/desorption process was monitored using the proposed MW sensor. The experimental setup used to monitor the dielectric properties of adsorbents consisted of a 2-port VNA (S5065, Copper Mountain Technologies) and data acquisition software. The VNA was connected to the reader through high-frequency cables (SB-SMA-MM-78, Maury Microwave). The reader part was implemented on a substrate (RT/duroid5880, Rogers Corporation) with a relative permittivity of 2.2, a loss factor of 0.0003, and a thickness of 1.52 mm. The sensing tag was designed on a flexible substrate (Ultralam 3850, Rogers Corporation) with a relative permittivity of 3, a loss factor of 0.003, and a thickness of 130  $\mu\text{m}$  (Figure 7-1.b). For real-time dielectric properties monitoring, the tag was mounted on the quartz adsorbent container measuring the resonant frequency variations while the reader was placed outside the bed and at a 30 mm distance from the tag. This time-based measurement was performed using a developed LabVIEW interface. Measurements of dielectric properties were conducted from 500 MHz to 1.1 GHz during VOC adsorption and desorption. The schematic of the proposed real-time desorption monitoring sensor, including the chip-less tag and the MW reader, is shown in Figure 7-2.a.

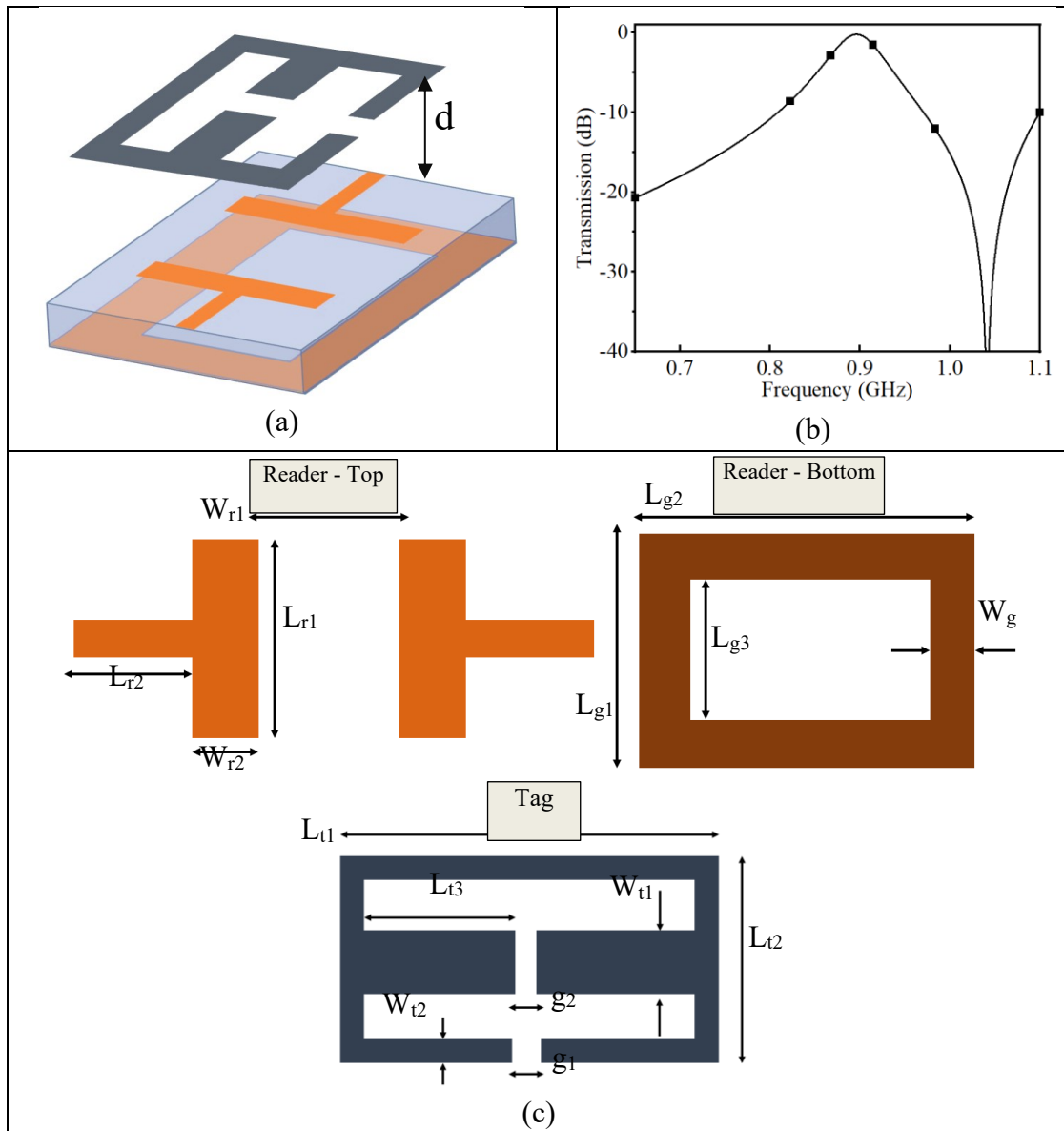


Figure 7-2. (a) The main structure of the chip-less MW sensor, (b) the transmission response of the system indicating a resonance in the spectrum of the whole structure. (c) the tag, reader, and the ground plane with their dimensions identified in mm:  $W_{r1}=33.3$ ,  $L_{r1}=25.4$ ,  $W_{r2}=7$ ,  $L_{r2}=24.6$ ,  $L_{g1}=57.27$ ,  $L_{g2}=95.8$ ,  $L_{g3}=40$ ,  $W_g=14$ ,  $L_{t1}=45$ ,  $L_{t2}=21.4$ ,  $L_{t3}=20.5$ ,  $W_{t1}=9$ ,  $W_{t2}=1$ , and  $g_1, g_2=1.4$ .

The main sensing element of the structure is the tag, which is an open-loop MW SRR placed at 35 mm vertical distance from a MW reader circuit. The tag is in the form of simple copper traces, and the resonance frequency of the tag is reflected in the spectrum of the transmission response (Figure 7-2.b). The 3D electromagnetic simulation of the structure results has been performed in Ansys HFSS. The structure of the reader circuit demonstrates gap coupled transmission lines in the top layer while the bottom layer is the defected ground structure (Figures 7-2.a & 7-2.c). The tag resonator (Figure 7-2.c) was designed on a flexible and thin substrate which makes it easier to be mounted on different adsorbent bed configurations.

The sensor design procedure starts with designing the tag resonator and the reader. The resonant frequency of the tag is initially designed at 880 MHz (Figure 7-2.b). Eq. 1 relates the resonant frequency of the sensor to its physical length ( $l \approx L_{t1} + 2 * (L_{t2} + L_{t3})$ ):

$$f_r = \frac{c}{2l\sqrt{\epsilon_{eff}}} \quad (\text{Eq. 1})$$

where  $f_r$  is the resonant frequency (Hz),  $c$  is the speed of light (m/s), and  $\epsilon_{eff}$  is the effective permittivity (F/m) of the resonator medium that is determined by the material surrounding the tag resonator. The 880 MHz has been the frequency where the design is optimized for both the size of the structure and the distance between the tag and the reader. The parameters that define the sensitivity of the MW sensor are variations in resonance frequency, amplitude, and quality factor of the frequency response, which are used for analyzing the sensing performance of the structure. The resonant profile of the sensor (transmission response) is observed and recorded during the adsorption/desorption process, and resonant frequency ( $f_r$ ) is extracted from the resonant profile. The resonant frequency can be defined as the frequency at which the maximum power transmission

occurs. Unlike  $l$  which is a design parameter,  $\epsilon_{eff}$  will affect the resonance frequency to shift into higher/lower frequencies. In an analysis of  $\epsilon_{eff}$ , Zarifi et al. found that  $\epsilon_{eff}$  is a function of adsorbate filling factor and permittivity of adsorbent/adsorbate system.<sup>22</sup> Since the thickness of the resonator is very small (100  $\mu\text{m}$ ), adsorption/desorption of VOC molecules in the adsorbent bed under the tag acts as the most effecting element to change  $\epsilon_{eff}$ , making the tag suitable for VOC sensing applications.<sup>8,30</sup> In this study, Dowex Optipore V503 ( $\epsilon_{r\_V503} \approx 1.5 - 2$ <sup>31</sup>) was selected as the major parameter that impacts  $\epsilon_{eff}$  variation during the adsorption/desorption.

Figure 7-3 shows the electromagnetic simulation results of the structure for different vertical distances between the tag (as shown in Figure 7-2.a) and the reader varying between 10 mm and 60 mm. As expected from the  $\epsilon_{eff}$  impact on resonance frequency in Eq. 1, the resonance frequency of the resonator shifts toward the higher frequency and the quality factor increases by decreasing the distance.

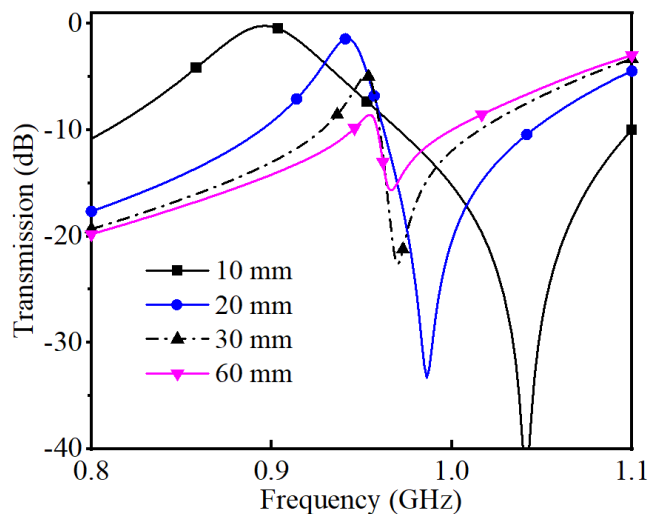


Figure 7-3. Transmission response of the tag-reader sensor while the distance between the tag and reader changes from 10 mm to 60 mm.

To analyze the sensitivity of the proposed sensor design with the permittivity change in the surrounding media, samples with different permittivity were placed at 15 mm distance from the reader and transmission was recorded between 0.6 to 1.3 GHz (Figure 7-4). As shown in Figure 7-4, the frequency shift was more than 0.3 GHz when the permittivity of the sample layer above the tag was changed from  $\epsilon_r = 1$  to  $\epsilon_r = 10$ . If we define the sensitivity of the sensing system as  $\Delta f/\Delta\epsilon_r$ , the presented sensitivity is -34.7 MHz/(unit  $\epsilon_r$ ). This considerable sensitivity despite using a thin layer of the sample over the tag, emphasizes the potential of the proposed sensor in measuring permittivity variation in small volume scale applications.

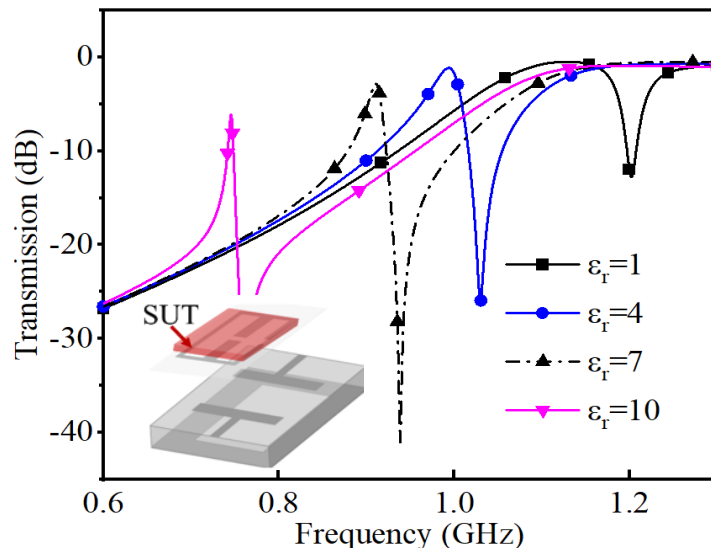


Figure 7-4. Simulation results showing the resonant frequency variation for four different effective permittivities ( $\epsilon_r$ ) of the sample under the test (SUT).

### 7.3.4 VOC Adsorption Isotherm

Adsorption isotherms were measured with a gravimetric method at 25 °C. The main elements of the system include a microbalance (Cahn Instruments, C-1000) in a nitrogen (99.9 %) purged environment, two mass flow controllers, syringe pump, quartz cells, and stainless-steel pans. A data-acquisition was used to continuously record the microbalance output. VOC adsorption experiments were performed by increasing the inlet concentration from 20 ppm to 1500 ppm in an ultra-pure nitrogen (99.9 %) stream. Adsorption continued until equilibrium state was achieved (i.e., < 0.01wt% change in 5 min). Samples' weight changes were recorded to calculate adsorption capacity at each relative pressure.

## 7.4 Result and discussion

### 7.4.1 Thermal stability

As mentioned earlier, the proposed VOC detection method is based on the detection of dielectric properties variation around the tag due to VOC adsorption/desorption. Previous studies show that dielectric property of material can change at elevated temperatures.<sup>32,33</sup> Therefore, the dielectric properties of the adsorbent bed was measured at the regeneration temperature (175 °C) to evaluate the extent of dielectric property variation. Figure 7-5 shows the temperature evolution in the bed and transmitted frequency shift versus the heating time. Obtained results show a stable transmission of frequency data, with the average frequency shift around 0.015 MHz at temperatures up to 175 °C. This small frequency shift due to the temperature increase can be used to correct the measured frequency shift during the regeneration process.

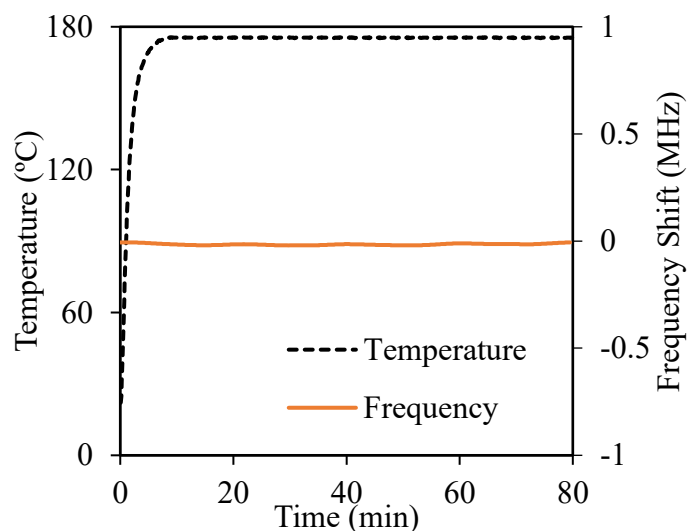


Figure 7-5. Change in temperature and frequency shift during the heating of the adsorbent bed.

### 7.4.2 VOC adsorption/desorption monitoring

After illustrating the effect of temperature on the transmitted frequency shift from the bed, the proposed sensor design was used to conduct VOC adsorption/desorption monitoring. Two VOC concentrations (100 ppm and 1000 ppm) in the inlet air stream were selected based on the adsorption isotherms (Figure 7-6) to evaluate the sensitivity of the sensor at two different VOC loads on the adsorbent. Effluent adsorbate concentration and sensor's resonance frequency were recorded during the adsorption/desorption process to assess the sensor's performance in VOC load monitoring.

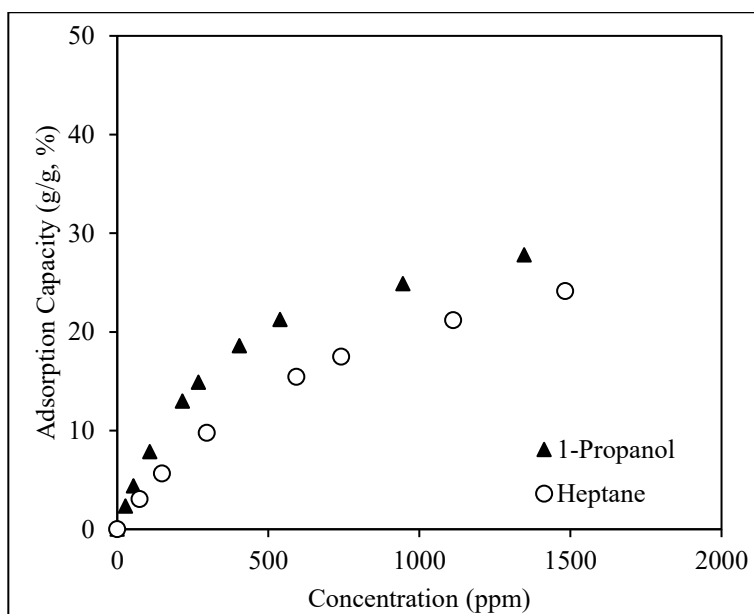


Figure 7-6. Heptane and 1-propanol adsorption isotherms.

Figure 7-7 presents the breakthrough curves, Dowex Optipore V503 adsorption capacities of each adsorbate, effluent adsorbate concentrations during the desorption, and frequency shift during adsorption/desorption. As expected from VOC adsorption isotherms (Figure 7-6), 1-propanol

adsorption took a longer time to reach the saturation state than heptane at the same inlet concentration (Figure 7-7.a). For a given concentration, the longer saturation time means a larger adsorption capacity (Figure 7-7.b).<sup>34</sup> Therefore, a higher amount of 1-propanol desorbed in the Dowex Optipore V503 regeneration results in higher concentration peaks compared to corresponding heptane desorption tests (Figure 7-7.c). From the data in Figure 7-7.d, it is apparent that 1-propanol showed larger frequency shift than heptane at the frequency shift plateau. This difference can be explained by the fact that 1-propanol has a larger dielectric constant and adsorption capacity on the adsorbent (Table 1 and Figure 7-7.b). Both parameters result in a larger change in the  $\epsilon_{eff}$  of adsorbent bed and transmitted frequency shift from the bed. These results support evidence from previous observations by Zarifi et al. and Fayaz et al. who found the direct relation of adsorbate load and adsorbate permittivity with the  $\epsilon_{eff}$ .<sup>22,31,35</sup> Additionally, Figure 7-7.d shows that the frequency shift gradually decreases during VOC adsorption and increases during VOC desorption till it gets back to the starting value after complete regeneration. This is consistent with the earlier sensitivity analysis (Figure 7-4) that shows a negative value (-34.7 MHz/unit  $\epsilon_r$ ) for the frequency shift per unit of permittivity change. In fact, VOC adsorption increases the effective permittivity of the bed by filling the adsorbent pores with VOC molecules which creates a downshift trend in the frequency shift. However, adsorbent regeneration decreases the effective permittivity and creates an increasing trend in the frequency shift as the bed loses adsorbed VOC molecules.

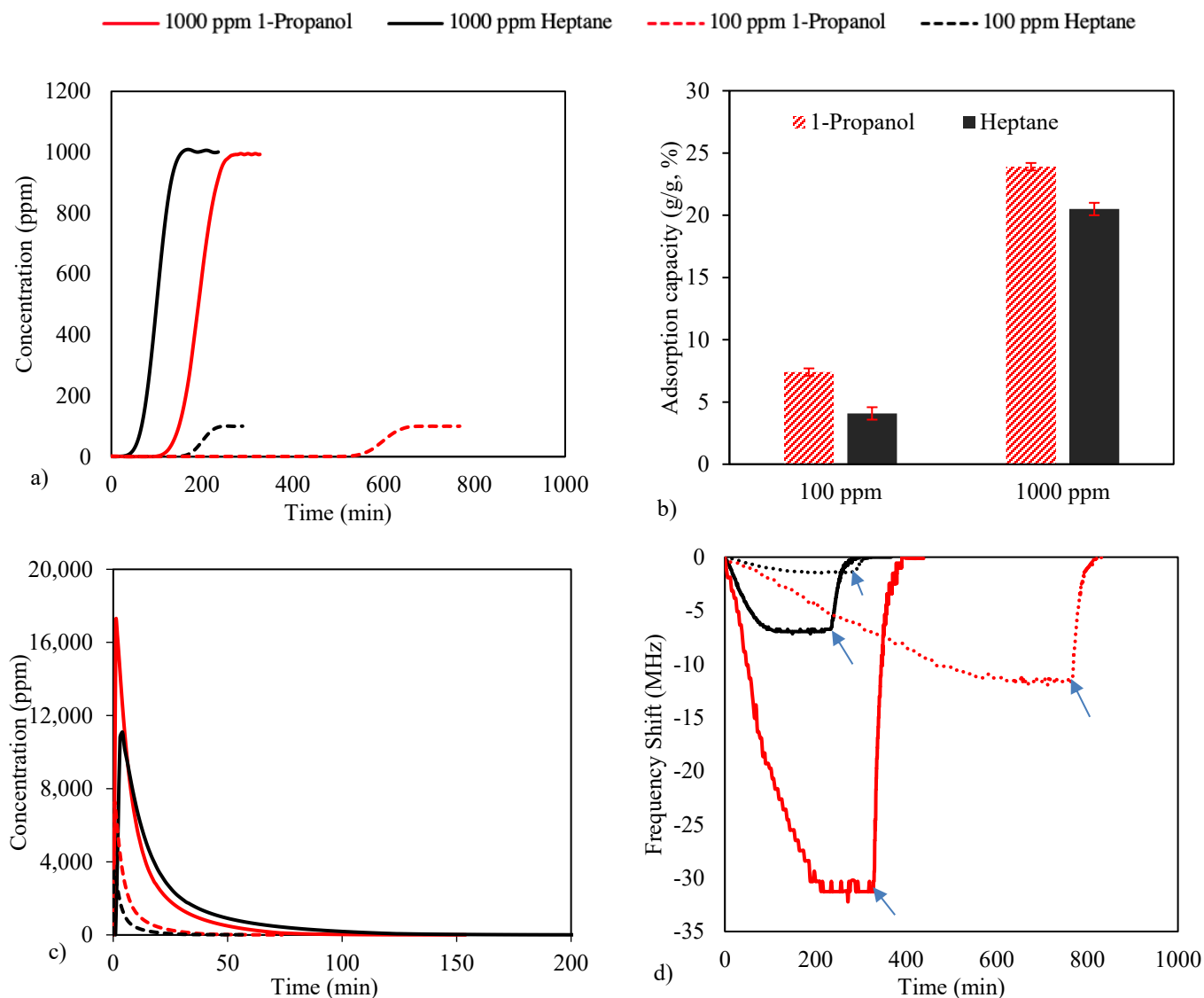
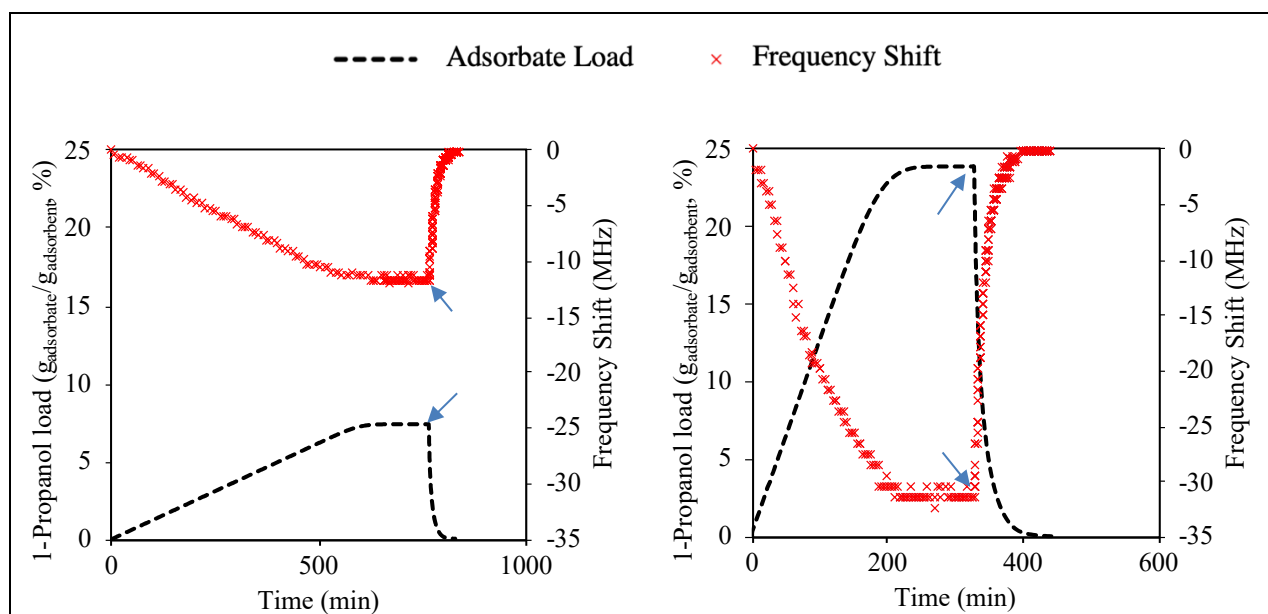


Figure 7-7. a) Adsorption breakthrough curves, b) Dowex Optipore V503 adsorption capacities, c) effluent VOC concentration during the desorption, and d) frequency shift variation during the adsorption and consecutive desorption. Error bars represent the standard deviation of three rounds of analysis. Arrows indicate the transition from the adsorption to the desorption.

To better illustrate the relation between the VOC load and the frequency shift, 1-Propanol/Heptane load on Dowex Optipore V503 were calculated based on the concentration data and ideal gas law

during the adsorption/desorption and compared to the time-based frequency shift results (Figure 7-8). Figure 7-8 shows an immediate change in the VOC loads and frequency shifts after the plateau which is related to the initiation of the regeneration process and VOC desorption from the bed. These results demonstrate that the frequency shifts in all experiments returned to the initial value after regeneration. Therefore, regardless of frequency shift value at saturation state, successful regeneration can be determined when the frequency shift value is approaching the initial value before the VOC adsorption. In other words, this method can be applied to any desorption process with minimum calibration requirement, which is an important achievement.



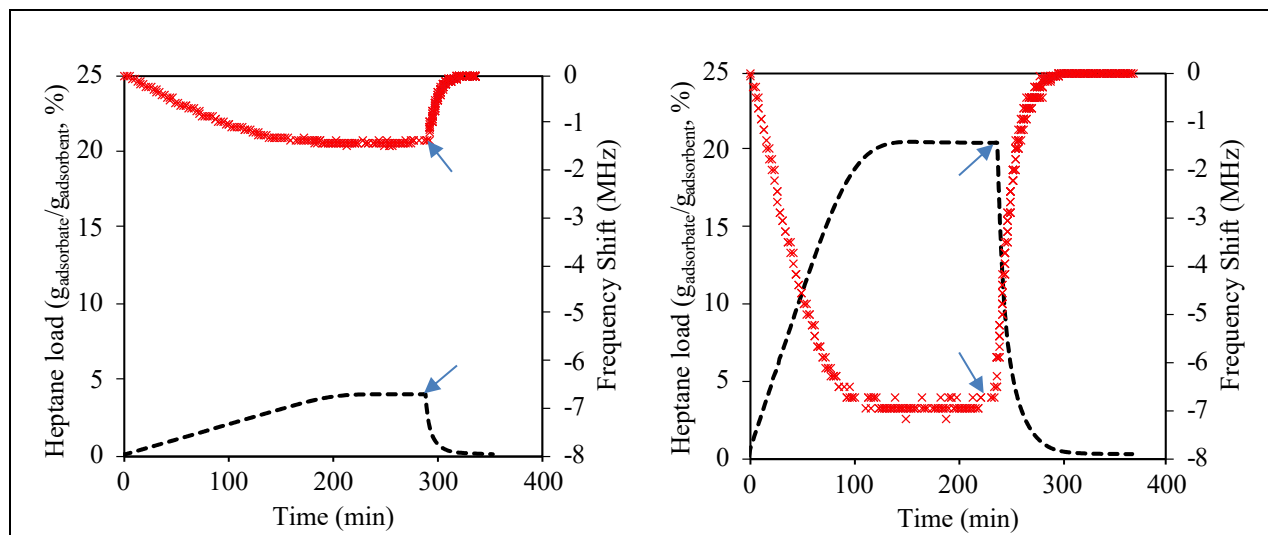


Figure 7-8. Adsorbate load and frequency shift change during adsorption/desorption of a) 100 ppm 1-Propanol, b) 1000 ppm 1-propanol, c) 100 ppm Heptane, and d) 1000 ppm Heptane.

Arrows indicate the transition from the adsorption to the desorption.

To evaluate the accuracy of the sensor in predicting VOC load on the adsorbent, recorded frequency shift and VOC load data during adsorption/desorption were normalized to their maximum values at the equilibrium state (plateau) and plotted versus each other. Figure 7-9 shows the linear relation of frequency shift with adsorbate load. Comparing the  $R^2$  values for the linear regression of frequency and concentration data demonstrate that the variation of 1-propanol load on the adsorbent can be estimated more accurately than heptane load using the resonant frequency data. In accordance with the present results, Fayaz et al. demonstrated a similar linear correlation between the frequency shift and heel, undesorbed VOC, on activated carbon.<sup>35</sup> Figure 7-10 illustrates that 1 wt % of 1-propanol creates more than 4 times larger frequency shift compared to 1 wt % heptane on the adsorbent. Therefore, variation of 1-propanol load on the adsorbent can be estimated with a higher level of accuracy than heptane load variation.

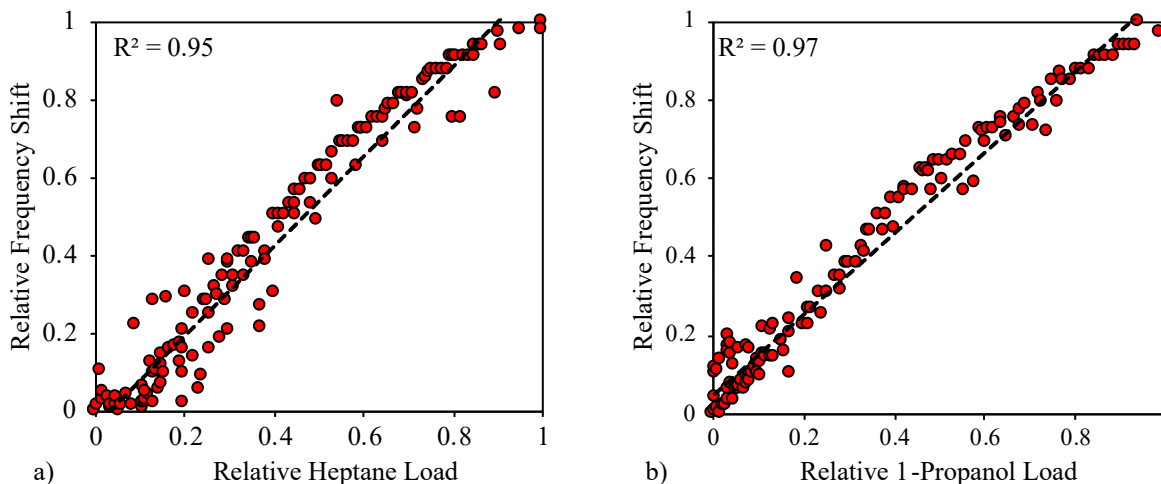


Figure 7-9. Relative frequency shift versus relative adsorbate load in adsorption/desorption of a) Heptane and b) 1-Propanol.

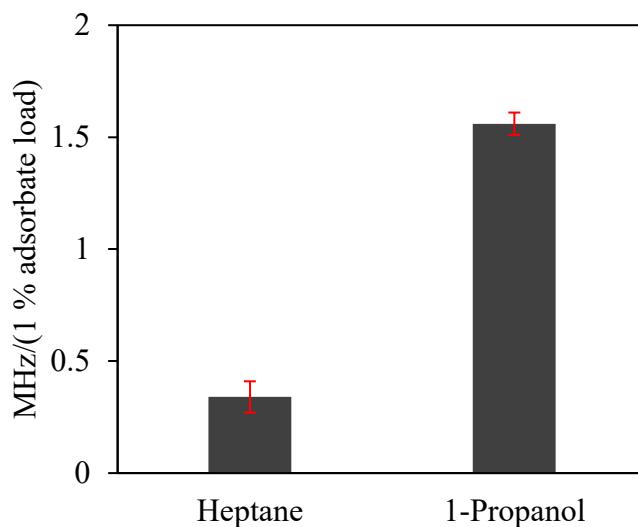


Figure 7-10. Resonant frequency shift of adsorbent with 1 % adsorbate load. Error bars show the standard deviation of three rounds of experiments.

### 7.4.3 Saturation & Regeneration time prediction

As mentioned earlier, this sensor design can potentially be used to measure saturation and regeneration time in the adsorption process. Therefore, obtained frequency and concentration data

during the adsorption/desorption cycle were used to evaluate the performance of the sensor in predicting both saturation ( $t_{\text{Sat.}}$ ) and regeneration time ( $t_{\text{Reg.}}$ ). In this study,  $t_{\text{Sat.}}$  is defined, based on the concentration data, as the time at which adsorbate concentration in the effluent gas stream reaches 99 % of inlet concentration and  $t_{\text{Reg.}}$  is defined as the time at which effluent gas concentration reaches 1 % of feed gas concentration. Based on frequency shift data,  $t_{\text{Sat.}}$  is defined as the time that resonant frequency shift reaches 99 % of its value at the saturation stage, and  $t_{\text{Reg.}}$  is defined as the time at which resonant frequency shift reaches 1 % of its value at the saturation stage. Figure 7-11.a indicates that, for both adsorbate types, the difference between the measured saturation time by frequency and by concentration data is less than 5 %. However, using frequency data, heptane and 1-propanol desorption times were underestimated by 9 to 13 % and 25 to 33 %, respectively (Figure 7-11.b). Larger error and underestimation of regeneration times compared to saturation times are related to the sensor's detection limit at low adsorbate loads.

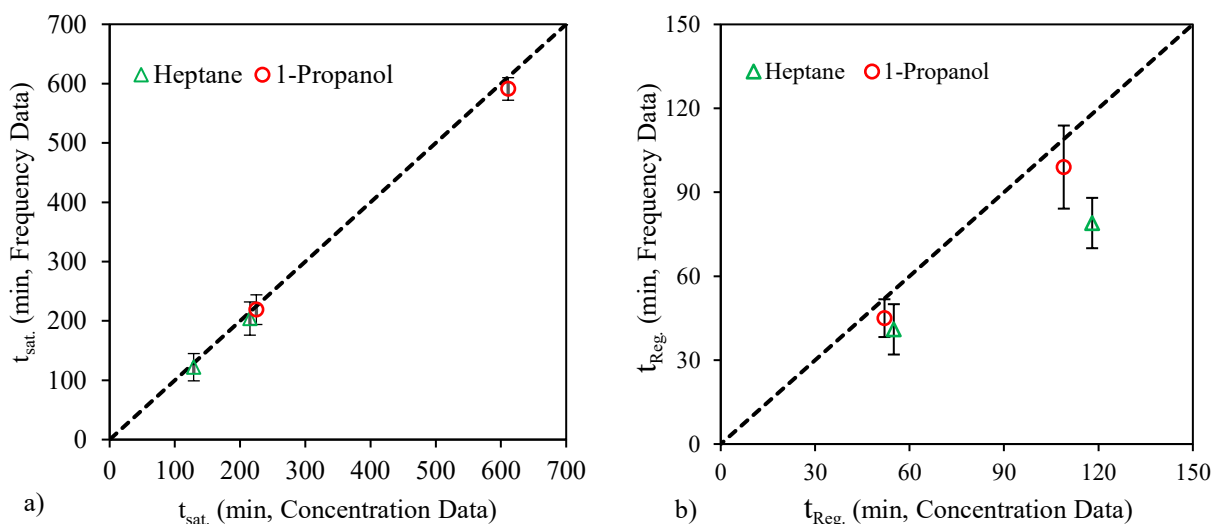


Figure 7-11. Measured adsorbent saturation time,  $t_{\text{Sat.}}$  (a) and regeneration time,  $t_{\text{Reg.}}$  (b) based on concentration and frequency data. Error bars show the standard deviation of three rounds of experiments.

## 7.5 Conclusions

In summary, a contactless distant MW sensor was designed for real-time monitoring of desorption process. Proposed sensor showed acceptable performance up to 60 mm away from the media. Sensitivity analysis of sensor showed more than -34 MHz/(unit  $\epsilon_r$ ) at 15 mm distance from the tag. Stable transmission of frequency data with less than 0.015 MHz frequency shift at temperatures up to 175 °C was observed from the thermal stability analysis. The proposed sensor exhibited an impressive sensitivity for the VOC load variation during the adsorption and desorption process. A linear correlation ( $R^2 > 0.95$ ) was observed between frequency shift data and adsorbate load on the adsorbent. Saturation and regeneration times were predicted using frequency data. Obtained results demonstrate more than 95 % and 75 % accuracy in predicting adsorbent saturation time and regeneration time, respectively. These results could be considered as a paradigm shift in MW sensors for harsh environment applications such as high temperature desorption process and pave the way towards their commercialization.

## 7.6 References

- (1) Schork, J. M.; Fair, J. R. Parametric Analysis of Thermal Regeneration of Adsorption Beds. *Ind. Eng. Chem. Res.* **1988**, 27 (3), 457–469. <https://doi.org/10.1021/ie00075a016>.
- (2) Hwang, K. S.; Choi, D. K.; Gong, S. Y.; Cho, S. Y. Adsorption and Thermal Regeneration of Methylene Chloride Vapor on an Activated Carbon Bed. *Chem. Eng. Sci.* **1997**. [https://doi.org/10.1016/S0009-2509\(96\)00470-8](https://doi.org/10.1016/S0009-2509(96)00470-8).
- (3) Lashaki, M. J.; Fayaz, M.; Wang, H. (Helena); Hashisho, Z.; Philips, J. H.; Anderson, J. E.; Nichols, M. Effect of Adsorption and Regeneration Temperature on Irreversible Adsorption of Organic Vapors on Beaded Activated Carbon. *Environ. Sci. Technol.* **2012**, 46 (7), 4083–4090. <https://doi.org/10.1021/es3000195>.
- (4) Zhang, G.; Feizbakhshan, M.; Zheng, S.; Hashisho, Z.; Sun, Z.; Liu, Y. Effects of Properties of Minerals Adsorbents for the Adsorption and Desorption of Volatile Organic Compounds (VOC). *Appl. Clay Sci.* **2019**, 173, 88–96. <https://doi.org/10.1016/j.clay.2019.02.022>.
- (5) Kim, J. H.; Lee, S. J.; Kim, M. B.; Lee, J. J.; Lee, C. H. Sorption Equilibrium and Thermal Regeneration of Acetone and Toluene Vapors on an Activated Carbon. *Ind. Eng. Chem. Res.* **2007**. <https://doi.org/10.1021/ie0609362>.
- (6) Huang, C. -C.; Fair, J. R. Parametric Analysis of Thermal Swing Cycles for Multicomponent Adsorption. *AIChE J.* **1989**. <https://doi.org/10.1002/aic.690351011>.
- (7) Yun, J. H.; Choi, D. K.; Moon, H. Benzene Adsorption and Hot Purge Regeneration in Activated Carbon Beds. *Chem. Eng. Sci.* **2000**. [https://doi.org/10.1016/S0009-2509\(00\)00189-5](https://doi.org/10.1016/S0009-2509(00)00189-5).
- (8) Abbasi, Z.; Daneshmand, M. Contactless PH Measurement Based on High Resolution Enhanced Q Microwave Resonator. In *2018 IEEE/MTT-S International Microwave Symposium-IMS*; IEEE, 2018; pp 1156–1159.

- (9) Kazemi, N.; Schofield, K.; Musilek, P. A High-Resolution Reflective Microwave Planar Sensor for Sensing of Vanadium Electrolyte. *Sensors* **2021**, *21* (11), 3759.
- (10) Kazemi, N.; Abdolrazzagh, M.; Musilek, P. Comparative Analysis of Machine Learning Techniques for Temperature Compensation in Microwave Sensors. *IEEE Trans. Microw. Theory Tech.* **2021**.
- (11) Vélez, P.; Muñoz-Enano, J.; Ebrahimi, A.; Herrojo, C.; Paredes, F.; Scott, J.; Ghorbani, K.; Martín, F. Single-Frequency Amplitude-Modulation Sensor for Dielectric Characterization of Solids and Microfluidics. *IEEE Sens. J.* **2021**, *21* (10), 12189–12201.
- (12) Abdolrazzagh, M.; Member, S.; Daneshmand, M.; Member, S. Dual Active Resonator for Dispersion Coefficient Measurement of Asphaltene Nano-Particles. **2017**, *17* (22), 7248–7256.
- (13) Baghelani, M.; Abbasi, Z.; Daneshmand, M. Noncontact High Sensitivity Chipless Tag Microwave Resonator for Bitumen Concentration Measurement at High Temperatures. *Fuel* **2020**, *265*. <https://doi.org/10.1016/j.fuel.2019.116916>.
- (14) Ebrahimi, A.; Withayachumnankul, W.; Al-Sarawi, S. F.; Abbott, D. Microwave Microfluidic Sensor for Determination of Glucose Concentration in Water. In *Microwave Symposium (MMS), 2015 IEEE 15th Mediterranean*; IEEE, 2015; pp 1–3.
- (15) Abbasi, Z.; Baghelani, M.; Daneshmand, M. High-Resolution Chipless Tag RF Sensor. *IEEE Trans. Microw. Theory Tech.* **2020**.
- (16) Kazemi, N.; Abdolrazzagh, M.; Musilek, P.; Daneshmand, M. A Temperature-Compensated High-Resolution Microwave Sensor Using Artificial Neural Network. *IEEE Microw. Wirel. Components Lett.* **2020**.
- (17) Jang, C.; Park, J.-K.; Lee, H.-J.; Yun, G.-H.; Yook, J.-G. Non-Invasive Fluidic Glucose Detection Based on Dual Microwave Complementary Split Ring Resonators with a

- Switching Circuit for Environmental Effect Elimination. *IEEE Sens. J.* **2020**, *20* (15), 8520–8527.
- (18) Albishi, A. M.; El Badawe, M. K.; Nayyeri, V.; Ramahi, O. M. Enhancing the Sensitivity of Dielectric Sensors with Multiple Coupled Complementary Split-Ring Resonators. *IEEE Trans. Microw. Theory Tech.* **2020**, *68* (10), 4340–4347.
- (19) Salim, A.; Naqvi, A. H.; Pham, A. D.; Lim, S. Complementary Split-Ring Resonator (CSRR)-Loaded Sensor Array to Detect Multiple Cracks: Shapes, Sizes, and Positions on Metallic Surface. *IEEE Access* **2020**, *8*, 151804–151816.
- (20) Abbasi, Z.; Shariaty, P.; Hashisho, Z.; Daneshmand, M. SilicaGel-Integrated Chipless RF Tag for Humidity Sensing. In *2018 18th International Symposium on Antenna Technology and Applied Electromagnetics (ANTEM)*; IEEE, 2018; pp 1–2.
- (21) Abbasi, Z.; Zarifi, M. H.; Shariati, P.; Hashisho, Z.; Daneshmand, M. Flexible Coupled Microwave Ring Resonators for Contactless Microbead Assisted Volatile Organic Compound Detection. In *Microwave Symposium (IMS), 2017 IEEE MTT-S International*; IEEE, 2017; pp 1228–1231.
- (22) Zarifi, M. H.; Shariaty, P.; Hashisho, Z.; Daneshmand, M. A Non-Contact Microwave Sensor for Monitoring the Interaction of Zeolite 13X with CO<sub>2</sub> and CH<sub>4</sub> in Gaseous Streams. *Sensors Actuators B Chem.* **2017**, *238*, 1240–1247.
- (23) Kim, N. Y.; Dhakal, R.; Adhikari, K. K.; Kim, E. S.; Wang, C. A Reusable Robust Radio Frequency Biosensor Using Microwave Resonator by Integrated Passive Device Technology for Quantitative Detection of Glucose Level. *Biosens. Bioelectron.* **2015**, *67*, 687–693.
- (24) Boybay, M. S.; Jiao, A.; Glawdel, T.; Ren, C. L. Microwave Sensing and Heating of Individual Droplets in Microfluidic Devices. *Lab Chip* **2013**, *13* (19), 3840–3846.

- (25) Moghadas, H.; Mushahwar, V. K. Passive Microwave Resonant Sensor for Detection of Deep Tissue Injuries. *Sensors Actuators B Chem.* **2018**, *277*, 69–77.
- (26) Nelson, R. D.; Lide, D. R.; Maryott, A. A. Selected Values of Electric Dipole Moments for Molecules in the Gas Phase. *National Standard Reference Series - National Bureau of Standards 10*; United States Department of Commerce, 1967; pp 1–49.
- (27) Reichardt, C.; Welton, T. *Solvents and Solvent Effects in Organic Chemistry*; Wiley-VCH Verlag GmbH & Co. KGaA: Weinheim, Germany, 2010. <https://doi.org/10.1002/9783527632220>.
- (28) Casas Espínola, J. L.; Hernández Contreras, X. A. Effect of Dielectric Constant on Emission of CdSe Quantum Dots. *J. Mater. Sci. Mater. Electron.* **2017**, *28* (10). <https://doi.org/10.1007/s10854-017-6539-9>.
- (29) Méndez-Bermúdez, J. G.; Dominguez, H.; Pusztai, L.; Guba, S.; Horváth, B.; Szalai, I. Composition and Temperature Dependence of the Dielectric Constant of 1-Propanol/Water Mixtures: Experiment and Molecular Dynamics Simulations. *J. Mol. Liq.* **2016**, *219*. <https://doi.org/10.1016/j.molliq.2016.02.053>.
- (30) Meaney, P. M.; Fox, C. J.; Geimer, S. D.; Paulsen, K. D. Electrical Characterization of Glycerin: Water Mixtures: Implications for Use as a Coupling Medium in Microwave Tomography. *IEEE Trans. Microw. Theory Tech.* **2017**, *65* (5), 1471–1478.
- (31) Fayaz, M.; Zarifi, M. H.; Abdolrazzaghi, M.; Shariaty, P.; Hashisho, Z.; Daneshmand, M. A Novel Technique for Determining the Adsorption Capacity and Breakthrough Time of Adsorbents Using a Noncontact High-Resolution Microwave Resonator Sensor. *Environ. Sci. Technol.* **2016**, *51* (1), 427–435.
- (32) Cherbański, R.; Molga, E. Intensification of Desorption Processes by Use of Microwaves- An Overview of Possible Applications and Industrial Perspectives. *Chem. Eng. Process. Process Intensif.* **2009**. <https://doi.org/10.1016/j.cep.2008.01.004>.

- (33) Lin, G.; Liu, C.; Zhang, L.; Hu, T.; Peng, J.; Li, J.; Wang, S. High Temperature Dielectric Properties of Spent Adsorbent with Zinc Sulfate by Cavity Perturbation Technique. *J. Hazard. Mater.* **2017**. <https://doi.org/10.1016/j.jhazmat.2017.02.010>.
- (34) Kim, K.-J.; Ahn, H.-G. The Effect of Pore Structure of Zeolite on the Adsorption of VOCs and Their Desorption Properties by Microwave Heating. *Microporous Mesoporous Mater.* **2012**, *152*, 78–83. <https://doi.org/10.1016/j.micromeso.2011.11.051>.
- (35) Fayaz, M.; Jahandar Lashaki, M.; Abdolrazzaghi, M.; Zarifi, M. H.; Hashisho, Z.; Daneshmand, M.; Anderson, J. E.; Nichols, M. Monitoring the Residual Capacity of Activated Carbon in an Emission Abatement System Using a Non-Contact, High Resolution Microwave Resonator Sensor. *Sensors Actuators B Chem.* **2019**, *282*, 218–224. <https://doi.org/10.1016/j.snb.2018.11.038>.

## **CHAPTER 8: CONCLUSIONS AND RECOMMENDATIONS**

### **8.1 Dissertation Overview**

Adsorbents with high surface area, thermal stability, and microwave (MW) absorption ability are highly desired for cyclic adsorption and MW-assisted regeneration processes. However, there are many adsorbents such as porous polymers which cannot be regenerated by MW due to poor MW absorption ability.

MW resonators have been widely used for sensing applications in environmental system monitoring. A very attractive application for the MW planar structure is VOC sensing. So far MW sensors have been used in low to medium range temperature process (<100 °C) which limits their application in harsh environments such as VOC sensing in thermal regeneration process.

This research is one of the first investigations that developed novel methods to improve MW-assisted regeneration of porous MW-transparent adsorbents and a new MW sensor for VOC sensing at high temperature desorption process.

### **8.2 Conclusions**

In chapter 3, the effect of purge gas relative humidity on MW absorption of Zeolite and Optipore V503 was investigated at a range of MW applied power. Higher temperature was achieved when adsorbents were purged with humid purge gas compared to dry purge gas. To elucidate the reason behind this, water vapor adsorption experiments were performed on both adsorbents under MW irradiation (0-400 W). After each adsorption test, the adsorption capacity and dielectric properties of the adsorbent samples were measured. Dielectric property measurements showed that the

dielectric constant and loss factor of the adsorbents decreased with increasing MW applied power. This trend is attributed to the water adsorption amount on zeolite and Optipore V503 which was reduced by more than 93 % and 97 %, respectively, due to the MW irradiation and corresponding adsorbent temperature increase. Further investigation revealed that water vapor concentration in the purge gas and the interaction of water molecules with the adsorbent surface are two major factors governing the extent of MW heating at constant applied power. Additionally, VOC adsorption on /MW assisted desorption of zeolite/Optipore V503 was performed to study the effect of purge gas humidity on the regeneration of adsorbents. Using humidified purge gas enhanced the VOC desorption rate by 86 % and decreased the energy required to reach 99 % desorption efficiency by 73 %.

In chapter 4, the effect of CNT addition to Optipore V503 was studied. CNTs were selected as a MAM due to their large loss factor and electrical conductivity. Different levels of CNT (0-0.3 wt%) were deposited on the adsorbent surface using an aqueous solution with SDS:CNT ratio of 10:1. Results obtained from HIM imaging and Raman spectroscopy showed that adsorbent beads can be successfully coated with CNT using SDS/CNT suspension. Nitrogen and heptane adsorption analysis revealed that BET surface area and adsorption performance of the adsorbent decreased due to SDS diffusion into the micropores during CNT coating. CNT-coated and as received adsorbent samples demonstrated similar thermal stability based on TGA analysis. Coating Optipore with 0.3 wt% of CNT enhanced its dielectric constant and loss factor by 160% and 2790%, respectively. The enhancement in the dielectric properties by CNTs led to a considerable reduction (more than 98%) in the MW energy needed to heat the bed. Finally, cyclic heptane adsorption/MW regeneration experiments showed more than 284% improvement in the desorption

efficiency of CNT coated samples. Improved VOC desorption during MW heating increased the working capacity of coated samples by 237 %.

In chapter 5, a series of CB/HCP composites of different CB contents were prepared through in-situ polymerization and Friedel-Crafts reactions. FTIR analysis and HIM images confirmed the synthesis of HCP and CB/HCP, respectively. The HIM images showed formation of CB agglomerates that can act as a conductive network within the matrix. TGA analysis showed more than a 60 percent increase in the residual weight at 880 °C in CB filled polymers which shows higher thermal stability of CB-filled composites. This is a particularly important feature since adsorbents can reach elevated temperatures in MW-heating. Nitrogen and toluene adsorption isotherm analysis indicated that the composites have well-developed micropore and mesopore structures. The CB content of 4 wt% was found to be optimum as disproportionally larger reductions in pore volume and adsorption capacity were observed above this filler content. Dielectric property measurement of HCP with 4 wt % CB showed more than 2 and 21-times enhancement in dielectric constant and loss factor, respectively. These increases are attributed to the formation of a conductive CB network inside the polymer structure which provided more paths for electron migration and therefore conduction loss inside the composite. MW-assisted desorption of HCP with 4 wt% CB showed a 139 °C increase in the desorption temperature compared to pristine HCP at the same applied MW power. As a result, hexane could completely desorb from the CB-filled composite and the desorption efficiency improved by more than 73 % compared to that of HCP.

In chapter 6, solution mixing method was selected to minimize the filler agglomeration in the composite. In this regard, polymers of 4, 4'-bis ((chloromethyl)-1, 1' -biphenyl- benzyl chloride)

were synthesized through the Friedel-Crafts reactions. GO nanosheets were synthesized by Hummer's method to be used as the MW absorptive filler that could potentially have a low percolation threshold due to its large aspect ratio. XRD, FTIR, SEM, HIM, and TEM studies showed the successful synthesis of HCPs and GO, and the proper dispersion of GO inside the HCP matrix. TGA analysis revealed that even a small amount of GO (1 wt%) profoundly increases the thermal stability of HCP. The small reduction in BET surface area and total pore volume of nanocomposites by GO content was attributed to the nonporous structure of GO sheets. Dielectric measurement results revealed that filling HCP with 8 wt% of GO enhances the dielectric constant and loss factor by more than 3 and 28 times, respectively. The consumed MW energy to heat the the polymer with 8 wt% GO by 1 °C was reduced by 99% in the MW heating experiments. More than 160 °C and 4 times enhancement in the desorption temperature and toluene desorption efficiency were achieved by addition of 4 wt% of GO to the polymer.

In chapter 7, a non-contact MW sensor was designed for real-time monitoring of desorption process. The sensor showed acceptable performance up to 60 mm away from the media. Sensitivity analysis of sensor showed more than -34 MHz/(unit  $\epsilon_r$ ) at 15 mm distance from the tag. Stable transmission of frequency data with less than 0.015 MHz frequency shift at temperatures up to 175 °C was observed from the thermal stability analysis. The proposed sensor exhibited a high sensitivity for the VOC load variation during the adsorption and desorption process. A linear correlation ( $R^2 > 0.95$ ) was observed between frequency shift data and adsorbate load on the adsorbent. Saturation and regeneration times were predicted using frequency data. Obtained results demonstrate more than 95 % and 75 % accuracy in predicting adsorbent saturation time and

regeneration time, respectively. These results could set the stage for the use of MW sensors in harsh environment applications such as high temperature desorption process.

### 8.3 Recommendations

In this research four methods were identified to improve the MW-assisted regeneration of MW-transparent adsorbents. Different characterization tests were used to show the advantages and disadvantages of each method. Based on the findings of this research, the following recommendations can be made for future investigations:

- Due to its tunable porosity and chemical versatility, HCPs are considered as a suitable candidate in many VOC adsorption applications. Nevertheless, commercially available polymeric adsorbents suffer from undefined bed porosity, high pressure drop and abrasion since they are typically provided in the form of spherical particles. These obstacles could be overcome through the free design offered by 3D printing. Further research could usefully explore the preparation of porous HCP honeycombs by 3D printing.
- This study showed the critical impact of MAMs (e.g., water, CNT, CB, GO) on the MW-assisted regeneration of MW-transparent adsorbents. While the presence of a MAM in the structure of adsorbent is needed for an efficient MW heating, it reduced the adsorption capacity of adsorbent based on the selected MAM. Future research could explore the effect of hybrid fillers (e.g., polymer/CNT nanofillers) as MAMs which could potentially result in better VOC adsorption and MW assisted regeneration of adsorbents.
- The cyclical performance of an adsorbent has a close relationship to its thermal stability at elevated temperatures. This study showed that the presence of MAM fillers (e.g., CB, GO)

in the polymer structure substantially increases the thermal stability of prepared composite. However, there are other nanofillers such  $\text{Al}_2\text{O}_3$  which has been reported in the literature for thermal stability improvement of non-porous composites. Further research might explore the effect of such nanoparticles on the thermal stability of porous composites.

- Adsorbent beads can be under a large mechanical stress in the packed bed, which directly affect the adsorbent life span. Due to high mechanical strength, carbonaceous fillers such as CNTs have been used to enhance the mechanical strength of non-porous polymer composites. A further study could assess the effect of CNTs on the mechanical strength of porous composite adsorbents.

## BIBLIOGRAPHY

- Abbasi, Zahra, Masoud Baghelani, and Mojgan Daneshmand. 2020. "High-Resolution Chipless Tag RF Sensor." *IEEE Transactions on Microwave Theory and Techniques*.
- Abbasi, Zahra, and Mojgan Daneshmand. 2018. "Contactless PH Measurement Based on High Resolution Enhanced Q Microwave Resonator." In *2018 IEEE/MTT-S International Microwave Symposium-IMS*, 1156–59. IEEE.
- Abbasi, Zahra, Pooya Shariaty, Zaher Hashisho, and Mojgan Daneshmand. 2018. "SilicaGel-Integrated Chipless RF Tag for Humidity Sensing." In *2018 18th International Symposium on Antenna Technology and Applied Electromagnetics (ANTEM)*, 1–2. IEEE.
- Abbasi, Zahra, Mohammad Hossein Zarifi, Pooya Shariati, Zaher Hashisho, and Mojgan Daneshmand. 2017. "Flexible Coupled Microwave Ring Resonators for Contactless Microbead Assisted Volatile Organic Compound Detection." *IEEE MTT-S International Microwave Symposium Digest* 2: 1228–31. <https://doi.org/10.1109/MWSYM.2017.8058827>.
- Abdolrazzaghi, Mohammad, Student Member, Mojgan Daneshmand, and Senior Member. 2017. "Dual Active Resonator for Dispersion Coefficient Measurement of Asphaltene Nano-Particles" *17* (22): 7248–56.
- Águeda, Vicente I., Barry D. Crittenden, José A. Delgado, and Steve R. Tennison. 2011. "Effect of Channel Geometry, Degree of Activation, Relative Humidity and Temperature on the Performance of Binderless Activated Carbon Monoliths in the Removal of Dichloromethane from Air." *Separation and Purification Technology* 78 (2): 154–63. <https://doi.org/10.1016/j.seppur.2011.01.036>.
- Aimoto, Atsuko, and Takashi Matsumoto. 1996. "Noninvasive Method for Measuring the Electrical Properties of Deep Tissues Using an Open-Ended Coaxial Probe." *Medical Engineering and Physics* 18 (8). [https://doi.org/10.1016/S1350-4533\(96\)00026-4](https://doi.org/10.1016/S1350-4533(96)00026-4).

## Bibliography

- Akram, Zikra, Ayesha Kausar, and Muhammad Siddiq. 2016. "Review on Polymer/Carbon Nanotube Composite Focusing Polystyrene Microsphere and Polystyrene Microsphere/Modified CNT Composite: Preparation, Properties, and Significance." *Polymer-Plastics Technology and Engineering* 55 (6): 582–603. <https://doi.org/10.1080/03602559.2015.1098696>.
- Albishi, Ali M, Mohamed K El Badawe, Vahid Nayyeri, and Omar M Ramahi. 2020. "Enhancing the Sensitivity of Dielectric Sensors with Multiple Coupled Complementary Split-Ring Resonators." *IEEE Transactions on Microwave Theory and Techniques* 68 (10): 4340–47.
- Amorim, Suélen M., Gabriel Steffen, Joel M.N. de S Junior, Claiton Z. Brusamarello, Ana P. Romio, and Michele D. Domenico. 2020. "Synthesis, Characterization, and Application of Polypyrrole/TiO<sub>2</sub> Composites in Photocatalytic Processes: A Review." *Polymers and Polymer Composites*. <https://doi.org/10.1177/0967391120949489>.
- Ania, C. O., J. A. Menéndez, J. B. Parra, and J. J. Pis. 2004. "Microwave-Induced Regeneration of Activated Carbons Polluted with Phenol. A Comparison with Conventional Thermal Regeneration." In *Carbon*. Vol. 42. <https://doi.org/10.1016/j.carbon.2004.01.010>.
- Ania, C. O., J. B. Parra, J. A. Menéndez, and J. J. Pis. 2005. "Effect of Microwave and Conventional Regeneration on the Microporous and Mesoporous Network and on the Adsorptive Capacity of Activated Carbons." *Microporous and Mesoporous Materials* 85 (1–2): 7–15. <https://doi.org/10.1016/j.micromeso.2005.06.013>.
- Antonio, Christian, and Rowan T. Deam. 2007. "Can 'Microwave Effects' Be Explained by Enhanced Diffusion?" *Physical Chemistry Chemical Physics* 9 (23): 2976–82. <https://doi.org/10.1039/b617358f>.
- Arief, Injamamul, Sourav Biswas, and Suryasarathi Bose. 2017. "FeCo-Anchored Reduced Graphene Oxide Framework-Based Soft Composites Containing Carbon Nanotubes as Highly Efficient Microwave Absorbers with Excellent Heat Dissipation Ability." *ACS Applied Materials and Interfaces* 9 (22). <https://doi.org/10.1021/acsami.7b04053>.

## Bibliography

- Baghelani, M., Z. Abbasi, and M. Daneshmand. 2020. "Noncontact High Sensitivity Chipless Tag Microwave Resonator for Bitumen Concentration Measurement at High Temperatures." *Fuel* 265. <https://doi.org/10.1016/j.fuel.2019.116916>.
- Barochi, Guillaume, Jérôme Rossignol, and Marcel Bouvet. 2011. "Development of Microwave Gas Sensors." *Sensors and Actuators B: Chemical* 157 (2): 374–79. <https://doi.org/10.1016/j.snb.2011.04.059>.
- Bernou, Catherine, Dominique Rebière, and Jacques Pistré. 2000. "Microwave Sensors: A New Sensing Principle. Application to Humidity Detection." *Sensors and Actuators B: Chemical* 68 (1–3): 88–93. [https://doi.org/10.1016/S0925-4005\(00\)00466-4](https://doi.org/10.1016/S0925-4005(00)00466-4).
- Bibi, Saira, Tariq Yasin, Safia Hassan, Muhammad Riaz, and Mohsan Nawaz. 2015. "Chitosan/CNTs Green Nanocomposite Membrane: Synthesis, Swelling and Polyaromatic Hydrocarbons Removal." *Materials Science and Engineering: C* 46 (January): 359–65. <https://doi.org/10.1016/j.msec.2014.10.057>.
- Boybay, Muhammed S, Austin Jiao, Tomasz Glawdel, and Carolyn L Ren. 2013. "Microwave Sensing and Heating of Individual Droplets in Microfluidic Devices." *Lab on a Chip* 13 (19): 3840–46.
- Bradshaw, S. M., E. J. Van Wyk, and J. B. De Swardt. 1998. "Microwave Heating Principles and the Application to the Regeneration of Granular Activated Carbon." *Journal of The South African Institute of Mining and Metallurgy* 98 (4): 201–10.
- Brodie, Graham, Mohan V. Jacob, and Peter Farrell. 2015. "6 Techniques for Measuring Dielectric Properties." In *Microwave and Radio-Frequency Technologies in Agriculture*, 52–77. De Gruyter Open Poland. <https://doi.org/10.1515/9783110455403-007>.
- Brown, S. D. M., A. Jorio, M. S. Dresselhaus, and G. Dresselhaus. 2001. "Observations of the D -Band Feature in the Raman Spectra of Carbon Nanotubes." *Physical Review B* 64 (7): 073403. <https://doi.org/10.1103/PhysRevB.64.073403>.

## Bibliography

- Bruce, Chrystal D., Max L. Berkowitz, Lalith Perera, and Malcolm D. E. Forbes. 2002. "Molecular Dynamics Simulation of Sodium Dodecyl Sulfate Micelle in Water: Micellar Structural Characteristics and Counterion Distribution." *The Journal of Physical Chemistry B* 106 (15): 3788–93. <https://doi.org/10.1021/jp013616z>.
- Burkholder, Harvey R., Glenn E. Fanslow, and Delwyn D. Bluhm. 1986. "Recovery of Ethanol from a Molecular Sieve by Using Dielectric Heating." *Industrial and Engineering Chemistry Fundamentals* 25 (3). <https://doi.org/10.1021/i100023a019>.
- Casas Espínola, J. L., and X. A. Hernández Contreras. 2017. "Effect of Dielectric Constant on Emission of CdSe Quantum Dots." *Journal of Materials Science: Materials in Electronics* 28 (10). <https://doi.org/10.1007/s10854-017-6539-9>.
- Cha, Chang Yul, and Charlie T. Carlisle. 2001. "Microwave Process for Volatile Organic Compound Abatement." *Journal of the Air and Waste Management Association* 51 (12): 1628–41. <https://doi.org/10.1080/10473289.2001.10464389>.
- Chandrasekaran, S., Srinivasan Ramanathan, and Tanmay Basak. 2012. "Microwave Material Processing—a Review." *AIChE Journal* 58 (2): 330–63. <https://doi.org/10.1002/aic.12766>.
- Che, R. C., L.-M. Peng, X. F. Duan, Qing Chen, and X. L. Liang. 2004. "Microwave Absorption Enhancement and Complex Permittivity and Permeability of Fe Encapsulated within Carbon Nanotubes." *Advanced Materials* 16 (5): 401–5. <https://doi.org/10.1002/adma.200306460>.
- Chen, Cheng, Limei Pan, Senchuan Jiang, Shuang Yin, Xiaoyun Li, Jingxian Zhang, Yongbao Feng, and Jian Yang. 2018. "Electrical Conductivity, Dielectric and Microwave Absorption Properties of Graphene Nanosheets/Magnesia Composites." *Journal of the European Ceramic Society* 38 (4): 1639–46. <https://doi.org/10.1016/j.jeurceramsoc.2017.11.052>.
- Chen, Chun-Yu, Nen-Wen Pu, Yih-Ming Liu, Sheng-Yao Huang, Chia-Hung Wu, Ming-Der Ger, Yan-Jhang Gong, and Yu-Chieh Chou. 2017. "Remarkable Microwave Absorption

## Bibliography

- Performance of Graphene at a Very Low Loading Ratio.” *Composites Part B: Engineering* 114 (April): 395–403. <https://doi.org/10.1016/j.compositesb.2017.02.016>.
- Cherbański, R., and E. Molga. 2009. “Intensification of Desorption Processes by Use of Microwaves-An Overview of Possible Applications and Industrial Perspectives.” *Chemical Engineering and Processing: Process Intensification*. <https://doi.org/10.1016/j.cep.2008.01.004>.
- Cherbański, Robert. 2018. “Regeneration of Granular Activated Carbon Loaded with Toluene – Comparison of Microwave and Conductive Heating at the Same Active Powers.” *Chemical Engineering and Processing - Process Intensification* 123 (January): 148–57. <https://doi.org/10.1016/j.cep.2017.11.008>.
- Cherbański, Robert, Magdalena Komorowska-Durka, Georgios D. Stefanidis, and Andrzej I. Stankiewicz. 2011. “Microwave Swing Regeneration vs Temperature Swing Regeneration—Comparison of Desorption Kinetics.” *Industrial & Engineering Chemistry Research* 50 (14): 8632–44. <https://doi.org/10.1021/ie102490v>.
- Chiang, Yu-Chun, Pen-Chi Chiang, and E.-E. Chang. 2001. “Effects of Surface Characteristics of Activated Carbons on VOC Adsorption.” *Journal of Environmental Engineering*. [https://doi.org/10.1061/\(asce\)0733-9372\(2001\)127:1\(54\)](https://doi.org/10.1061/(asce)0733-9372(2001)127:1(54)).
- Chiang, Yu Chun, Pen Chi Chiang, and Chin Pao Huang. 2001. “Effects of Pore Structure and Temperature on VOC Adsorption on Activated Carbon.” *Carbon* 39 (4). [https://doi.org/10.1016/S0008-6223\(00\)00161-5](https://doi.org/10.1016/S0008-6223(00)00161-5).
- Chihara, Kazuyuki, Kanji Oomori, Takao Oono, and Yosuke Mochizuki. 1997. “Supercritical CO<sub>2</sub> Regeneration of Activated Carbon Loaded with Organic Adsorbates.” *Water Science and Technology* 35 (7). [https://doi.org/10.1016/S0273-1223\(97\)00139-X](https://doi.org/10.1016/S0273-1223(97)00139-X).
- Chin, Woo Seok, and Dai Gil Lee. 2007. “Development of the Composite RAS (Radar Absorbing Structure) for the X-Band Frequency Range.” *Composite Structures* 77 (4): 457–65. <https://doi.org/10.1016/j.compstruct.2005.07.021>.

## Bibliography

- Chowdhury, Tamanna, Meng Shi, Zaher Hashisho, James A. Sawada, and Steven M. Kuznicki. 2012. "Regeneration of Na-ETS-10 Using Microwave and Conductive Heating." *Chemical Engineering Science* 75 (June): 282–88. <https://doi.org/10.1016/j.ces.2012.03.039>.
- Clark, David E., Diane C. Folz, and Jon K. West. 2000. "Processing Materials with Microwave Energy." *Materials Science and Engineering: A* 287 (2): 153–58. [https://doi.org/10.1016/S0921-5093\(00\)00768-1](https://doi.org/10.1016/S0921-5093(00)00768-1).
- Clark, David E., and Willard H. Sutton. 1996. "Microwave Processing of Materials." *Annual Review of Materials Science* 26 (1): 299–331. <https://doi.org/10.1146/annurev.ms.26.080196.001503>.
- Coss, P. Moses, and Chang Yul Cha. 2000. "Microwave Regeneration of Activated Carbon Used for Removal of Solvents from Vented Air." *Journal of the Air and Waste Management Association* 50 (4): 529–35. <https://doi.org/10.1080/10473289.2000.10464038>.
- Dang, Zhi-Min, Jin-Ping Wu, Hai-Ping Xu, Sheng-Hong Yao, Mei-Juan Jiang, and Jinbo Bai. 2007. "Dielectric Properties of Upright Carbon Fiber Filled Poly(Vinylidene Fluoride) Composite with Low Percolation Threshold and Weak Temperature Dependence." *Applied Physics Letters* 91 (7): 072912. <https://doi.org/10.1063/1.2770664>.
- Das, Chapal Kumar, Pallab Bhattacharya, and Swinderjeet Singh Kalra. 2012. "Graphene and MWCNT: Potential Candidate for Microwave Absorbing Materials." *Journal of Materials Science Research* 1 (2). <https://doi.org/10.5539/jmsr.v1n2p126>.
- Das, Chapal Kumar, and Avinandan Mandal. 2011. "Microwave Absorbing Properties of DBSA-Doped Polyaniline/BaTiO<sub>3</sub>-Ni<sub>0.5</sub>Zn<sub>0.5</sub>Fe<sub>2</sub>O<sub>4</sub> Nanocomposites." *Journal of Materials Science Research* 1 (1). <https://doi.org/10.5539/jmsr.v1n1p45>.
- Deng, Qinqin, Xudong Yang, and Jianshun Zhang. 2009. "Study on a New Correlation between Diffusion Coefficient and Temperature in Porous Building Materials." *Atmospheric Environment* 43 (12): 2080–83. <https://doi.org/10.1016/j.atmosenv.2008.12.052>.

## Bibliography

- Deshmukh, Kalim, M. Basheer Ahamed, S. K. Khadheer Pasha, Rajendra R. Deshmukh, and Pundlik R. Bhagat. 2015a. "Highly Dispersible Graphene Oxide Reinforced Polypyrrole/Polyvinyl Alcohol Blend Nanocomposites with High Dielectric Constant and Low Dielectric Loss." *RSC Advances* 5 (76): 61933–45. <https://doi.org/10.1039/c5ra11242g>.
- Deshmukh, Kalim, M Basheer Ahamed, S. K. Khadheer Pasha, Rajendra R Deshmukh, and Pundlik R Bhagat. 2015b. "Highly Dispersible Graphene Oxide Reinforced Polypyrrole/Polyvinyl Alcohol Blend Nanocomposites with High Dielectric Constant and Low Dielectric Loss." *RSC Advances* 5 (76): 61933–45. <https://doi.org/10.1039/C5RA11242G>.
- Dominguez, Ana, Aurora Fernandez, Noemi Gonzalez, Emilia Iglesias, and Luis Montenegro. 1997. "Determination of Critical Micelle Concentration of Some Surfactants by Three Techniques." *Journal of Chemical Education* 74 (10): 1227. <https://doi.org/10.1021/ed074p1227>.
- Dou, Baojuan, Qin Hu, Jinjun Li, Shizhang Qiao, and Zhengping Hao. 2011. "Adsorption Performance of VOCs in Ordered Mesoporous Silicas with Different Pore Structures and Surface Chemistry." *Journal of Hazardous Materials* 186 (2–3): 1615–24. <https://doi.org/10.1016/j.jhazmat.2010.12.051>.
- Duan, Wen Hui, Quan Wang, and Frank Collins. 2011. "Dispersion of Carbon Nanotubes with SDS Surfactants: A Study from a Binding Energy Perspective." *Chemical Science* 2 (7): 1407. <https://doi.org/10.1039/c0sc00616e>.
- Dunn, Russell F., and Mahmoud M. El-Halwagi. 1994. "Optimal Design of Multicomponent VOC Condensation Systems." *Journal of Hazardous Materials* 38 (1): 187–206. [https://doi.org/10.1016/0304-3894\(94\)00014-X](https://doi.org/10.1016/0304-3894(94)00014-X).
- Dykas, M M, K Poddar, S L Yoong, V Viswanathan, S Mathew, A Patra, S Saha, G Pastorin, and T Venkatesan. 2018. "Enhancing Image Contrast of Carbon Nanotubes on Cellular

## Bibliography

- Background Using Helium Ion Microscope by Varying Helium Ion Fluence.” *Journal of Microscopy* 269 (1): 14–22. <https://doi.org/10.1111/jmi.12604>.
- Ebrahimi-Tazangi, Fatemeh, Seyedeh Hoda Hekmatara, and Jamileh Seyed-Yazdi. 2021. “Remarkable Microwave Absorption of GO-SiO<sub>2</sub>/Fe<sub>3</sub>O<sub>4</sub> via an Effective Design and Optimized Composition.” *Journal of Alloys and Compounds* 854 (February): 157213. <https://doi.org/10.1016/j.jallcom.2020.157213>.
- Ebrahimi, Amir, Withawat Withayachumnankul, Said F Al-Sarawi, and Derek Abbott. 2015. “Microwave Microfluidic Sensor for Determination of Glucose Concentration in Water.” In *Microwave Symposium (MMS), 2015 IEEE 15th Mediterranean*, 1–3. IEEE.
- “Facile and Economic Synthesis of Silica Nanoparticles.” 2009. *Journal of Ovonic Research* 5 (5).
- Fakhouri, M.O., and H.S. Ramaswamy. 1993. “Temperature Uniformity of Microwave Heated Foods as Influenced by Product Type and Composition.” *Food Research International* 26 (2): 89–95. [https://doi.org/10.1016/0963-9969\(93\)90062-N](https://doi.org/10.1016/0963-9969(93)90062-N).
- Falciglia, Pietro P., Paolo Roccaro, Lorenzo Bonanno, Guido De Guidi, Federico G.A. Vagliasindi, and Stefano Romano. 2018. “A Review on the Microwave Heating as a Sustainable Technique for Environmental Remediation/Detoxification Applications.” *Renewable and Sustainable Energy Reviews* 95 (November): 147–70. <https://doi.org/10.1016/j.rser.2018.07.031>.
- Fayaz, Mohammadreza, Masoud Jahandar Lashaki, Mohammad Abdolrazzaghi, Mohammad H Zarifi, Zaher Hashisho, Mojgan Daneshmand, James E Anderson, and Mark Nichols. 2019. “Monitoring the Residual Capacity of Activated Carbon in an Emission Abatement System Using a Non-Contact, High Resolution Microwave Resonator Sensor.” *Sensors and Actuators B: Chemical* 282 (March): 218–24. <https://doi.org/10.1016/j.snb.2018.11.038>.
- Fayaz, Mohammadreza, Pooya Shariaty, John D. Atkinson, Zaher Hashisho, John H. Phillips, James E. Anderson, and Mark Nichols. 2015a. “Using Microwave Heating To Improve the

## Bibliography

- Desorption Efficiency of High Molecular Weight VOC from Beaded Activated Carbon.” *Environmental Science & Technology* 49 (7): 4536–42. <https://doi.org/10.1021/es505953c>.
- Fayaz, Mohammadreza, Pooya Shariaty, John D Atkinson, Zaher Hashisho, John H Phillips, James E Anderson, and Mark Nichols. 2015b. “Using Microwave Heating To Improve the Desorption Efficiency of High Molecular Weight VOC from Beaded Activated Carbon.” *Environmental Science & Technology* 49 (7): 4536–42. <https://doi.org/10.1021/es505953c>.
- Fayaz, Mohammadreza, Mohammad H. Zarifi, Mohammad Abdolrazzaghi, Pooya Shariaty, Zaher Hashisho, and Mojgan Daneshmand. 2017. “A Novel Technique for Determining the Adsorption Capacity and Breakthrough Time of Adsorbents Using a Noncontact High-Resolution Microwave Resonator Sensor.” *Environmental Science and Technology* 51 (1): 427–35. <https://doi.org/10.1021/acs.est.6b03418>.
- Feng, Aihu, Yang Yu, Le Mi, Yunzhen Cao, Yun Yu, and Lixin Song. 2019. “Structural, Textural and Toluene Adsorption Properties of NH<sub>4</sub>HF<sub>2</sub> and Alkali Modified USY Zeolite.” *Microporous and Mesoporous Materials* 290 (December): 109646. <https://doi.org/10.1016/j.micromeso.2019.109646>.
- Fonseca, B. De, J. Rossignol, I. Bezverkhyy, J. P. Bellat, D. Stuerger, and P. Pribetich. 2014. “VOCs Detection by Microwave Transduction Using Zeolites as Sensitive Material.” *Procedia Engineering* 87 (January): 1019–22. <https://doi.org/10.1016/J.PROENG.2014.11.334>.
- Fuertes, A.B, G. Marbán, and D.M Nevskaia. 2003. “Adsorption of Volatile Organic Compounds by Means of Activated Carbon Fibre-Based Monoliths.” *Carbon* 41 (1): 87–96. [https://doi.org/10.1016/S0008-6223\(02\)00274-9](https://doi.org/10.1016/S0008-6223(02)00274-9).
- Funawatashi, Yuichi, and Tateyuki Suzuki. 2003. “Numerical Analysis of Microwave Heating of a Dielectric.” *Heat Transfer - Asian Research* 32 (3): 227–36. <https://doi.org/10.1002/htj.10087>.

## Bibliography

- Funck, Andreas, and Walter Kaminsky. 2007. "Polypropylene Carbon Nanotube Composites by in Situ Polymerization." *Composites Science and Technology* 67 (5). <https://doi.org/10.1016/j.compscitech.2006.01.034>.
- Funke, Hans H., Andrew M. Argo, Chelsey D. Baertsch, John L. Falconer, and Richard D. Noble. 1996. "Separation of Close-Boiling Hydrocarbons with Silicalite Zeolite Membranes." *Journal of the Chemical Society, Faraday Transactions* 92 (13): 2499. <https://doi.org/10.1039/ft9969202499>.
- Geedipalli, S. S.R., V. Rakesh, and A. K. Datta. 2007. "Modeling the Heating Uniformity Contributed by a Rotating Turntable in Microwave Ovens." *Journal of Food Engineering* 82 (3): 359–68. <https://doi.org/10.1016/j.jfoodeng.2007.02.050>.
- Germain, Jonathan, Frantisek Svec, and Jean M.J. Fréenet. 2008. "Preparation of Size-Selective Nanoporous Polymer Networks of Aromatic Rings: Potential Adsorbents for Hydrogen Storage." *Chemistry of Materials* 20 (22): 7069–76. <https://doi.org/10.1021/cm802157r>.
- Ghafari, Mohsen, and John D. Atkinson. 2018. "Impact of Styrenic Polymer One-Step Hyper-Cross-Linking on Volatile Organic Compound Adsorption and Desorption Performance." *Journal of Hazardous Materials* 351 (June): 117–23. <https://doi.org/10.1016/j.jhazmat.2018.02.051>.
- Ghafari, Mohsen, and John D Atkinson. 2017. "One-Step Hyper-Cross-Linking of Porous Styrenic Polymers Using Dichloroalkane Cross-Linkers to Maintain Hydrophobicity." *Polymer* 116 (May): 278–86. <https://doi.org/10.1016/j.polymer.2017.03.082>.
- Gibson, C., I. Matthews, and A. Samuel. 1988. "Microwave Enhanced Diffusion in Polymeric Materials." *Journal of Microwave Power and Electromagnetic Energy* 23 (1): 17–28. <https://doi.org/10.1080/08327823.1988.11688033>.
- Gupta, Manoj, and Wong Wai Leong Eugene. 2007. *Microwaves and Metals. Microwaves and Metals*. Singapore: John Wiley & Sons (Asia) Pte Ltd. <https://doi.org/10.1002/9780470822746>.

## Bibliography

- Haggenmueller, R., H. H. Gommans, A. G. Rinzler, J. E. Fischer, and K. I. Winey. 2000. "Aligned Single-Wall Carbon Nanotubes in Composites by Melt Processing Methods." *Chemical Physics Letters* 330 (3–4). [https://doi.org/10.1016/S0009-2614\(00\)01013-7](https://doi.org/10.1016/S0009-2614(00)01013-7).
- Han, Zhidong, and Alberto Fina. 2011. "Thermal Conductivity of Carbon Nanotubes and Their Polymer Nanocomposites: A Review." *Progress in Polymer Science* 36 (7): 914–44. <https://doi.org/10.1016/j.progpolymsci.2010.11.004>.
- Hashisho, Zaher, Mark J. Rood, Suhail Barot, and Jennifer Bernhard. 2009. "Role of Functional Groups on the Microwave Attenuation and Electric Resistivity of Activated Carbon Fiber Cloth." *Carbon* 47 (7): 1814–23. <https://doi.org/10.1016/j.carbon.2009.03.006>.
- He, Fuan, Sienting Lau, Helen Laiwa Chan, and Jintu Fan. 2009. "High Dielectric Permittivity and Low Percolation Threshold in Nanocomposites Based on Poly(Vinylidene Fluoride) and Exfoliated Graphite Nanoplates." *Advanced Materials* 21 (6): 710–15. <https://doi.org/10.1002/adma.200801758>.
- Hiura, H., T. W. Ebbesen, K. Tanigaki, and H. Takahashi. 1993. "Raman Studies of Carbon Nanotubes." *Chemical Physics Letters*. [https://doi.org/10.1016/0009-2614\(93\)90040-8](https://doi.org/10.1016/0009-2614(93)90040-8).
- Horikoshi, Satoshi, Robert F. Schifffmann, Jun Fukushima, and Nick Serpone. 2017. *Microwave Chemical and Materials Processing: A Tutorial*. *Microwave Chemical and Materials Processing: A Tutorial*. <https://doi.org/10.1007/978-981-10-6466-1>.
- Horikoshi, Satoshi, and Nick Serpone. 2020. *RF Power Semiconductor Generator Application in Heating and Energy Utilization*. Edited by Satoshi Horikoshi and Nick Serpone. *RF Power Semiconductor Generator Application in Heating and Energy Utilization*. Singapore: Springer Singapore. <https://doi.org/10.1007/978-981-15-3548-2>.
- Huang, Chen-Chia -C, and James R. Fair. 1989. "Parametric Analysis of Thermal Swing Cycles for Multicomponent Adsorption." *AIChE Journal*. <https://doi.org/10.1002/aic.690351011>.

## Bibliography

- Huang, Jing, and S Richard Turner. 2018. "Polymer Reviews Hypercrosslinked Polymers: A Review Hypercrosslinked Polymers: A Review." *Polymer Reviews* 58 (1): 1–41. <https://doi.org/10.1080/15583724.2017.1344703>.
- Huang, Yan Yan, and Eugene M. Terentjev. 2012. "Dispersion of Carbon Nanotubes: Mixing, Sonication, Stabilization, and Composite Properties." *Polymers* 4 (1): 275–95. <https://doi.org/10.3390/polym4010275>.
- Hughes, J. V., and H. L. Armstrong. 1952. "The Dielectric Constant of Dry Air." *Journal of Applied Physics* 23 (5): 501–4. <https://doi.org/10.1063/1.1702240>.
- Hwang, Kye Soon, Dae Ki Choi, Sung Yong Gong, and Sung Yong Cho. 1997. "Adsorption and Thermal Regeneration of Methylene Chloride Vapor on an Activated Carbon Bed." *Chemical Engineering Science* 52 (7): 1111–23. [https://doi.org/10.1016/S0009-2509\(96\)00470-8](https://doi.org/10.1016/S0009-2509(96)00470-8).
- Ismail, H., Pooria Pasbakhsh, M.N. Ahmad Fauzi, and A. Abu Bakar. 2008. "Morphological, Thermal and Tensile Properties of Halloysite Nanotubes Filled Ethylene Propylene Diene Monomer (EPDM) Nanocomposites." *Polymer Testing* 27 (7): 841–50. <https://doi.org/10.1016/j.polymertesting.2008.06.007>.
- Jahandar Lashaki, Masoud, John D. Atkinson, Zaher Hashisho, John H. Phillips, James E. Anderson, and Mark Nichols. 2016. "The Role of Beaded Activated Carbon's Pore Size Distribution on Heel Formation during Cyclic Adsorption/Desorption of Organic Vapors." *Journal of Hazardous Materials* 315 (September): 42–51. <https://doi.org/10.1016/j.jhazmat.2016.04.071>.
- Jahandar Lashaki, Masoud, Mohammadreza Fayaz, Saeid Niknaddaf, and Zaher Hashisho. 2012. "Effect of the Adsorbate Kinetic Diameter on the Accuracy of the Dubinin–Radushkevich Equation for Modeling Adsorption of Organic Vapors on Activated Carbon." *Journal of Hazardous Materials* 241–242 (November): 154–63. <https://doi.org/10.1016/j.jhazmat.2012.09.024>.

## Bibliography

- James, Alex M., Samuel Harding, Thomas Robshaw, Neil Bramall, Mark D. Ogden, and Robert Dawson. 2019. "Selective Environmental Remediation of Strontium and Cesium Using Sulfonated Hyper-Cross-Linked Polymers (SHCPs)." *ACS Applied Materials & Interfaces* 11 (25): 22464–73. <https://doi.org/10.1021/acsami.9b06295>.
- Jang, Chorom, Jin-Kwan Park, Hee-Jo Lee, Gi-Ho Yun, and Jong-Gwan Yook. 2020. "Non-Invasive Fluidic Glucose Detection Based on Dual Microwave Complementary Split Ring Resonators with a Switching Circuit for Environmental Effect Elimination." *IEEE Sensors Journal* 20 (15): 8520–27.
- Jayalakshmi, C. G., A. Inamdar, A. Anand, and B. Kandasubramanian. 2018. "Polymer Matrix Composites as Broadband Radar Absorbing Structures for Stealth Aircrafts." *Journal of Applied Polymer Science*, December, 47241. <https://doi.org/10.1002/app.47241>.
- Jia, Guo-Zhu, Qian Jie, and Wang Feng. 2015. "Hydrogen Bond Analysis in Alcohol (1-Propanol, 2-Propanol and Glycerol)-DMF Mixtures Based on Dielectric Spectroscopy." *Journal of Molecular Structure* 1100 (November): 354–58. <https://doi.org/10.1016/j.molstruc.2015.07.065>.
- Jogdand, A.P., and Dr. P.L. Kadam. 2014. "Dielectric Behavior of Acetonitrile + Methanol Binary Mixtures at Microwave Frequency." *IOSR Journal of Applied Physics* 6 (1): 14–22. <https://doi.org/10.9790/4861-06121422>.
- Jones, D.A., T.P. Lelyveld, S.D. Mavrofidis, S.W. Kingman, and N.J. Miles. 2002. "Microwave Heating Applications in Environmental Engineering—a Review." *Resources, Conservation and Recycling* 34 (2): 75–90. [https://doi.org/10.1016/S0921-3449\(01\)00088-X](https://doi.org/10.1016/S0921-3449(01)00088-X).
- Justh, Nóra, Barbara Berke, Krisztina László, and Imre Miklós Szilágyi. 2018. "Thermal Analysis of the Improved Hummers' Synthesis of Graphene Oxide." *Journal of Thermal Analysis and Calorimetry* 131 (3): 2267–72. <https://doi.org/10.1007/s10973-017-6697-2>.

## Bibliography

- Kazemi, Nazli, Mohammad Abdolrazzaghi, and Petr Musilek. 2021. "Comparative Analysis of Machine Learning Techniques for Temperature Compensation in Microwave Sensors." *IEEE Transactions on Microwave Theory and Techniques*.
- Kazemi, Nazli, Mohammad Abdolrazzaghi, Petr Musilek, and Mojgan Daneshmand. 2020. "A Temperature-Compensated High-Resolution Microwave Sensor Using Artificial Neural Network." *IEEE Microwave and Wireless Components Letters*.
- Kazemi, Nazli, Calvin Schofield, and Petr Musilek. 2021. "A High-Resolution Reflective Microwave Planar Sensor for Sensing of Vanadium Electrolyte." *Sensors* 21 (11): 3759.
- Khan, Faisal I., and Alope Kr. Ghoshal. 2000. "Removal of Volatile Organic Compounds from Polluted Air." *Journal of Loss Prevention in the Process Industries*.  
[https://doi.org/10.1016/S0950-4230\(00\)00007-3](https://doi.org/10.1016/S0950-4230(00)00007-3).
- Kim, Jong Hwa, Sang Jin Lee, Min Bae Kim, Jang Jae Lee, and Chang Ha Lee. 2007. "Sorption Equilibrium and Thermal Regeneration of Acetone and Toluene Vapors on an Activated Carbon." *Industrial and Engineering Chemistry Research*.  
<https://doi.org/10.1021/ie0609362>.
- Kim, Ki-Joong, and Ho-Geun Ahn. 2012. "The Effect of Pore Structure of Zeolite on the Adsorption of VOCs and Their Desorption Properties by Microwave Heating." *Microporous and Mesoporous Materials* 152 (April): 78–83.  
<https://doi.org/10.1016/j.micromeso.2011.11.051>.
- Kim, N Y, R Dhakal, K K Adhikari, E S Kim, and C Wang. 2015. "A Reusable Robust Radio Frequency Biosensor Using Microwave Resonator by Integrated Passive Device Technology for Quantitative Detection of Glucose Level." *Biosensors and Bioelectronics* 67: 687–93.
- Kim, Seong-Ick, Takashi Aida, and Hiroo Niiyama. 2005. "Binary Adsorption of Very Low Concentration Ethylene and Water Vapor on Mordenites and Desorption by Microwave

## Bibliography

- Heating.” *Separation and Purification Technology* 45 (3): 174–82. <https://doi.org/10.1016/j.seppur.2005.03.006>.
- Kirkby, N. 1988. “Gas Separation by Adsorption Processes.” *Gas Separation & Purification* 2 (1): 41. [https://doi.org/10.1016/0950-4214\(88\)80042-2](https://doi.org/10.1016/0950-4214(88)80042-2).
- Komarov, V., S. Wang, and J. Tang. 2005. “Permittivity and Measurements.” In *Encyclopedia of RF and Microwave Engineering*. Hoboken, NJ, USA: John Wiley & Sons, Inc. <https://doi.org/10.1002/0471654507.eme308>.
- Kostas, Emily T., Daniel Beneroso, and John P. Robinson. 2017. “The Application of Microwave Heating in Bioenergy: A Review on the Microwave Pre-Treatment and Upgrading Technologies for Biomass.” *Renewable and Sustainable Energy Reviews*. Elsevier Ltd. <https://doi.org/10.1016/j.rser.2017.03.135>.
- Kosuge, Katsunori, Shiori Kubo, Nobuyuki Kikukawa, and Makoto Takemori. 2007. “Effect of Pore Structure in Mesoporous Silicas on VOC Dynamic Adsorption/Desorption Performance.” *Langmuir*. <https://doi.org/10.1021/la062616t>.
- Koyuncu, Filiz, Fuat Güzel, and Hasan Saygılı. 2018. “Role of Optimization Parameters in the Production of Nanoporous Carbon from Mandarin Shells by Microwave-Assisted Chemical Activation and Utilization as Dye Adsorbent.” *Advanced Powder Technology* 29 (9): 2108–18. <https://doi.org/10.1016/j.apt.2018.05.019>.
- Kraus, Markus, Ulf Trommler, Frank Holzer, Frank Dieter Kopinke, and Ulf Roland. 2018. “Competing Adsorption of Toluene and Water on Various Zeolites.” *Chemical Engineering Journal* 351. <https://doi.org/10.1016/j.cej.2018.06.128>.
- Krishnamoorthy, Karthikeyan, Murugan Veerapandian, Kyusik Yun, and S.-J. Kim. 2013. “The Chemical and Structural Analysis of Graphene Oxide with Different Degrees of Oxidation.” *Carbon* 53 (March): 38–49. <https://doi.org/10.1016/j.carbon.2012.10.013>.

## Bibliography

- Kruželák, Ján, Andrea Kvasničáková, Klaudia Hložeková, and Ivan Hudec. 2021. "Progress in Polymers and Polymer Composites Used as Efficient Materials for EMI Shielding." *Nanoscale Advances*. Royal Society of Chemistry. <https://doi.org/10.1039/d0na00760a>.
- Kuila, Tapas, Saswata Bose, Chang Eui Hong, Md Elias Uddin, Partha Khanra, Nam Hoon Kim, and Joong Hee Lee. 2011. "Preparation of Functionalized Graphene/Linear Low Density Polyethylene Composites by a Solution Mixing Method." *Carbon*. <https://doi.org/10.1016/j.carbon.2010.10.031>.
- Kulkarni, Sunil, and Jayant Kaware. 2014. "Regeneration and Recovery in Adsorption- a Review." *International Journal of Innovative Science, Engineering & Technology(IJISSET)* 1 (8).
- Kutluay, Sinan, and Farabi Temel. 2021. "Silica Gel Based New Adsorbent Having Enhanced VOC Dynamic Adsorption/Desorption Performance." *Colloids and Surfaces A: Physicochemical and Engineering Aspects* 609. <https://doi.org/10.1016/j.colsurfa.2020.125848>.
- Lai, Cui, Zhihong Wang, Lei Qin, Yukui Fu, Bisheng Li, Mingming Zhang, Shiyu Liu, et al. 2021. "Metal-Organic Frameworks as Burgeoning Materials for the Capture and Sensing of Indoor VOCs and Radon Gases." *Coordination Chemistry Reviews* 427 (January): 213565. <https://doi.org/10.1016/j.ccr.2020.213565>.
- Lashaki, Masoud Jahandar, Mohammadreza Fayaz, Haiyan (Helena) Wang, Zaher Hashisho, John H. Philips, James E. Anderson, and Mark Nichols. 2012a. "Effect of Adsorption and Regeneration Temperature on Irreversible Adsorption of Organic Vapors on Beaded Activated Carbon." *Environmental Science & Technology* 46 (7): 4083–90. <https://doi.org/10.1021/es3000195>.
- Lashaki, Masoud Jahandar, Mohammadreza Fayaz, Haiyan (Helena) Wang, Zaher Hashisho, John H Philips, James E Anderson, and Mark Nichols. 2012b. "Effect of Adsorption and Regeneration Temperature on Irreversible Adsorption of Organic Vapors on Beaded

## Bibliography

- Activated Carbon.” *Environmental Science & Technology* 46 (7): 4083–90. <https://doi.org/10.1021/es3000195>.
- Lee, Dong-Geun, Jong-Hwa Kim, and Chang-Ha Lee. 2011. “Adsorption and Thermal Regeneration of Acetone and Toluene Vapors in Dealuminated Y-Zeolite Bed.” *Separation and Purification Technology* 77 (3): 312–24. <https://doi.org/10.1016/j.seppur.2010.12.022>.
- Legras, Benoit, Isabelle Polaert, Lionel Estel, and Michel Thomas. 2011. “Mechanisms Responsible for Dielectric Properties of Various Faujasites and Linde Type A Zeolites in the Microwave Frequency Range.” *The Journal of Physical Chemistry C* 115 (7): 3090–98. <https://doi.org/10.1021/jp111423z>.
- Leng, Chi Cheng, and Neville G. Pinto. 1996. “An Investigation of the Mechanisms of Chemical Regeneration of Activated Carbon.” *Industrial and Engineering Chemistry Research* 35 (6). <https://doi.org/10.1021/ie950576a>.
- Levchik, Galina F., Kun Si, Sergei V. Levchik, G. Camino, and Charles A. Wilkie. 1999. “Correlation between Cross-Linking and Thermal Stability: Cross-Linked Polystyrenes and Polymethacrylates.” *Polymer Degradation and Stability*. [https://doi.org/10.1016/S0141-3910\(99\)00028-2](https://doi.org/10.1016/S0141-3910(99)00028-2).
- Li, Junfei, Ming Gao, Yudong Zheng, Yueping Guan, and Deqi Yi. 2020. “Effects of Low-Load Boron/Silicon-Based Graphene Oxide on Combustion and Thermal Degradation of Flame-Retardant Unsaturated Polyester Resin.” *Macromolecular Materials and Engineering* 305 (12): 2000454. <https://doi.org/10.1002/mame.202000454>.
- Li, Mi, Xingyi Huang, Chao Wu, Haiping Xu, Pingkai Jiang, and Toshikatsu Tanaka. 2012. “Fabrication of Two-Dimensional Hybrid Sheets by Decorating Insulating PANI on Reduced Graphene Oxide for Polymer Nanocomposites with Low Dielectric Loss and High Dielectric Constant.” *Journal of Materials Chemistry* 22 (44). <https://doi.org/10.1039/c2jm34683d>.

## Bibliography

- Li, Xiuquan, Li Zhang, Zhongqing Yang, Peng Wang, Yunfei Yan, and Jingyu Ran. 2020. “Adsorption Materials for Volatile Organic Compounds (VOCs) and the Key Factors for VOCs Adsorption Process: A Review.” *Separation and Purification Technology* 235. <https://doi.org/10.1016/j.seppur.2019.116213>.
- Lin, Guo, Chenhui Liu, Libo Zhang, Tu Hu, Jinhui Peng, Jing Li, and Shixing Wang. 2017. “High Temperature Dielectric Properties of Spent Adsorbent with Zinc Sulfate by Cavity Perturbation Technique.” *Journal of Hazardous Materials*. <https://doi.org/10.1016/j.jhazmat.2017.02.010>.
- Long, Chao, Ying Li, Weihua Yu, and Aimin Li. 2012a. “Adsorption Characteristics of Water Vapor on the Hypercrosslinked Polymeric Adsorbent.” *Chemical Engineering Journal*. <https://doi.org/10.1016/j.cej.2011.11.019>.
- . 2012b. “Removal of Benzene and Methyl Ethyl Ketone Vapor: Comparison of Hypercrosslinked Polymeric Adsorbent with Activated Carbon.” *Journal of Hazardous Materials* 203–204 (February): 251–56. <https://doi.org/10.1016/j.jhazmat.2011.12.010>.
- Luo, Juhua, Pan Shen, Wei Yao, Cuifeng Jiang, and Jianguang Xu. 2016. “Synthesis, Characterization, and Microwave Absorption Properties of Reduced Graphene Oxide/Strontium Ferrite/Polyaniline Nanocomposites.” *Nanoscale Research Letters* 11 (1): 1–14. <https://doi.org/10.1186/s11671-016-1340-x>.
- Lv, Yuting, Jing Sun, Guanqun Yu, Wenlong Wang, Zhanlong Song, Xiqiang Zhao, and Yanpeng Mao. 2020a. “Hydrophobic Design of Adsorbent for VOC Removal in Humid Environment and Quick Regeneration by Microwave.” *Microporous and Mesoporous Materials* 294: 109869. <https://doi.org/10.1016/j.micromeso.2019.109869>.
- . 2020b. “Hydrophobic Design of Adsorbent for VOC Removal in Humid Environment and Quick Regeneration by Microwave.” *Microporous and Mesoporous Materials* 294 (March): 109869. <https://doi.org/10.1016/j.micromeso.2019.109869>.

## Bibliography

- Ma, Feng Ji, Shu Xia Liu, Da Dong Liang, Guo Jian Ren, Feng Wei, Ya Guang Chen, and Zhong Min Su. 2011. "Adsorption of Volatile Organic Compounds in Porous Metal-Organic Frameworks Functionalized by Polyoxometalates." *Journal of Solid State Chemistry*. <https://doi.org/10.1016/j.jssc.2011.09.002>.
- Ma, Liang, Mengya He, Pengbo Fu, Xia Jiang, Wenjie Lv, Yuan Huang, Yi Liu, and Hualin Wang. 2020. "Adsorption of Volatile Organic Compounds on Modified Spherical Activated Carbon in a New Cyclonic Fluidized Bed." *Separation and Purification Technology*. <https://doi.org/10.1016/j.seppur.2019.116146>.
- Ma, Peng Cheng, Naveed A. Siddiqui, Gad Marom, and Jang Kyo Kim. 2010. "Dispersion and Functionalization of Carbon Nanotubes for Polymer-Based Nanocomposites: A Review." *Composites Part A: Applied Science and Manufacturing*. Elsevier Ltd. <https://doi.org/10.1016/j.compositesa.2010.07.003>.
- Macintyre, Fiona S., and David C. Sherrington. 2004. "Control of Porous Morphology in Suspension Polymerized Poly(Divinylbenzene) Resins Using Oligomeric Porogens." *Macromolecules* 37 (20): 7628–36. <https://doi.org/10.1021/ma0491053>.
- Maitlo, Hubdar Ali, Ki-Hyun Kim, Azmatullah Khan, Jan E. Szulejko, Jo Chun Kim, Hee Nam Song, and Wha-Seung Ahn. 2019. "Competitive Adsorption of Gaseous Aromatic Hydrocarbons in a Binary Mixture on Nanoporous Covalent Organic Polymers at Various Partial Pressures." *Environmental Research* 173: 1–11. <https://doi.org/10.1016/j.envres.2019.03.028>.
- Makeiff, Darren A., and Trisha Huber. 2006. "Microwave Absorption by Polyaniline-Carbon Nanotube Composites." *Synthetic Metals* 156 (7–8). <https://doi.org/10.1016/j.synthmet.2005.05.019>.
- Manickavasagan, A., D. S. Jayas, and N. D.G. White. 2006. "Non-Uniformity of Surface Temperatures of Grain after Microwave Treatment in an Industrial Microwave Dryer." *Drying Technology* 24 (12): 1559–67. <https://doi.org/10.1080/07373930601030796>.

## Bibliography

- Mao, Haiyan, Dingguo Zhou, Zaher Hashisho, Sunguo Wang, Heng Chen, and Haiyan Helena Wang. 2015. "Constant Power and Constant Temperature Microwave Regeneration of Toluene and Acetone Loaded on Microporous Activated Carbon from Agricultural Residue." *Journal of Industrial and Engineering Chemistry* 21 (January): 516–25. <https://doi.org/10.1016/j.jiec.2014.03.014>.
- Marcano, Daniela C., Dmitry V. Kosynkin, Jacob M. Berlin, Alexander Sinitskii, Zhengzong Sun, Alexander Slesarev, Lawrence B. Alemany, Wei Lu, and James M. Tour. 2010. "Improved Synthesis of Graphene Oxide." *ACS Nano* 4 (8): 4806–14. <https://doi.org/10.1021/nn1006368>.
- Marsland, T. P., and S. Evans. 1987. "Dielectric Measurements with an Open-Ended Coaxial Probe." *IEE Proceedings H: Microwaves, Antennas and Propagation* 134 (4). <https://doi.org/10.1049/ip-h-2.1987.0068>.
- Meaney, Paul M, Colleen J Fox, Shireen D Geimer, and Keith D Paulsen. 2017. "Electrical Characterization of Glycerin: Water Mixtures: Implications for Use as a Coupling Medium in Microwave Tomography." *IEEE Transactions on Microwave Theory and Techniques* 65 (5): 1471–78.
- Meier, Matthias, Michael Turner, Steven Vallee, William C. Conner, Kyu Ho Lee, and Karl S. Yngvesson. 2009. "Microwave Regeneration of Zeolites in a 1 Meter Column." *AICHE Journal* 55 (7): 1906–13. <https://doi.org/10.1002/aic.11793>.
- Méndez-Bermúdez, José G., Hector Dominguez, László Pusztai, Sándor Guba, Barnabás Horváth, and István Szalai. 2016. "Composition and Temperature Dependence of the Dielectric Constant of 1-Propanol/Water Mixtures: Experiment and Molecular Dynamics Simulations." *Journal of Molecular Liquids* 219. <https://doi.org/10.1016/j.molliq.2016.02.053>.
- Meng, Qing Bo, Go-Su Yang, and Youn-Sik Lee. 2013. "Preparation of Highly Porous Hypercrosslinked Polystyrene Adsorbents: Effects of Hydrophilicity on the Adsorption

## Bibliography

- and Microwave-Assisted Desorption Behavior toward Benzene.” *Microporous and Mesoporous Materials* 181 (November): 222–27.  
<https://doi.org/10.1016/j.micromeso.2013.07.027>.
- . 2014. “Sulfonation of a Hypercrosslinked Polymer Adsorbent for Microwave-Assisted Desorption of Adsorbed Benzene.” *Journal of Industrial and Engineering Chemistry* 20 (4): 2484–89. <https://doi.org/10.1016/j.jiec.2013.10.030>.
- Metaxas, A.C., and R.J. Meredith. 1989. “Book Review: Industrial Microwave Heating.” *Journal of Microwave Power and Electromagnetic Energy* 24 (2): 108–108.  
<https://doi.org/10.1080/08327823.1989.11688082>.
- Micheli, Davide, Antonio Vricella, Roberto Pastore, and Mario Marchetti. 2014. “Synthesis and Electromagnetic Characterization of Frequency Selective Radar Absorbing Materials Using Carbon Nanopowders.” *Carbon* 77 (October): 756–74.  
<https://doi.org/10.1016/j.carbon.2014.05.080>.
- Min, Dandan, Wancheng Zhou, Yuchang Qing, Fa Luo, and Dongmei Zhu. 2017. “Enhanced Microwave Absorption Properties of Oriented Carbonyl Iron/Carbon Black Composite Induced by Shear Force.” *Journal of Electronic Materials* 46 (8): 4903–11.  
<https://doi.org/10.1007/s11664-017-5493-x>.
- Mishra, Radha Raman, and Apurbba Kumar Sharma. 2016. “Microwave–Material Interaction Phenomena: Heating Mechanisms, Challenges and Opportunities in Material Processing.” *Composites Part A: Applied Science and Manufacturing* 81 (February): 78–97.  
<https://doi.org/10.1016/j.compositesa.2015.10.035>.
- Mittal, Garima, Vivek Dhand, Kyong Yop Rhee, Soo-Jin Park, and Wi Ro Lee. 2015. “A Review on Carbon Nanotubes and Graphene as Fillers in Reinforced Polymer Nanocomposites.” *Journal of Industrial and Engineering Chemistry* 21 (January): 11–25.  
<https://doi.org/10.1016/j.jiec.2014.03.022>.

## Bibliography

- Moghadas, Hamid, and Vivian K Mushahwar. 2018. "Passive Microwave Resonant Sensor for Detection of Deep Tissue Injuries." *Sensors and Actuators B: Chemical* 277: 69–77.
- Moldoveanu, Serban C., and Victor David. 2013. "Mobile Phases and Their Properties." In *Essentials in Modern HPLC Separations*. <https://doi.org/10.1016/b978-0-12-385013-3.00007-0>.
- Mondal, Avijit, Dinesh Agrawal, and Anish Upadhyaya. 2009. "Microwave Heating of Pure Copper Powder with Varying Particle Size and Porosity." *Journal of Microwave Power and Electromagnetic Energy* 43 (1). <https://doi.org/10.1080/08327823.2008.11688599>.
- Morales Mendoza, N, S Goyanes, C Chilotte, V Bekeris, G Rubiolo, and R Candal. 2012. "Magnetic Binary Nanofillers." *Physica B: Condensed Matter* 407 (16): 3203–5. <https://doi.org/10.1016/j.physb.2011.12.065>.
- Moulart, Alexandre, Courtney Marrett, and Jonathan Colton. 2004. "Polymeric Composites for Use in Electronic and Microwave Devices." *Polymer Engineering and Science* 44 (3): 588–97. <https://doi.org/10.1002/pen.20053>.
- Mu, Bin, Paul M. Schoenecker, and Krista S. Walton. 2010. "Gas Adsorption Study on Mesoporous Metal–Organic Framework UMCM-1." *The Journal of Physical Chemistry C* 114 (14): 6464–71. <https://doi.org/10.1021/jp906417z>.
- Neimark, Alexander V, Yangzheng Lin, Peter I Ravikovitch, and Matthias Thommes. 2009. "Quenched Solid Density Functional Theory and Pore Size Analysis of Micro-Mesoporous Carbons." *Carbon* 47 (7): 1617–28. <https://doi.org/10.1016/j.carbon.2009.01.050>.
- Nelson, Ralph. D, David R. Lide, and Arthur A. Maryott. 1967. "Selected Values of Electric Dipole Moments for Molecules in the Gas Phase." In *National Standard Reference Series - National Bureau of Standards 10*, 1–49. United States Department of Commerce.
- Nigar, H., N. Navascués, O. de la Iglesia, R. Mallada, and J. Santamaría. 2015. "Removal of VOCs at Trace Concentration Levels from Humid Air by Microwave Swing Adsorption, Kinetics

## Bibliography

- and Proper Sorbent Selection.” *Separation and Purification Technology* 151 (September): 193–200. <https://doi.org/10.1016/j.seppur.2015.07.019>.
- Nikfar, Nafiseh, Yasser Zare, and Kyong Yop Rhee. 2018. “Dependence of Mechanical Performances of Polymer/Carbon Nanotubes Nanocomposites on Percolation Threshold.” *Physica B: Condensed Matter* 533 (March): 69–75. <https://doi.org/10.1016/j.physb.2018.01.008>.
- Niknaddaf, Saeid, John D. Atkinson, Pooya Shariaty, Masoud Jahandar Lashaki, Zaher Hashisho, John H. Phillips, James E. Anderson, and Mark Nichols. 2016. “Heel Formation during Volatile Organic Compound Desorption from Activated Carbon Fiber Cloth.” *Carbon* 96 (January): 131–38. <https://doi.org/10.1016/j.carbon.2015.09.049>.
- Norkhairunnisa, M., A. Azizan, M. Mariatti, H. Ismail, and LC Sim. 2012. “Thermal Stability and Electrical Behavior of Polydimethylsiloxane Nanocomposites with Carbon Nanotubes and Carbon Black Fillers.” *Journal of Composite Materials* 46 (8): 903–10. <https://doi.org/10.1177/0021998311412985>.
- Oh, Jung-Hoon, Kyung-Sub Oh, Chun-Gon Kim, and Chang-Sun Hong. 2004. “Design of Radar Absorbing Structures Using Glass/Epoxy Composite Containing Carbon Black in X-Band Frequency Ranges.” *Composites Part B: Engineering* 35 (1): 49–56. <https://doi.org/10.1016/j.compositesb.2003.08.011>.
- Ondon, B. S., B. Sun, Z. Y. Yan, X. M. Zhu, and H. Liu. 2014. “Effect of Microwave Heating on the Regeneration of Modified Activated Carbons Saturated with Phenol.” *Applied Water Science* 4 (4): 333–39. <https://doi.org/10.1007/s13201-013-0147-5>.
- Penner, N. A., P. N. Nesterenko, M. M. Hyin, M. P. Tsyurupa, and V. A. Davankov. 1999. “Investigation of the Properties of Hypercrosslinked Polystyrene as a Stationary Phase for High-Performance Liquid Chromatography.” *Chromatographia* 50 (9–10): 611–20. <https://doi.org/10.1007/BF02493669>.

## Bibliography

- Peyravi, Arman, Peyman Keshavarz, and Darioush Mowla. 2015. "Experimental Investigation on the Absorption Enhancement of CO<sub>2</sub> by Various Nanofluids in Hollow Fiber Membrane Contactors." *Energy and Fuels*. <https://doi.org/10.1021/acs.energyfuels.5b01956>.
- Pezolt, Daniel J., Scott J. Collick, Herbert A. Johnson, and Lanny A. Robbins. 1997. "Pressure Swing Adsorption for VOC Recovery at Gasoline Loading Terminals." *Environmental Progress* 16 (1): 16–19. <https://doi.org/10.1002/ep.3300160115>.
- Polaert, Isabelle, Lionel Estel, Raphaël Huyghe, and Michel Thomas. 2010. "Adsorbents Regeneration under Microwave Irradiation for Dehydration and Volatile Organic Compounds Gas Treatment." *Chemical Engineering Journal* 162: 941–48. <https://doi.org/10.1016/j.cej.2010.06.047>.
- Pourjavid, Mohammad Reza, Masoud Arabieh, Seyed Reza Yousefi, Mohammad Reza Jamali, Mohammad Rezaee, Majid Haji Hosseini, and Ali Akbari Sehat. 2015. "Study on Column SPE with Synthesized Graphene Oxide and FAAS for Determination of Trace Amount of Co(II) and Ni(II) Ions in Real Samples." *Materials Science and Engineering: C* 47 (February): 114–22. <https://doi.org/10.1016/j.msec.2014.11.028>.
- Pozar, David M. 2012. *Microwave Engineering, 4th Edition*. John Wiley & Sons, Inc.
- Price, David W., and Philip S. Schmidt. 1998a. "VOC Recovery through Microwave Regeneration of Adsorbents: Process Design Studies." *Journal of the Air & Waste Management Association* 48 (12): 1135–45. <https://doi.org/10.1080/10473289.1998.10463758>.
- Price, David W., and Philip S. Schmidt. 1998b. "VOC Recovery through Microwave Regeneration of Adsorbents: Process Design Studies." *Journal of the Air & Waste Management Association* 48 (12): 1135–45. <https://doi.org/10.1080/10473289.1998.10463758>.
- Qin, F., and C. Brosseau. 2012. "A Review and Analysis of Microwave Absorption in Polymer Composites Filled with Carbonaceous Particles." *Journal of Applied Physics* 111 (6): 061301. <https://doi.org/10.1063/1.3688435>.

## Bibliography

- Qing, Yuchang, Xuan Wang, Yingying Zhou, Zhibin Huang, Fa Luo, and Wancheng Zhou. 2014. "Enhanced Microwave Absorption of Multi-Walled Carbon Nanotubes/Epoxy Composites Incorporated with Ceramic Particles." *Composites Science and Technology* 102 (October): 161–68. <https://doi.org/10.1016/j.compscitech.2014.08.006>.
- Raganati, Federica, Riccardo Chirone, and Paola Ammendola. 2020. "CO<sub>2</sub> Capture by Temperature Swing Adsorption: Working Capacity As Affected by Temperature and CO<sub>2</sub> Partial Pressure." *Industrial & Engineering Chemistry Research* 59 (8): 3593–3605. <https://doi.org/10.1021/acs.iecr.9b04901>.
- Ramesh, K., K. Sammi Reddy, I. Rashmi, and A. K. Biswas. 2014. "Nanostructured Natural Zeolite: Surface Area, Meso-Pore and Volume Distribution, and Morphology." *Communications in Soil Science and Plant Analysis* 45 (22). <https://doi.org/10.1080/00103624.2014.956934>.
- Ramezanipour Penchah, Hamid, Hossein Ghanadzadeh Gilani, and Ahad Ghaemi. 2020. "CO<sub>2</sub>, N<sub>2</sub>, and H<sub>2</sub> Adsorption by Hyper-Cross-Linked Polymers and Their Selectivity Evaluation by Gas-Solid Equilibrium." *Journal of Chemical and Engineering Data* 65 (10): 4905–13. <https://doi.org/10.1021/acs.jced.0c00541>.
- Reichardt, Christian, and Thomas Welton. 2010. *Solvents and Solvent Effects in Organic Chemistry. Solvents and Solvent Effects in Organic Chemistry: Fourth Edition*. Weinheim, Germany: Wiley-VCH Verlag GmbH & Co. KGaA. <https://doi.org/10.1002/9783527632220>.
- Renukappa, N. M., Siddaramaiah, R. D. Sudhaker Samuel, J. Sundara Rajan, and Joong Hee Lee. 2009. "Dielectric Properties of Carbon Black: SBR Composites." *Journal of Materials Science: Materials in Electronics* 20 (7). <https://doi.org/10.1007/s10854-008-9780-4>.
- Richard, Cyrille. 2003. "Supramolecular Self-Assembly of Lipid Derivatives on Carbon Nanotubes." *Science* 300 (5620): 775–78. <https://doi.org/10.1126/science.1080848>.

## Bibliography

- Roussy, Georges, Andre Zoulalian, Martine Charreyre, and Jean Marie Thiebaut. 1984. "How Microwaves Dehydrate Zeolites." *The Journal of Physical Chemistry* 88 (23): 5702–8. <https://doi.org/10.1021/j150667a049>.
- RUHL, M. 1993. "Recover VOCs via Adsorption on Activated Carbon." *Chemical Engineering Progress* 89 (7).
- Saini, Parveen, and Manju Aror. 2012. "Microwave Absorption and EMI Shielding Behavior of Nanocomposites Based on Intrinsically Conducting Polymers, Graphene and Carbon Nanotubes." In *New Polymers for Special Applications*. InTech. <https://doi.org/10.5772/48779>.
- Saleem, Hareema, Mobeen Haneef, and Hina Y Abbasi. 2018. "Synthesis Route of Reduced Graphene Oxide via Thermal Reduction of Chemically Exfoliated Graphene Oxide." *Materials Chemistry and Physics* 204 (January): 1–7. <https://doi.org/10.1016/j.matchemphys.2017.10.020>.
- Salim, Ahmed, Aqeel Hussain Naqvi, Anh Duc Pham, and Sungjoon Lim. 2020. "Complementary Split-Ring Resonator (CSRR)-Loaded Sensor Array to Detect Multiple Cracks: Shapes, Sizes, and Positions on Metallic Surface." *IEEE Access* 8: 151804–16.
- Salvador, Francisco, Nicolas Martin-Sanchez, Ruth Sanchez-Hernandez, Maria Jesus Sanchez-Montero, and Carmen Izquierdo. 2015. "Regeneration of Carbonaceous Adsorbents. Part I: Thermal Regeneration." *Microporous and Mesoporous Materials* 202 (January): 259–76. <https://doi.org/10.1016/j.micromeso.2014.02.045>.
- Schork, Joan M., and James R. Fair. 1988. "Parametric Analysis of Thermal Regeneration of Adsorption Beds." *Industrial & Engineering Chemistry Research* 27 (3): 457–69. <https://doi.org/10.1021/ie00075a016>.
- Shao, Min, Sihua Lu, Ying Liu, Xin Xie, Chichung Chang, Shan Huang, and Zhongmin Chen. 2009. "Volatile Organic Compounds Measured in Summer in Beijing and Their Role in

## Bibliography

- Ground-level Ozone Formation.” *Journal of Geophysical Research* 114 (7): D00G06. <https://doi.org/10.1029/2008JD010863>.
- Shariaty, Pooya, Masoud Jahandar Lashaki, Zaher Hashisho, James Sawada, Steven Kuznicki, and Ron Hutcheon. 2017. “Effect of ETS-10 Ion Exchange on Its Dielectric Properties and Adsorption/Microwave Regeneration.” *Separation and Purification Technology* 179 (May): 420–27. <https://doi.org/10.1016/j.seppur.2017.02.016>.
- Shen, Xiang-Zhong, Shan-Mei Xie, Jun Guo, and Zhi-Cheng Liu. 2009. “Microwave Absorbing Properties of Ternary Linear Low-Density Polyethylene/Carbonyl Iron Powder/Carbon Black Composites.” *Journal of Applied Polymer Science* 114 (6): 3434–39. <https://doi.org/10.1002/app.30666>.
- Shi, Qiuyi, Xinyu Yang, Liuyan Wu, Huijuan Liu, Jian Zhang, Feng Zhang, and Chao Long. 2018. “Binary Adsorption Equilibrium and Breakthrough of Toluene and Cyclohexane on Macroporous and Hypercrosslinked Polymeric Resins.” *Microporous and Mesoporous Materials* 271 (November): 73–82. <https://doi.org/10.1016/j.micromeso.2018.05.034>.
- Shi, Sui-Lin, Ling-Zhen Zhang, and Jun-Shou Li. 2009. “Electrical and Dielectric Properties of Multiwall Carbon Nanotube/Polyaniline Composites.” *Journal of Polymer Research* 16 (4): 395–99. <https://doi.org/10.1007/s10965-008-9241-z>.
- Singh, Sandeep Kumar, Mohammad Jaleel Akhtar, and Kamal K. Kar. 2018. “Hierarchical Carbon Nanotube-Coated Carbon Fiber: Ultra Lightweight, Thin, and Highly Efficient Microwave Absorber.” *ACS Applied Materials and Interfaces* 10 (29). <https://doi.org/10.1021/acsami.8b06673>.
- Srivastava, Anjali, and Dipanjali Mazumdar. 2011. “Monitoring and Reporting VOCs in Ambient Air.” In *Air Quality Monitoring, Assessment and Management*. InTech. <https://doi.org/10.5772/16774>.
- “Steam Regeneration of Adsorbents: An Experimental and Technical Review.” 2013. *Chemical Science Transactions* 2 (4). <https://doi.org/10.7598/cst2013.545>.

## Bibliography

- Stobinski, L., B. Lesiak, A. Malolepszy, M. Mazurkiewicz, B. Mierzwa, J. Zemek, P. Jiricek, and I. Bieloshapka. 2014. "Graphene Oxide and Reduced Graphene Oxide Studied by the XRD, TEM and Electron Spectroscopy Methods." *Journal of Electron Spectroscopy and Related Phenomena* 195 (August): 145–54. <https://doi.org/10.1016/j.elspec.2014.07.003>.
- Sudan, Sylvain, Andrzej Gładysiak, Bardiya Valizadeh, Jung-Hoon Lee, and Kyriakos C. Stylianou. 2020. "Sustainable Capture of Aromatic Volatile Organic Compounds by a Pyrene-Based Metal–Organic Framework under Humid Conditions." *Inorganic Chemistry* 59 (13): 9029–36. <https://doi.org/10.1021/acs.inorgchem.0c00883>.
- Sui, Hong, Hangxi Liu, Ping An, Lin He, Xingang Li, and Shan Cong. 2017. "Application of Silica Gel in Removing High Concentrations Toluene Vapor by Adsorption and Desorption Process." *Journal of the Taiwan Institute of Chemical Engineers*. <https://doi.org/10.1016/j.jtice.2017.02.019>.
- Sun, Genban, Bingxiang Dong, Minhua Cao, Bingqing Wei, and Changwen Hu. 2011. "Hierarchical Dendrite-Like Magnetic Materials of Fe<sub>3</sub>O<sub>4</sub>,  $\gamma$ -Fe<sub>2</sub>O<sub>3</sub>, and Fe with High Performance of Microwave Absorption." *Chemistry of Materials* 23 (6): 1587–93. <https://doi.org/10.1021/cm103441u>.
- Sun, Zhenyu, Valeria Nicolosi, David Rickard, Shane D. Bergin, Damian Aherne, and Jonathan N. Coleman. 2008. "Quantitative Evaluation of Surfactant-Stabilized Single-Walled Carbon Nanotubes: Dispersion Quality and Its Correlation with Zeta Potential." *The Journal of Physical Chemistry C* 112 (29): 10692–99. <https://doi.org/10.1021/jp8021634>.
- Taguchi, Akira, and Ferdi Schüth. 2005. "Ordered Mesoporous Materials in Catalysis." *Microporous and Mesoporous Materials*. <https://doi.org/10.1016/j.micromeso.2004.06.030>.
- Tang, Jin, Song Bi, Xin Wang, Gen liang Hou, Xun jia Su, Chao hui Liu, Yang yang Lin, and Hao Li. 2019. "Excellent Microwave Absorption of Carbon Black/Reduced Graphene Oxide

## Bibliography

- Composite with Low Loading.” *Journal of Materials Science* 54 (22): 13990–1. <https://doi.org/10.1007/s10853-019-03902-0>.
- Thakur, Vijay Kumar, and Michael R. Kessler. 2015. “Self-Healing Polymer Nanocomposite Materials: A Review.” *Polymer* 69. <https://doi.org/10.1016/j.polymer.2015.04.086>.
- Tian, Chunhua, Yunchen Du, Chunsheng Cui, Zhiliang Deng, Jianlei Xue, Ping Xu, Rong Qiang, Ying Wang, and Xijiang Han. 2017. “Synthesis and Microwave Absorption Enhancement of Yolk–Shell Fe<sub>3</sub>O<sub>4</sub>@C Microspheres.” *Journal of Materials Science* 52 (11): 6349–61. <https://doi.org/10.1007/s10853-017-0866-3>.
- Uematsu, M., and E. U. Frank. 1980. “Static Dielectric Constant of Water and Steam.” *Journal of Physical and Chemical Reference Data* 9 (4): 1291–1306. <https://doi.org/10.1063/1.555632>.
- Urban, Jiri, Frantisek Svec, and Jean M.J. Fréchet. 2010. “Hypercrosslinking: New Approach to Porous Polymer Monolithic Capillary Columns with Large Surface Area for the Highly Efficient Separation of Small Molecules.” *Journal of Chromatography A* 1217 (52): 8212–21. <https://doi.org/10.1016/j.chroma.2010.10.100>.
- Vadivel, M., R. Ramesh Babu, M. Arivanandhan, K. Ramamurthi, and Y. Hayakawa. 2015. “Role of SDS Surfactant Concentrations on the Structural, Morphological, Dielectric and Magnetic Properties of CoFe<sub>2</sub>O<sub>4</sub> Nanoparticles.” *RSC Advances* 5 (34): 27060–68. <https://doi.org/10.1039/C5RA01162K>.
- Vélez, Paris, Jonathan Muñoz-Enano, Amir Ebrahimi, Cristian Herrojo, Ferran Paredes, James Scott, Kamran Ghorbani, and Ferran Martín. 2021. “Single-Frequency Amplitude-Modulation Sensor for Dielectric Characterization of Solids and Microfluidics.” *IEEE Sensors Journal* 21 (10): 12189–201.
- Venkatesh, M. S., and G. S.V. Raghavan. 2005. “An Overview of Dielectric Properties Measuring Techniques.” *Canadian Biosystems Engineering / Le Genie Des Biosystems Au Canada*.

## Bibliography

- Vermoortele, Frederik, Bart Bueken, Gaëlle Le Bars, Ben Van de Voorde, Matthias Vandichel, Kristof Houthoofd, Alexandre Vimont, et al. 2013. "Synthesis Modulation as a Tool To Increase the Catalytic Activity of Metal–Organic Frameworks: The Unique Case of UiO-66(Zr)." *Journal of the American Chemical Society* 135 (31): 11465–68. <https://doi.org/10.1021/ja405078u>.
- Vikrant, Kumar, Yao Qu, Ki-Hyun Kim, Danil W. Boukhvalov, and Wha-Seung Ahn. 2020. "Amine-Functionalized Microporous Covalent Organic Polymers for Adsorptive Removal of a Gaseous Aliphatic Aldehyde Mixture." *Environmental Science: Nano* 7 (11): 3447–68. <https://doi.org/10.1039/D0EN00537A>.
- Vinodh, Rajangam, Eui Min Jung, Mani Ganesh, Mei Mei Peng, Aziz Abidov, Muthiahpillai Palanichamy, Wang Seog Cha, and Hyun Tae Jang. 2015. "Novel Microporous Hypercross-Linked Polymers as Sorbent for Volatile Organic Compounds and CO<sub>2</sub> Adsorption." *Journal of Industrial and Engineering Chemistry* 21 (January): 1231–38. <https://doi.org/10.1016/j.jiec.2014.05.039>.
- Wang, Chao, Xijiang Han, Ping Xu, Xiaolin Zhang, Yunchen Du, Surong Hu, Jingyu Wang, and Xiaohong Wang. 2011. "The Electromagnetic Property of Chemically Reduced Graphene Oxide and Its Application as Microwave Absorbing Material." *Applied Physics Letters* 98 (7): 1–4. <https://doi.org/10.1063/1.3555436>.
- Wang, Gang, Baojuan Dou, Junhui Wang, Wanqiu Wang, and Zhengping Hao. 2013. "Adsorption Properties of Benzene and Water Vapor on Hyper-Cross-Linked Polymers." *RSC Advances* 3 (43): 20523–31. <https://doi.org/10.1039/c3ra41450g>.
- Wang, HaiLin, Lie Nie, Jing Li, YuFei Wang, Gang Wang, JunHui Wang, and ZhengPing Hao. 2013. "Characterization and Assessment of Volatile Organic Compounds (VOCs) Emissions from Typical Industries." *Chinese Science Bulletin* 58 (7): 724–30. <https://doi.org/10.1007/s11434-012-5345-2>.

## Bibliography

- Wang, Jing, Akihiro Yoshida, Peifen Wang, Tao Yu, Zhongde Wang, Xiaogang Hao, Abuliti Abudula, and Guoqing Guan. 2020. "Catalytic Oxidation of Volatile Organic Compound over Cerium Modified Cobalt-Based Mixed Oxide Catalysts Synthesized by Electrodeposition Method." *Applied Catalysis B: Environmental* 271 (August): 118941. <https://doi.org/10.1016/j.apcatb.2020.118941>.
- Wang, Junhui, Wan-Qiu Wang, Zhengping Hao, Gang Wang, Yang Li, Jian-Gang Chen, Miaomiao Li, Jie Cheng, and Zhao-Tie Liu. 2016. "A Superhydrophobic Hyper-Cross-Linked Polymer Synthesized at Room Temperature Used as an Efficient Adsorbent for Volatile Organic Compounds." *RSC Advances* 6 (99): 97048–54. <https://doi.org/10.1039/C6RA18687D>.
- Wang, Lan, and Zhi-Min Dang. 2005. "Carbon Nanotube Composites with High Dielectric Constant at Low Percolation Threshold." *Applied Physics Letters* 87 (4): 042903. <https://doi.org/10.1063/1.1996842>.
- Wang, Lina, Xilai Jia, Yongfeng Li, Fan Yang, Liqiang Zhang, Liping Liu, Xiao Ren, and Haitao Yang. 2014a. "Synthesis and Microwave Absorption Property of Flexible Magnetic Film Based on Graphene Oxide/Carbon Nanotubes and Fe<sub>3</sub>O<sub>4</sub> Nanoparticles." *Journal of Materials Chemistry A* 2 (36): 14940. <https://doi.org/10.1039/C4TA02815E>.
- . 2014b. "Synthesis and Microwave Absorption Property of Flexible Magnetic Film Based on Graphene Oxide/Carbon Nanotubes and Fe<sub>3</sub>O<sub>4</sub> Nanoparticles." *Journal of Materials Chemistry A* 2 (36): 14940. <https://doi.org/10.1039/C4TA02815E>.
- Wang, Shuangshuang, Liang Zhang, Chao Long, and Aimin Li. 2014. "Enhanced Adsorption and Desorption of VOCs Vapor on Novel Micro-Mesoporous Polymeric Adsorbents." *Journal of Colloid and Interface Science* 428 (August): 185–90. <https://doi.org/10.1016/j.jcis.2014.04.055>.
- Wang, Wan-Qiu, Junhui Wang, Jian-Gang Chen, Xiu-Shan Fan, Zhao-Tie Liu, Zhong-Wen Liu, Jinqiang Jiang, and Zhengping Hao. 2015. "Synthesis of Novel Hyper-Cross-Linked

## Bibliography

- Polymers as Adsorbent for Removing Organic Pollutants from Humid Streams.” *Chemical Engineering Journal* 281 (December): 34–41. <https://doi.org/10.1016/j.cej.2015.06.095>.
- Wang, Xiaomei, Han Ou, and Jianhan Huang. 2019. “One-Pot Synthesis of Hyper-Cross-Linked Polymers Chemically Modified with Pyrrole, Furan, and Thiophene for Phenol Adsorption from Aqueous Solution.” *Journal of Colloid and Interface Science* 538 (March): 499–506. <https://doi.org/10.1016/j.jcis.2018.12.021>.
- Weng, Ling, Qian Shan Xia, Li Wen Yan, Li Zhu Liu, and Zhi Sun. 2016. “In Situ Preparation of Polyimide/Titanium Carbide Composites with Enhanced Dielectric Constant.” *Polymer Composites* 37 (1). <https://doi.org/10.1002/pc.23162>.
- Wu, Fan, Aming Xie, Mengxiao Sun, Yuan Wang, and Mingyang Wang. 2015. “Reduced Graphene Oxide (RGO) Modified Spongelike Polypyrrole (PPy) Aerogel for Excellent Electromagnetic Absorption.” *Journal of Materials Chemistry A* 3 (27): 14358–69. <https://doi.org/10.1039/C5TA01577D>.
- Wu, L. Z., J. Ding, H. B. Jiang, L. F. Chen, and C. K. Ong. 2005. “Particle Size Influence to the Microwave Properties of Iron Based Magnetic Particulate Composites.” *Journal of Magnetism and Magnetic Materials* 285 (1–2). <https://doi.org/10.1016/j.jmmm.2004.07.045>.
- Wusiman, Kuerbanjiang, Hyomin Jeong, Kelimu Tulugan, Handry Afrianto, and Hanshik Chung. 2013. “Thermal Performance of Multi-Walled Carbon Nanotubes (MWCNTs) in Aqueous Suspensions with Surfactants SDBS and SDS.” *International Communications in Heat and Mass Transfer* 41 (February): 28–33. <https://doi.org/10.1016/j.icheatmasstransfer.2012.12.002>.
- Xiao, Feng Shou, and Xiangju Meng. 2016. *Zeolites in Sustainable Chemistry. Zeolites in Sustainable Chemistry: Synthesis, Characterization and Catalytic Applications*.

## Bibliography

- Xiu, Guo-hua, Ping Li, and Alirio E. Rodrigues. 2002. "Sorption-Enhanced Reaction Process with Reactive Regeneration." *Chemical Engineering Science* 57 (18): 3893–3908. [https://doi.org/10.1016/S0009-2509\(02\)00245-2](https://doi.org/10.1016/S0009-2509(02)00245-2).
- Xu, Shujun, Yali Luo, and Bien Tan. 2013. "Recent Development of Hypercrosslinked Microporous Organic Polymers." *Macromolecular Rapid Communications* 34 (6): 471–84. <https://doi.org/10.1002/marc.201200788>.
- Yacubowicz, J., M. Narkis, and L. Benguigui. 1990. "Electrical and Dielectric Properties of Segregated Carbon Black-Polyethylene Systems." *Polymer Engineering and Science* 30 (8): 459–68. <https://doi.org/10.1002/pen.760300806>.
- Yang, Hui, Jian Shan, Jinglin Li, and Shangting Jiang. 2019. "Microwave Desorption and Regeneration Methods for Activated Carbon with Adsorbed Radon." *Adsorption* 25 (2): 173–85. <https://doi.org/10.1007/s10450-019-00019-3>.
- Yang, Ralph T. 2003. *Adsorbents: Fundamentals and Applications*. *Adsorbents: Fundamentals and Applications*. <https://doi.org/10.1002/047144409x>.
- Yi, Fen Yun, Xiao Dan Lin, Shui Xia Chen, and Xiao Qun Wei. 2009. "Adsorption of VOC on Modified Activated Carbon Fiber." *Journal of Porous Materials* 16 (5). <https://doi.org/10.1007/s10934-008-9228-5>.
- Yu, Yong, Shuangqi Song, Zhixiang Bu, Xiaofeng Gu, Gangbing Song, and Li Sun. 2013. "Influence of Filler Waviness and Aspect Ratio on the Percolation Threshold of Carbon Nanomaterials Reinforced Polymer Nanocomposites." *Journal of Materials Science* 48 (17): 5727–32. <https://doi.org/10.1007/s10853-013-7364-z>.
- Yuen, Foo Keng, and B.H. Hameed. 2009. "Recent Developments in the Preparation and Regeneration of Activated Carbons by Microwaves." *Advances in Colloid and Interface Science* 149 (1–2): 19–27. <https://doi.org/10.1016/j.cis.2008.12.005>.

## Bibliography

- Yun, Jeong Ho, Dae Ki Choi, and Hee Moon. 2000. "Benzene Adsorption and Hot Purge Regeneration in Activated Carbon Beds." *Chemical Engineering Science*. [https://doi.org/10.1016/S0009-2509\(00\)00189-5](https://doi.org/10.1016/S0009-2509(00)00189-5).
- Zarifi, Mohammad H., Mohammadreza Fayaz, Jordan Goldthorp, Mohammad Abdolrazzaghi, Zaher Hashisho, and Mojgan Daneshmand. 2015. "Microbead-Assisted High Resolution Microwave Planar Ring Resonator for Organic-Vapor Sensing." *Applied Physics Letters* 106 (6): 062903. <https://doi.org/10.1063/1.4907944>.
- Zarifi, Mohammad H., Pooya Shariaty, Zaher Hashisho, and Mojgan Daneshmand. 2017a. "A Non-Contact Microwave Sensor for Monitoring the Interaction of Zeolite 13X with CO<sub>2</sub> and CH<sub>4</sub> in Gaseous Streams." *Sensors and Actuators, B: Chemical* 238: 1240–47. <https://doi.org/10.1016/j.snb.2016.09.047>.
- . 2017b. "A Non-Contact Microwave Sensor for Monitoring the Interaction of Zeolite 13X with CO<sub>2</sub> and CH<sub>4</sub> in Gaseous Streams." *Sensors and Actuators B: Chemical* 238 (January): 1240–47. <https://doi.org/10.1016/j.snb.2016.09.047>.
- Zeng, Shao Zhong, Limin Guo, Qianjun He, Yu Chen, Peng Jiang, and Jianlin Shi. 2010. "Facile One-Pot Synthesis of Nanoporous Hypercrosslinked Hydroxybenzene Formaldehyde Resins with High Surface Area and Adjustable Pore Texture." *Microporous and Mesoporous Materials* 131 (1–3): 141–47. <https://doi.org/10.1016/j.micromeso.2009.12.014>.
- Zhang-Steenwinkel, Y., L.M. van der Zande, H.L. Castricum, A. Blik, R.W. van den Brink, and G.D. Elzinga. 2005. "Microwave-Assisted in-Situ Regeneration of a Perovskite Coated Diesel Soot Filter." *Chemical Engineering Science* 60 (3): 797–804. <https://doi.org/10.1016/j.ces.2004.09.042>.
- Zhang, Guangxin, Mohammad Feizbakhshan, Shuilin Zheng, Zaher Hashisho, Zhiming Sun, and Yangyu Liu. 2019. "Effects of Properties of Minerals Adsorbents for the Adsorption and

## Bibliography

- Desorption of Volatile Organic Compounds (VOC).” *Applied Clay Science* 173 (June): 88–96. <https://doi.org/10.1016/j.clay.2019.02.022>.
- Zhang, Liang, Xiaofei Song, Jian Wu, Chao Long, Aimin Li, and Quanxing Zhang. 2012. “Preparation and Characterization of Micro-Mesoporous Hypercrosslinked Polymeric Adsorbent and Its Application for the Removal of VOCs.” *Chemical Engineering Journal*. <https://doi.org/10.1016/j.cej.2012.03.071>.
- Zhang, Tingting, Wenbin Huang, Nan Zhang, Ting Huang, Jinghui Yang, and Yong Wang. 2017. “Grafting of Polystyrene onto Reduced Graphene Oxide by Emulsion Polymerization for Dielectric Polymer Composites: High Dielectric Constant and Low Dielectric Loss Tuned by Varied Grafting Amount of Polystyrene.” *European Polymer Journal* 94 (111): 196–207. <https://doi.org/10.1016/j.eurpolymj.2017.07.008>.
- Zhang, Xiaodong, Yang Yang, Xutian Lv, Yuxin Wang, Ning Liu, Dan Chen, and Lifeng Cui. 2019. “Adsorption/Desorption Kinetics and Breakthrough of Gaseous Toluene for Modified Microporous-Mesoporous UiO-66 Metal Organic Framework.” *Journal of Hazardous Materials*. <https://doi.org/10.1016/j.jhazmat.2018.11.099>.
- Zhang, Xueyang, Bin Gao, Anne Elise Creamer, Chengcheng Cao, and Yuncong Li. 2017. “Adsorption of VOCs onto Engineered Carbon Materials: A Review.” *Journal of Hazardous Materials*. <https://doi.org/10.1016/j.jhazmat.2017.05.013>.
- Zhang, Yinhang, Jang Rak Choi, and Soo Jin Park. 2018. “Interlayer Polymerization in Amine-Terminated Macromolecular Chain-Grafted Expanded Graphite for Fabricating Highly Thermal Conductive and Physically Strong Thermoset Composites for Thermal Management Applications.” *Composites Part A: Applied Science and Manufacturing* 109. <https://doi.org/10.1016/j.compositesa.2018.04.001>.
- Zhao, Ping, Shifa Wang, Alec Kadlec, Zhaodong Li, and Xudong Wang. 2016. “Properties of Cement–Sand-Based Piezoelectric Composites with Carbon Nanotubes Modification.”

## Bibliography

- Ceramics International* 42 (13): 15030–34.  
<https://doi.org/10.1016/j.ceramint.2016.06.153>.
- Zhou, Bing, Bin Sun, Wenjuan Qiu, Ying Zhou, Junqian He, Xiao'ai Lu, and Hanfeng Lu. 2019. "Adsorption/Desorption of Toluene on a Hypercrosslinked Polymeric Resin in a Highly Humid Gas Stream." *Chinese Journal of Chemical Engineering*.  
<https://doi.org/10.1016/j.cjche.2018.09.027>.
- Zhou, Xufeng, and Zhaoping Liu. 2010. "A Scalable, Solution-Phase Processing Route to Graphene Oxide and Graphene Ultralarge Sheets." *Chemical Communications* 46 (15): 2611. <https://doi.org/10.1039/b914412a>.

## APPENDIX A: SUPPLEMENTARY INFORMATION

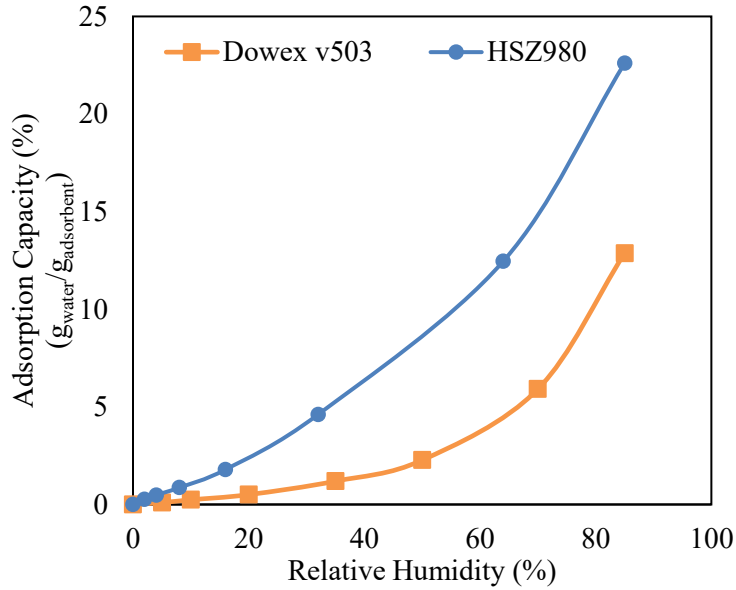
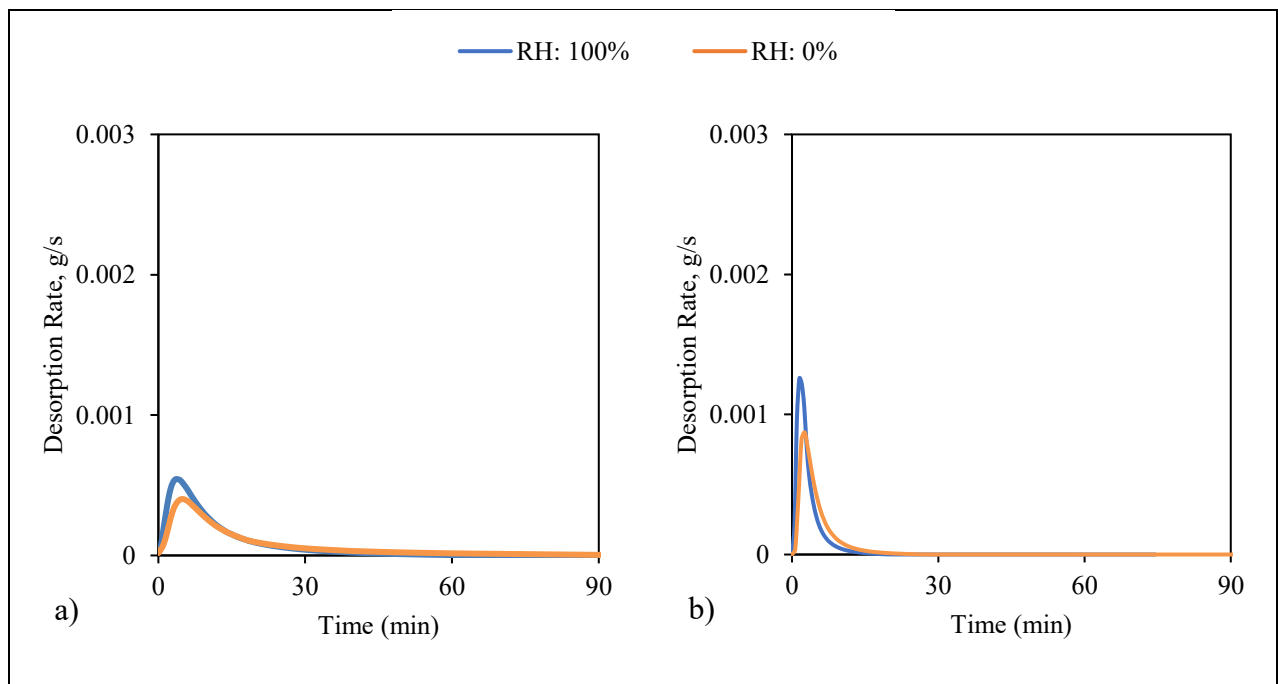


Figure 0-1. Adsorption isotherms of water vapor on Zeolite HSZ980 and Optipore V503 without MW heating.



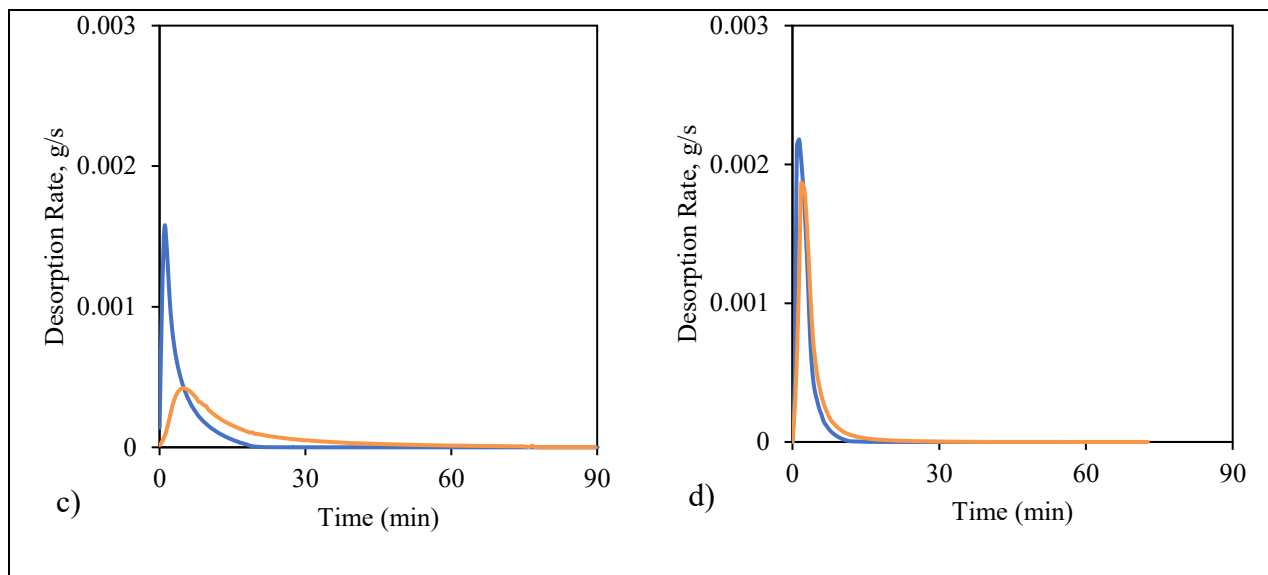


Figure 0-2. Desorption rate of a) Cyhex from Optipore V503, b) IPA from Optipore V503, c) Cyhex from Zeolite HSZ980, and d) IPA from Zeolite HSZ980 at 0 and 100 % RH and constant applied power of 380 W.

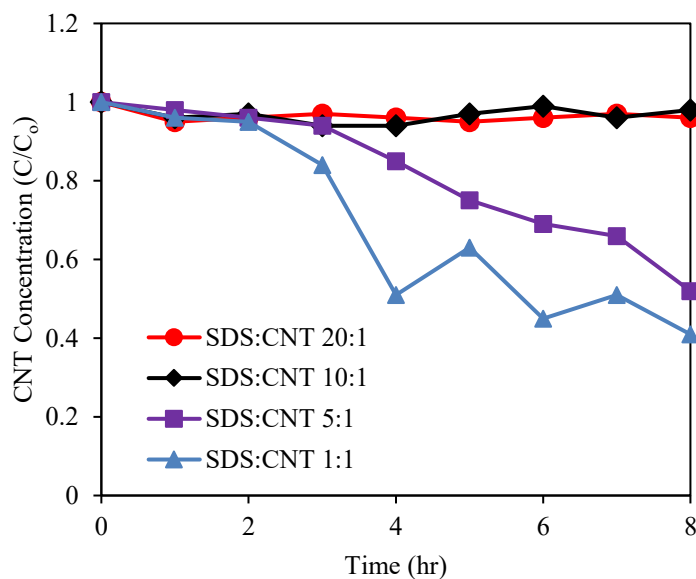


Figure 0-3. Dispersed CNT concentration versus time.